MICROFLUIDIC REDUCTION OF OSMOTIC STRESS IN OOCYTE AND ZYGOTE VITRIFICATION

by

David Lai

A dissertation submitted in partial fulfillment
of the requirements for the degree of
Doctor of Philosophy
(Biomedical Engineering)
in The University of Michigan
2014

Doctoral Committee:

Professor Shuichi Takayama, Chair
Professor Joseph L. Bull
Professor Katsuo Kurabayashi
Professor Gary D. Smith

To my mom and dad

…for supporting me and giving me two baby brothers

and to Joshua and Samuel.

…my childhood would be so different if I didn't spend it beating you up.

ACKNOWLEDGEMENTS

This dissertation contains research written with

extensive contributions and support of all my colleagues and friends.

TABLE OF CONTENTS

DEDICATION ii

ACKNOLEDGEMENTS iii

LIST OF FIGURES viii

LIST OF APPENDICES xi

CHAPTERS

Part 1:

1. Microfluidics for Assisted Reproductive Technologies 1

1.1 Introduction 1

1.2 Gamete Manipulations 3

1.3 *In Vitro* Fertilization 9

1.4 Cryopreservation 11

1.5 Embryo Culture 14

1.6 Embryo Analysis 16

1.7 Conclusions 18

1.8 References 33

2. Microfluidic Reduction of Osmotic Stress in Oocyte and Zygote Vitrification 36

2.1 Introduction 36

2.2 Materials and Methods 39

2.3 Results and Discussion 45

2.4Conclusions 53

2.5 References 58

3. Conclusions and Future Direction 60

Part 2:

4. Rounded Multi-level Microchannels with Orifices Made in One Exposure Enabled Aqueous Two-Phase System Droplet Microfluidics 64

4.1 Introduction 64

4.2 Materials and Methods 65

4.3 Results and Discussion 67

4.4. Conclusions 70

4.5 References 77

5. Precisely Targeted Delivery of Cells and Biomolecules Within Microchannels Using Aqueous Two-Phase Systems 79

5.1 Introduction 79

5.2 Materials and Methods 82

5.3 Results and Discussion 86

5.4. Conclusions 91

5.5 References 97

6. Simple Multi-level Microchannel Fabrication by pseudo-Grayscale Backside Diffused Light Lithography 100

6.1 Introduction 101

6.2 Materials and Methods 103

6.3 Results and Discussion 106

6.4. Conclusions 110

6.5 References 118

7. Label-Free Direct Visual Analysis of Hydrolytic Enzyme Activity Using Aqueous Two-Phase System Droplet Phase Transitions 120

7.1 Introduction 120

7.2 Materials and Methods 122

7.3 Results and Discussion 128

7.4. Conclusions 132

7.5 References 139

APPENDICES 141

LIST OF FIGURES

Fig. 1.1	Microfluidic sperm sorter	20
Fig. 1.2	Sperm microfluorometer	21
Fig. 1.3	Sperm motility sorting	22
Fig. 1.4	Sperm fluorescence activated sorting	23
Fig. 1.5	Microfluidic zygote denuding	24
Fig. 1.6	Magnetically driven microtools	25
Fig. 1.7	Weir-type microfluidic fertilization	26
Fig. 1.8	Microfluidic CPA exposures for slow-rate freezing	27
Fig. 1.9	Microfluidic permeable CPA exposure for vitrification	28
Fig. 1.10	Microfluidic embryo culture	29
Fig. 1.11	Microfunnel embryo culture and buffer flow chip	30
Fig. 1.12	Multilayer designs for fully automated microfluidics	31
Fig. 1.13	Braille driven microfluidic device for spent media analysis	32
Fig. 2.1	Kedem Katchalsky model and zygote morphology	54
Fig. 2.2	Roughness index and sphericity of murine zygotes	55
Fig. 2.3	Microfluidic device characterization for vitrification	56
Fig. 2.4	Lipid retention and developmental competence	57
Fig. 3.1	Generic phase diagram for vitrification	63
Fig. 4.1	Schematic for orifice fabrication for BDLL	71
Fig. 4.2	Schematic for generic BDLL	72
Fig. 4.3	Photomask for orifice fabrication for BDLL	73
Fig. 4.4	BDLL device	74

Fig. 4.5	BDLL multi-level characterization	75
Fig. 4.6	ATPS droplet characterization	76
Fig. 5.1	ATPS laminar flow characterization	92
Fig. 5.2	ATPS laminar flow cell patterning	93
Fig. 5.3	ATPS droplet flow cell patterning	94
Fig. 5.4	ATPS laminar trypsin delivery	95
Fig. 5.5	ATPS partition and laminar flow schematic	96
Fig. 6.1	pGD BDLL photomask, device, and schematic	112
Fig. 6.2	SEM images of BDLL devices	113
Fig. 6.3	pGS BDLL fabrication height characterization: exposure time	114
Fig. 6.4	pGS BDLL fabrication height characterization: exposure energy	115
Fig. 6.5	pGS BDLL red blood cell sorting	116
Fig. 6.6	pGS BDLL ovarian follicle sorting	117
Fig. 7.1	ATPS binodial phase diagram shifts	133
Fig. 7.2	DEX chain length and concentrations for ATPS	134
Fig. 7.3	ATPS binodial curves for temperatures and pH	135
Fig. 7.4	ATPS phase change with dextranase	136
Fig. 7.5	ATPS dextranase with microfluidics	137
Fig. A.1	Braille display for driving microfluidic devices	158
Fig. A.2	Braille driven microfunnel embryo culture	159
Fig. A.3	Passively driven sperm sorting	160
Fig. A.4	Microfluidic sperm counting microfluorometer	161
Fig. A.5	OET sperm sorting	162
Fig. A.6	Optics and hydrodynamics for sperm sorting	163
Fig. A.7	Absorption spectra for analysis of oocyte maturity	164
Fig. A.8	Highly programmable complex Braille operations	165

Fig. A.9	Predictive algorithms of embryo development	166
Fig. A.10	Challenges of integrating photonics and microfluidics	167
Fig. B.1	Schematic for microfluidic IVF	196
Fig. B.2	Microfluidic laminar flow sperm sorting	197
Fig. B.3	Microfluidic weir-type IVF	198
Fig. B.4	Microfluidics for mammalian embryo culture	199
Fig. B.5	Microfluidic co-culture embryo platforms	200
Fig. B.6	Microfluidic CPA exposure devices	201
Fig. B.7	Microfluidics for embryo metabolism analysis	202
Fig. C.1	Timeline of fluidic actuation and control systems	229
Fig. C.2	Microfluidic multiplexers	230
Fig. C.3	Microfluidic logic gates	231
Fig. C.4	Microfluidic oscillator	232
Fig. C.5	Applications of microfluidic multiplexers	233
Fig. C.6	Droplet microfluidic operations	234
Fig. C.7	Applications of droplet microfluidics	235

LIST OF APPENDICES

APPENDIX

A. Lab-on-a-Chip Biophotonics: Its Application to Assisted Reproductive Technologies 142

A.1 Introduction 142

A.2 Basic Use of Biophotonics in LOC ART 144

A.3 Advanced Use of Biophotonics in LOC ART 147

A.4 Future of Biophotonics in LOC ART 153

A.5 References 168

B. Thinking Big by Thinking Small: Application of Microfluidic Technology to Improve ART 171

B.1 Introduction 171

B.2 Andrology 172

B.3 Embryology 177

B.4 Cryopreservation 188

B.5 Future Directions 190

B.6 Conclusions 195

B.7 References 203

C. Microfluidic Automation Using Elastomeric Valves and Droplets: Reducing Reliance on External Controllers 208

C.1 Introduction 208

C.2 History of Macroscale Fluidic Control 210

C.3 Advent of Elastomeric Microfluidic Devices 212

C.4 Droplet Circuits 221

C.5 Outlook and Perspectives 225

C.6 References 236

Part 1

Chapter 1

Microfluidics for Assisted Reproductive Technologies

1.1 Introduction

Infertility affects almost 10% of couples in the United States and the causes are roughly equal between male and female derived infertility[1]. As reproduction is a major quality of life issue: there is a large motivation for the advancement of assisted reproductive technology. Although a relatively new field, microfluidics has already demonstrated the benefits of automation, consistency, sensitivity, and precision to the field of assisted reproductive technologies (ARTs). Efforts in this field utilize the high-throughput nature of microfluidics as well as the potential to perform highly sensitive non-destructive tests for gamete/embryo quality to overcome some of the toughest and most laborious challenges faced by assisted reproductive technologies.

One of the most common benefits of microfluidics is its cost efficiency due to the low amounts of materials used, however in the field of ART, this benefit is of secondary importance. The advantage of highly accurate high-throughput gamete sorting and the identification of the most suitable male and female gamete to use for fertilization justify the use of microfluidics even if it were more expensive to operate.

Male gamete quality assessment chips typically operate at a relatively high-throughput range due to the large quantities of available material, while female gamete quality assessment chips are the complete opposite in terms of sorting speed as the low amounts of available sample justify the use of sophisticated biophotonic non-destructive tests of gamete quality. Fertilization-on-chip devices either mimic existing ART techniques or incorporate selectivity barriers within the microfluidic device based on sperm motility to mimic the motility selection of the uterus and fallopian tube.

Cryopreservation has been key to increasing the efficiency of fertility treatments in ART. Cryopreservation devices focus on reducing osmotic stress particularly for vitrification where concentrations of cryoprotectant agents (CPA) are particularly high. Microfluidic cryopreservation devices also reliably standardize the vitrification protocol with precision and accuracy to the fluid transfer of the CPA exchange: addressing the large unknown that is the variable fluid behavior in current manual pipetting even within the best trained and skilled personnel.

Microfluidic embryo cultures have also employed biomimicry of the fallopian tubes in multiple strategies to assist embryos into developing with superior developmental competence. Such strategies include mimicry of the mechanical stimulation provided by fallopian tube flow as well as the recirculation of secreted factors that chemically stimulate embryo growth. As developmental competence increases with technological advancement of each stage whether using conventional clinical lab techniques or lab on a chip (LOC) techniques, it is increasingly more sensible and feasible to perform single embryo transfers (SETs). The chances of multiple births, typically an unfavorable outcome, exponentially decrease with each

embryo transferred beyond one. It is therefore paramount in this stage to select the best embryo to transfer as to maximize the chance of a successful SET. To address this issue, multiple non-destructive tests have been developed to determine embryo quality after embryo culture and these include advanced spectroscopy techniques that directly examine the embryo, indirect metabolite analysis of spent culture media as well as real-time embryo development monitoring combined with predictive algorithms for selecting the best embryo for.

1.2 Gamete Manipulations

Gamete manipulations using lab-on-a-chip technologies focus on non-destructive quality analysis of sperm and oocytes. Andrology strategies take advantage of the high-throughput characteristics of microfluidics due to the high number of gametes available and are particularly useful for individuals with low numbers of viable sperm. On the contrary, gynecology strategies focus on in-depth analysis due to the limited number of gametes and the high importance of oocyte quality on subsequent embryo development. Despite the widespread acceptance that morphology is a poor indication of future developmental success[2], it is still the primary measure of quality. Female lab-on-a-chip devices employ the precision and accuracy provided by microfluidic devices to develop more sophisticated measures of oocyte quality assessment.

Male gamete sorting

The determination of viability for sperm is rather simple as the sole concern is DNA integrity as advanced assisted reproductive technologies such as intracytoplasmic sperm injection (ICSI) is capable of overcoming numerous infertility issues that

complicate natural conception. Intracytoplasmic sperm injection is such a powerful technique that it is possible to use dying or even dead sperm to achieve fertilization. However, it is well known that the use of dead or dying sperm for ICSI results in adverse outcomes including low fertilization, poor embryo development, high abortion rates, and prevalent childhood diseases[3]. Due to the large number of sperm available, it is rare that live and motile sperm cannot be found even if in low number for the majority of male infertility cases. As ICSI only requires a single viable sperm and the significant adverse result of using dead or dying sperm, the first conventional sorting criterion is that the sperm be motile: evidence that it is alive. The second criterion is that it has normal morphology in the absence of defects such as multiple heads, multiple tails, large or small heads, or abnormal mid-sections. Such defects in morphology indicate defected genotype on which it is based and are discarded during conventional sperm sorting.

For lab-on-a-chip applications, mobility provides a simple mechanism for separation as non-motile sperm and debris are incapable of crossing streamlines in laminar flow regime. The enclosed system of microfluidic devices as well as the high level of fluid control allow sorting of non-motile sperm and debris with high accuracy and at high-throughput speeds. Conveniently for microfluidic applications, the second conventional criterion for sorting: abnormal morphology also often affects motility. When designing the microfluidic device with high safety factors (where only highly motile sperm are selected), the device would also eliminate abnormal albeit motile sperms simultaneously from the sample.

One passively driven microfluidic device to sort sperm by motility used gravity to create two streams flowing in a laminar regime[4] (Fig. 1.1). It relies on the

motile sperm's ability to cross enough streamlines by traveling in the transverse direction to flow. The passive flow of the microfluidic device delivers the sperm to the collection chamber separate from the waste collection chamber. Viable sperm sorted into the collection chamber can then be collected for ICSI. The continuously separating nature of the microfluidic device allows for reasonable volumes of sample to be sorted for easy identification of viable sperm even in cases of severe male infertility.

In another example, a microfluidic device with a long hydrostatic channel connected to a detection cuvette allowed for the screening of male subfertility with the staining of sperm with calcein-AM[5] (Fig. 1.2a-b). The long hydrostatic channel served as a selective barrier for motile sperm: allowing only the sperm of healthy motility to traverse the long distance to reach and populate the detection cuvette (Fig. 1.2c-f). The fluorescence profile is monitored by microfluorometer over a 50 minute period (Fig. 1.2g-h). As the detection cuvette is populated by more sperm, the fluorescence from the combined calcein-AM increases the fluorescence intensity proportionally to the number of sperm in the detection cuvette over time. This fluorescence profile of each sample can then be screened relative to a reference sample to determine their subfertility level. The device, being small and disposable, has shown promise as an accurate in-home screening technique for male subfertility.

It was a microfluidic study that definitively demonstrated that sperm behave predictably in certain well defined flow conditions. The study determined that the sperm would tend to either swim towards or against flow depending on the intensity of the flow velocity[6]. This device demonstrated the predictability of this behavior and applied it to separate, align, and orient sperm of mouse, bull, and human species.

One recent advancement of note in male infertility microfluidic devices employ an integrated charge-coupled device (CCD) to the microfluidic device to provide a wide field of view to sort and track sperm populations[7] (Fig. 1.2i) The sophisticated automated sperm monitoring algorithm is capable of determining sperm average velocity, straight line velocity, straightness of swim path, and average acceleration. The attention given by the software to each individual sperm provides the capability to identify the most motile sperm, which by conventional wisdom is the healthiest, for potential applications in ICSI. Such detailed quantification of sperm quality eliminates the arbitrary elements of conventional sperm selection when there are numerous viable sperm available.

Even more recent advances in sperm quality assessment by microfluidic devices include a device that quantifies both sperm concentration and motile percentage[8] (Fig. 1.3a-i). The device uses a microfluidic component for the separation of motile sperm of similar mechanisms as its predecessors and is designed to be centrifuged to sediment the sperm sample for quantification. Concurrently, a sophisticated method for quantifying human sperm quality was developed using a microfluidic resistive pulse technique (RPT)[9]. The change in current over time from the resistive properties of the sperm is measured as it travels along a long narrow aperture where the voltage is applied. The signal profile can be easily analyzed for the sperm's swimming behavior in terms of beat frequency and swim velocity as well as the sperm's volume. Such proposed techniques offer economic advances to comparable sperm analysis provided by conventional computer assisted sperm analysis (CASA).

The latest microfluidic assay for determining sperm DNA integrity demonstrates strong evidence that sperm motility is a strong indication of high chromatin and DNA integrity[10] (Fig. 1.3j). The device is capable of using raw semen and uses a viscoelastic medium and long hydrostatic channels that mimic the motility selection process of the female reproductive tract. The length of the device can be adjusted according to the subfertility of the sample for an optimal level of motility-based sorting.

Although not strictly lab-on-a-chip, fluorescence activated cell sorting (FACS) uses a cytometer in combination with DNA-binding dyes and fluorescence detection. It has been used for detecting minute differences in fluorescence signal originating from a 3.8% difference in total DNA content between X and Y chromosome bearing bovine spermatozoa[11] (Fig. 1.4). When the difference in DNA content is detected, an applied electric field sorts the droplet containing the spermatozoa into X and Y chromosome bearing bins. The system can reach up to 25,000 individual spermatozoa per second and is useful in agricultural industries. However it is known that high shear stress and high voltage cause extensive DNA fragmentation[12, 13]. This is a concern that should not be ignored as both high shear stress and voltage exist in the cytometer and sorting region of FACS.

Female gamete quality assessment

Oocyte quality is a large factor that affects later developmental success during and after fertilization. Despite the importance of oocyte selection, especially for SETs, the determination of oocyte quality is typically based on highly subjective morphological properties. However, a more sophisticated analysis of oocyte quality must not compromise the quality of the oocyte as it needs to be retrieved for further use. As

such, there are significant challenges in developing the appropriate tools to probe the oocyte for a quantitative analysis of its quality.

One such microfluidic device that studied this problem developed an optical solution to study the refractive index and optical absorption of the oocyte to determine its maturity as well as a microindentor to measure the hardness and reduced Young modulus of the oocyte: a tool that can be used for further study of the oocyte[14] (Fig. 1.5e-f). The optical probe was capable of detecting a significant difference in absorption spectra between mature and immature oocytes. This development provides a solution to alleviate some of the subjectivity that exists in oocyte selection for ART.

During common ART procedures such as *in vitro* maturation (IVM), *in vitro* fertilization (IVF) and *in vitro* embryo culture (IVC), the oocyte or zygote undergoes a process where its cumulus cells are removed, sometimes called denuding. The most common form of denuding requires a technician to repeatedly flush the cumulus oocyte complex (COC) into and out of a narrow pipette tip. Such a procedure is known to cause high mechanical stress[15]. As such, a novel micromanipulation device was designed using the precise control provided by microfluidics. The device is capable of reorienting the cumulus into a ring around a zygote. The cumulus ring surrounding the zygote is then attached to a removal port, which combined with the suction from an adjacent port, rotates the COC to remove the ring: leaving the denuded zygote with less mechanical stress[16] (Fig. 1.5a-d). The ability to precisely control the zygote position by device geometry and fluid control enable predictable and reliable cumulus removal.

Recent advances in microelectromechanical systems (MEMS) for ART developed a set of magnetically driven microtools (MMTs) that upon actuation

enucleated oocytes[17]. Enucleation is a process where the nucleus is removed from the cell body: a key component in the cloning process. Such a technique is normally performed by highly trained technicians but typically still suffers from low success rates and repeatability. The use of this device overcomes limitations of conventional enucleation by providing precision and reproducibility. The group also demonstrated the combination of MMT with ultrasonic vibration doubled the output force of the MMT to improve the positioning accuracy by 100-fold[18] (Fig. 1.6).

Optofluidic devices are a specialized research field that combines microfluidic and optics designs. One such optofluidic device was developed using optical ablation for microsurgery of oocytes[19]. While microfluidic channels have been shown to be effective at cell positioning as well as long-term and real-time monitoring, optical ablation is an effective noninvasive method to destroy intracellular organelles. Such microsurgery techniques are a valuable tool that can provide insight about the functions of the organelle and developmental repercussions for damaged oocytes.

1.3 *In Vitro* Fertilization

There are two prevalent methods of fertilization in ART that are modified in lab-on-a-chip devices. The first method is the use of fertilization medium and conventional insemination with sperm and the default method of IVF. However if it is deemed that conventional insemination is likely to be unsuccessful, ICSI will be used in ART. The conventional insemination IVF technique is relatively simple where medium containing washed sperm is mixed and incubated with medium containing oocytes. A sperm will make contact with oocyte where it penetrates the zona pellucida as it

would naturally for fertilization. The second method is ICSI, a powerful technique that overcomes numerous male and female infertility challenges. Intracellular sperm injection overcomes many stages of fertilization where complications may occur by assisting the sperm in penetrating the egg through direct injection of the sperm into the egg cytoplasm.

There have been a significant amount of microfluidic fertilization devices that enhances the conventional insemination and IVF technique. Depending on the design, it can boast higher fertilization efficiency with lower total number and concentrations of sperm needed. The device can also increase primary outcomes by lowering instances of polyspermic penetration compared to conventional fertilization medium.

One such IVF microfluidic device was designed using polydimethylsiloxane(PDMS)/borosilicate material and was driven passively by hydrostatic pressure[20] (Fig. 1.7a). The device employed a now commonly used weir-type trap design for oocytes while sperm are allowed to flow through the device. This device demonstrated that by limiting the time the oocytes were exposed to the sperm, as the sperm had a limited chance to penetrate the oocyte as the flowed by, the device design allowed for significantly lower rates of polyspermy.

Another device of similarly inspired weir-type design focused its study on low-sperm count fertilization. The device demonstrated that although the rate of fertilization decreases in a microfluidic device for high sperm count samples, the microfluidic device was effective at significantly increasing the fertilization rate of low sperm count samples[21] (Fig. 1.7b). This result is primarily due to the geometry and scale of the microfluidic device that increases the effective concentration of

sperm in the area surrounding the oocyte thus greatly increasing the chances of fertilization.

More sophisticated devices later emerged that also used weir-type traps to individually compartmentalize oocytes within the microfluidic device[22] (Fig. 1.7c). The device applied the microfluidic enhancement of the conventional insemination IVF technique and the individual compartments were capable of providing single embryo development tracking over 96 hours. Such a device demonstrates great potential for a microfluidic device to provide a fully integrated and automated system for ART research and clinical applications.

The microfluidic enhancement to conventional insemination IVF is clear, but the advancement in microfluidic system in ICSI has just begun. Recently, there has been effort in producing a fully integrated and automated microfluidic system for ICSI[23]. The device uses sperm separation by motility to select viable sperm for ICSI and is further combined with a chemical and mechanical cumulus denuding compartment. A series of embedded electrodes are used to orient the oocyte and laser trapping is used to immobilize the selected sperm. The actual ICSI procedure is performed on-chip by a piezo-actuator driven needle. The device then releases the fertilized zygote to individualized compartments for single embryo long term culture and monitoring. This fully integrated system is one of the first to fully integrate both male and female gamete processing and selection for usage, ICSI, and long term single embryo culture and monitoring.

1.4 Cryopreservation

Cryopreservation is now an essential part of assisted reproductive technology and substantially increases the efficiency of techniques/processes such as SETs, donor-recipient cycle synchronizations, and oncofertility preservation with both embryo[24] and oocyte[25] cryopreservation. There are two prevalent strategies of cryopreservation: 1) slow-rate freezing or equilibrium freezing; and 2) ultra-rapid cooling or vitrification.

The microfluidic designs used to explore microfluidic cryopreservation, like the chronological development of conventional cryopreservation, started with slow-rate freezing. The unprecedented control of fluid osmolality was capable of minimizing osmotic stress using diffusion and laminar flow[26] (Fig. 1.8). By lowering the osmotic stress, the device improved post-thaw survivability by up to 25% on average over convention cryopreservation techniques.

With recent technological advancements to vitrification, recent studies on mature human oocyte cryopreservation demonstrated that vitrification has enhanced outcome in terms of higher survival rates, cleavage, and pregnancy rates compared to its slow-rate freezing alternative[27]. The osmotic fluid control provided by microfluidics gives an unprecedented level of precision and osmolality control not available with manual pipetting. This is particularly important in vitrification where higher concentrations of cryoprotectant agents (CPAs) are used. In an effort to lower the osmotic stress the cells experience, a protocol for fluid exchange was developed that moves the cell into solutions of sequentially increasing concentrations of CPAs so that it lessens the osmotic change per step and divides the osmotic change necessary for vitrification over several steps over time. Some groups have demonstrated that the increase in the number of steps, and therefore the less osmotic stress introduced per

step, the higher cryosurvival[28] and development[29]. However the significantly increased number of pipetting steps in a fixed amount of time became increasingly difficult to perform manually. Microfluidics provides the capability of continuous perfusion, essentially an infinite amount of steps, and is capable of providing real-time and continuous optical microscopy and lab-on-a-chip automation for reproducibility by eliminating operator variability. Facing these current limitations, the motivations for using microfluidics for CPA exposure of oocytes and embryos for vitrification is clear and many groups have begun microfluidic designs for study.

A computerized microfluidic control of media exposure for human cleavage embryos was designed to permit gradual cryoprotectant exposure to limit the large osmolality changes currently used in manual pipetting vitrification. It demonstrated that the microfluidic method produced similar embryo survival, morula formation, cavitation, and blastocyst formation rates compared to its conventional manual pipetting method alternative[30]. This device was the first to explore gradual CPA exposure for vitrification.

Osmotic stress can be accurately predicted using computer modelling by Kedem-Katchalsky equations and known permeability parameters[31]. This was first explored using a device with only permeable CPAs demonstrating that the Kedem-Katchalsky model which has historically been used to model step-wise increases in CPA concentration can also be reliably used to model osmotic stress behavior of cells exposed to continuously changing CPA concentrations by microfluidic perfusion[32] (Fig. 1.9). The microfluidic device design however had limited access to cells for loading and removal which limited its ability to explore cryosurvival and developmental response to the different CPA exposure regime. The device also lacked

impermeable solutes that are highly recommended and present for practical vitrification solutions due to their low toxicity and its thermodynamic contributions towards vitrification[33].

Most recently, another microfluidic device using both permeable and impermeable solutes was designed to further confirm the remarkable accuracy of the Kedem-Katchalsky equations to model osmotic stress of oocytes and zygotes for vitrification. By using a combination of both permeable and impermeable solutes, the device was capable of controlling the shrinkage rate of the cell independently of its minimum cell volume. The study demonstrated the importance of shrinkage rate and its effect on sub-lethal damages[34]. The minimization of shrinkage rate had no effect on cryosurvival of murine zygotes as both manual and microfluidic CPA exposure had 100% cryosurvival. The shrinkage rate however did have an effect on sub-lethal damages. The lowering of shrinkage rate, and therefore sub-lethal damage, significantly increased the developmental competence of cryopreserved murine zygotes. This study is the first to experimentally and mathematically separate the effects of shrinkage rate from minimum shrinkage volume and is first to demonstrate a sub-lethal improvement in cryopreserved embryos.

1.5 Embryo Culture

Microfluidic techniques provide embryo culture devices with mechanical fluid stimulation, automated culture media renewal, real-time and long-term imaging, as well as autocrine factor retention. Currently, only up to half of human embryos fertilized by IVF develops into the blastocyst stage in *in vitro* culture with

approximately another 50% that attains successful implantation. The motivation of microfluidic design typically aims to simulate the natural environment of the *in vivo* environment. As in cryopreservation, automation also eliminates much of the user variability. Such control of physical and chemical parameters is needed for the careful dissection of experimental parameters necessary to further improve embryo culture outcomes[35] (Fig. 1.10a).

Early studies of microfluidic embryo culture devices studied the effect of microchannel culture as well as the material selection for microfluidic device fabrication. The foundation for microfluidic *in vivo* embryo culture was laid with the demonstration of advanced blastocyst development, higher survival rates, and fewer degenerated embryos in both silicon/borosilicate and PDMS/borosilicate devices[36] (Fig. 1.10b). This study employed static (no flow) microchannel culture allowing for a direct comparison with static microdrop systems. The improved developmental outcome is presumably due to the lower volume and the embryo's enhanced ability to regulate its microenvironment with paracrine and/or autocrine factors.

Although the addition of flow conditions is more similar to *in vivo* environments of embryo culture, it was discovered that simple continuous media perfusion within a microchannel and weir-type trap during embryo development was detrimental to embryo development across a range of flow rates[37]. Multiple reasons for the poor outcome were suggested, but the primary reason may be the loss of paracrine and autocrine factors and the inability of embryo self-regulation of its microenvironment. Subsequently developed was a dynamic microfunnel embryo culture system that provides mechanical stimulation from fluid flow while retaining biochemical stimulations by allowing the retention of autocrine factors from the

embryo's attempt to regulate its microenvironment[38] (Fig. 1.11a). The Murine embryos subjected to microfunnel pulsatile culture had significantly higher number of blastomeres per blastocyst. The more advanced embryo development was also shown to result in enhanced implantation and pregnancy rate than static culture controls.

The embryo culture devices so far have been preimplantation embryos. Microfluidic devices can also be used for zebrafish embryo development into zebrafish larvae. The use of the devices showed no increase in gross malformations of zebrafish larvae[39] (Fig. 1.11b). The cost effectiveness of the zebrafish model combined with low reagent volumes used during the microfluidic device embryo culture could be used for new analytic assays for the pharmaceutical industry.

More recently, more sophisticated microfluidic automation demonstrates fully integrated devices to culture and analyze developing zebrafish embryos[40] Microfluidic automation demonstrated the fluid control for automatic embryo loading, immobilization, medium perfusion, and release of viable embryos. It also had embedded control systems to control chemical and mechanical fluid stimulations, as well as temperature regulation. The ability to simultaneously perform automatic image acquisition and real-time monitoring provided the functionality to analyze subtle indications of developmental quality.

1.6 Embryo Analysis

As the practice of SETs become more prevalent in assisted reproductive technology, the importance of embryo selection for the best embryo becomes paramount to improve implantation rates. Current research direction is toward non-destructive

analysis of embryo quality. While non-destructive direct analysis on the embryo is uncommon, some recent solutions have been developed that uses advanced photonics such as light induced dielectrophoresis (DEP) or coherent anti-stokes raman spectroscopy (CARS). Neither technique currently has lab-on-a-chip applications, but has a great potential for on-chip integration. Current microfluidic devices for non-destructive embryo analysis employ indirect analysis of embryo quality such as spent medium metabolite analysis. Current limitations of such devices however are resulted from the devices being designed as targeted assays that measure specific metabolites of interest, therefore the microfluidic design becomes exponentially complex with each additional metabolite of interest. Such limitations highlight the strength of advanced spectroscopy capable of analyzing a broad spectrum of metabolites.

DEP devices have been used to directly evaluate the quality of preimplantation murine embryos. The electrical admittance of the embryo changes according to its development. This change, when controlled using the appropriate optoelectronic tweezer (OET) medium and in the presence of an OET induced DEP, can attract early stage development embryos while repelling late stage development embryos[41]. Such a non-invasive sorting mechanism uses a reproducible and quantitative measurement to determine embryonic developmental stages without the subjectivity of morphology assessment.

Another recent advancement in spectroscopy that has proved powerful for direct measurements of cell metabolism is CARS. The technique is capable of non-invasively monitor lipid concentration and distribution within the cell[42]. This label-free method of monitoring lipid content over time allows for the assessment of lipid metabolism of embryos.

In an effort to avoid exposure of embryos to intense UV light needed for metabolite assays, a reasonable strategy is to physically separate the embryo development with spent medium aspirate analysis into two separate microfluidic devices. One group demonstrated such potential with a fully automated analysis for performing the necessary aliquotting, mixing, data acquisition, and data analysis operations to quantify glucose, pyruvate, and lactate levels[43] (Fig. 1.12).

Another strategy to avoid harmful UV light exposure to developing embryos is to use longer emission and excitation wavelengths of UV light and to spatially segregate optical interrogation from embryo culture. The device was capable of fluid priming, fluid mixing, chemical reaction, fluid washing and injections to analyze glucose metabolism[44] (Fig. 1.13). With integrated embryo culture, this device is capable of performing real-time and continuous culture aspirate measurements for over 6 hours.

Although not yet integrated into microfluidic devices, many powerful broad spectrum analysis techniques have been used to analyze embryo metabolism. Such techniques not only simplify the analysis of multiple metabolites of interest, but also provide the possibility to study metabolites that one would not initially expect to be interesting. They also benefit from high sensitivity in addition to versatility and include nuclear magnetic resonance (NMR), mass spectroscopy (MS), near-infrared spectroscopy (NIR), and regular raman spectroscopy[45].

1.7 Conclusions

One of the most pressing challenges for ART as the trend for SET continues to grow is a method to non-invasively evaluate embryo and gamete quality. This challenge is also compounded by the now accepted realization that morphology, the most conventional method, is a poor indication of quality. Microfluidics has already shown promise to provide alternative methods of quality measurement with strategies tailored to the gamete or embryo analyzed using automation and sensitivity and sometimes combined with sophisticated biophotonic analysis. It is worthy to note that the use of microfluidic devices will not eliminate the need for an embryologist but will enhance outcome and reduce variability. The operation of complex microfluidic processes such as a series of mixing, dilutions, and sorting as well as sophisticated biophotonic techniques require a large amount of supporting equipment. Research effort in embedded microfluidic designs aim to decrease the amount of supporting equipment needed. Future device design should consider usability and adoptability for embryologists. Embryologists would also require additional training to include a change in current procedures to incorporate microfluidic techniques. As microfluidic devices for ART matures, this would be considered as enhanced job training as an ongoing effort to adopt the newest, most effective techniques[46].

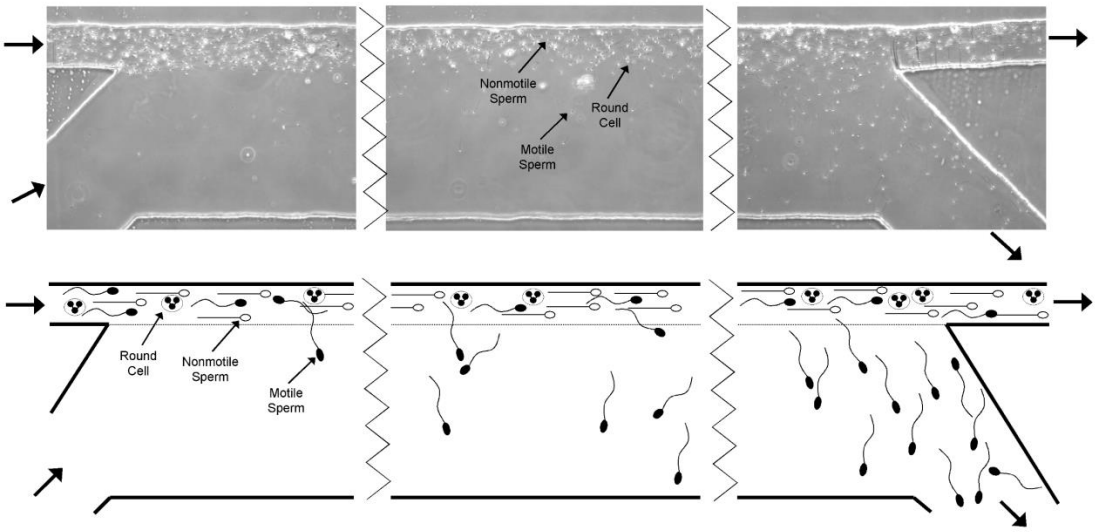

Fig. 1.1 Image captures and illustrations of the movement of sperm sample during sorting. Non-motile and dead sperm will be transported along the laminar streamline from the top left inlet reservoir to the top right channel while motile sperm can move across the streamlines into the collection outlet at the bottom right corner.

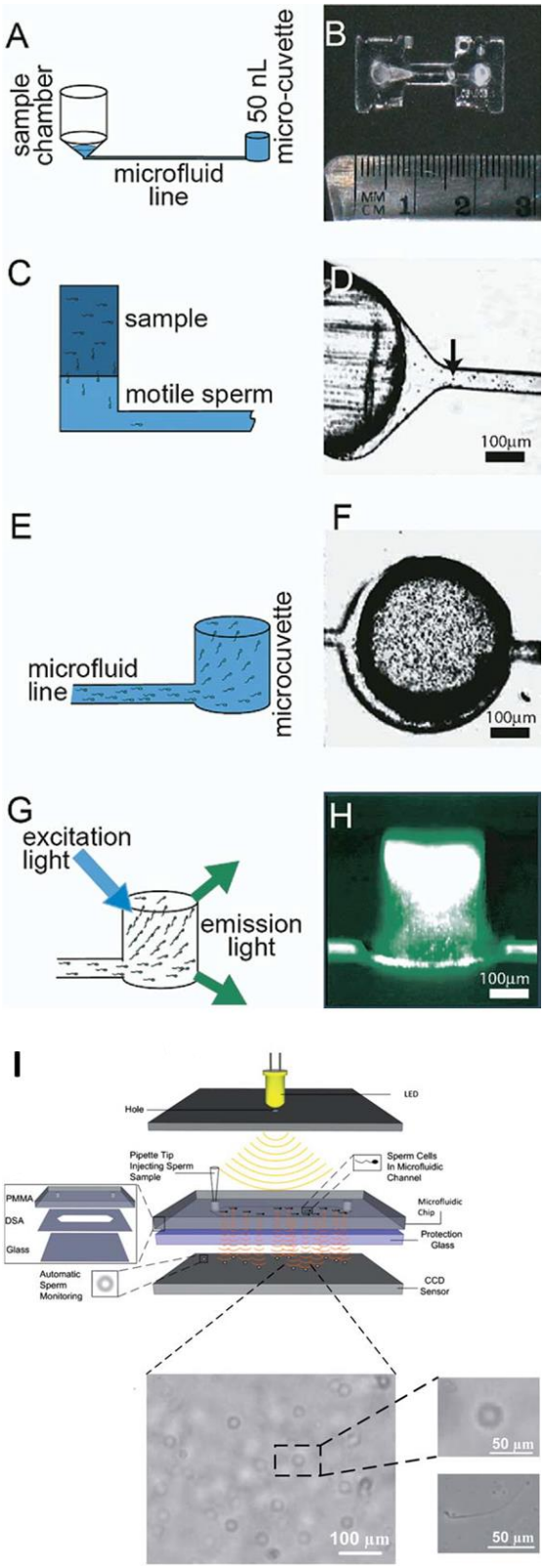

Fig. 1.2 (A-H) Sperm assessment with microfluorometer. (I)Schematic representation of the multi-layer microfluidic chip for simultaneous sperm motility sorting and CCD monitoring.

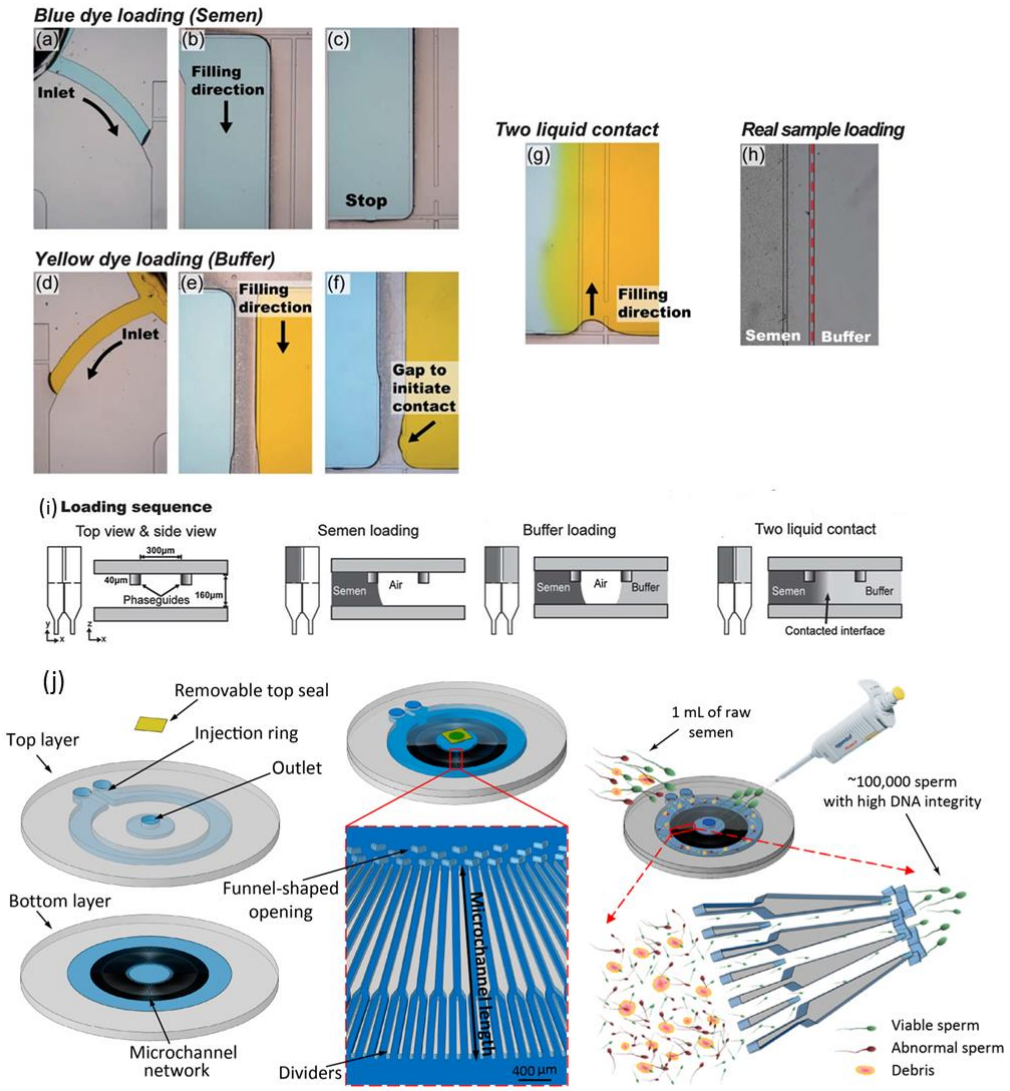

Fig. 1.3 (A-I) Motility sorting based on phase-guide structure. The motile sperm will cross the interface barrier to the buffer zone. (J) Sperm motility selection based on microchannels filled with viscoelastic medium are used to mimic reproductive tracts.

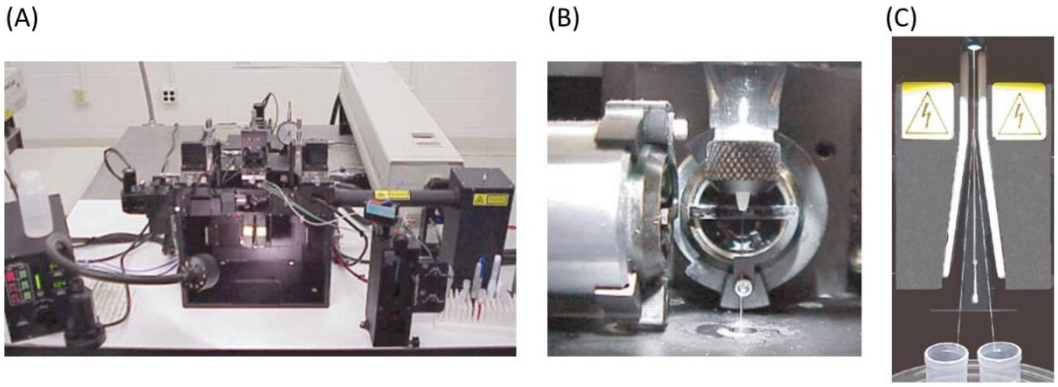

Fig. 1.4 (A) Overview of sperm sorter set up. (B) Fluorescence detector integrated with hydrodynamics system. (C) Droplets containing spermatozoa are sorted to positive or negative charge depending on its sex chromosome.

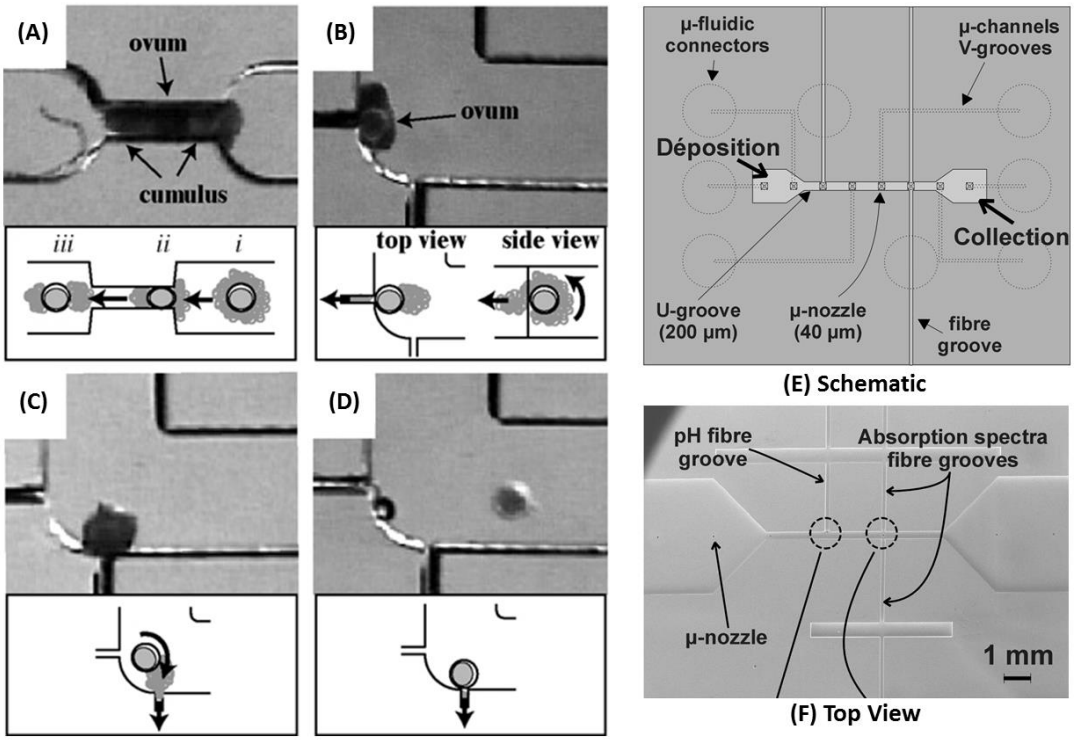

Fig. 1.5 (A-D) Stepwise denuding of zygote. (E-F) Schematic and top view of optical sensor.

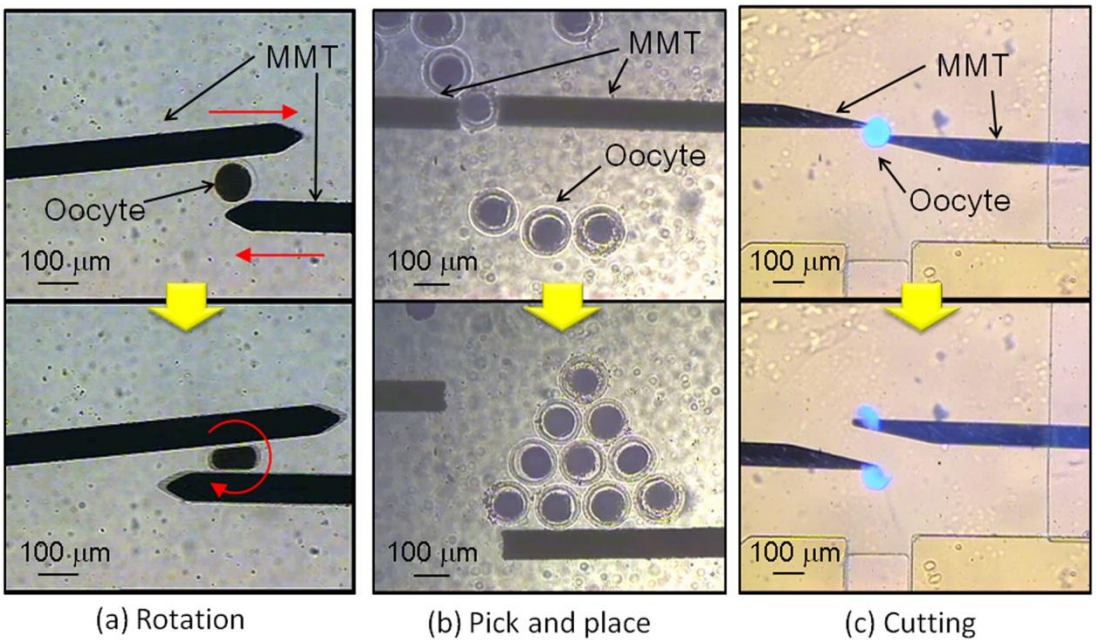

Fig. 1.6 Magnetically driven microtools with ultrasonic vibration for oocytes manipulation in a microfluidic environment.

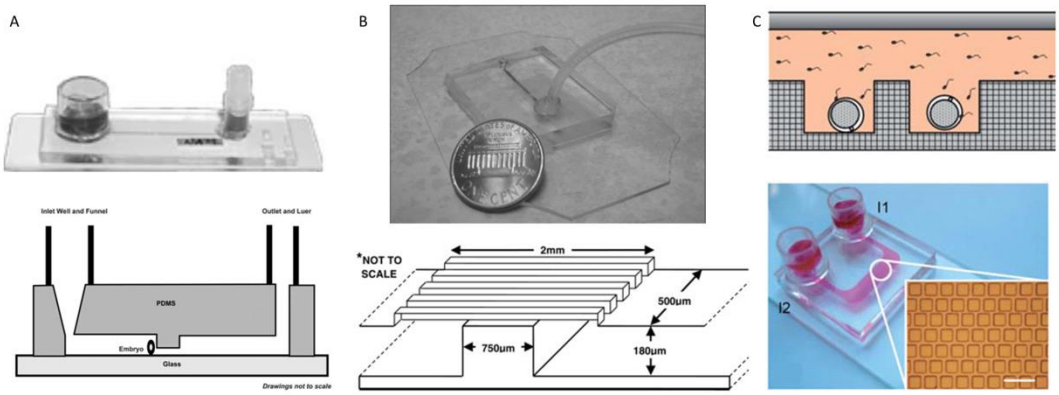

Fig. 1.7 (A) Weir-type trap design for fertilization. (B) Small scale design of microfluidic device promotes the effectiveness of fertilization. (C) Compartmentalized fertilization chambers for multiple embryos.

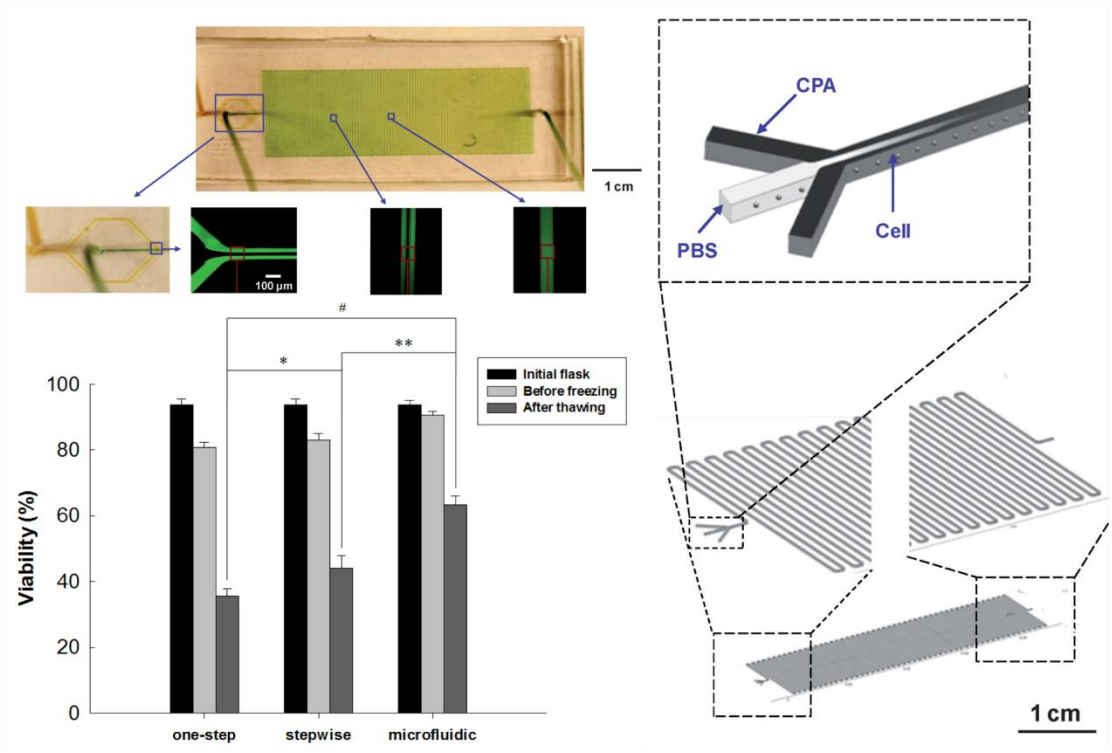

Fig. 1.8 Increased viability is achieved by reducing osmotic shock during cryopreservation process through gradual exposure of CPA concentration to the cells.

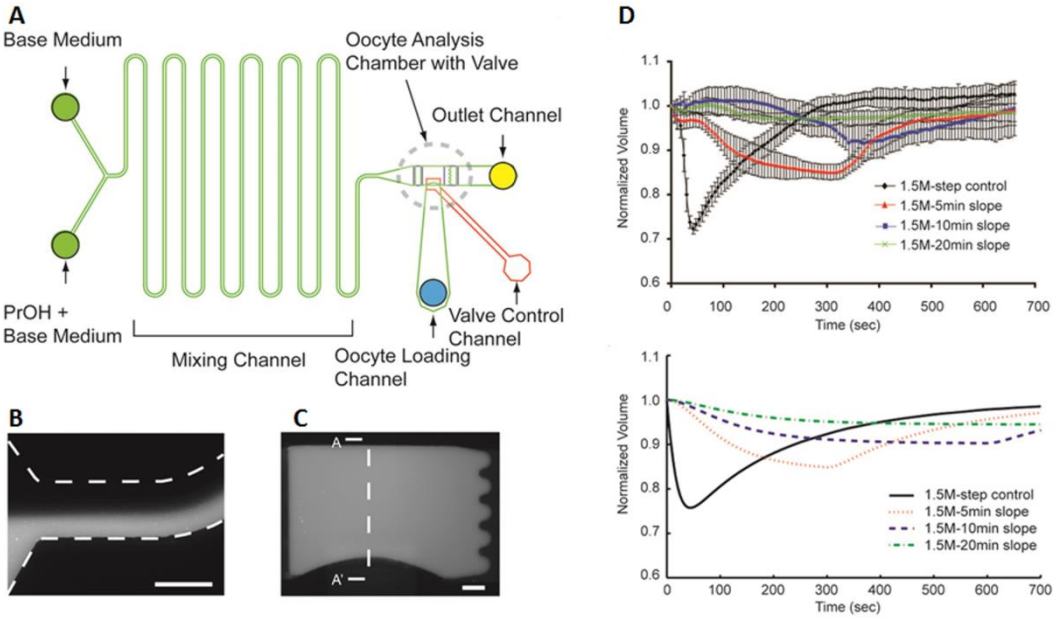

Fig. 1.9 (A)Schematic of microfluidic network. (B) Separation of two streams at the inlet channel. (C) Mixing of streams in the analysis chamber. (D) Volumetric response showed decreasing volume excursion with increasing linear change in CPA.

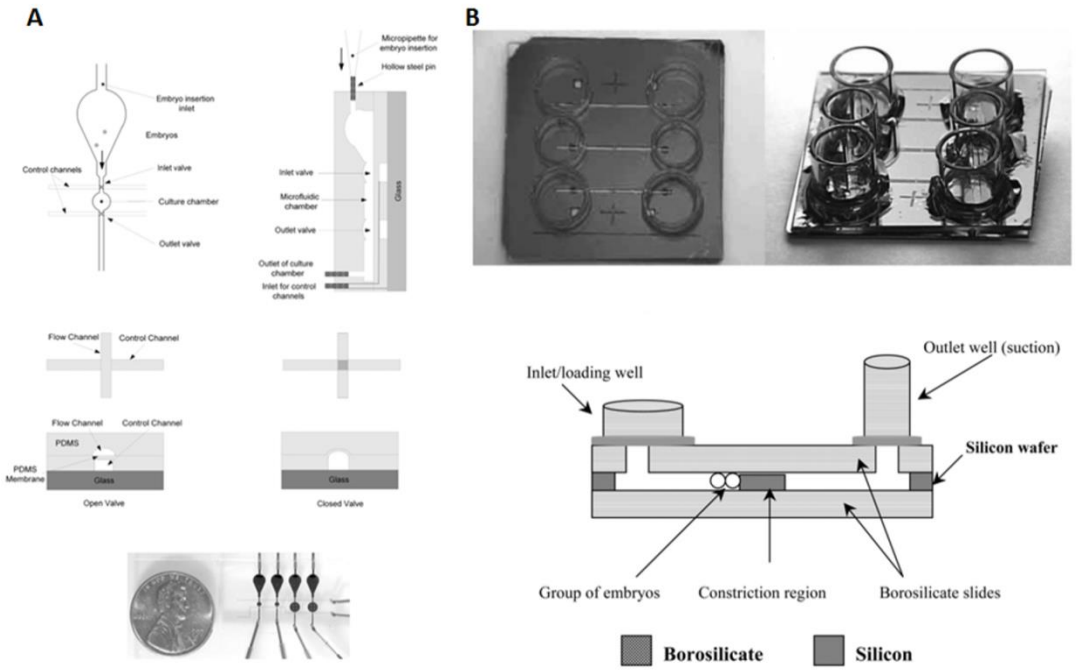

Fig. 1.10 (A) Flow channels design for sub-microliter volume culture. (B) Silicon/borosilicate device for microchannel culture.

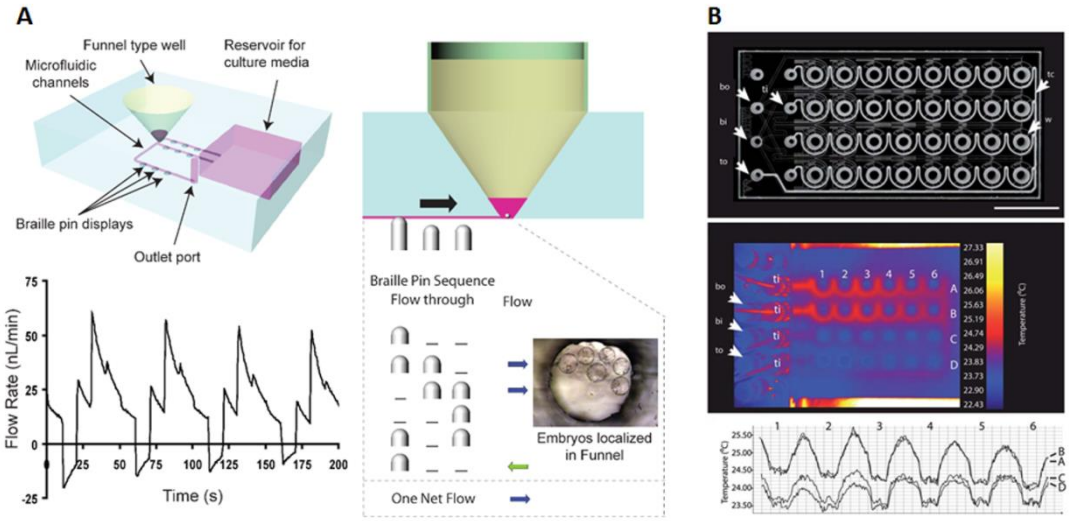

Fig. 1.11 (A) Microfunnel with Braille pin piezoelectric actuators providing dynamic controls to enhance embryo culture. (B) Zebrafish embryo culture to larvae in a continuous buffer flow microchip.

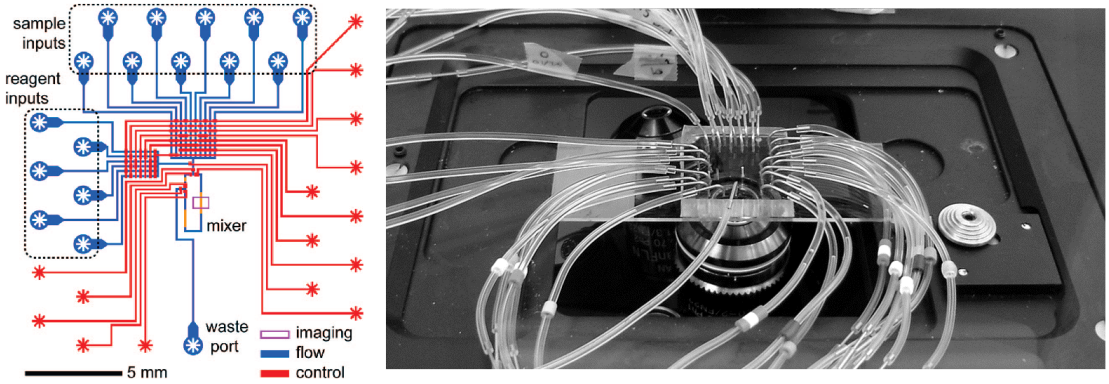

Fig. 1.12 Multilayer design for a fully automated system.

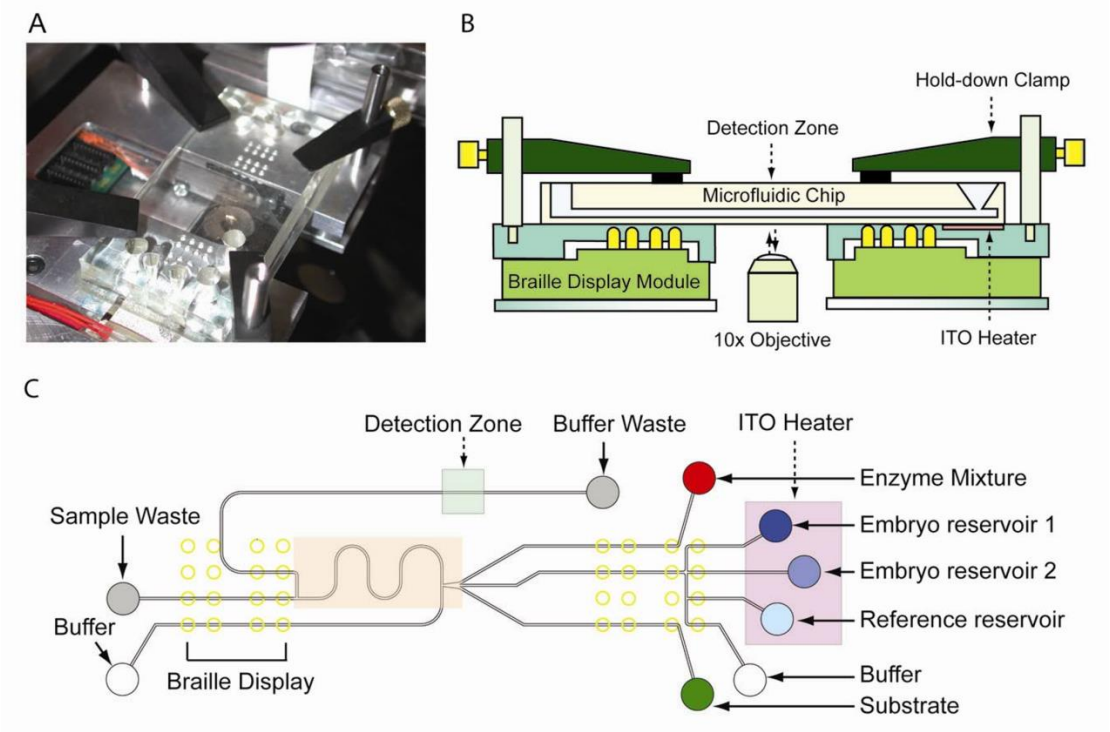

Fig. 1.13 Braille driven microfluidic device for spent media analysis.

1.8 References

1. V. M. Brugh, 3rd and L. I. Lipshultz, *The Medical clinics of North America*, 2004, **88**, 367-385.

2. A. Borini, C. Lagalla, M. Cattoli, E. Sereni, R. Sciajno, C. Flamigni and G. Coticchio, *Reproductive BioMedicine Online*, 2005, **10**, 653-668.

3. S. E. Lewis and R. J. Aitken, *Cell and tissue research*, 2005, **322**, 33-41.

4. B. S. Cho, T. G. Schuster, X. Zhu, D. Chang, G. D. Smith and S. Takayama, *Analytical Chemistry*, 2003, **75**, 1671-1675.

5. M. C. McCormack, S. McCallum and B. Behr, *The Journal of Urology*, 2006, **175**, 2223-2227.

6. D.-b. Seo, Y. Agca, Z. C. Feng and J. K. Critser, *Microfluidics and Nanofluidics*, 2007, **3**, 561-570.

7. X. Zhang, I. Khimji, U. A. Gurkan, H. Safaee, P. N. Catalano, H. O. Keles, E. Kayaalp and U. Demirci, *Lab on a chip*, 2011, **11**, 2535-2540.

8. C. Y. Chen, T. C. Chiang, C. M. Lin, S. S. Lin, D. S. Jong, V. F. Tsai, J. T. Hsieh and A. M. Wo, *The Analyst*, 2013, **138**, 4967-4974.

9. Y. A. Chen, K. C. Chen, V. F. Tsai, Z. W. Huang, J. T. Hsieh and A. M. Wo, *Clinical chemistry*, 2013, **59**, 493-501.

10. R. Nosrati, M. Vollmer, L. Eamer, M. C. San Gabriel, K. Zeidan, A. Zini and D. Sinton, *Lab on a chip*, 2014, **14**, 1142-1150.

11. G. E. Seidel and D. Garner, *Reproduction*, 2002, **124**, 733-743.

12. D. H. Triyoso and T. A. Good, *The Journal of Physiology*, 1999, **515**, 355-365.

13. M. Stacey, J. Stickley, P. Fox, V. Statler, K. Schoenbach, S. J. Beebe and S. Buescher, *Mutation Research/Genetic Toxicology and Environmental Mutagenesis*, 2003, **542**, 65-75.

14. R. Zeggari, B. Wacogne, C. Pieralli, C. Roux and T. Gharbi, *Sensors and Actuators B: Chemical*, 2007, **125**, 664-671.

15. Y. Agca, J. Liu, J. J. Rutledge, E. S. Critser and J. K. Critser, *Molecular Reproduction and Development*, 2000, **55**, 212-219.

16. I. K. Glasgow, H. C. Zeringue, D. J. Beebe, S. J. Choi, J. T. Lyman, N. G. Chan and M. B. Wheeler, *IEEE transactions on bio-medical engineering*, 2001, **48**, 570-578.

17. N. Inomata, T. Mizunuma, Y. Yamanishi and F. Arai, *Journal of Microelectromechanical Systems*, 2011, **20**, 383-388.

18. M. Hagiwara, T. Kawahara, Y. Yamanishi, T. Masuda, L. Feng and F. Arai, *Lab on a chip*, 2011, **11**, 2049-2054.

19. C. Chandsawangbhuwana, L. Z. Shi, Q. Zhu, M. C. Alliegro and M. W. Berns, *Journal of biomedical optics*, 2012, **17**, 015001.

20. S. G. Clark, K. Haubert, D. J. Beebe, C. E. Ferguson and M. B. Wheeler, *Lab on a chip*, 2005, **5**, 1229-1232.

21. R. S. Suh, X. Zhu, N. Phadke, D. A. Ohl, S. Takayama and G. D. Smith, *Human reproduction*, 2006, **21**, 477-483.

22. C. Han, Q. Zhang, R. Ma, L. Xie, T. Qiu, L. Wang, K. Mitchelson, J. Wang, G. Huang, J. Qiao and J. Cheng, *Lab on a chip*, 2010, **10**, 2848-2854.

23. A. Giglio, S. H. Cheong, Q. V. Neri, Z. Rosenwaks and G. D. Palermo, *Fertility and Sterility*, 2013, **100**, S479.

24. A. Trounson and L. Mohr, *Nature*, 1983, **305**, 707-709.

25. M. Kuwayama, G. Vajta, O. Kato and S. P. Leibo, *Reproductive BioMedicine Online*, 2005, **11**, 300-308.

26. Y. S. Song, S. Moon, L. Hulli, S. K. Hasan, E. Kayaalp and U. Demirci, *Lab on a chip*, 2009, **9**, 1874-1881.

27. G. D. Smith, P. C. Serafini, J. Fioravanti, I. Yadid, M. Coslovsky, P. Hassun, J. R. Alegretti and E. L. Motta, *Fertil Steril*, 2010, **94**, 2088-2095.

28. M. Kuwayama, S. Hamano and T. Nagai, *Reproduction*, 1992, **96**, 187-193.

29. T. Otoi, K. Yamamoto, N. Koyama, S. Tachikawa and T. Suzuki, *Cryobiology*, 1998, **37**, 77-85.

30. L. Meng, X. Huezo, B. A. Stone, K. Baek, G. Ringler and R. P. Marrs, *Fertility and Sterility*, 2011, **96**, S207.

31. O. Kedem and A. Katchalsky, *Biochimica et Biophysica Acta*, 1958, **27**, 229-246.

32. Y. S. Heo, H. J. Lee, B. A. Hassell, D. Irimia, T. L. Toth, H. Elmoazzen and M. Toner, *Lab on a chip*, 2011, **11**, 3530-3537.

33. L. L. Kuleshova, D. R. MacFarlane, A. O. Trounson and J. M. Shaw, *Cryobiology*, 1999, **38**, 119-130.

34. D. Lai, J. Ding, G. D. Smith and S. Takayama, *Fertility and Sterility*, 2013, **100**, S107.

35. J. Melin, A. Lee, K. Foygel, D. E. Leong, S. R. Quake and M. W. Yao, *Developmental dynamics : an official publication of the American Association of Anatomists*, 2009, **238**, 950-955.

36. S. Raty, E. M. Walters, J. Davis, H. Zeringue, D. J. Beebe, S. L. Rodriguez-Zas and M. B. Wheeler, *Lab on a chip*, 2004, **4**, 186-190.

37. D. L. Hickman, D. J. Beebe, S. L. Rodriguez-Zas and M. B. Wheeler, *Comp Med*, 2002, **52**, 122-126.

38. Y. S. Heo, L. M. Cabrera, C. L. Bormann, C. T. Shah, S. Takayama and G. D. Smith, *Human reproduction*, 2010, **25**, 613-622.

39. E. M. Wielhouwer, S. Ali, A. Al-Afandi, M. T. Blom, M. B. Riekerink, C. Poelma, J. Westerweel, J. Oonk, E. X. Vrouwe, W. Buesink, H. G. vanMil, J. Chicken, R. van't Oever and M. K. Richardson, *Lab on a chip*, 2011, **11**, 1815-1824.

40. K. I. Wang, Z. Salcic, J. Yeh, J. Akagi, F. Zhu, C. J. Hall, K. E. Crosier, P. S. Crosier and D. Wlodkowic, *Biosensors & bioelectronics*, 2013, **48**, 188-196.

41. J. K. Valley, P. Swinton, W. J. Boscardin, T. F. Lue, P. F. Rinaudo, M. C. Wu and M. M. Garcia, *PloS one*, 2010, **5**, e10160.

42. A. Enejder, C. Brackmann and F. Svedberg, *IEEE Journal of Selected Topics in Quantum Electronics*, 2010, **16**, 506-515.

43. J. P. Urbanski, M. T. Johnson, D. D. Craig, D. L. Potter, D. K. Gardner and T. Thorsen, *Anal Chem*, 2008, **80**, 6500-6507.

44. Y. S. Heo, L. M. Cabrera, C. L. Bormann, G. D. Smith and S. Takayama, *Lab on a chip*, 2012, **12**, 2240-2246.

45. D. Lai, G. D. Smith and S. Takayama, *Journal of biophotonics*, 2012.

46. J. E. Swain, D. Lai, S. Takayama and G. D. Smith, *Lab on a chip*, 2013, **13**, 1213-1224.

Chapter 2

Microfluidic Reduction of Osmotic Stress in Oocyte and Zygote Vitrification

Microfluidic cryoprotectant exchange enables vitrification of murine zygotes with superior morphology as indicated by a smoother cell surface and higher developmental competence compared to conventional methods. Bovine oocyte vitrification also benefit as evidenced by higher lipid retention. Experimental observations and mathematical analysis demonstrate that the microfluidic advantage arise predominantly from eliminating high shrinkage rates associated with abrupt and uneven exposure to vitrification solutions that readily occur in current manual protocols. The microfluidic cryoprotectant exchange method described has immediate applications for improving animal and human oocyte, zygote, and embryo cryopreservation. On a fundamental level, the clear demonstration that at the same minimum cell volume, cell shrinkage rate affects sub-lethal damage should be broadly useful for cryobiology.

2.1 Introduction

The successful cryopreservation of embryos and oocytes has significantly expanded the scope of infertility treatment[1,2]. A major concern in cryobiology is the osmotic stress that cells experience as their water content is exchanged with cryoprotectant

agents (CPA) to eliminate formation of damaging intracellular ice crystals. While immediately lethal osmotic stress has largely been overcome, sub-lethal effects still remain and affect overall embryo development and treatment outcomes. This concern is particularly high for the fast cooling protocol called vitrification where the CPA used have high osmolality and non-cell permeable components[3]. Compared to mammalian cells with diameters on the order of 10 micrometers, oocytes and zygotes with diameters on the order of 100 micrometers have ~1000 times larger volume of water that needs to be replaced with CPAs. However, the cell surface area does not increase proportionally making the required water-CPA exchange through the cell membrane difficult and the cell highly susceptible to osmotic stress. Early studies on osmotic stress suggested the existence of a threshold minimum cell volume where shrinkage becomes sufficient to cause lethal damage to cell membrane integrity[4]. This theory formed the basis of many prominent osmotic stress studies investigating the threshold minimum cell volume in different cell types[5,6]. In an attempt to reduce osmotic stress, one common method for oocyte and zygote vitrification involves a 3-step equilibration process where the cells are manually pipetted into subsequently higher levels of CPA concentrations to avoid sudden changes of osmolality[7], allowing the cell to shrink in stages, and sometimes to re-expand, to avoid the critical minimum cell volume.

In species with oocytes, zygotes, and embryos that are difficult to cryopreserve, it has been shown that higher number of equilibration steps increases the rate of cryosurvival[8] and developmental competence[9]. However despite improved outcome, protocols with high number of equilibration steps have not been clinically adopted due to their impracticality. The Demirci group has developed a microfluidic device

for slow-rate freezing[10] and recently, the Toner group pioneered the use of microfluidic CPA exchange to overcome limitations of manual pipetting[11]. They demonstrated precise control of fluid exchange to maintain a large cell volume during CPA exchange. However, the study did not incorporate impermeable solutes highly recommended for cryopreservation[12] nor was the device designed for cell removal after CPA exchange to allow actual vitrification. Consequently, while the oocyte was maintained at large volumes, it is not clear whether the protocol could produce developmentally competent cells after vitrification and warming.

Early studies of osmotic stress focused primarily on minimum cell volume particularly because cryosurvival was a major concern in cryobiology and the minimum cell volume was experimentally easy to observe. Currently, the issues of cryosurvival have largely been overcome and the field is focusing efforts on increasing developmental competence in order to increase the effectiveness of single embryo transfers (SETs) to exponentially decrease chances of unintended multiple births while still achieving live births. The current methods of CPA mixing are incapable of separating the minimum cell volume effects from the shrinkage rate. It also suffers from poor mixing efficiency as well as a lack of controllability and consistency. Although previous studies using these manual pipetting techniques demonstrated that the minimum cell volume is lethal, the effects of shrinkage rate (which increase as minimum cell volume decreases) is unknown. Here we report a novel microfluidic device that overcomes these challenges. Using this device we provide an evaluation of the impact of microfluidic CPA exchange procedures on cryosurvival, cell health as evaluated by lipid content, and developmental competence. Because of the highly controlled nature of this microfluidic CPA exchange procedure,

we were able to distinguish effects of cell shrinkage rate independent of minimum cell volume. Our results demonstrate for the first time that for a constant minimum cell volume and CPA exposure time, minimizing the cell shrinkage rate leads to improved outcomes.

2.2 Materials and Methods

Kedem-Katchalsky Modeling. The device was designed to minimize osmotic stress by Kedem-Katchalsky equations using MatLAB (MathWorks, Natick, MA). The osmolarity contributions of each CPA component in the VS is assumed to be additive. L_p is $8.94*10^{-7}$ cm/sec/atm, ω_{DMSO} is $2.54*10^{-5}$ cm/sec, ω_{EG} is $1.0*10^{-5}$ cm/sec. t_f is the user-defined time duration of CPA exchange, and n is the step number of computer analysis. The solvent/solute interaction, σ did not have a dramatic effect on model. The ideal shrinkage regime will have the most gradual and a constant shrinkage rate, thus the deviation $\gamma = 0$. Using an n of 820 000 to facilitate faster computation, the deviation γ of each shrinkage regime was calculated and compared with the ideal $\gamma = 0$.

Device design and fabrication. Microfluidic devices were made using conventional photolithography and soft lithography using polydimethylsiloxane (PDMS) (Dow Corning, Midland, MI). The device consists of two layers: The microfluidic channel layer (150 μm) that houses the oocytes/zygotes as well as delivers the CPA solutions and the holding pipette layer (20 μm) that provides the vacuum for the oocytes/zygotes to remain stationary under constant volumetric flow rate but changing CPA concentrations and associated viscosity and fluid density.

The device was designed with a serpentine mixing channel, an oocyte/zygote exposure chamber and a set of height-differential (10 cm) powered suction microchannels. The loading and withdrawal of oocytes or zygotes from the device was achieved through a port drilled by a 200 µm microdrill bit (Kyocera, Kyoto, Japan) into a glass slide (Fisher Scientific, Waltham, MA) on which the PDMS is bonded to provide laminar flow in and out of the device. This combined with control of vacuum created an effective method of retrieval with no edges or corners for oocytes / zygotes to be trapped within the device.

Fluorescence quenching and fluorescence microscopy. Fluorescence quenching mixing characterization was achieved using VS supplemented with 20 µM fluorescein (Sigma-Aldrich, St. Louis, MO) mixed with culture media with 2 M potassium iodide (KI, Sigma-Aldrich, St. Louis, MO). Both solutions were flowed into the microfluidic device at 350 µL / hr. As the two solutions mix, the binding of iodide with fluorescence shifts the excitation spectrum to decrease captured fluorescence signal from fluorescence microscopy. For normalization, the channels were filled with 1) premixed equal volumes of VS supplemented with fluorescein and culture media supplemented with potassium iodide, 2) just VS supplemented with fluorescein, and 3) VS supplemented with fluorescein premixed at equal volumes with culture media without potassium iodide.

Regular fluorescence microscopy was used to characterize the increasing CPA concentrations over time. The VS solution was supplemented with 20 µM fluorescein and the culture media had no potassium iodide. The VS syringe pump operated from 0 to 700 µL / hr while the culture media syringe pump operated from 700 to 0 µL / hr. After serpentine channel mixing, the fluorescence signal contributed by the VS

solution as it increases is proportional to the CPA concentration for that mixed solution in time.

Oocyte / zygote loading, trapping, and withdrawal. Loading of oocyte / zygotes through the loading/withdrawal port is achieved by activation of the suction channel powered by a negative height differential (~10 cm) in the absence of syringe pump flow. The activation and deactivation of the suction channel is operated by a 3-way valve at the end of the height differential. The exposure chamber contains 15 holding microchannels where up to 15 oocytes/zygotes are immobilized via the continued activation of the suction port. The cells are released out of the device through the loading / withdrawal port by the termination of suction port in the presence of syringe pump flow.

Automated and manual vitrification. Automated vitrification was achieved by two programmable syringe pumps (Chemyx, Stafford, TX) capable of providing linear gradients. The vitrification solution syringe pump was programmed to provide a linearly increasing flow rate from 0 to 700 µL / hr in 10 minutes. The culture media syringe pump was programmed to provide a linearly decreasing flow rate from 700 to 0 µL / hr in 10 minutes. After mixture by serpentine channel, the solution of constantly flow rate ~700 µL / hr but changing CPA concentrations from culture media to vitrification solution conditions is delivered to the exposure chamber to exposure cells. During operation, the spent fluid escapes via the loading / withdrawal port as well as the suction port. The media that escapes from the loading / withdrawal port is discarded.

Manual vitrification for MII oocytes and zygotes were performed by fully trained individuals using a previously described technique[22] with slight modification.

Mouse or bovine MII oocytes were transferred to 20 μL washing solution drop for 1 min and then merged with two 20 μL equilibration solution drops sequentially for 2 min each merging, then oocytes were transferred to equilibration solution for 2-3 min. After equilibration, oocytes were transferred through three 20 μL vitrification solution drops for 5 sec, 5 sec and 10 sec, and then stayed in the fourth drop of vitrification solution until cryopreservation. High Security Vitrification (HSV) straws (CryoBio Systems, L'Aigle, France) were used for loading oocytes and the loaded straws were plunged into liquid nitrogen within a 90 second interval. Mouse zygotes vitrification procedures were similar as those for oocytes, except longer incubation (8 min) in equilibration solution.

Oocyte and zygote harvest. All procedures described within were reviewed and approved by The University Committee on Use and Care of Animals at the University of Michigan and were performed in accordance with the Guiding Principles for the Care and Use of Laboratory Animals.

Bovine ovaries were obtained from a local abattoir at random stages of the estrous cycle or pregnancy and transported to the laboratory in warmed PBS containing antibiotics. Cumulus-oocyte complexes were aspirated from follicles of 2-6 mm diameter and matured for 24h in M199 medium (Sigma-Aldrich, St. Louis, MO) at 39°C in 5% CO_2, 5%O_2, 90% N_2. Mature oocytes were then denuded of cumulus cells before use.

Meiotically competent germinal vesicle intact (GVI) oocytes were collected from antral follicles of 21-23d old CF-1 female (Harlan, Indianapolis, IN) ovaries 44-46h after 5 IU equine chorionic gonadotropin (eCG, Sigma-Aldrich, St. Louis, MO) stimulation. Denuded GVI oocytes were triple washed in HTFH (human tubal fluid-

HEPES, Irvine Scientific, Santa Ana, CA) /0.3% BSA and cultured in HTF/0.3% BSA at 37ºC in 5% CO_2 incubator for 18h to obtain MII oocytes.

To collect zygotes female B6C3F1 mice at 6 to 8 weeks old were injected with 5 IU equine chorionic gonadotropin (eCG, Sigma-Aldrich, St. Louis, MO). Forty-eight h later mice were injected with 5 IU human chronically gonadotropin (hCG, Sigma-Aldrich, St. Louis, MO). Upon hCG injection, female mice were placed with mature B6C3F1 males of known fertility until sacrificed 18h later. Zygotes were released from the ampulla, denuded in human tubal fluid-HEPES (HTFH, Irvine Scientific, Santa Ana, CA) / 0.1% Hyaluronidase, triple washed in HTFH / 0.3% BSA and placed in pre-equilibrated potassium simplex optimized medium (KSOM) + amino acids (AA) (Millipore, Billerica, MA) at 37ºC in 5% CO_2 incubator until use.

Phase contrast microscopy, roughness index, and sphericity. Zygotes were analyzed at 400x magnification for phase contrast microscopy. The RI was quantified as standard deviation of the grey values within the region of interest (ROI). The ROI was defined as the middle 50% of cell surface so that edge effects are nullified. The zygotes were oriented such that the polar bodies do not visually obstruct the center of the zygote. Zygotes exposed to CPA by automated or manual pipetting protocols were stained by Hoechst 33342 at 5µg /ml for 10 min but unwashed to retain cytoplasmic staining. The Hoechst stained zygotes used were analyzed using confocal microscopy. The volume and surface area were then quantified using ImageJ to calculate sphericity.

Warming, embryo culture, and developmental competence analysis. Murine oocyte and zygote warming were performed by fully trained individuals using a previously described technique[22]. Murine zygotes, either NVE or vitrified and warmed were transferred to 50µl pre-equilibrated KSOM+AA microdrops under oil

and cultured at 37ºC in 5% CO_2, 5% O_2, 90% N_2 gaseous conditions. Embryo morphologies in each experimental group were assessed at 96h of culture for blastocyst development using an inverted microscope (200x; Leica DM2RB, Wetzlar, Germany).

Cytoplasmic lipid content. Bovine oocytes in control, automated and manually vitrified groups were fixed on Poly-L-Lysine coated coverslips separately overnight using 2% paraformaldehyde. Fixed oocyte samples were triple washed with 1xPBS the next day, stained with 100 nM Nile Red (Sigma-Aldrich, St. Louis, MO) for 20 min at room temperature, then washed one time with 1xPBS and stained with Hoechst 33342 (5µg /ml) for 10 min. After Hoechst staining, oocyte samples were triple washed with 1xPBS and mounted in 90% Glycerol with anti-fading reagent. Lipid contents in bovine oocytes were visualized under confocal microscopy and were quantified with ImageJ.

Developmental competence analysis. To count the total number of cells (blastomeres) in blastocysts derived following no treatment (control) or automated and manually vitrified and warming; blastocysts were placed on Poly-L-Lysine coated coverslips and fixed overnight with 2% paraformaldehyde. Fixed blastocyst samples were triple washed in 1xPBS the next day, stained with Hoechst 33342 (5 µg/ml) for 10 min, triple washed with 1xPBS, and then mounted in 90% Glycerol with anti-fading reagent. Blastomere numbers were counted under fluorescent microscopy (400x) by two individuals, both blinded to knowledge of treatment, and reported values were averages of counts.

2.3 Results and Discussion

Kedem-Katchalsky Modeling. A cell's volumetric change in response to a defined input of CPA concentrations can be accurately modeled[13–15]. Kedem-Katchalsky equations (Eq 1-2) typically use step-wise input functions of CPA concentrations as this is the experimental limitation of manual pipetting. However with the use of microfluidics, we expand the experimental possibilities to include continuous temporal gradients of CPA concentrations using ethylene glycol (EG), dimethyl sulfoxide (DMSO), and sucrose. We note that although a related mathematical analysis was performed by Heo and colleagues, they did not consider the inclusion of impermeable CPAs, such as sucrose, in the vitrification solution (VS) as is highly recommended for practical cryopreservation[12] and necessary to control shrinkage rate independently of minimum cell volume (Fig. 2.1A).

Eq 1:

$$J_v = -L_p RT(\Delta C_i + \sigma \Delta C_s)$$

Eq 2:

$$J_s = \omega RT \Delta C_s + J_v(1-\sigma)\overline{C_s}$$

How ideal a CPA exchange protocol is in terms of avoiding abrupt cell shrinkage can be mathematically appreciated as the deviation (%volume / sec) of the shrinkage (%volume / sec) (Eq 3) over time. Where f(t) is the function of cell volume shrinkage over time (Eq 4). The ideal shrinkage regime would have constant cell

shrinkage over time, and thus the deviation $\gamma = 0$ % volume / sec. Such a rate will allow the shrinkage rate to be minimized while still transitioning the cell to its minimum cell volume by the end of the user-defined duration. The direct exposure had the fastest maximal shrinkage rate of 7.51 % volume / sec. Manual-pipetting caused a large deviation, $\gamma = 0.19$ % volume / sec where the zygote is at times shrinking quickly while other times static and sudden introduction of CPA from manual-pipetting also produced a fast maximal shrinkage rate of 4.13 % volume / sec. Auto-microfluidics reduces the shrinkage regime deviation, $\gamma = 0.09$ % volume / sec and prevents instances of quick cell shrinkage by eliminating sudden changes in osmolality producing maximum shrinkage rates of only 0.35 % volume / sec.

Eq 3:

$$\lim_{n\to\infty} \gamma = \sqrt{\frac{1}{n-1}\sum_{i=0}^{n}\left(f(\frac{i * t_f}{n}) - \frac{1}{t_f}\int_0^{t_f} f(t)dt\right)^2}$$

Eq 4:

$$f(t) = \frac{dv}{dt}$$

Zygote vitrification affecting morphology and cryosurvival. Fresh murine zygotes (Fig. 2.1C,H) were subjected to defined CPA exposure regimes (Fig. 2.1D-G). The direct exposure (Fig. 2.1G,L) represents a transfer of zygotes directly from culture media to VS, a protocol known to be detrimental to cryosurvival (59.6 ± 3.2%, n=40).

Manual-pipetting (Fig. 2.1D,I) and auto-microfluidic (Fig. 2.1E,J) fluid exchange both had high cryosurvival (100 ± 0%, n=200 and 100 ± 0%, n=224) and experimental cell shrinkage agreed with models (Fig. 2.1B). Despite no significant difference between manual-pipetting and auto-microfluidic CPA exposure on cryosurvival, high magnification reveal significant morphological improvement with a more uniform and gradual shrinkage rate (Fig. 2.1I,J). Confocal images further demonstrate distinct morphological differences between manual-pipetting and auto-microfluidic CPA exchange. Additional morphological studies (Fig. 2.1F,K) demonstrate the importance of applying sucrose, the impermeable component of the vitrification solution gradually for a smooth cell surface and simulated direct VS exposures by microfluidics (Fig. 2.1G,L) demonstrate the importance of avoiding abrupt CPA exposures to avoiding the large crater-like deformations on the cell membrane that are sometimes visible in manual-pipetting protocols (Fig. 2.1I) where cell water volume may escape unevenly due to high gradient of CPA concentrations preferentially on one side of the cell.

Zygote surface smoothness can be assessed while in vitrification solution under 400X magnification and phase contrast microscopy. Rough surfaces cast dark and light areas on the cell surface under phase contrast. The roughness index (RI) can then be quantified as the standard deviation of the grey value of the cell. Zygotes exposed to automated microfluidic CPA exposure (Fig. 2.1E,J; RI=23.50, standard error (StdErr)=0.11, n=27) are significantly ($p<0.001$) smoother than its manual pipetting analogue (Fig. 2.1D,I; RI=33.72, StdErr=0.09, n=26) (Fig. 2.2A) . Abrupt sucrose also had rough surfaces statistically comparable to manual pipetting which also consists of an abrupt exposure to sucrose (RI=34.32, StdErr=0.23, n=20). Direct

exposure curiously had smooth surfaces despite an abrupt exposure to all CPAs: EG, DMSO, and sucrose (RI=25.08, StdErr=0.30, n=20). Non-Vitrified or CPA Exposed (NVE) zygotes, alternatively referred to as fresh zygotes, had visual occlusions that cast dark regions in phase microscopy due to significant differences in refractive indexes within its cytoplasmic content. The lack of EG and DMSO, which have an added benefit of homogenizing refractive indexes of cytoplasmic content, prevented the direct comparison of NVE zygotes to other experimental groups. This roughness index is non-invasive and can be instantly quantified with real-time monitoring within the microfluidic device.

Zygote sphericity is calculated by measuring the cell surface area and volume by confocal microscopy. Zygotes exposed to CPA by automated microfluidics (Fig. 2.1E,J) has significantly ($p<0.001$) more spherical morphology than zygotes exposed to CPA by manual pipetting (Fig. 2.1D,I). Abrupt sucrose, which consists of an abrupt exposure sucrose, causes rough cell surfaces and some deformations in cell shape that negatively affects sphericity (sphericity = 0.780, StdErr = 0.002, n=16). CPA Manual pipetting, which also consists of an abrupt exposure to sucrose, causes ripples and deformations in cell shape (sphericity = 0.790, StdErr = 0.001, n=24) that is statistically comparable to the abrupt sucrose group. Automated microfluidic CPA exposure retains a smooth cell surface and a lack of deformations to cell shape that allows the cell to retain its spherical morphology (sphericity = 0.956, StdErr = 0.001, n = 27; Fig. 2.2B) that is statistically similar to the sphericity of NVE zygotes (sphericity = 0.965, StdErr = 0.001 , n= 20). Direct exposure causes large deformations in cell shape that, despite its smooth surface, have the largest impact on sphericity (sphericity = 0.586, StdErr = 0.004, n = 18).

Microfluidic device design. Continuous temporal gradient of CPA concentrations is realized by two synchronized programmable syringe pumps connected to the inlets of the microfluidic device with geometry-mediated CPA mixing and exposure embedded into device design (Fig. 2.3A). Immobilized by holding microchannels within the exposure chamber, the microfluidic device allows for real-time monitoring by microscopy (Fig. 2.3B). The loading/withdrawal port is a microdrilled hole within the glass substrate that is aligned to the end of the PDMS channel. It loads cells when the suction is activated in the absence of syringe flow and a cell withdrawal port when the suction is deactivated in the presence of syringe flow. The suction microchannels (20 μm by 20 μm) were powered by a negative height differential and is activated / deactivated by a 3-way valve. Abnormal deformation in the zona pellucida was observed at ~18 cm. As such, a height differential of ~10 cm was used and the flow velocity was adjusted such that the cells would remain trapped during syringe flow. The small size of the cell loading / withdrawal port (~200 μm diameter) allow for laminar flow as well as the absence of the weir-type geometries or dead space at the outlet that may trap the cell within the device. We demonstrate the reliability and versatility of the automated microfluidic device by vitrifying 474 murine or bovine oocytes and zygotes with 100 % recovery as well as the capability of vitrifying up to 15 oocytes/zygotes simultaneously.

Increased bovine cytoplasmic lipid retention. Bovine oocyte from the manual-pipetting and auto-microfluidic methods were studied to demonstrate the biological advantages of lowering shrinkage rate. Confocal images of bovine oocytes with Nile Red staining were normalized to NVE oocytes at 100 ± 0.01 % (mean ± StdErr; n = 17) lipid content to characterize post-warming cytoplasmic lipid retention. Vitrified

oocytes using manual-pipetting CPA exposure have significantly lower cytoplasmic lipid retention 51.8 ± 0.01% (n = 18) than bovine oocytes vitrified using auto-microfluidic CPA exposure 76.6 ± 0.02 % (n = 17; $p < 0.01$; Fig. 2.4A).

Increased developmental competence. To demonstrate the effects of sub-lethal damage from shrinkage rate on embryo developmental competence, we assessed number of blastomeres per blastocyst after 96h culture of NVE murine zygotes as control with zygotes vitrified with manual-pipetting and auto-microfluidic CPA exchange. NVE zygotes have 109 ± 4 blastomeres (n = 46) after 96h embryo development. Both vitrification methods caused sub-lethal damage that significantly reduced blastomeres per blastocyst verses controls. Furthermore, the vitrification method with the faster shrinkage rate (manual-pipetting) resulted in significantly less blastomeres per blastocyst (89 ± 3 blastomeres, n = 35) compared to the method with reduced shrinkage rate (auto-microfluidic; 98 ± 3 blastomeres, n = 46, $p < 0.05$). Thus, sub-lethal damage was significantly decreased using vitrification by auto-microfluidic CPA exposure which preserved zygotes with higher developmental competence compared to its manual-pipetting analogue (Fig. 2.4B).

For the rapid cooling cryopreservation method of vitrification, the pre-cooling CPA exchange protocol plays a critical role in the overall outcome. The challenge is that there are multiple conflicting needs that must be met. Introducing sufficient amount of CPA into the cell is critical to avoid ice formation. On the other hand, it is also important to avoid excess CPA exposure time and concentrations as the chemicals are inherently toxic to cells. This confounding factor gives rise to the desire to decrease the time spent to reduce toxicity effects which directly conflicts with the desire to increase time spent to reduce osmotic stress. What all the specific

mechanisms are that contribute to osmotic stress is however still unclear. One of the most prevalent theories of osmotic stress is that there is a minimum cell volume below which a cell will become lethally damaged. This was achieved in early studies of osmotic stress primarily because lethality and minimum cell volume are experimentally simple to quantify. However there could be other factors contributing to osmotic stress and as the field of reproductive sciences focus on increasing the efficiency of single embryo transfers, the focus has changed from lethality or cryosurvival to cell health and developmental competence. Impressive and painstaking work by Kuwayama and coworkers and Otoi and colleagues that utilized multiple pipetting steps suggests that a gradual exchange of CPA is important[8,9]. These and other previous studies on the role of CPA-induced cell damage were unable to distinguish osmotic stress caused by rapid shrinkage rates independently and in a well-controlled manner from that caused by the cells reaching a certain minimum volume. Here, we demonstrate using both mathematical modelling and experimental validation that shrinkage rate can be independently controlled while keeping the minimum cell volume reached the same. Furthermore, we show that maintaining a low shrinkage rate throughout the CPA exchange procedure is critical for reducing sub-lethal cell damage. These experiments are enabled by precise control of cell CPA exposure using microfluidic cell immobilization, microfluidic-enabled continuous gradual increase of CPA concentrations, and the use of impermeable solutes as a key component in VS.

More specifically, the oocytes or zygotes are trapped within the exposure chamber by weir-type holding microchannels powered by a negative height differential for suction (Fig. 2.3B). The loading / withdrawal port is a simple but

effective 200 μm diameter hole. Immobilized oocytes or zygotes within the microfluidic exposure chamber enabled real-time and high magnification imaging that is often lost during manual pipetting as stereoscopes are often used for their wide field of view but low magnification. Mixing of CPA within the microfluidic device is achieved by conventional serpentine channel geometries (Fig. 2.3C) to provide linearly increasing concentrations of CPA (Fig. 2.3D) to the cell exposure chamber. Using this system, we controlled minimum cell volume to be identical for all experimental groups while varying the maximal shrinkage rate and shrinkage profile.

One challenge for comparing CPA exchange protocols and their sub-lethal effects is the readout. Unlike lethal damage, the differences are more subtle. With improved vitrification protocols that now largely avoid lethal damage; the use of vitrification is become widespread. Measurement and improvement of sub-lethal damage associated with vitrification is thus timely and critical. We analyzed qualitative differences in cell morphology (Fig. 2.1H-J, Fig. 2.2) that demonstrate significant differences in morphology despite no difference in cryosurvival: a now clearly insufficient readout in cryopreservation of gametes and embryos. Interestingly, the amount of osmotic stress from shrinkage rate had a direct relationship with its impact on sphericity. To address the readout challenge, we quantified developmental competence by cryopreserving murine zygotes and comparing cell numbers of blastocysts (Fig. 2.4B). We additionally quantified cytoplasmic lipid retention of bovine zygotes (Fig. 2.4A). Cytoplasmic lipid content is a major energy source, inversely related to sub-lethal cell damage, and a contributor to developmental competence[16–19]. There are reports that lipid content can be predictive of future developmental success[20]. The significant difference in post-warm cytoplasmic lipid

between auto and manual exposure groups is evidence that the shrinkage rate and its effect on morphology is more energetically costly to the zygote, although the exact mechanism of energetic cost is yet unknown. All measures show that the microfluidic gradual CPA exchange protocol that minimized cell shrinkage rate is superior.

2.4 Conclusions

In addition to the fundamental insights obtained, the automated microfluidic CPA exchange method developed has important practical implications. The variability with manual pipetting in terms of pipetting volume error as well as pipetting rigor and its associated convective forces make the commonly-used protocols difficult to reproduce exactly even within a single operator. This operator variability can be a source of dramatically different cryosurvival rates reported in the past[21]. Such variability makes standardization and the identification of the most optimized vitrification method and vitrification solution difficult within the field of cryobiology. The automated microfluidic system provides unprecedented accuracy and precision in fluid control and is a suitable tool that eliminates operator variability in the discovery and use of new CPA formulation and procedures in the continuous development of cryopreservation technology. In this regard it is important to note that the microfluidic cell introduction and recovery rate for 474 oocytes and zygotes has been 100%. Beyond direct applicability of the described protocols to enhance oocyte and zygote vitrification, we anticipate the new mechanistic insights that complement and add to the minimum cell volume theory to be generally helpful in guiding future improvements in cell, organoid, and tissue cryopreservation.

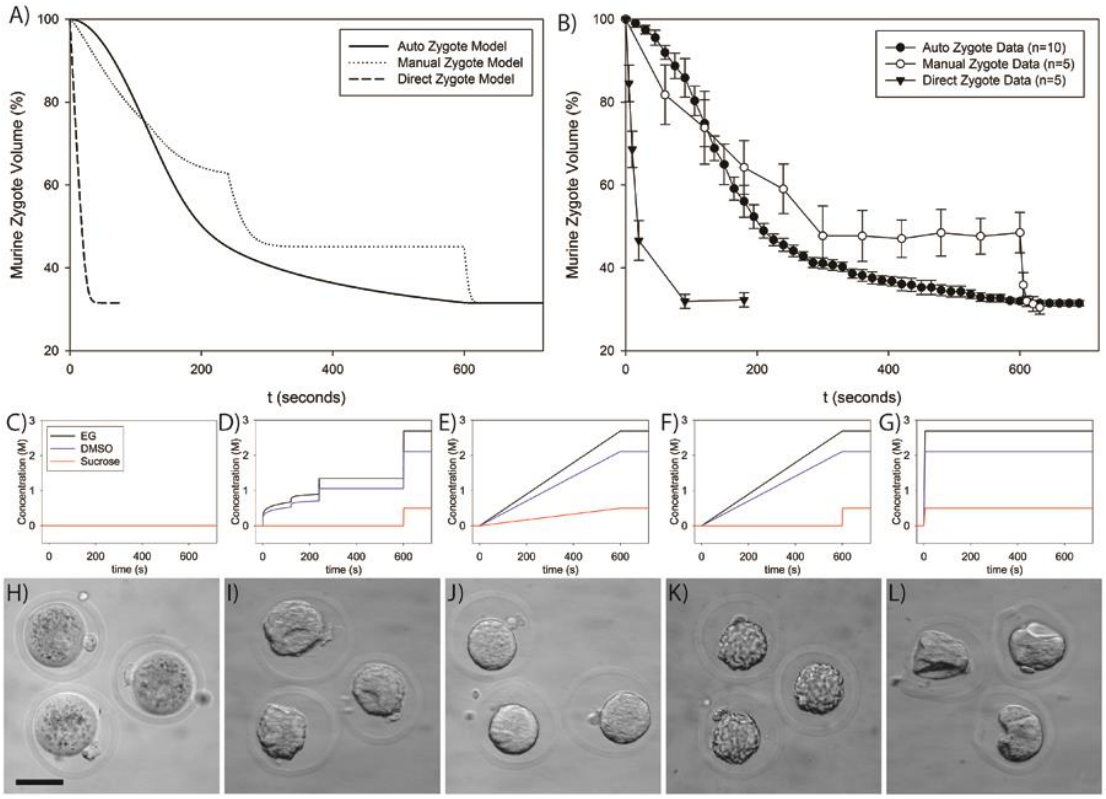

Fig. 2.1 A) Kedem-Katchalsky model predictions of zygote shrinkage during different cryoprotectant agent (CPA) exchange protocols. Auto represents automated-microfluidic CPA exposure. Manual represents manual-pipetting CPA exposure. Direct represents direct exposure from culture medium to VS known to be detrimental to cryosurvival. All shrinkage regimes had similar minimum cell volume but significantly different shrinkage patterns. B) Experimental observation of zygote volumes matched that of predictive models. CPA exchange profiles for: C) No CPA exposure, D) Commonly used manual pipetting protocols, E) Automated microfluidic protocol with gradual addition of all CPA components, F) Gradual exposure of permeable CPA components but abrupt exposure to the impermeable component sucrose, and G) Direct and sudden exposure from culture media to VS. Black line represents EG, Blue line represents DMSO, and Red represents sucrose. H) Murine zygote before CPA exposure. I-L) show representative zygote morphology after exposure to each of the CPA protocols represented in the graphs above each image. J) Zygotes exposed to gradual CPA exchange show a smooth and round morphology whereas zygotes exposed to other protocols show small ripple-like or large crater-like deformations. Error bars: standard deviation. Scale bar: 50 µm.

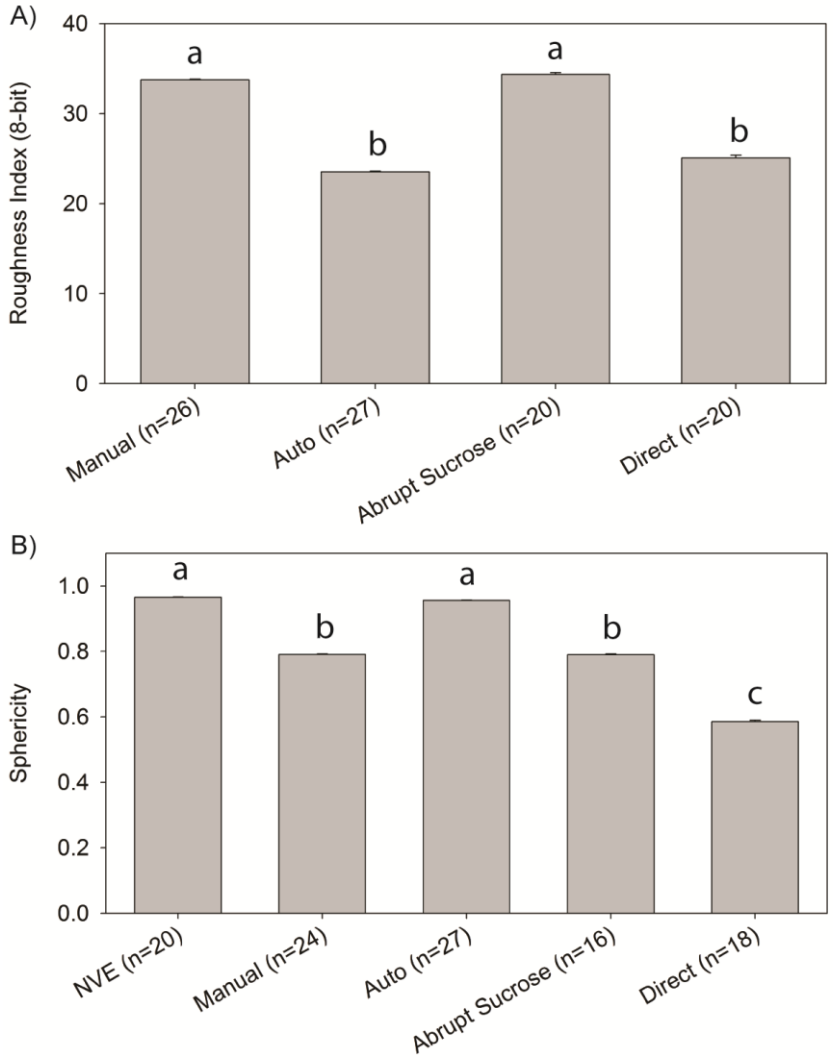

Fig. 2.2 A) Murine zygotes subjected to automated microfluidic CPA exposure had significantly ($p<0.001$) smoother cell surface than their counterparts subjected to manual pipetting-based CPA exposure. Sudden exposures to sucrose formed cell surfaces with similar roughness to that of manual pipetting. Direct exposure had smooth cell surfaces comparable with automated CPA exposure. The RI analysis is non-invasive and can be quantified in real-time within the microfluidic device. Non-Vitrified or CPA Exposed (NVE) zygotes had visual occlusions that cast dark regions in phase microscopy due to significant differences in refractive indexes within its cytoplasmic content due to the lack of EG and DMSO that prevent direct comparison from other experimental groups. B) Confocal microscopy reveals that murine zygotes subjected to automated microfluidic CPA exposure have significantly high spherical morphology ($p<0.001$) than manual pipetting and direct CPA exposure and maintains its surface smoothness and sphericity at a level statistically comparable to NVE zygotes. Manual pipetting and abrupt sucrose CPA exposure forms ripples and some large deformations in cell shape that produced comparably low sphericity. Direct exposure causes large deformations in cell shape that, despite its smooth surface, have the largest impact on sphericity. Error bars: standard error. Different letters signify statistical significance $p<0.05$.

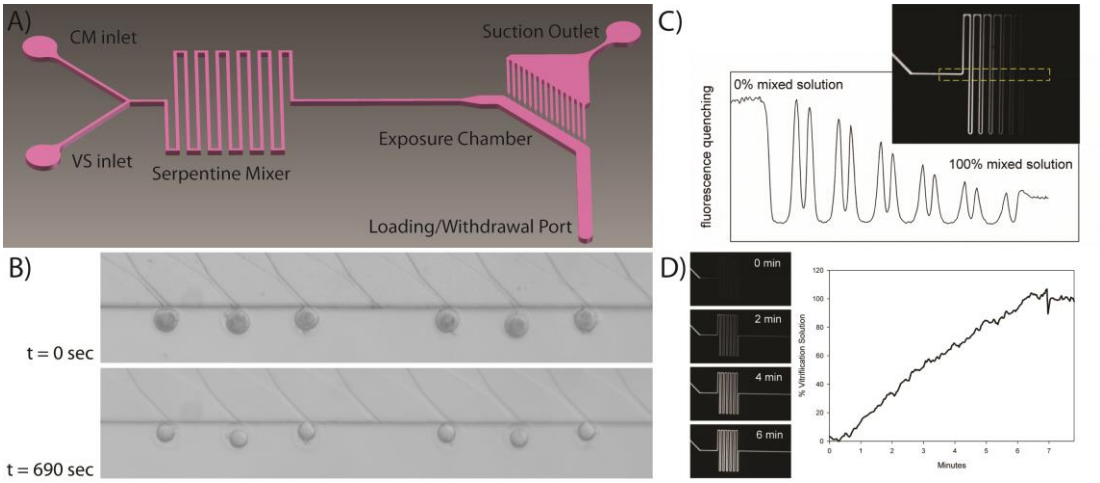

Fig. 2.3 A) Device schematic. B) Holding microchannels immobilize cells within the exposure chamber allowing for real-time morphological assessment during CPA exchange. C) Fluorescence quenching experiment demonstrating efficient mixing. D) Synchronized syringe pumps combined with the serpentine channel provide linearly increasing CPA profile.

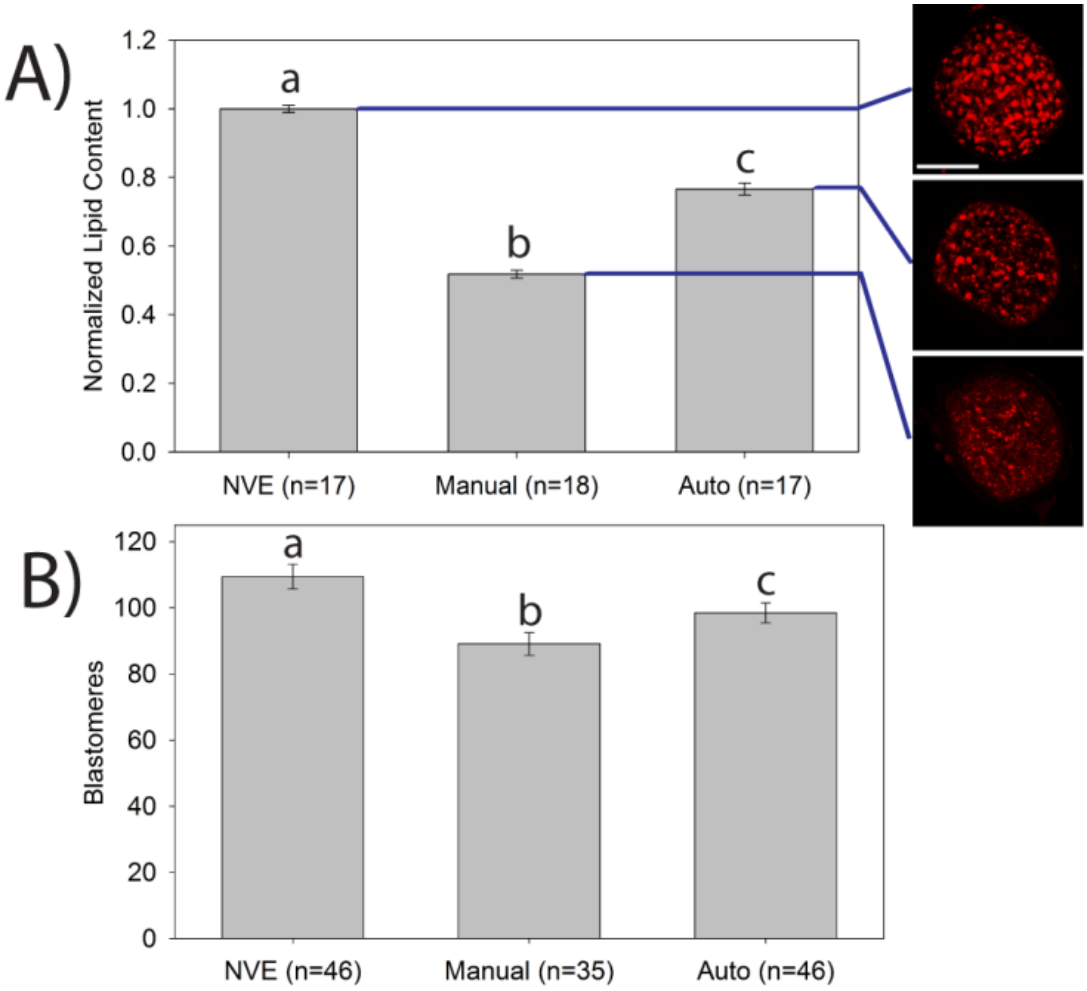

Fig. 2.4 A) Vitrification causes a loss of cytoplasmic lipid for bovine oocytes. However the use of automated-microfluidic CPA exposure increases cytoplasmic lipid retention compared to manual-pipetting CPA ($p<0.01$). Inlets demonstrate difference in lipid droplet size and distribution. Scale bar: 50 µm. B) Vitrification-derived sub-lethal damage decreases developmental competence after 96 hours of embryo culture of murine zygotes. However automated-microfluidic CPA exposure significantly increases number of blastomeres per blastocyst compared to its manual-pipetting analogue and provides evidence that sub-lethal damage was reduced. Error bars: standard error. Different letters signify statistical significance $p<0.05$.

2.5 References

1. Trounson, A. & Mohr, L. Human pregnancy following cryopreservation, thawing and transfer of an eight-cell embryo. *Nature* **305,** 707–709 (1983).

2. Kuwayama, M., Vajta, G., Kato, O. & Leibo, S. P. Highly efficient vitrification method for cryopreservation of human oocytes. *Reprod. Biomed. Online* **11,** 300–308 (2005).

3. Rall, W. F. & Fahy, G. M. Ice-free cryopreservation of mouse embryos at −196 °C by vitrification. *Nature* **313,** 573–575 (1985).

4. Meryman, H. T. Osmotic stress as a mechanism of freezing injury. *Cryobiology* **8,** 489–500 (1971).

5. Mullen, S. F., Li, M., Li, Y., Chen, Z.-J. & Critser, J. K. Human oocyte vitrification: the permeability of metaphase II oocytes to water and ethylene glycol and the appliance toward vitrification. *Fertil. Steril.* **89,** 1812–1825 (2008).

6. Agca, Y., Liu, J., Rutledge, J. J., Critser, E. S. & Critser, J. K. Effect of osmotic stress on the developmental competence of germinal vesicle and metaphase II stage bovine cumulus oocyte complexes and its relevance to cryopreservation. *Mol. Reprod. Dev.* **55,** 212–219 (2000).

7. Smith, G. D. *et al.* Prospective randomized comparison of human oocyte cryopreservation with slow-rate freezing or vitrification. *Fertil. Steril.* **94,** 2088–2095 (2010).

8. Kuwayama, M., Hamano, S. & Nagai, T. Vitrification of bovine blastocysts obtained by in vitro culture of oocytes matured and fertilized in vitro. *Reproduction* **96,** 187–193 (1992).

9. Otoi, T., Yamamoto, K., Koyama, N., Tachikawa, S. & Suzuki, T. Cryopreservation of Mature Bovine Oocytes by Vitrification in Straws. *Cryobiology* **37,** 77–85 (1998).

10. Song, Y. S. *et al.* Microfluidics for cryopreservation. *Lab. Chip* **9,** 1874 (2009).

11. Heo, Y. S. *et al.* Controlled loading of cryoprotectants (CPAs) to oocyte with linear and complex CPA profiles on a microfluidic platform. *Lab. Chip* **11,** 3530 (2011).

12. Kuleshova, L. L., MacFarlane, D. R., Trounson, A. O. & Shaw, J. M. Sugars Exert a Major Influence on the Vitrification Properties of Ethylene Glycol-Based Solutions and Have Low Toxicity to Embryos and Oocytes. *Cryobiology* **38,** 119–130 (1999).

13. Kedem, O. & Katchalsky, A. Thermodynamic analysis of the permeability of biological membranes to non-electrolytes. *Biochim. Biophys. Acta* **27,** 229–246 (1958).

14. Pfaff, R. Water and DMSO membrane permeability characteristics of in-vivo- and in- vitro-derived and cultured murine oocytes and embryos. *Mol. Hum. Reprod.* **4,** 51–59 (1998).

15. Paynter, S. J., Fuller, B. J. & Shaw, R. W. Temperature Dependence of Kedem–Katchalsky Membrane Transport Coefficients for Mature Mouse Oocytes in the Presence of Ethylene Glycol. *Cryobiology* **39,** 169–176 (1999).

16. Sutton-McDowall, M. L., Feil, D., Robker, R. L., Thompson, J. G. & Dunning, K. R. Utilization of endogenous fatty acid stores for energy production in bovine preimplantation embryos. *Theriogenology* **77,** 1632–1641 (2012).

17. Dunning, K. R., Akison, L. K., Russell, D. L., Norman, R. J. & Robker, R. L. Increased Beta-Oxidation and Improved Oocyte Developmental Competence in Response to L-Carnitine During Ovarian In Vitro Follicle Development in Mice. *Biol. Reprod.* **85,** 548–555 (2011).

18. Chankitisakul, V., Somfai, T., Inaba, Y., Techakumphu, M. & Nagai, T. Supplementation of maturation medium with L-carnitine improves cryo-tolerance of bovine in vitro matured oocytes. *Theriogenology* **79,** 590–598 (2013).

19. Somfai, T. *et al.* Enhancement of lipid metabolism with L-carnitine during in vitro maturation improves nuclear maturation and cleavage ability of follicular porcine oocytes. *Reprod. Fertil. Dev.* **23,** 912 (2011).

20. Wong, C. C. *et al.* Non-invasive imaging of human embryos before embryonic genome activation predicts development to the blastocyst stage. *Nat. Biotechnol.* **28,** 1115–1121 (2010).

21. Tsang, W. H. & Chow, K. L. Cryopreservation of mammalian embryos: Advancement of putting life on hold. *Birth Defects Res. Part C Embryo Today Rev.* **90,** 163–175 (2010).

22. Smith G, Fioravanti J. Oocyte and embryo cryopreservation. In: Gardner D, ed. In vitro fertilization: a practical approach. New York: Informa Healthcare USA, Inc, 2007:331–64.

Chapter 3

Conclusions and Future Direction

Previous osmotic stress studies employ experimental groups with differing concentrations of permeable or impermeable cryoprotectants (CPAs). Those employing vitrification solutions (VSs) containing impermeable solutes have also introduced the impermeable CPA such as glucose, sucrose, sorbital or trehalose abruptly at the end of the CPA exchange procedure. As such, osmotic stress studies of the past have been unable to experimentally separate osmotic damage from minimum cell volume and shrinkage rate during CPA exposure.

The use of continuous CPA exposure by microfluidics and the use of impermeable solutes such as sucrose in the VS allowed for the ability to independently control shrinkage rate and minimum cell volume. The lowering of shrinkage rate during CPA exposure lowered sub-lethal osmotic stress to increase cytoplasmic lipid retention of bovine oocytes and developmental competence of murine zygotes. When considering shrinkage rate as strain rate and minimum cell volume as strain, it is then evident that the observed improved quality agree with fundamental principles of materials science.

Recent developments in fabrication techniques such as carbon vapor deposition (CVD) diamond microfluidic devices that have low thermal mass. Such a microfluidic devices would allow for an enclosed vitrification vehicle that allows high cooling rate to facilitate vitrification as well as an enclosure that prevents cell loss and eliminate risk of liquid nitrogen contamination.

There is evidence that different VSs are more preferable depending on the cell type to be vitrified. However, a single cell type may have different VSs where there are conflicting studies that one is better than the other. This can at times be attributed to confounding factors such as user variability. The use of a microfluidic device that eliminates user variability can more easily determine the most optimal VS between opposing views.

Current VSs employ a high concentration of vitrification solution. The toxicity concerns fuel an ever present desire to decrease the CPA concentration in the VS however this is limited by the cooling rate (Fig. 3.1). As new cooling techniques are developed to increase cooling rate, it will become possible in the future to develop new VSs with lower CPA concentration and toxicity. The use of a microfluidic device without user variability will facilitate the development of new VSs as cooling technology continues to improve.

The mechanistic principles studied in CPA exposure can be applied to CPA removal in post-vitrification warming. The lowering of expansion rate of cells during post-vitrification warming is expected to also improve oocyte, zygote, and embryo

quality. The development of a microfluidic device for post-vitrification warming has the added benefit of facilitating donor oocyte transport.

A fully integrated microfluidic device with the capability to perform CPA exposure, function as a vehicle for vitrification , and CPA removal will allow for full automation for the entire cryopreservation process. The microfluidic device would be capable of performing protocols not possible with conventional techniques to eliminate pipetting variability and minimize mechanical and chemical stress on cells.

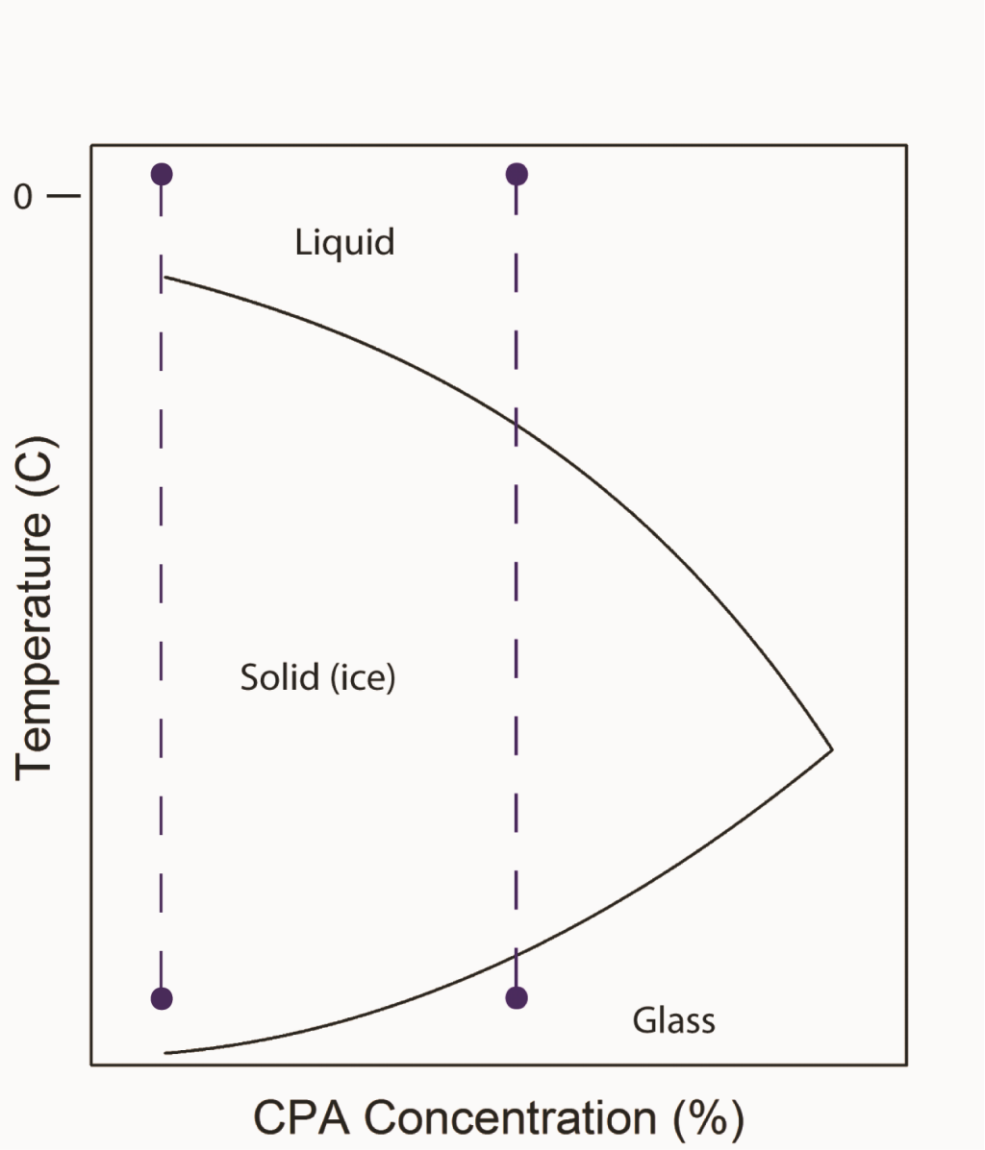

Fig. 3.1 Generic phase diagram. The length of the dotted blue line signifies the cooling rate provided by current cooling technology. The ever present desire to decrease CPA concentration is thwarted by the inability to achieve safe vitrification phase transition due to insufficient cooling rate.

Part 2

Chapter 4:

Rounded multi-level microchannels with orifices made in one exposure enable aqueous two-phase system droplet microfluidics

Exposure of a negative photoresist-coated glass slide with diffused light from the backside through a mask with disconnected features provides multi-level rounded channels with narrow orifices in one exposure. Using these structures, we construct microfluidic systems capable of creating aqueous two-phase system droplets where one aqueous phase forms droplets and the other aqueous phase forms the surrounding matrix. Unlike water-in-oil droplet systems, aqueous two-phase systems can have very low interfacial tensions that prevent spontaneous droplet formation. The multi-level channels fabricated by backside lithography satisfy two conflicting needs: (i) the requirement to have narrowed channels for efficient valve closure by channel deformation and (ii) the need to have wide channels to reduce the flow velocity, thus reducing the capillary number and enhancing droplet formation.

4.1 Introduction

Production of molds with multi-level rounded channel features to cast PDMS prepolymer against typically requires multiple steps or costly procedures.[1–5] Here, we use an inexpensive, single exposure, backside diffused light lithography (BDLL) procedure with photomasks that contain channel features of different widths and disconnected regions to generate multi-level rounded microchannels with strategically placed orifices. The effect of BDLL to generate channels with bell-shaped cross-sectional shapes that are wider than the original mask feature and differential height according to mask width[6] is used here to create narrow connections between multi-level features that are not connected on the original photomask (Fig. 4.1A and B). The rounded, narrow channel orifices allow for efficient channel constriction by Braille pin actuation[7] of channels that are otherwise too large to be closed reliably (Fig. 4.1C).

The system is demonstrated to be useful for generating aqueous two phase system (ATPS) droplets. Unlike oil/water microfluidic droplet systems that take advantage of high interfacial tensions to spontaneously generate droplets,[8–12] the most biocompatible ATPS systems with low polymer contents[13] have low interfacial tensions that prevent the practical use of spontaneous droplet formation.[14] The multi-level rounded channels with orifices fabricated by BDLL with disconnected photomask features (DPFs) allow for the efficient valve closure at the orifice as well as reduction of flow velocity in the widened downstream channel region to generate reliable ATPS droplet formation.

4.2 Materials and Methods

Channel characterization and device fabrication

To assess relative channel dimensions, a photomask of 500 μm squares with varying distances was used to expose the negative photoresist (SU-8) by BDLL (for varying durations proportionately to height) at heights of 30, 50, 90, 150 and 200 μm.[6] A schematic and brief explanation of the BDLL procedure and setup is shown in Fig. 4.2. The channel shapes, widths, and heights were determined using environmental scanning electron microscopy and fluorescence imaging of channels filled with 0.01% fluorescein.

A hydrodynamic focusing device was used to facilitate droplet formation. SU-8 was exposed for 90 s through a photomask containing a 400 μm DPF between the central channels (Fig. 4.3). The resulting PDMS replicas were bonded to 100 μm thick PDMS membranes to produce a closed channel system for Braille actuation.

ATPS threading regime and droplet formation

The ATPS used in this study was near critical-point at 3.2% w/w dextranM_w 500 000 (Pharmacosmos, Denmark) and 2.5% w/w PEG M_w 35 000 (Sigma-Aldrich, St Louis, MO) prepared as previously described.[13]A threading regime was produced using the device shown in Fig. 4.4 with flow rates of 0.01 mL h^{-1} and 0.10 mL h^{-1} for dextran and PEG phases using a syringe pump.

An actuating Braille pin was placed underneath the orifice in the centre channel to discontinue the dextran flow by valving. The Braille pin was controlled using a computer user interface[15,16] to actuate in a frequency range between 2.5 Hz and 0.83 Hz. Droplets were imaged using phase contrast light microscopy (Nikon TS100, Tokyo, Japan).

4.3 Results and Discussion

Characterization of BDLL

Channels resulting from BDLL are larger than the features on the photomask. A 500 μm photomask produced 955 μm channels with 100 s exposure in a 100 μm high photoresist with a standard deviation of 8 μm. For BDLL with a given DPF, increased photoresist thickness with associated increased exposure allows for a wider DPF to be connected on the developed photoresist. For every 50 μm in SU-8 thickness, the maximum DPF over which connections can be formed increases by 25 μm (Fig. 4.5C).

For a given photoresist thickness, by adjusting the exposure times, mask line widths, and DPF positions and sizes, we can separately control the heights of different sections of channels and orifices (Fig. 4.5D and E). For a given sub-saturating exposure, channel height increases with increasing the mask line width. The constricted orifice height, however, can be independently adjusted to decrease by increasing the size of the DPFs. This method produces a multi-level channel with a channel orifice as evidenced by fluorescence images (Fig. 4.5A) and phase contrast cross-sectional images (not shown, but similar to Fig. 1 in ref. 6). A profile plot shows the calculated channel height across the *x*-axis based on the fluorescence intensity (Fig. 4.5B). The channel is multi-level, starting from a 45 μm height, narrowing to an orifice with only a 16 μm height, then widening to a 90 μm high channel.

Monodisperse droplet formation

For a fixed channel geometry, the volumetric flow and the capillary number, Ca = $\eta V/\gamma$ (the ratio of viscous stresses to surface stresses) dictate droplet formation, where η is the viscosity, V is the characteristic velocity, and γ is the interfacial tension. Flow conditions of Ca < 1 are required for efficient droplet formation;[14] otherwise, the length of the channel (L_c) required for droplet formation to occur by Rayleigh instabilities becomes too large. Because ATPSs typically have extremely low interfacial tensions (≤0.1 mN m^{-1}) and high viscosity, the flow velocity required to achieve a Ca supportive of spontaneous droplet formation becomes too small for most applications. A 0.01 mN m^{-1} interfacial tension oil/water/surfactant system has been explored for droplet formation but using sub-centimetre scale channels where, despite the use of a slow flow velocity, much of the droplet breakup still occurs after a significant delay.[17] An ATPS droplet system was previously used to perform droplet sorting.[18] In this system, however, the ATPS phases were composed oftetrabutylammonium bromide and ammonium sulfate at concentrations of 15% and 30% w/w making them possess a very high interfacial tension (4–5 mN m^{-1}) that is advantageous for spontaneous droplet formation but negating much of the bio- and cyto-compatibility advantage of ATPSs. More recently, droplets of an ATPS with a relatively low interfacial tension of 0.1 mN m^{-1} were prepared with biocompatible polymers by generating instabilities with a piezoelectric bending plate.[19]

Here, we used a microfluidic system that utilizes rounded channels with orifices combined with Braille pin valving (Fig. 4.1) to allow droplet formation (Fig. 4.6) using a near-critical point ATPS with the lowest interfacial tensions among ATPS droplet systems demonstrated to date. The ATPS had measured viscosities of 3.1 cP

for the dextran-rich and 4.9 cP for the PEG-rich phases with an estimated interfacial tension of 0.010 mN m^{-1}.[13] As expected, the channel alone generated no droplets, with laminar streams of ATPS being stable for at least 27 mm at a flow rate of 0.01 mL h^{-1}. The flow rate required to achieve a Ca ≈ 1 required for spontaneous droplet formation in our channel would be 0.5 μL h^{-1}. However, the periodic valve closure at the channel orifices of a hydrodynamic focusing junction using Braille actuation (Fig. 4.1C and D) effectively generated droplets. We observed that sample evaporation did not have a dramatic effect on droplets for the two hour duration of our experiments performed under room temperature conditions.

A range of monodisperse droplets of defined sizes and inter-droplet spacings could be formed by varying either the dextran/PEG flow ratio, the Braille pin actuation frequency, or both (Fig. 4.6). We produced droplet sizes between 0.9 nL and 3.4 nL with droplet spacings between 200 μm and 1400 μm. Increasing the PEG flow rate increased the spacing between droplets but not the size of the droplets (Fig. 4.6A). Decreasing the Braille actuation frequency increased both the droplet volume and the distance between drops (Fig. 4.6B).

Although not all combinations of flow ratios and Braille actuation frequencies were tested, our results indicate that a large combination of droplet sizes and droplet spacings can be achieved by adjusting both the flow ratio and the Braille actuation frequency. Due to the high capillary number, droplets in motion assume a teardrop shape but assume a spherical shape once the flow is arrested (Fig. 4.6C and D). Thus, we demonstrate highly controlled low interfacial tension droplet formation using a multi-level device formed through a single photolithographic exposure.

4.4 Conclusions

We demonstrate an extension of a previously described backside diffused light lithography (BDLL) method[6] to produce multi-level channels with strategically positioned channel orifices. The fabrication equipment required is inexpensive compared to conventional photolithography and the procedure is also straightforward involving only a single exposure and no alignment steps that are required in multi-step multiple-mask procedures conventionally used for fabrication of multi-level features. Using our multi-level channel, we formed ATPS droplets at the lowest interfacial tensions reported to date. Such ATPS droplet formation capabilities are useful for biocompatible droplet-based cell patterning[13,20] and production of monodisperse hydrogel particles.[19] We also envision this straightforward microchannel orifice fabrication method to be useful for many applications beyond ATPS droplet formation such as cell and particle trapping.[1]

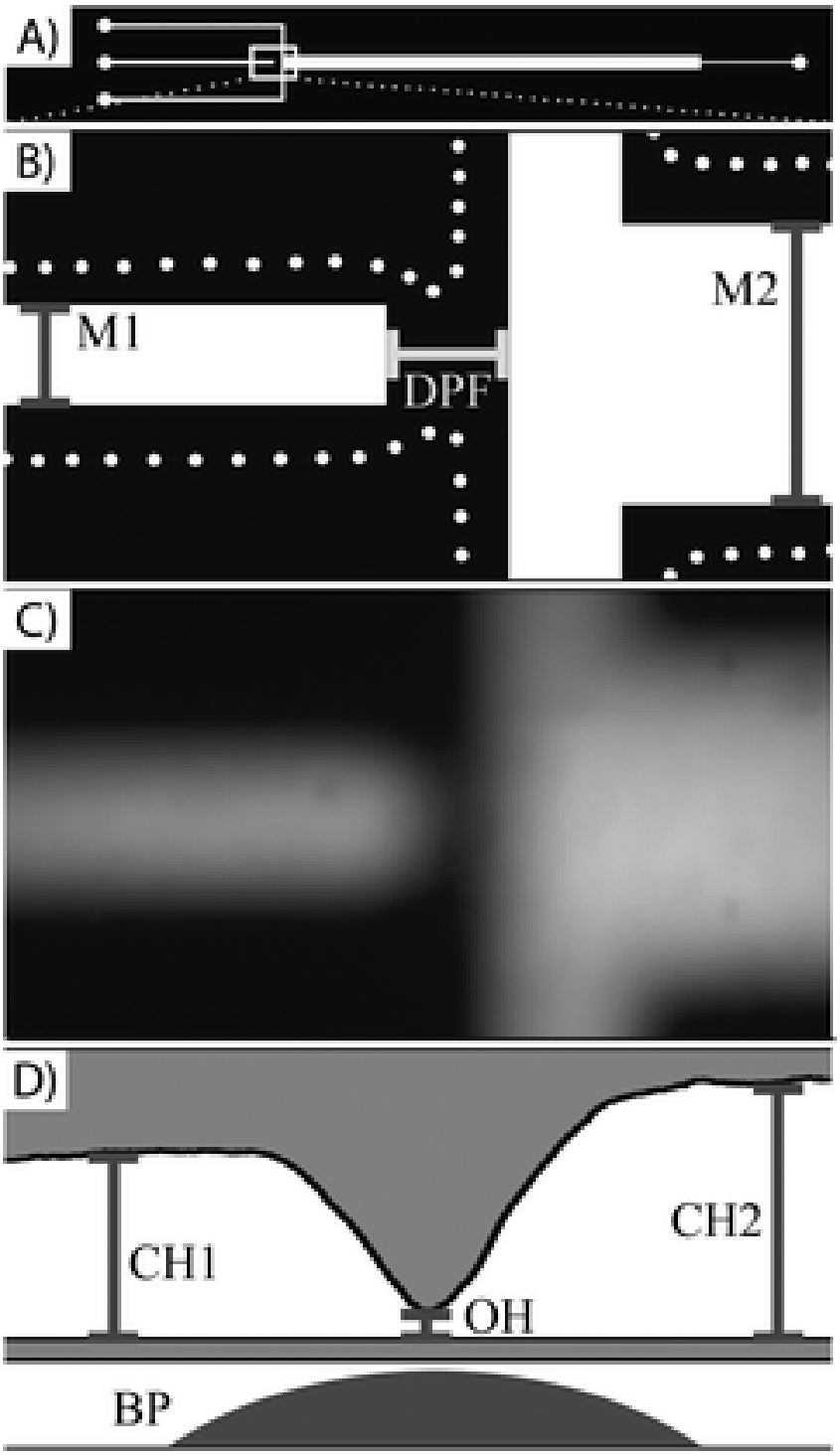

Fig. 4.1 (A) Photomask feature used to generate multi-level channels for ATPS droplet generation. White box: area of interest for (B, C and D). (B) Close-up view of the junction region of the photomask. White regions represent transparent portions of the mask. Dotted lines outline the actual channel feature obtained from this mask due to the channel widening effect of BDLL. M1: mask line width 1, M2: mask line width 2, DPF: disconnected photomask feature. (C) Fluorescent image of an actual channel obtained from the mask. (D) Schematic of the side-view of the device shown in (C). A Braille pin aligned to the shallow orifice region allows for efficient channel valving. CH1: channel height 1, CH2: channel height 2, OH: orifice height, BP: Braille pin.

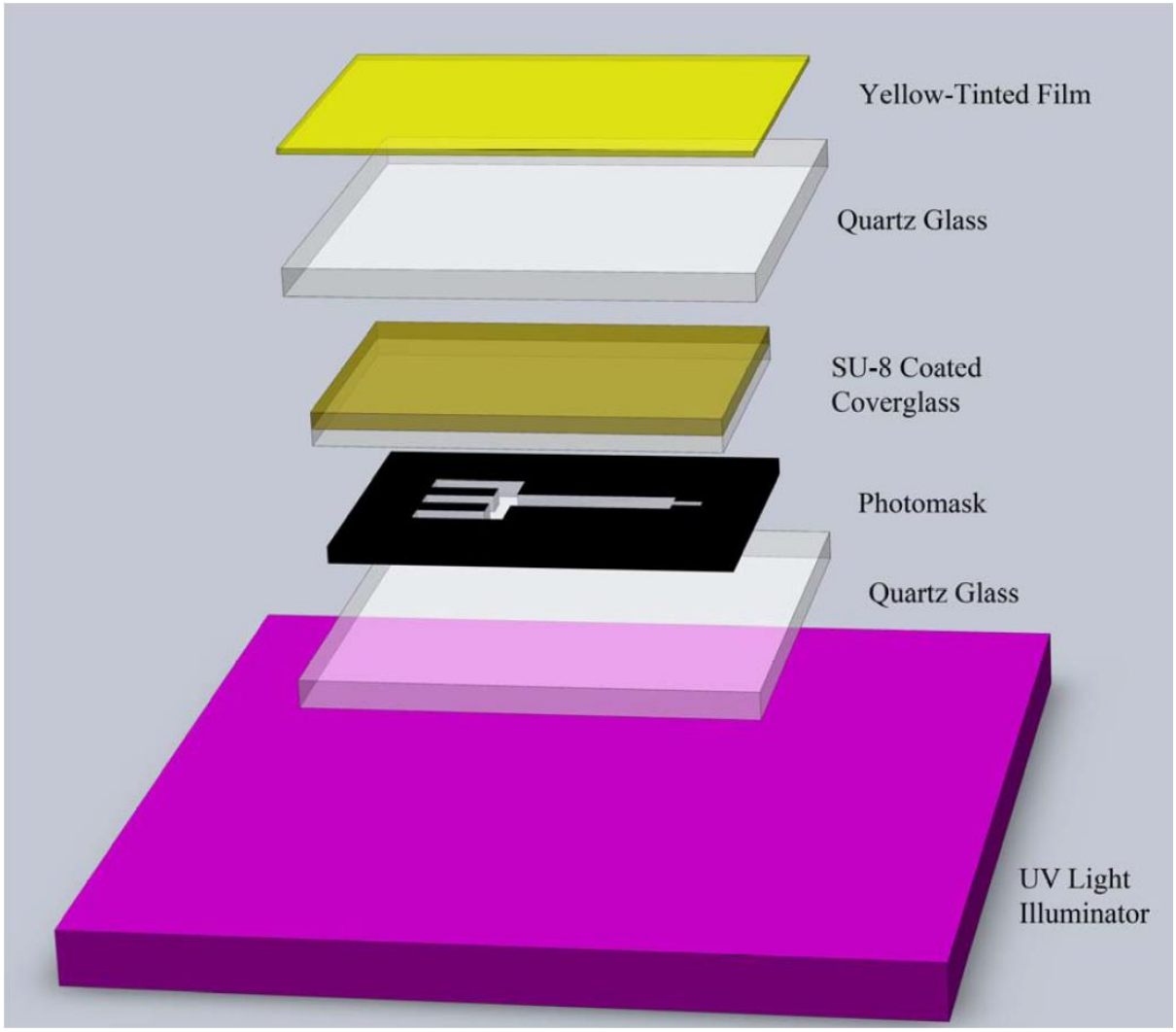

Fig. 4.2 Schematic of Backside Diffused Light Lithography. UV light passing the photomask diffuses radially in the cover glass to expose an area wider than the area of the photomask. The rounded shape results from a spatial-intensity profile that results from diffused and diffracted light. More detail and characterization of this process is described by Futai et al[6].

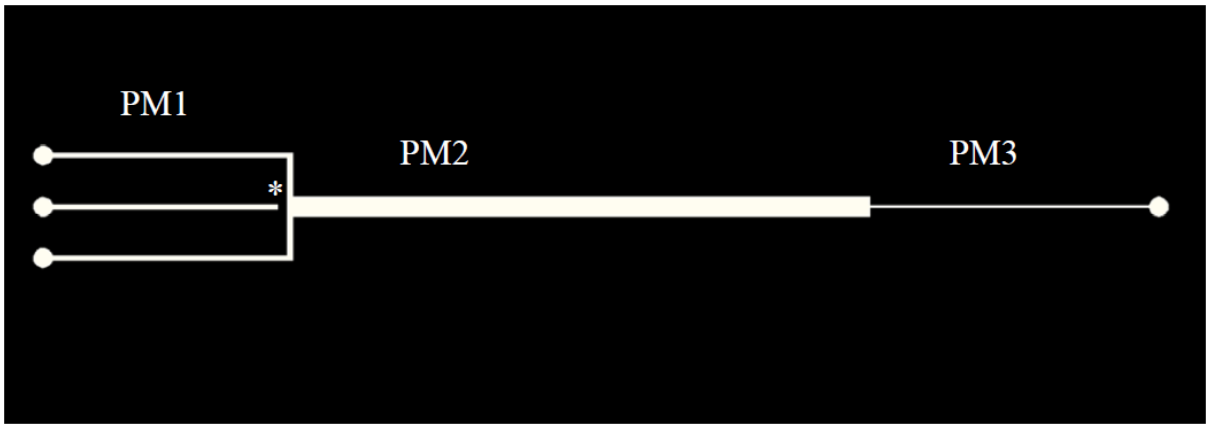

Fig. 4.3 Photomasked for device in Fig.4.4. The device is of basic hydrodynamic focusing design save for Disconnected Photomask Feature (*) for the center channel that eventually becomes an orifice after BDLL. Photomask dimensions. PM1 L: 10.5 mm, PM1 W: 300 μm, PM2 L: 27 mm, PM2W: 1 mm, PM3 L: 13 mm, PM3 W:150 μm.

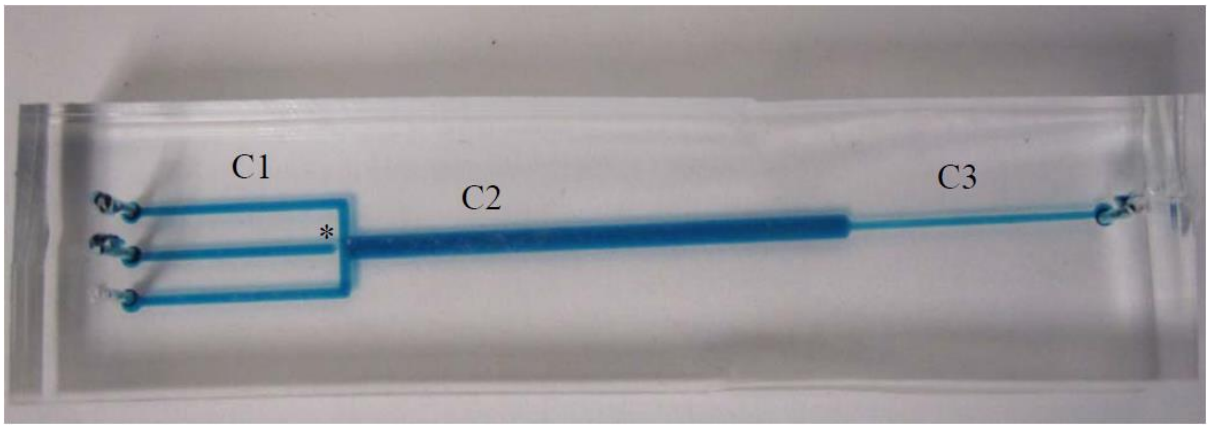

Fig. 4.4 Device used for droplet generation. The device is of basic hydrodynamic focusing design save for a small orifice (*) for the center channel that allows for efficient channel valving by Braille actuation. Channel dimensions. C1 L: 10.6 mm, C1 W: 587 μm, C2 L: 27.1 mm, C2W: 1.24 mm, C3 L: 13.2 mm, C3 W: 413 μm.

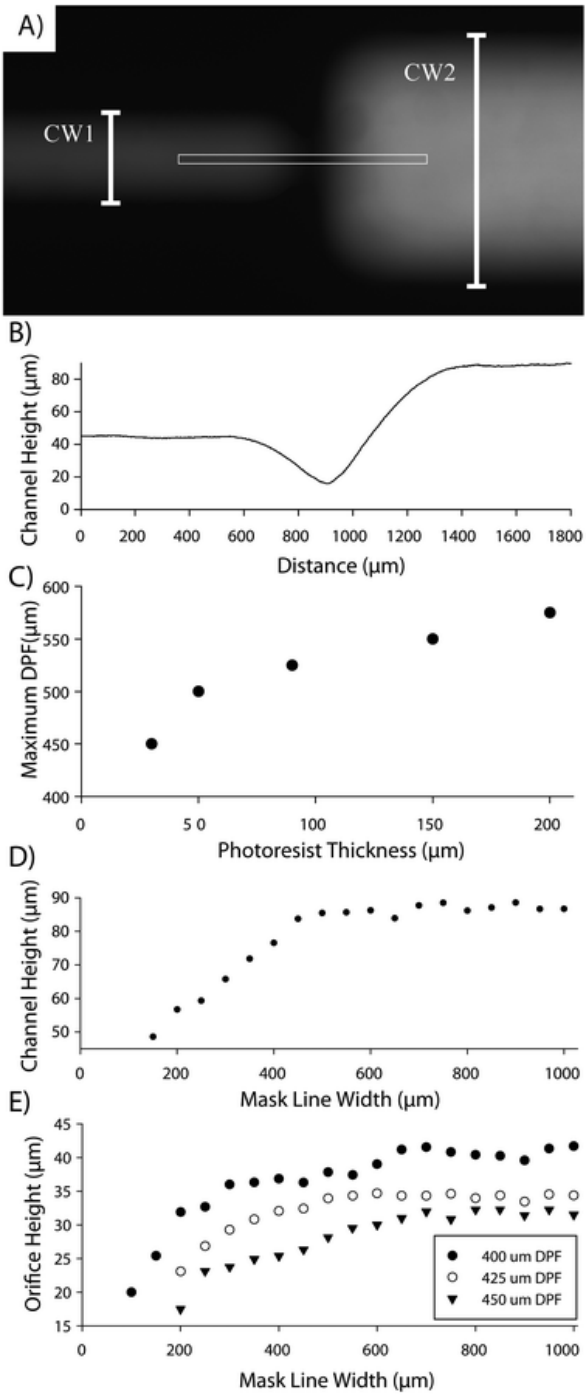

Fig. 4.5 (A) Fluorescent image of a multi-level channel with an orifice. The white box indicates the area used for profile plotting. CW1: channel width 1, CW2: channel width 2. (B) Profile plot indicating the calculated channel heights. (C) The maximum DPF that produces orifices. The increased photoresist thickness and associated light exposure allow for a larger DPF to be connected after development. All conditions below the points will form connected orifices (smaller DPF gives larger orifices). (D) Channel feature heights are smaller for smaller mask line widths. (E) For a fixed DPF and mask line width 2 of 1 mm (feature that gives rise to CW2 in (A)), the orifice height and width decrease with decreasing mask line width 1 (the mask feature that gives rise to CW1). With a large mask line width 1, the DPF needs to be increased to obtain narrow orifices.

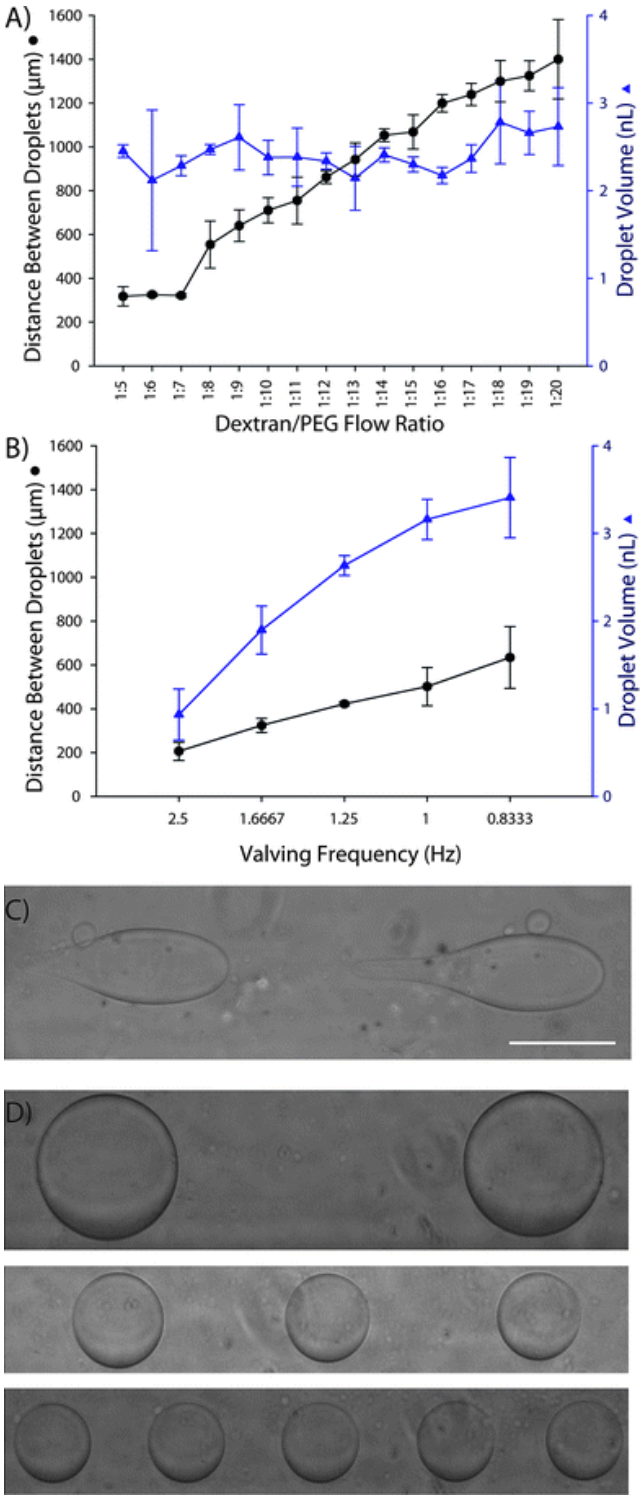

Fig. 4.6 Formation of aqueous two phase system (ATPS) droplets with a very low interfacial tension. (A) Varying dextran/PEG flow ratio changes distance between droplets, but the volumes of droplets remain constant. (B) Decreasing valving frequency increases the droplet volume and the inter-droplet distance. (C) Droplets in motion assume a teardrop shape due to the high capillary number of the system. (D) Phase contrast image of droplets at 1 : 7 flow ratio with 2.5 Hz, 1.25 Hz and 0.8333 Hz shows that droplets conform to a spherical shape when the flow is terminated. Scale bar: 200 µm.

4.5 References

1. X. Liu, Q. Wang, J. Qin and B. Lin, *Lab Chip*, 2009, **9**, 1200–1205.
2. B. Wagner, H. J. Quenzer, W. Henke, W. Hoppe and W. Pilz, *Sens. Actuators, A*, 1995, **46**, 89–94.
3. M. W. Toepke and P. J. A. Kenis, *J. Am. Chem. Soc.*, 2005, **127**, 7674–7675.
4. A. W. Browne, M. J. Rust, W. S. Jung, S. H. Lee and C. H. Ahn, *Lab Chip*, 2009, **9**, 2941–2946.
5. J. T. Cabral, S. D. Hudson, C. Harrison and J. F. Douglas, *Langmuir*, 2004, **20**, 10020–10029.
6. N. Futai, W. Gu and S. Takayama, *Adv. Mater.*, 2004, **16**, 1320–1323.
7. W. Gu, X. Zhu, N. Futai, B. S. Cho and S. Takayama, *Proc. Natl. Acad. Sci. U. S. A.*, 2004, **101**, 15861–15866.
8. R. Tewhey, J. B. Warner, M. Nakano, B. Libby, M. Medkova, P. H. David, S. K. Kotsopoulos, M. L. Samuels, J. B. Hutchison, J. W. Larson, E. J. Topol, M. P. Weiner, O. Harismendy, J. Olson, D. R. Link and K. A. Frazer, *Nat. Biotechnol.*, 2009, **27**, 1025–1031.
9. Y. C. Tan, J. S. Fisher, A. I. Lee, V. Cristini and A. P. Lee, *Lab Chip*, 2004, **4**, 292–298.
10. S. Xu, Z. Nie, M. Seo, P. Lewis, E. Kumacheva, H. A. Stone, P. Garstecki, D. B. Weibel, I. Gitlin and G. M. Whitesides, *Angew. Chem.*, 2005, **117**, 734–738.
11. J. C. Baret, O. J. Miller, V. Taly, M. Ryckelynck, A. El-Harrak, L. Frenz, C. Rick, M. L. Samuels, J. B. Hutchison, J. J. Agresti, D. R. Link, D. A. Weitz and A. D. Griffiths, *Lab Chip*, 2009, **9**, 1850–1858.
12. K. Vijayakumar, S. Gulati, A. J. deMello and J. B. Edel, *Chem. Sci.*, 2010, **1**, 447–452.
13. H. Tavana, B. Mosadegh and S. Takayama, *Adv. Mater.*, 2010, **24**, 2628–2631.
14. T. Cubaud and T. G. Mason, *Phys. Fluids*, 2008, **20**, 053302.
15. N. Futai, W. Gu, J. W. Song and S. Takayama, *Lab Chip*, 2006, **6**, 149–154.
16. G. Mehta, K. Mehta, D. Sud, J. W. Song, T. Bersano-Begey, N. Futai, Y. S. Heo, M.-A. Mycek, J. J. Linderman and S. Takayama, *Biomed. Microdevices*, 2007, **9**, 123–134.
17. M. Hashimoto, P. Gerstecki, H. A. Stone and G. M. Whitesides, *Soft Matter*, 2008, **4**, 1403–1413.

18. Y. H. Choi, Y. S. Song and D. H. Kim, *J. Chromatogr., A*, 2010, **1217**, 3723–3728.

19. I. Ziemecka, V. van Steijn, G. J. M. Koper, M. Rosso, A. M. Brizard, J. H. van Esch and M. T. Kreutzer, *Lab Chip*, 2011, **11**, 620–624.

20. J. P. Frampton, D. Lai, H. Sriram and S. Takayama, *Biomed. Microdevices* DOI:10.1007/s10544-011-9574-7.

Chapter 5

Precisely targeted delivery of cells and biomolecules within microchannels using aqueous two-phase systems

Laminar and pulsatile flow of aqueous solutions in microfluidic channels can be useful for controlled delivery of cells and molecules. Dispersion effects resulting from diffusion and convective disturbances, however, result in reagent delivery profiles becoming blurred over the length of the channels. This issue is addressed partially by using oil-in-water phase systems. However, there are limitations in terms of the biocompatibility of these systems for adherent cell culture. Here we present a fully biocompatible aqueous two-phase flow system that can be used to pattern cells within simple microfluidic channel designs, as well as to deliver biochemical treatments to cells according to discrete boundaries. We demonstrate that aqueous two-phase systems are capable of precisely delivering cells as laminar patterns, or as islands by way of forced droplet formation. We also demonstrate that these systems can be used to precisely control chemical delivery to preformed monolayers of cells growing within channels. Treatments containing trypsin were localized more reliably using aqueous two-phase delivery than using conventional delivery in aqueous medium.

5.1 Introduction

Microfluidic systems have been used extensively for analysis of drug and chemical actions on cells and to reveal mechanisms of cell-cell signaling through soluble factors (Torisawa et al. *2010*; Wu et al. *2010*; Young and Beebe *2010*). Such systems provide a range of capabilities that are not available in conventional petri dish culture including the abilities to precisely manipulate small liquid volumes, localize treatments within cell populations and perform analyses on small numbers of cells (Olofsson et al. *2009*; Villa-Diaz et al. *2009*; Jovic et al. *2010*; Liu et al. *2010*). This is usually accomplished through generation of either laminar or pulsatile flow (Gu et al. *2004*; Bransky et al. *2008*).

Laminar flow is among the most common methods for selective delivery of cells and molecules within microfluidic channels. This method has been used to deliver bacteria, blood cells, and many other mammalian cell types in controlled fashions (Takayama et al. *1999*; Regenberg et al. *2004*; Lucchetta et al.*2005*; Berthier et al. *2011*). It has also featured in experiments that probe cell functions through delivery of selective treatments (Sawano et al. *2002*). However, for most small molecules and proteins, as well as some larger particles, selective laminar flow delivery is usually limited to several millimeters from the convergence point of the laminar streams. Further downstream, diffusive effects can result in the formation of concentration gradients. It is possible to increase the distance over which selective treatments can be applied by increasing the velocity of flow, but this requires the use of either significantly larger sample volumes or significantly smaller channel sizes, and may result in undesirable consequences to cells or confounding factors related to increased fluid flow rate (e.g. shear stresses).

Pulsatile flow is also useful for treating cells in microchannels and has been used in a variety of cell signaling experiments (Gu et al. *2004*; Jovic et al. *2010*). However, dispersion of materials during pulsatile flow is even more problematic than for laminar flow, limiting selectivity of treatments to the time/frequency domain. Furthermore, pulsatile flow is not amenable to cell patterning because most types of cells sediment as they move through channels resulting in rapid loss of pattern fidelity.

Although diffusion gradients and dispersion of materials may be desirable for certain experiments, one can envisage a great number of experiments that could benefit from stable delivery of materials over the entire channel length. Therefore, in order to perform a more extensive repertoire of cell-based experiments in microfluidic channels it is necessary to establish methods for more selective in-channel cell patterning and chemical delivery over greater channel distances.

This need is partially satisfied with biphasic flow, the most commonly used systems consisting of air-and-water or oil-and-water (Zheng et al. *2004*; Guillot and Colin *2005*; Teh et al. *2008*; Brouzes et al. *2009*; Vijayakumar et al. *2010*). These systems provide high precision chemical separation and delivery; however, neither air nor oil are fully biocompatible with cells and can result in cells death due to mechanical disruption caused by surface stresses or non-biocompatible phase components (Bilek et al. *2003*; Wei-Heong Tan*2007*). Recently, aqueous two-phase systems (ATPSs) have been incorporated in several cell-based microfluidic applications, including collection of plant and animal cells, separation of erythrocytes and leukocytes from whole blood, and production of polyethylene glycol diacrylate hydrogel microspheres (Yamada et al. *2004*; Nam et al. *2005*; Soohoo and Walker *2009*; Tsukamoto et al. *2009*; Ziemecka et al.*2011*). Other applications of

ATPSs in microfluidic systems include separation of proteins and nucleotides through continuous partitioning or by electrophoresis across the interface between the two polymer solutions (Hahn et al. *2011a, b*). In contrast to other biphasic flow systems, ATPSs are fully biocompatible and are composed of phases that differ from each other only by the polymer constituents. The most commonly used ATPS for cell and biomolecule applications is the polyethylene glycol (PEG)-dextran system. Both PEG and dextran can dissolve in aqueous media, including cell culture media, at concentrations low enough to avoid damage to cells (Tavana et al. *2009*). Furthermore, the PEG-dextran ATPS is capable of partitioning materials, i.e. the biomolecules or cells of interest can distribute preferentially to either PEG or dextran (Albertsson *1972*; Yamada et al. *2004*).

Here we report the use of ATPSs in microfluidic channels for delivery of adherent cells and biomolecules to discrete channel regions. We demonstrate that mammalian cells can be directly patterned in precise laminar patterns or as islands by ATPS-mediated delivery. Furthermore we demonstrate that ATPSs can be used to deliver chemical treatments to cells growing within microfluidic channels with higher precision than conventional aqueous buffers.

5.2 Materials and Methods

ATPS compositions

ATPSs were formed by mixing equal volumes of stock solutions comprised of the following: *i*. 5.0% wt/wt PEG Mr 35,000 kDa (Sigma, St Louis MO) and 6.4% wt/vol dextran Mr 500,000 kDa (Pharmacosmos A/S, Denmark) or *ii*. 14.0% wt/wt PEG Mr

35,000 kDa and 14.0% wt/wt dextran Mr 10,000 kDa (Pharmacosmos). The resulting emulsions contained final concentrations of 2.5% PEG and 3.2% dextran for the dextran Mr 500,000 kDa system and 7.0% PEG and 7.0% dextran for the dextran Mr 10,000 kDa system. The emulsions could be separated into distinct phases by gradual overnight equilibration or by centrifugation at 4000 RCF for 15 min. For cell patterning, polymers were dissolved in DMEM containing 10% FBS by gently triturating the solutions until all polymer particles were completely dissolved. For trypsin delivery, polymers were dissolved in F12K CO_2 independent medium without FBS.

To improve partitioning to the dextran phase, trypsin was mixed with negatively charged carboxymethyl dextran (CM-dextran) (Sigma) prior to addition to the equilibrated dextran phase. The final concentration of CM-dextran in the dextran phase was 0.1 mg/mL. The final concentration of trypsin (Worthington, Lakewood, NJ) was 900 Units/mL.

Channel Designs

Simple microfluidic channel designs were selected to highlight the general utility of ATPS-mediated cell and reagent delivery. Laminar flow was generated using several flow focusing channels of varying geometries that were created using standard photolithographic and soft lithographic processes (McDonald et al. *2000*). The first of these designs was a flow focusing channel with three inlet channels and a main channel of 25 mm in length and either 1.5 or 1 mm in width, 0.1 mm in height. The width of the central channel in the hydrodynamically focusing geometry (PEG channel) was either 0.25 or 0.5 mm and could be used to adjust the width of the PEG divider stream in the main channel independent of volumetric flow rate. The second

design consisted of seven inlets with a 25 mm-long main channel, 1.5 mm wide and 0.1 mm in height. This device could be used to generate four laminar dextran streams separated by three PEG streams.

Droplet dispensing devices were created using backside photolithography and contained two dispensing orifices flanked by PEG focusing channels with a central PEG channel separating the two orifices (Futai et al. *2004*). PDMS replicas were bonded to 100 μm-thick PDMS membranes to permit Braille actuation at the orifices.

Cell Culture

The C2C12 myofibroblast cell line was used for all experiments. C2C12 cells were maintained in DMEM with 10%FBS in a humidified CO_2 incubator at 37°C. Cells were seeded in fibronectin-coated microfluidic devices at a final density of 20,000 cells/uL. Prior to seeding, cells were labeled with CellTracker dyes or Hoechst 33342 (both from Molecular Probes, Carlsbad, CA) as per manufacturer instructions and washed and centrifuged twice to remove excess dye. Cells were then suspended in dextran solutions and drawn into plastic syringes fitted with Tygon tubing to interface with microfluidic devices.

For laminar cell patterning, cells were seeded in the dextran phase into either three channel or seven channel devices with dextran/cell channels separated by PEG. Once two-phase laminar flow became stable, devices were disconnected from the flow sources and placed in a 37°C CO_2 incubator for 1 h to allow cells to attach. ATPS solutions were then replaced by cell culture medium and cells were incubated for an additional 24 h before microscopic analysis.

Islands of cells were seeded by way of Braille-actuated droplet formation in bell-shaped channels (Futai et al.*2004*; Gu et al. *2004*). FITC dextran was added to the cell dextran mixture to facilitate alignment of the dextran/cell dispensing orifices with the Braille actuation pins. Initial flow rates of 0.3 mL/h for PEG and 0.05 mL/h for dextran were used to establish laminar flow in Braille devices and clear the channels of loosely adherent cells that entered the channels during flow stabilization. This flow rate was gradually reduced to 0.15 mL for PEG and 0.002 mL/h for dextran to allow droplet formation to occur. Droplet size and spacing were controlled by modifying the Braille pin actuation interval and PEG/dextran flow ratio. After stable droplets containing cells were formed the channels were clamped shut at both upstream and downstream regions to arrest droplet movement. Cells were then allowed to attach to the channels for 1 h before the ATPS medium was replaced with culture medium.

Selective treatment of cells with biomolecules was demonstrated on cells cultured to confluence in laminar flow focusing devices. Trypsin was delivered to cells for 5 min. ATPS/trypsin treated regions were compared to both the non-treated side of the channel and channels treated with biomolecules dissolved in medium without the ATPS.

Staining, microscopy and statistical analysis

Cell-patterned devices were fixed in 4% paraformaldehyde after 24 h of culture and then washed twice with PBS. Devices used for biomolecule delivery were fixed immediately after treatment. Actin cytoskeleton staining was performed by staining cells with Alexa-568 phalloidin (Molecular Probes) as per manufacturer instructions. Nuclear staining was achieved by labeling cells with Hoechst 33342.

Imaging was performed on a Nikon SMZ 1500 stereoscope and Nikon TE300 inverted microscopes equipment with mercury excitation sources (Nikon, Tokyo, Japan). Image collection and analysis was performed using simple PCI (Hamamatsu, Sewickley, PA), Metamorph (Molecular Devices, Sunnyvale, CA) and Image J software. Statistical analyses were performed using SigmaPlot and SigmaStat (Systat Software, Chicago, IL)

5.3 Results and Discussion

Characteristics of ATPS flow in microchannels

ATPSs could be delivered as laminar streams using simple y-type or t-type channel designs. In contrast to laminar flow of polymer-free buffer solutions such as PBS, ATPS laminar flow required greater relative volumetric flow ratios of dextran to PEG to achieve similar channel occupancy of the laminar streams. The fractional channel occupancy differed for each phase systems due to viscosity differences between dextran and PEG which were dependent on both polymer concentration and molecular weight. Laminar streams of dextran and PEG could be differentiated based on the presence of discrete phase boundaries (Fig. 5.1(a)). As expected, molecules placed within one phase of the two-phase system were often strongly retained within that phase and displayed little diffusive dispersion in downstream channel regions as compared to PBS controls (Fig. 5.1(a-d)).

The lack of diffusive dispersion, due to molecule partitioning, is governed by specific energetic and affinity interactions between the molecules of interest and one or both of the phases(Albertsson *1972*). Red food colorant and Coomassie G250 both

partition almost exclusively to the PEG phase and clearly demonstrate that ATPS delivery in laminar streams can selectively confine chemicals to discrete channel regions more effectively than aqueous buffers alone (Fig. 5.1(c), (d)). Based on these initial observations, we sought to exploit ATPS partitioning properties to more effectively deliver both cells and bioactive molecules within microchannels. In order to more effectively control the delivery of these materials within channels we generated calibration curves for dextran/PEG channel occupancy as a function of volumetric flow ratio (Fig. 5.1(e)).

Patterning cells by ATPS laminar flow

Laminar flow of ATPS could be used to establish clear laminar patterns of adherent cell in t-type microchannels (Fig. 5.2(a-c)). By varying the number of inlet channels it was possible to establish up to four laminar streams for patterning adherent cells (Fig. 5.2(d), (e), (h)). By varying the width of the PEG spacing channel or by decreasing the dextran/PEG flow ratio it was possible to obtain cultures that displayed no gaps (Fig. 5.2(d), (h)), small gaps (Fig. 5.2(f)), or large gaps between cell populations. Using this method multiple populations of cells could be directly seeded into microchannels as laminar patterns. After devices were removed from the syringe lines cells attached to the channel surfaces within 1 h. Cells remained organized in their initial patterns for at least 24 h after seeding. We found that this method of cell delivery was compatible with both active pumping by syringe pump as well as gravity or capillary driven flow. Furthermore, ATPSs retained their patterns even after flow was removed, remaining laminar long enough for cells to sediment and begin attaching to the channels.

Laminar patterns of adherent cells will be useful for experiments that seek to investigate the interactions of multiple cell populations under flow conditions. Additionally, the ability to directly pattern gaps between populations of cells will facilitate in-channel migration assays.

Patterning islands of cells through forced ATPS droplet formation

Laminar cell patterning can be useful for a variety of migration and co-culture assays in which it is convenient for cells to be patterned on opposite sides of channels. However, some experiments may seek to explore radial migration phenomena and colony migration under flow conditions, or to observe effects of unidirectional signaling of soluble factors. Therefore, it will also be useful to pattern cells in additional configurations such as islands along the length of channels. This cannot be achieved by pulsatile flow of conventional aqueous solutions due to dispersion effects. However, ATPSs permits the formation of controlled dextran droplets surrounded by PEG. Cells are contained within the dextran droplets by the interfacial tension between the two polymer phases.

To control droplet formation, we used a computerized Braille microfluidic platform to valve bell shaped channels by way of pin actuation. This allowed us to control droplet size and spacing and to arrest the droplets for cell attachment to occur (Lai et al. *2011*). Using two actuation orifices, we were able to form alternating droplets of dextran within a PEG-filled channel (Fig. 5.3(a), (b)). After droplets were arrested in the channels, cells remained associated with the dextran phase (Fig. 5.3(b-d)). By alternating the actuation timing of the dextran channels we could rapidly produce alternating droplets containing different materials as indicated by the presence of alternating droplets containing either FITC or TRITC labeled dextran (Fig. 5.3(b)).

When cell tracker labeled C2C12 cells were incorporated into the dextran phase, alternating colonies of red and green Cell Tracker-labeled cells were observed that readily adhered to the channel surface (Fig. 5.3(c), (d)).

Selectivity of biomolecule delivery can be improved using ATPSs

Many biomolecules and particles partition within ATPSs to either dextran or PEG. Partitioning is influenced by the size of the molecule or particle, its charge, specific interactions with the phase-forming polymers, and properties related to phase system composition such as molecular weight of the polymers (Albertsson *1972*). Cells partition well in the dextran Mr 500,000 phase system; however, many biomolecules partition weakly to dextran in this phase system. Thus, in order to increase specificity for the dextran phase during delivery, we used dextrans of lower molecular weight and incorporated charged dextrans to interact electrostatically with the molecules of interest.

The effects of trypsin were more selective when ATPS was used as a delivery medium. Trypsin, a 23 kDa enzyme, can be used to rapidly dissociate cells from their substrate by cleaving a variety of proteins that mediate cell adhesion and has been used previously to remove cells within microfluidic channels (Takayama et al. *1999*; Nie et al. *2007*; Villa-Diaz et al. *2009*; van der Meer et al. *2010*). Trypsin exists primarily as a cationic protein, and thus we expected its selectivity for dextran to be enhanced through the addition of negatively charged dextran (CM-dextran). When an ATPS was used as the delivery medium, trypsin activity was confined exclusively to the dextran treatment phase (Fig. 5.4(a), (e), (g)). When a conventional aqueous delivery medium was used, cells on both sides of the channel were affected by trypsin, although cells on the treated side were more thoroughly dissociated (Fig. 5.4(b), (f),

(h)). The intensity profile of Hoechst-labeled cells served as a quantifiable measure of cell dissociation (Fig. 5.4(c), (d)). ATPS delivery resulted in a strict boundary, whereas conventional aqueous delivery resulted in a gradient effect (Fig. 5.4(c), (d)). This can be appreciated by measuring the slope of the signal intensity profile in the center of the laminar region of the channel (Fig. 5.4(d)). The effects of ATPS on trypsin selectivity could be readily observed both in upstream laminar regions (Fig. 5.4(e)) but also for laminar regions near the end of the channel (Fig. 5.4(g)).

Collectively these results demonstrate that ATPS delivery in microchannels is capable of more selective confinement of molecule to parts of microfluidic channels than is conventional aqueous delivery. This can result from several factors that influence selectivity. First the higher viscosity of the ATPS results in more limited diffusion than for other less viscous aqueous mediums. However, this factor alone cannot account for the apparent selectiveness of ATPS delivery. The most critical factor is the partitioning behavior of the ATPS. This will vary based on the molecule of interest and the composition of the ATPS, however most molecules partition to one phase or the other. Molecules that partition strongly to the dextran phase will be well maintained regardless of the flow rate or viscosity of the systems. Molecules that favor PEG can also be confined to half of the channel based on the configuration of the phase system. In this case molecules are confined to one side of the channel both by viscous-limitations to diffusion and active partitioning into a thin PEG divider. This concept is illustrated in Fig. 5.5.

Based on calculation for steady state diffusion from a semi-infinite source, we estimate that ATPS can perform at least twice as well as conventional laminar delivery under slow flow or arrested flow conditions (assuming only modest (kpart of

trypsin ~0.6) partitioning of molecules) (Takayama et al. *2003*; George et al.*2008*). If molecules display an even stronger preference for a single phase, this advantage is further enhance as a function of the partition coefficient. At higher flow rates we would expect the performance of the ATPS to be even better, although the advantage relative to conventional laminar flow becomes less dramatic. However, the only scenario in which ATPS does not provide enhanced selectivity is for molecules that distribute equally among phase, which rarely occurs.

5.4 Conclusions

We demonstrate that ATPSs can be used to compliment a variety of microfluidic techniques used to culture mammalian cells. We used both the interfacial and partitioning properties of the ATPS to enhance delivery of cells and molecules within microfluidic channels. For cell delivery we demonstrated that up to four populations of adherent cells can be patterned simultaneously. We also demonstrated that cells can be encapsulated within dextran droplets and delivered within PEG to produce patterns of small colonies or islands. Additionally, we achieved enhanced selectivity of chemical delivery to cells using an ATPS. This was accomplished for trypsin, and permitted more selective cell harvesting. We propose a model for selective delivery based on the viscosity of ATPS, partitioning behavior and configuration of the phases under laminar flow.

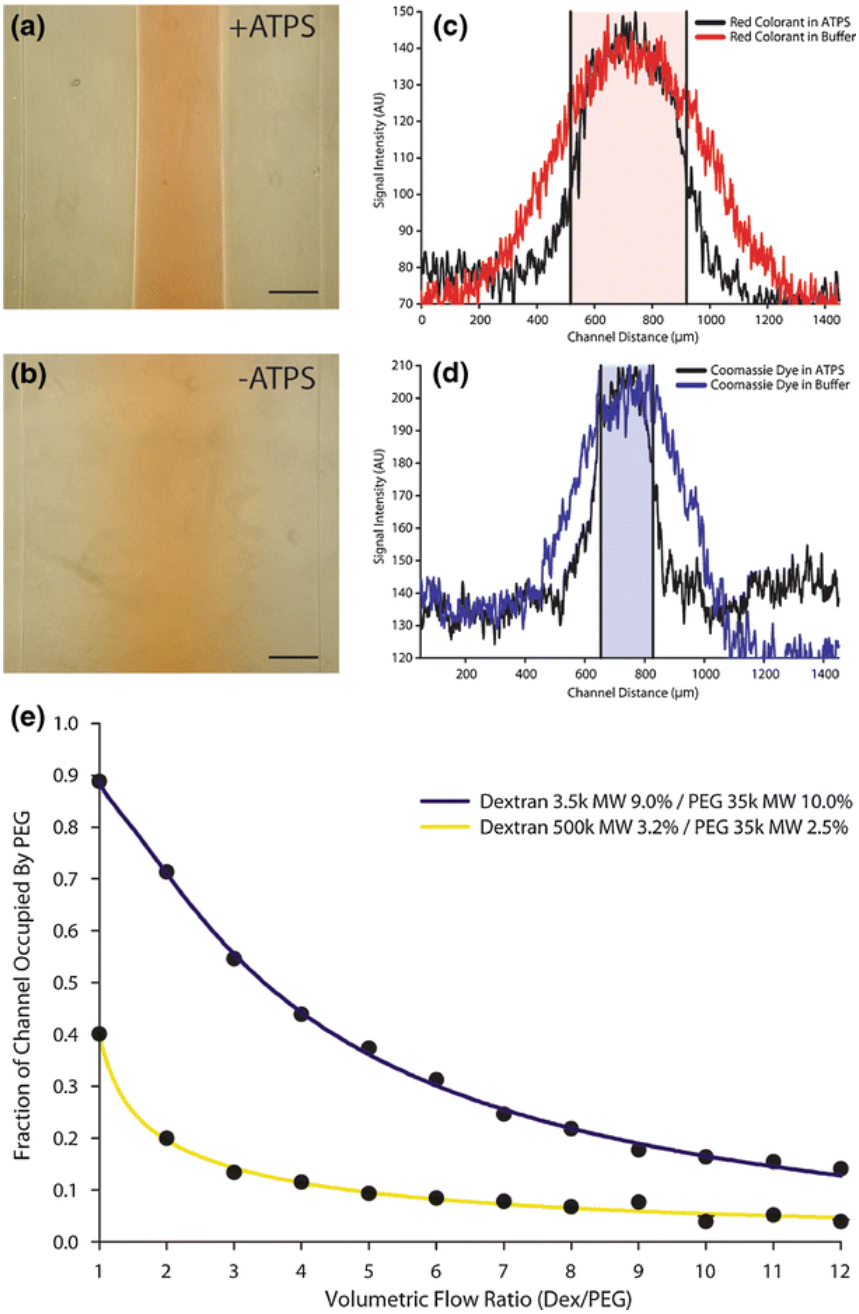

Fig. 5.1 Characteristics of ATPS flow in Microchannels. (**a**). An ATPS displays a clear phase boundary when delivered as laminar streams within a PDMS-glass microchannel. Food colorants are clearly retained in PEG within the phase boundary. (**b**). Buffer solution do not display partitioning and have no phase boundary. Molecules diffuse laterally as laminar streams move through the channel. The diffusion characteristics of red food colorant (**c**) and Coomassie G250 (**d**) were plotted based on intensity of dye across the channel. The shaded regions of these plots correspond to the actual channel occupancy of the stream immediately downstream from the channel junction. ATPS solutions maintain a strict boundary at regions further downstream whereas buffers allow molecules to diffuse from these regions. (**e**). Example of volumetric flow calibration curve used to determine fractional channel occupancy for different PEG-dextran flow conditions. Scale bar = 250 um, $n = 3$ observations

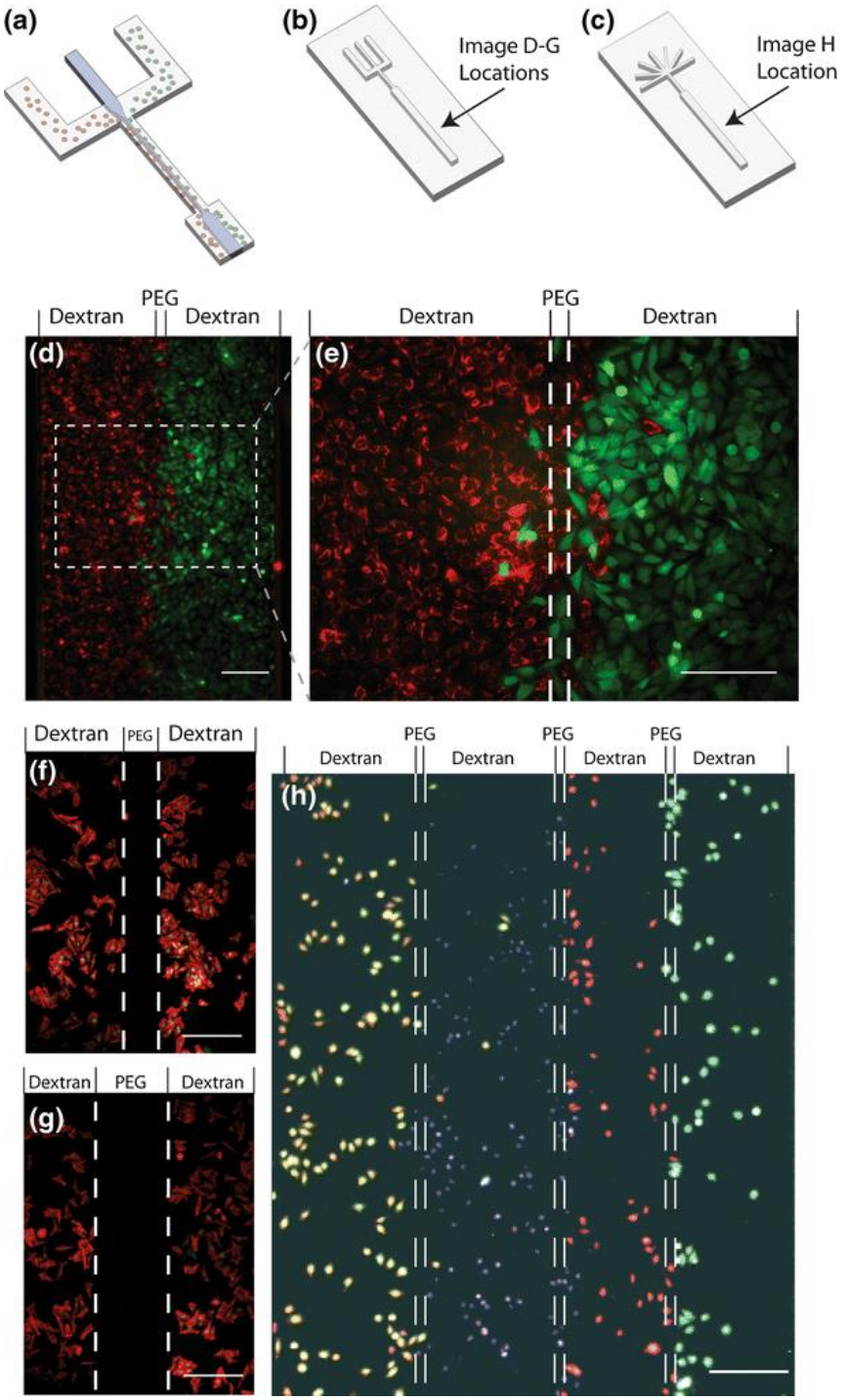

Fig. 5.2 Precise laminar patterns of adherent cells can be generated through ATPS laminar flow patterning. (**a**). Schematic of cell delivery in dextran with a central PEG spacer. (**b**). A two cell-type device design. (**c**). A four cell-type device design. (**d-e**). Two populations of C2C12 cells labeled with cell tracker green and cell tracker red were patterned using the minimum PEG spacer. (**f-e**). By using devices of different PEG channel width it is possible to change the gap between cell populations using identical volumetric flow conditions as evidence by actin-phalloidin staining of fixed patterned cells. (**h**). it was demonstrated that up to 4 cell populations can be patterned simultaneously. Patterned cells were pre-stained with green cell tracker, red cell tracker, red and green cell tracker, or Hoechst 33342. Scale bar = 250 um

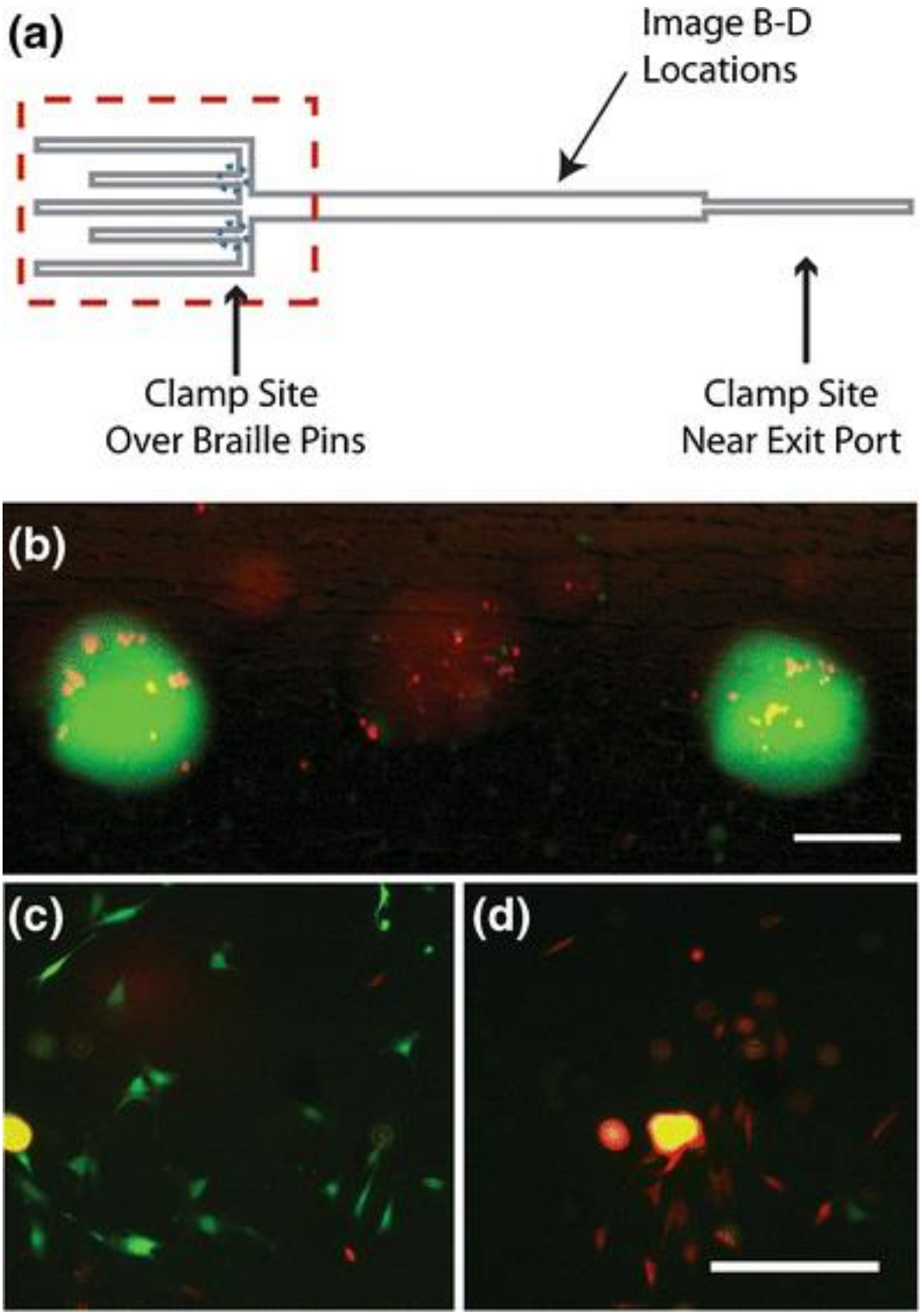

Fig. 5.3 Braille microfluidics can be used to directly pattern islands of cells by way of forced ATPS droplet formation. (**a**). Schematic of a Braille device with sites of actuation (*blue marks*) and clamp sites for arresting flow (*black arrows*). (**b**). Using alternating actuation of Braille orifices it is possible to deliver alternating droplets of dextran within PEG, as evidenced by several consecutive droplets containing either TRITC-dextran (*red*) or FITC-dextran (*green*) (**c**-**d**). When cells are incorporate into droplets it is possible to deposit alternating islands of cells that remain patterned for at least 24 h after adhering. Scale bar = 100 um

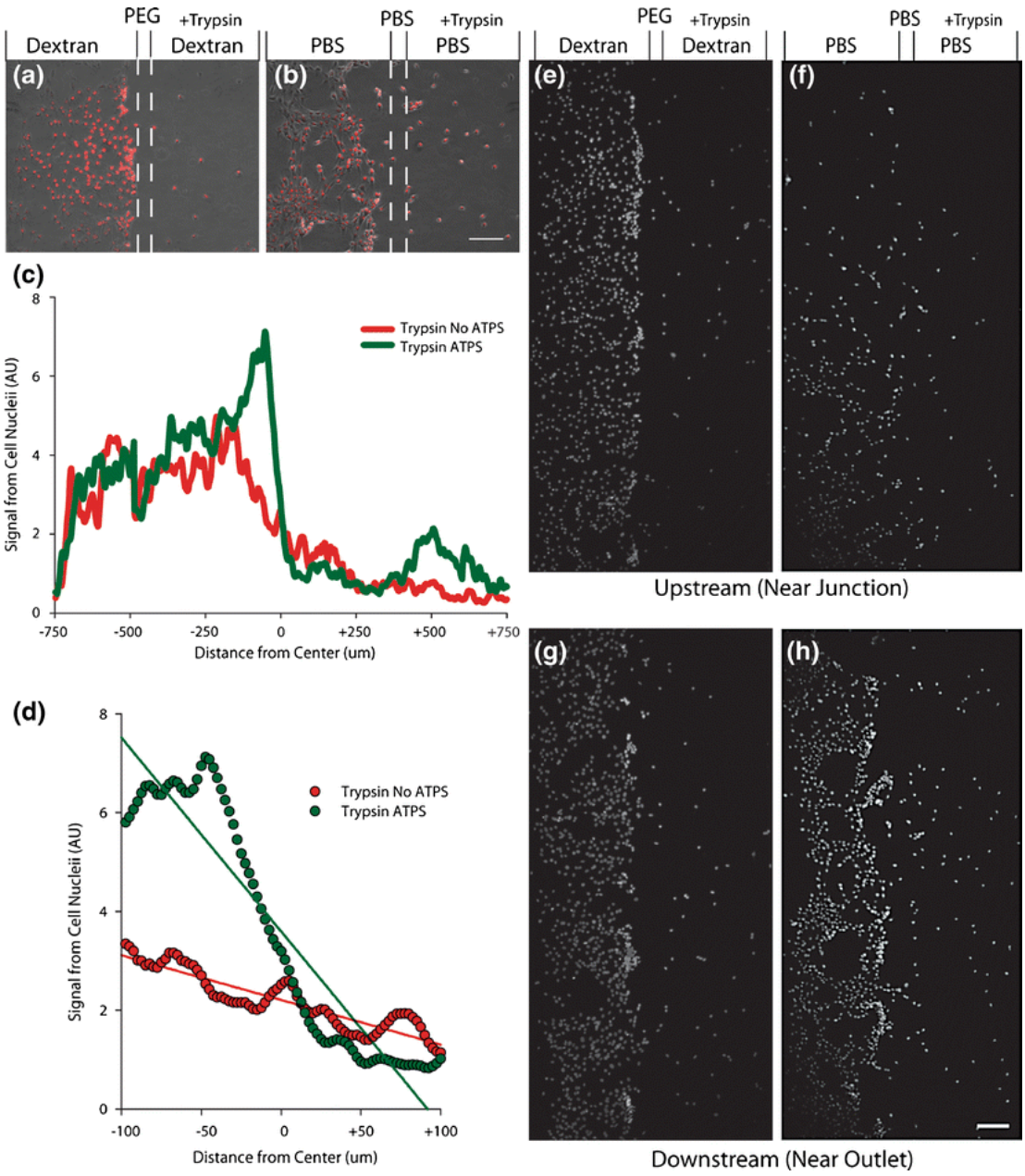

Fig. 5.4 Trypsin delivery is well confined by ATPSs. (**a**). Representative image of Phase Contrast/Hoechst-labeled cells following ATPS delivery of trypsin on the right side of the channel. (**b**). Representative image of aqueous delivery of trypsin showing effects on both sides of the channel. (**c**-**d**). Intensity profiles reveal a clear boundary for ATPS delivery and a gradient effect for aqueous delivery. (**e**-**h**). Boundaries are maintained in both upstream and downstream channel regions for ATPS delivery whereas aqueous delivery shows a gradient effect across the width of the channel that is apparent in all channel regions. Scale bar = 200 um, $n = 3$ observations, curves plotted as means

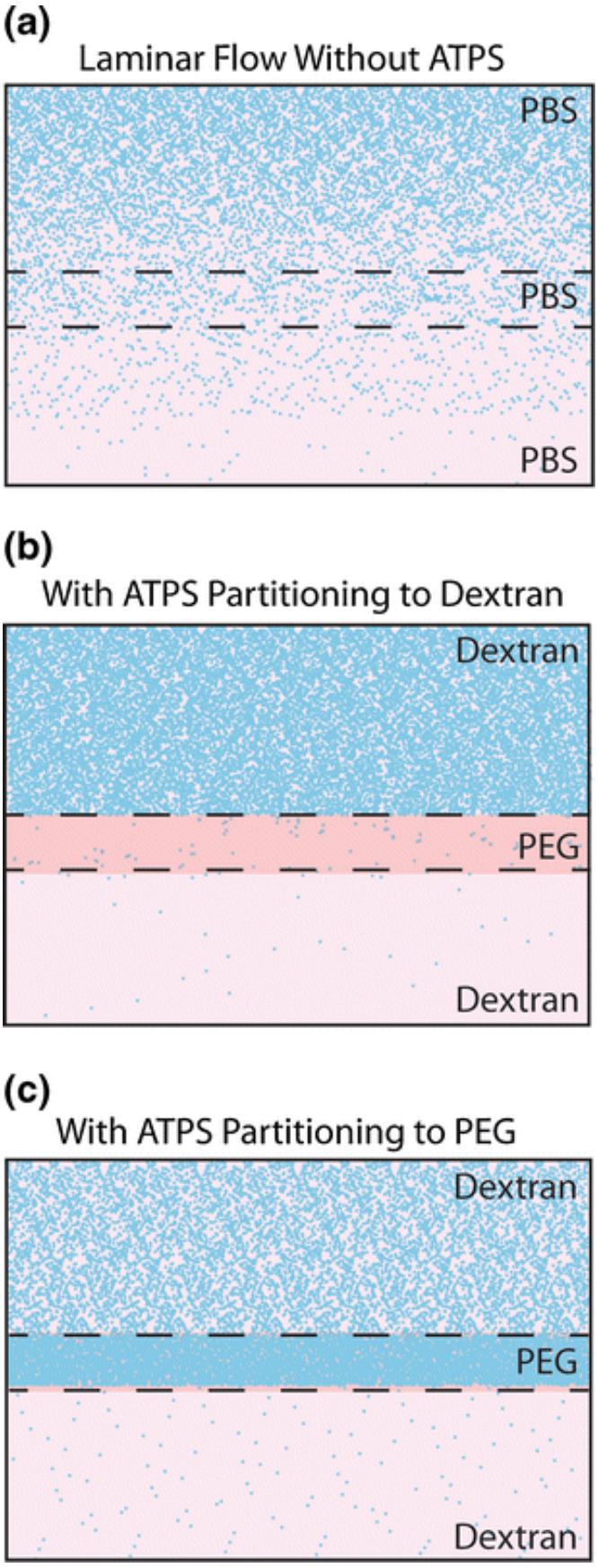

Fig. 5.5 Molecule or particle localization under various ATPS flow conditions.

5.5 References

P.A. Albertsson, *Partition of Cell Particles and Macromolecules* (Wiley, New York, 1972)

E. Berthier, J. Warrick, et al., Pipette-friendly laminar flow patterning for cell-based assays. Lab Chip. (2011)

A.M. Bilek, K.C. Dee et al., Mechanisms of surface-tension-induced epithelial cell damage in a model of pulmonary airway reopening. J. Appl. Physiol. **94**(2), 770–783 (2003)

A. Bransky, N. Korin et al., Experimental and theoretical study of selective protein deposition using focused micro laminar flows. Biomed. Microdevices **10**(3), 421–428 (2008)

E. Brouzes, M. Medkova et al., Droplet microfluidic technology for single-cell high-throughput screening. Proc. Natl. Acad. Sci. U.S.A. **106**(34), 14195–14200 (2009)

N. Futai, W. Gu, S. Takayama, Rapid prototyping of microstructures with bell-shaped cross-sections and its application to deformation-based microfluidic valves. Adv. Mater. **15**, 1320–1323 (2004)

A. George, F. Truskey, Y. David, F. Katz, *Transport Phenomena in Biological Systems*, (Prentice Hall, 2008)

W. Gu, X. Zhu et al., Computerized microfluidic cell culture using elastomeric channels and Braille displays. Proc. Natl. Acad. Sci. U.S.A. **101**(45), 15861–15866 (2004)

P. Guillot, A. Colin, Stability of parallel flows in a microchannel after a T junction. Phys. Rev. E Stat. Nonlin. Soft Matter Phys. **72**(6 Pt 2), 066301 (2005)

T. Hahn, S. Hardt, Size-dependent detachment of DNA molecules from liquid–liquid interfaces. Soft Matter, epub ahead of print (2011)

T. Hahn, G. Munchow et al., Electrophoretic transport of biomolecules across liquid-liquid interfaces. J. Phys. Condens. Matter **23**(18), 184107 (2011b)

A. Jovic, B. Howell et al., Phase-locked signals elucidate circuit architecture of an oscillatory pathway. PLoS Comput. Biol. **6**(12), e1001040 (2010)

D. Lai, J.P. Frampton, et al, *Rounded Microchannels with Constrictions Made in One Step by Backside Diffused Light Lithography Enables Aqueous Two-Phase System Droplet Microfluidics*. In Submission. (2011)

W. Liu, L. Li et al., An integrated microfluidic system for studying cell-microenvironmental interactions versatilely and dynamically. Lab Chip **10**(13), 1717–1724 (2010)

E.M. Lucchetta, J.H. Lee et al., Dynamics of Drosophila embryonic patterning network perturbed in space and time using microfluidics. Nature**434**(7037), 1134–1138 (2005)

J.C. McDonald, D.C. Duffy et al., Fabrication of microfluidic systems in poly(dimethylsiloxane). Electrophoresis **21**(1), 27–40 (2000)

K.H. Nam, W.J. Chang et al., Continuous-flow fractionation of animal cells in microfluidic device using aqueous two-phase extraction. Biomed. Microdevices **7**(3), 189–195 (2005)

F.Q. Nie, M. Yamada et al., On-chip cell migration assay using microfluidic channels. Biomaterials **28**(27), 4017–4022 (2007)

J. Olofsson, H. Bridle et al., Direct access and control of the intracellular solution environment in single cells. Anal. Chem. **81**(5), 1810–1818 (2009)

B. Regenberg, U. Kruhne et al., Use of laminar flow patterning for miniaturised biochemical assays. Lab Chip **4**(6), 654–657 (2004)

A. Sawano, S. Takayama et al., Lateral propagation of EGF signaling after local stimulation is dependent on receptor density. Dev. Cell **3**(2), 245–257 (2002)

J.R. Soohoo, G.M. Walker, Microfluidic aqueous two phase system for leukocyte concentration from whole blood. Biomed. Microdevices **11**(2), 323–329 (2009)

S. Takayama, J.C. McDonald et al., Patterning cells and their environments using multiple laminar fluid flows in capillary networks. Proc. Natl. Acad. Sci. U.S.A. **96**(10), 5545–5548 (1999)

S. Takayama, E. Ostuni et al., Selective chemical treatment of cellular microdomains using multiple laminar streams. Chem. Biol. **10**(2), 123–130 (2003)

H. Tavana, A. Jovic et al., Nanolitre liquid patterning in aqueous environments for spatially defined reagent delivery to mammalian cells. Nat. Mater.**8**(9), 736–741 (2009)

S.Y. Teh, R. Lin et al., Droplet microfluidics. Lab Chip **8**(2), 198–220 (2008)

Y.S. Torisawa, B. Mosadegh et al., Microfluidic platform for chemotaxis in gradients formed by CXCL12 source-sink cells. Integr. Biol. (Camb.) **2**(11–12), 680–686 (2010)

M. Tsukamoto, S. Taira et al., Cell separation by an aqueous two-phase system in a microfluidic device. Analyst **134**(10), 1994–1998 (2009)

A.D. van der Meer, K. Vermeul et al., A microfluidic wound-healing assay for quantifying endothelial cell migration. Am. J. Physiol. Heart Circ. Physiol. **298**(2), H719–H725 (2010)

K. Vijayakumar, S. Gulati, A.J. de Mello, J.B. Edel, Rapid cell extraction in aqueous two-phase microdroplet systems. Chem. Sci. **1**, 447–452 (2010)

L.G. Villa-Diaz, Y.S. Torisawa et al., Microfluidic culture of single human embryonic stem cell colonies. Lab Chip **9**(12), 1749–1755 (2009)

S.T. Wei-Heong Tan, Monodisperse alginate hydrogel microbeads for cell encapsulation. Adv. Mater **19**, 2696–2701 (2007)

M.H. Wu, S.B. Huang et al., Microfluidic cell culture systems for drug research. Lab Chip **10**(8), 939–956 (2010)

M. Yamada, V. Kasim et al., Continuous cell partitioning using an aqueous two-phase flow system in microfluidic devices. Biotechnol. Bioeng. **88**(4), 489–494 (2004)

E.W. Young, D.J. Beebe, Fundamentals of microfluidic cell culture in controlled microenvironments. Chem. Soc. Rev. **39**(3), 1036–1048 (2010)

B. Zheng, J.D. Tice, R.F. Ismagilov, Formation of arrayed droplets by soft lithography and two-phase fluid flow and application in protein crystallization. Adv. Mater. **16**(15), 1365–1368 (2004)

I. Ziemecka, V. van Steijn et al., Monodisperse hydrogel microspheres by forced droplet formation in aqueous two-phase systems. Lab Chip **11**(4), 620–624 (2011)

Chapter 6

Simple multi-level microchannel fabrication by pseudo-grayscale backside diffused light lithography

Photolithography of multi-level channel features in microfluidics is laborious and/or costly. Grayscale photolithography is mostly used with positive photoresists and conventional front side exposure, but the grayscale masks needed are generally costly and positive photoresists are not commonly used in microfluidic rapid prototyping. Here we introduce a simple and inexpensive alternative that uses pseudo-grayscale (pGS) photomasks in combination with backside diffused light lithography (BDLL) and the commonly used negative photoresist, SU-8. BDLL can produce smooth multi-level channels of gradually changing heights without use of true grayscale masks because of the use of diffused light. Since the exposure is done through a glass slide, the photoresist is cross-linked from the substrate side up enabling well-defined and stable structures to be fabricated from even unspun photoresist layers. In addition to providing unique structures and capabilities, the method is compatible with the "garage microfluidics" concept of creating useful tools at low cost since pGS BDLL can be performed with the use of only hot plates and a UV transilluminator: equipment commonly found in biology labs. Expensive spin coaters or collimated UV aligners are not needed. To demonstrate the applicability of pGS BDLL, a variety of weir-type cell traps were constructed with a single UV exposure to separate cancer

cells (MDA-MB-231, 10–15 μm in size) from red blood cells (RBCs, 2–8 μm in size) as well as follicle clusters (40–50 μm in size) from cancer cells (MDA-MB-231, 10–15 μm in size).

6.1 Introduction

The direction of microfluidics as a field is toward more complex operations, and complexity embedded within the device design is especially attractive. Multi-level channel designs have useful applications in microfluidic devices to embed complex operations into the device while insulating the complexity from the user (no need for additional external controls and robust function). Such multi-level channel designs have been used for chaotic mixers,[1] weir-type cell traps for cell isolation,[2] and weir-type cell traps for cell fusion.[3] The lack of moving parts allows for simple operation, however typical applications of such microfluidic devices necessitate the rapid-prototyping process to be quick and cost efficient.

Fabrication of multi-level channel features in microfluidics typically requires multiple exposures where each layer is serially spun, each photomask precisely aligned, and exposed by ultraviolet (UV) light. Alternative methods of producing multi-level channels such as hot embossing,[4] erosion,[5] etching,[6] laser fabrication,[7] photoresist reflow,[8] micro-milling,[9] 3D-printing,[10] electroplating,[11] deformable molds,[12] and liquid molding[13] are also laborious and/or require specialized equipment.

The intrinsic limitation of typical photomask-based photoresist patterning methods is the binary nature of an all-or-none illumination of exposed areas. Thus, many

groups have used grayscale photomasks to generate a range of illumination densities using a single exposure. Grayscale photolithography suffers from high costs because grayscale photomasks are generated using scanning lasers,[14] ultra-high resolution binary masks,[15] variable Inconel deposition on glass,[16] or High-Energy Beam Sensitive (HEBS) glass.[17] Low-cost alternatives to grayscale photolithography are complex, requiring the use of a microfluidic photomask.[18]Most grayscale photolithography use positive photoresists[14–18] that are less common in microfluidic device fabrication. Negative photoresists have been used in conjunction with grayscale exposure techniques, however the resulting channels were of low resolution and on the order of milimetres.[19] Others have used negative photoresists for multi-level photolithography with the use of 3D diffusers[20] and digital micro-mirror devices.[21] However each study was either unable to fabricate multi-level features independent of feature width in a single exposure or required a relatively sophisticated semiconductor mask that may deter non-microfluidic scientists from adopting microfluidic technology. BDLL has been used to create microfluidic devices with bell-shaped cross-section microchannels[22] and multi-layered orifices with disconnected photomask features.[23] While this technology has been capable of fine control of short-range tapering and orifice heights, the method has lacked the ability to sustain long channels of varying height. BDLL with pGS photomasks overcomes this shortcoming while maintaining cost-effectiveness and simplicity for the fabrication of microfluidic devices in a single UV exposure.

Cell separation by size is applicable to cancer research for uses including identification of metastatic cancer cells in blood[24] and separation of cancer cells from follicles in oncofertility preservation for young women.[25,26] We use pGS BDLL as a

tool to create multi-level weir-type cell traps using only equipment commonly found in many biology labs. This technology increases the accessibility of microfluidics, making a powerful and ever-expanding tool chest of experimental techniques available to more researchers in multiple fields.

6.2 Materials and Methods

Characterization of pGS BDLL

pGS masks were printed by CAD/Art Services (Bandon, OR) at 20 000 DPI. Individual pseudo-gray areas were created using an isotropic pattern of binary opaque and transparent 10 by 10 μm squares (Fig. 6.1a). With such patterns, areas of 100%, 25%, 19.8%, 16%, 13.2%, 11.1%, 9.5%, 8.2%, 7.1%, 6.2%, 5.5%, 4.9%, 4.4%, 4%, 3.6% and 3.3% transparent were printed at channel width and length dimensions between 10^2 and 10^4 μm on the photomask for pGS BDLL.

Device fabrication and channel characterization

pGS masks with varying per cent transparent areas were used for BDLL as described previously[22,23] and illustrated in Fig. 6.1b. Negative photoresist (SU-8 2075 and 2025, MicroChem, Newton, MA) was deposited on coverglass slides at 50 μm, 100 μm, and 200 μm with a spin coater and SU-8 2075 was also deposited onto the same coverglass slides (Fisher Scientific, Waltham, MA) without the use of a spin coater to produce a 1200 μm thick layer of photoresist (Fig. 6.1c).

Each thickness and per cent transparent condition was exposed at four durations: 90 s, 135 s, 180 s, and 225 s on an 8 mW cm^{-2} UV illuminator (816A Ultraviolet

Transilluminator, Fisher Scientific, Waltham, MA) to demonstrate the effect of per cent transparent and exposure time and spin/unspun height on resultant channel height on the SU-8 mold. Soft bake, and post exposure bake conditions were controlled according to spin height per manufacturer recommendations. In the unspun condition, since there was no manufacturer recommendation, a soft bake of 15 min at 65 °C and 90 min at 95 °C and a post exposure bake of 10 min at 65 °C and 30 min at 95 °C was used.

Conventional soft lithography was used on these SU-8 molds to produce polydimethylsiloxane (PDMS, Dow Corning, Midland, MI) devices. The resultant PDMS channel heights were determined using light microscopy as well as fluorescence microscopy of channels filled with 0.01% fluorescein as previously described.[23]

MDA-MB-231 cancer cell transfection and cell culture

We previously described MDA-MB-231 human breast cancer cells stably transduced with green fluorescent protein (GFP).[31] Growth media consisted of Dubelco's Modified Eagle Medium supplemented with 10% fetal bovine serum and 1% antibiotic–antimycotic (Life Technologies, Carlsbad, CA). Upon confluence, cells were washed with phosphate buffered saline, trypsinized, resuspended in growth medium, and used in experiments at the concentrations specified.

Enzymatic digestion of ovarian tissue and follicle isolation

For all experiments, we isolated ovaries from 6–8 days old female mice F1 CBA/JxC57BL/6N. Ovaries were extracted and separated from the connective tissues and enzymatically digested in 20 μL (13 Wünsch units per mL) liberase DH (Roche,

Indianapolis, IN) in 500 μL L15 (Leibovitz's) media (Sigma-Aldirch, St. Louis, MO). The total digestion time was 1 h at 30 °C and every 15 min, enzyme digested pieces were dispersed by gentle pipetting to isolate follicles.[32] The enzyme digestion was arrested by adding 10% serum and the suspension of the follicles and stromal cells were concentrated to a small volume. Five thousand cancer cells (5 μL of 10^6 mL^{-1} suspension) were added to the follicle-stromal cell suspension to mimic the scenario of cancer cell contaminated tissue. A dramatically higher amount of cancer cells than what is clinically expected was used to facilitate calculation of isolation efficiency.

Red blood cell, cancer cell and follicle sorting

Cells and follicles were sorted using multi-level channels to produce weir-type traps. Devices were fabricated using pGS BDLL with channel heights of 58 μm and weir-type traps of 21 to 8 μm in height for blood sorters and channel heights of 120 μm and 20 μm traps for the follicle sorters. Blood sorting devices were passively driven using a 3 cm positive height differential. The effectiveness of the weir-type trap can be qualitatively observed by MDA-MB-231 cancer cells (at 0.5×10^6 cells mL^{-1}) trapped within the channel while the RBCs (at 2×10^6 cells mL^{-1}, Lampire, Pipersville, PA) are freely allowed to pass through. Follicle sorting devices were driven passively in the form of a suction channel by a 7 cm negative height differential on the opposing end of the weir-type trap to filter 500 μL L15 medium containing ovarian follicles and cancer cells followed by 500 μL L15 media containing no cells to flush most remaining cells and debris through the follicle trap. Ovarian follicles were extracted by reversing the height differential between the inlet and the outlet and collecting ovarian follicles from the inlet in which they were introduced.

6.3 Results and Discussion

Characterization of pGS BDLL

pGS BDLL is capable of producing multi-level microfluidic devices at superior levels of cost-efficiency and simplicity over conventional photolithography, alternative multi-level fabrication techniques and previous grayscale photomask technologies. A relatively low-cost, low-resolution photomask printed on transparency sheets was used to create an isotropic pattern of binary opaque and transparent 10 by 10 μm squares to produce channels of different heights by BDLL with SU-8 negative photoresist (Fig. 6.1a and b). This same technique was also demonstrated using unspun layers of SU-8 approximately 1200 μm thick (Fig. 6.1c).

Of note, the rough surface of the unspun SU-8 yields smooth and uniform features (Fig. 6.1d) comparable to traditional photolithography masters. This is made possible by the relatively small effect of film height on resultant channel height especially for very thick SU-8 films (1200 μm) where even substantial (~100 μm) differences in film thickness have negligible effect on resultant channel height. Since UV light exposes the photoresist through the substrate in BDLL, a low amount of UV light is used such that the depth penetration of the UV light is small relative to the film thickness. The roughness of the film surface opposite of the UV light source has no effect on the resultant microchannel. As the UV light is uniformly and carefully controlled with the pGS photomask, uniform channel features can be fabricated from an unspun photoresist layer even with an extremely rough surface. A high-magnification SEM image of the resultant SU-8 molds (Fig. 6.2) to demonstrate

flatness of resultant channels. At 1200× magnification, it becomes clear that the surface contains dimple-shaped imperfections. The random manner of the imperfections suggests that they arise from UV light diffracted by dust and/or scratches on the UV transilluminator, quartz glass and/or coverglass and not from the repeating binary pattern of opaque and transparent squares.

To demonstrate the utility of pGS BDLL over conventional photolithography, we produced a device to separate red blood cells (RBC) from cancer cells (MDA-MB-231) using nine different levels of per cent transparent to produce an array of weir-type traps of eight different heights (one source channel height and eight weir-trap heights). The equivalent sorter device developed using conventional lithography would require 9 layers of photoresist deposition involving 5 different types of SU-8 photoresist (2075, 2025, 2005, 2002, and 2000.5) and 9 individual spin coating cycles, pre-exposure bakes, UV exposure, and post-exposure bakes.

Fabricated channel height can be finely controlled down to 8 μm by a combination of per cent transparent area of the pGS mask as well as the exposure time of the UV transilluminator. Furthermore, devices designed for cell sorters were fabricated using unspun SU-8 without the use of spin coaters. The effect of exposure time was characterized for each spin height and unspun photoresist thicknesses for 100% transparent photomasks (Fig. 6.3). Our findings show a relationship between exposure time and channel height and is in agreement with manufacturer specifications for suggested exposure times for conventional photolithography. We discovered that the resultant channel heights are somewhat dependent on film thickness especially at thinner film thicknesses but independent of over-baking during post-exposure bake (data not shown). The effect of pGS BDLL was further characterized by analysing the

effect of per cent transparent pGS photomasks for each photoresist thickness and exposure time. Together, these two parameters determine the exposure energy according to eqn (1): $E_{Total} = I_{UV}*T*t$, where E_{Total} is the total exposure energy [mJ cm^{-2}], I_{UV} is the intensity of the UV light source [mW cm^{-2}], T is the transparent fraction of the mask [unitless], and t is the exposure time [sec]. For a given film thickness (even unspun layers), exposure energy can be modulated to generate a wide range of feature sizes in a reproducible fashion (Fig. 6.4).

The usefulness of microfluidics for biological applications is clear, however, the adoption of microfluidic tools by biology labs is stunted by the need for specialized photolithography equipment such as spin coaters and collimated UV light aligners.[27] The characterization of pGS BDLL for the fabrication of microfluidic in this work makes sophisticated multi-level device fabrication accessible to a wide array of biology labs. pGS BDLL only requires hot plates and a UV transilluminator: equipment normally used for DNA and protein analysis and common to most biology labs. The adjustability of pGS BDLL was used to construct weir-type traps for two cell separation applications requiring distinctly different ranges of channel heights.

Cell sorting of MDA-MB-231 cancer cells from red blood cells (RBCs)

Blood analysis of cancer patients for circulating tumour cells (CTCs) is an active area of research with potential for advanced prognosis and identifying individual-specific therapeutic response.[28–30] As such, the effective use of microfluidics for the rapid detection of CTCs within patient blood has high potential to be a cost-effective method toward fast and individualized patient care.

Motivated by future applications in analyses of blood samples from cancer patients, we used pGS BDLL to generate a mold for soft lithography to produce multiple multi-level PDMS channels simultaneously and inexpensively. A prepared mixture of red blood cells and breast cancer cells were passed through a device with multiple types of weir structures with different sized traps to screen for the optimal structure where cancer cells could be trapped but red blood cells pass through. The effectiveness of the cancer cell trap diminished as the weir-type trap size increased from 8 to 21 μm, where it can no longer trap cells of similar size (Fig. 6.5).

Cell sorting of murine follicles from stromal cells and MDA-MB-231 cancer cells

Cell-size based separation of different cell types poses a potential application in the field of fertility preservation in cancer survivors. Ovarian tissue can be removed prior to the whole body exposure to toxic chemotherapy, cryopreserved and later transplanted back to the patient to restore fertility. The major drawback of the tissue autotransplantation is the potential risk of reintroduction of cancer cells back to the patient. Ovarian follicles, the functional units of the ovary, can be mechanically or enzymatically isolated from other cell types and transplanted back to the patient as a pure population of the reproductive units using current tissue engineering techniques. With future potential applications of clinical treatment-scale separation of ovarian follicles from cancer cells as a motivation, we used pGS BDLL to create a mold with a wide structure for soft lithography to produce a PDMS device with increased separation capacity to isolate the large ovarian follicles from the smaller cancer cells.

Our design was effective at sorting of follicles from stromal and cancer cells. In these trials, 88% of the cancer cells were removed while 84% of ovarian follicles were recovered, as shown from examination of cell mixture before and after sorting

by a microfluidic device (Fig. 6.6). Our experimental observations suggest a fraction of cancer cells failed to be isolated from follicles due to the cancer cells adhering to the extracellular matrix around the follicles. More experimentation will reveal the collagenase and liberase activity for the optimum cancer cell removal. In a clinically relevant scenario, we anticipate that an 88% contaminant removal may be enough to eliminate all cancer cells.

Disadvantages of pGS BDLL

Despite ease of fabrication of multi-level microchannels using pGS BDLL, it is difficult to stably fabricate microchannel features of width and length <100 μm. Due to the lower adhesion of SU-8 to the glass substrate relative to conventional silicon wafers, features of aspect ratio <1 are easily washed off during development process. Finally, although it is possible to fabricate multi-level microfluidic devices with unspun SU-8 films, the process uses a large amount of negative photoresist. Long and frequent use of pGS BDLL for device fabrication will eventually justify the purchase of a spin coater to decrease SU-8 usage per device fabricated.

6.4 Conclusions

Despite the proven usefulness of microfluidics for biological applications, its widespread use is still deterred by the need for specialized equipment needed for photolithography. This work demonstrates a microfluidic device fabrication technique using only equipment commonly found in biology labs. Furthermore, we show the ability of pGS BDLL to fabricate sophisticated multi-level devices that are otherwise highly laborious to create using conventional photolithography. To explore potential

cancer research applications as well as to demonstrate the range of structures pGS BDLL is capable of creating, we developed two application specific devices. One is a device with multi-channel, multi-height narrow weir-type traps that can screen designs that are best for trapping metastatic cancer cells in blood while letting red blood cells flow through. Another is a large-width weir-type trap for the isolation of follicle clusters from a mixture that contains unwanted stromal and cancer cells. While our demonstrations focused only on cancer diagnosis and oncofertility preservation, the technique should be broadly useful anywhere rapid prototyping of multi-height microstructures is needed.

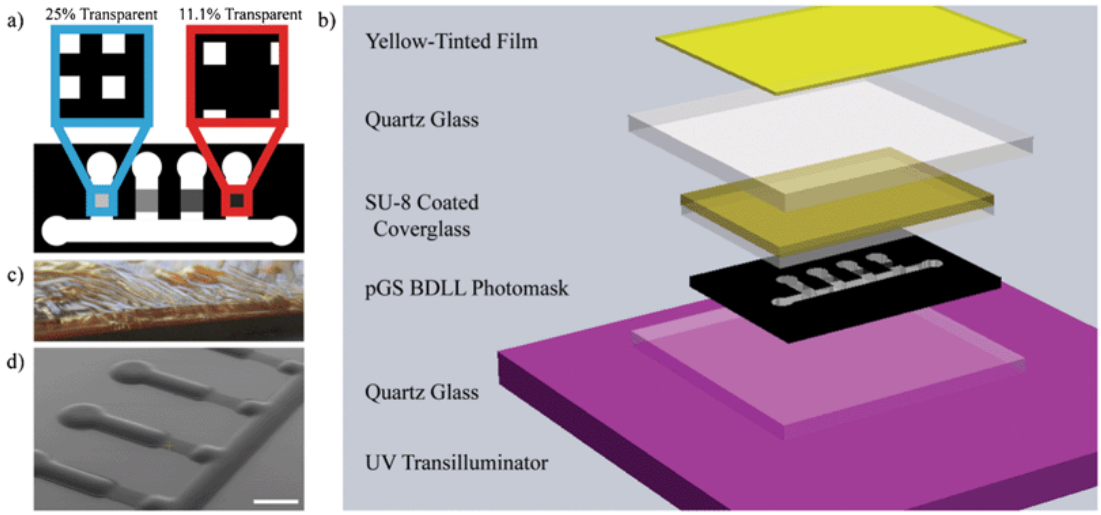

Fig. 6.1 a) pGS photomask. Binary patterns of transparent/opaque squares produce different levels of "gray". Transparent squares are 10 μm by 10 μm. b) Schematic of BDLL. UV light from the UV transilluminator passes through the pGS photomask and glass substrate to expose SU-8 to produce rounded channels of different height depending on how much energy is allowed to pass through the pGS photomask. c) Unspun layer (1200 μm) of SU-8 on glass slide. The surface is crude, normally ineffective for conventional photolithography. d) However, an unspun layer of SU-8 can be used to reliably fabricate multi-layered microfluidic channels using pGS BDLL. SEM image of resultant SU-8 molds. Scale bar: 1 mm.

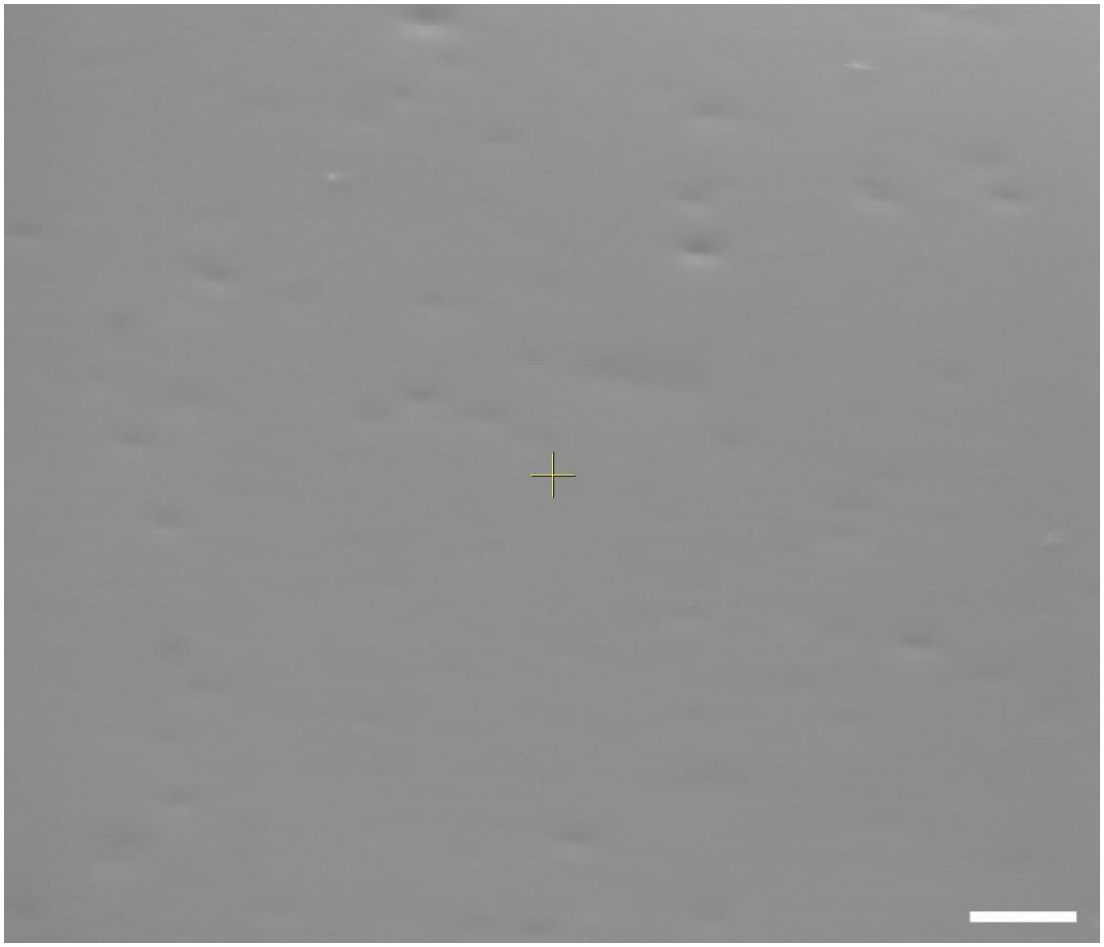

Fig. 6.2 SEM image of a 24 μm tall channel using unspun SU-8 at 8.16% transparent and 225s of UV exposure. Scale Bar: 20 μm

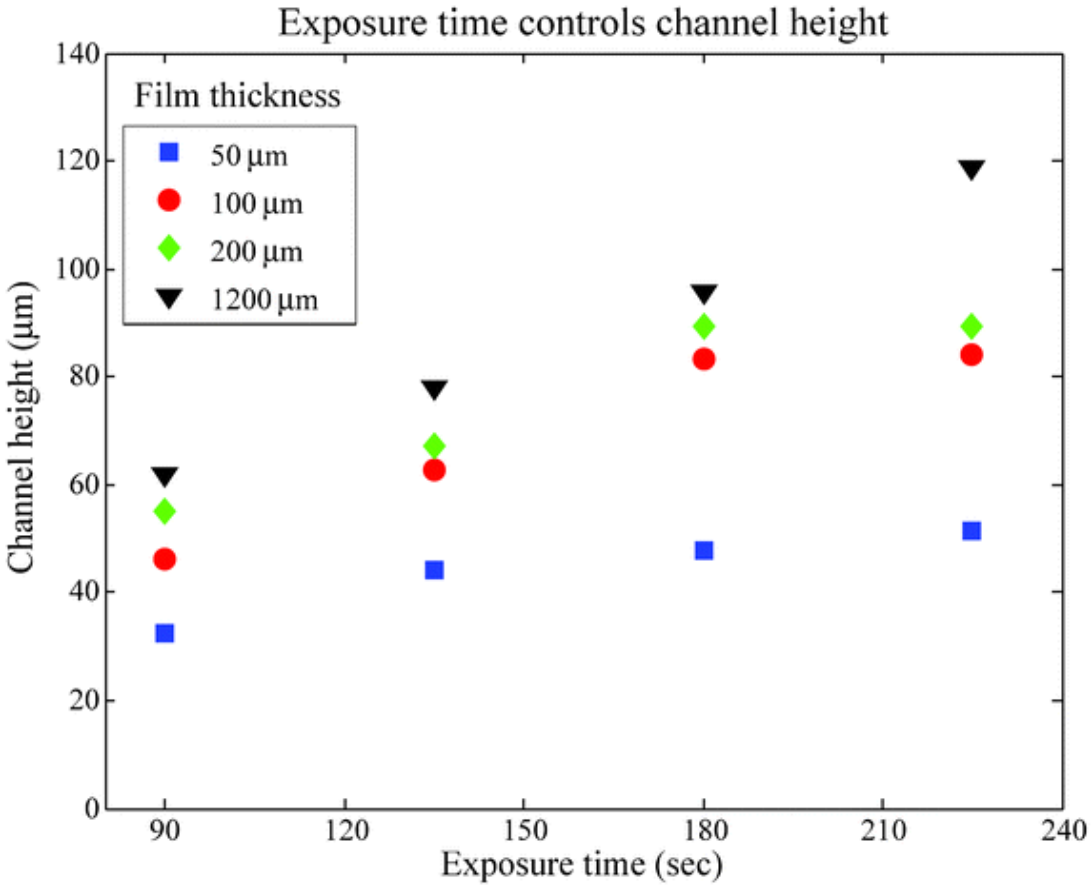

Fig. 6.3 Using 100% transparent photomasks, different heights can be generated by changing exposure time. The resultant channel height from BDLL is also dependent on SU-8 film thickness.

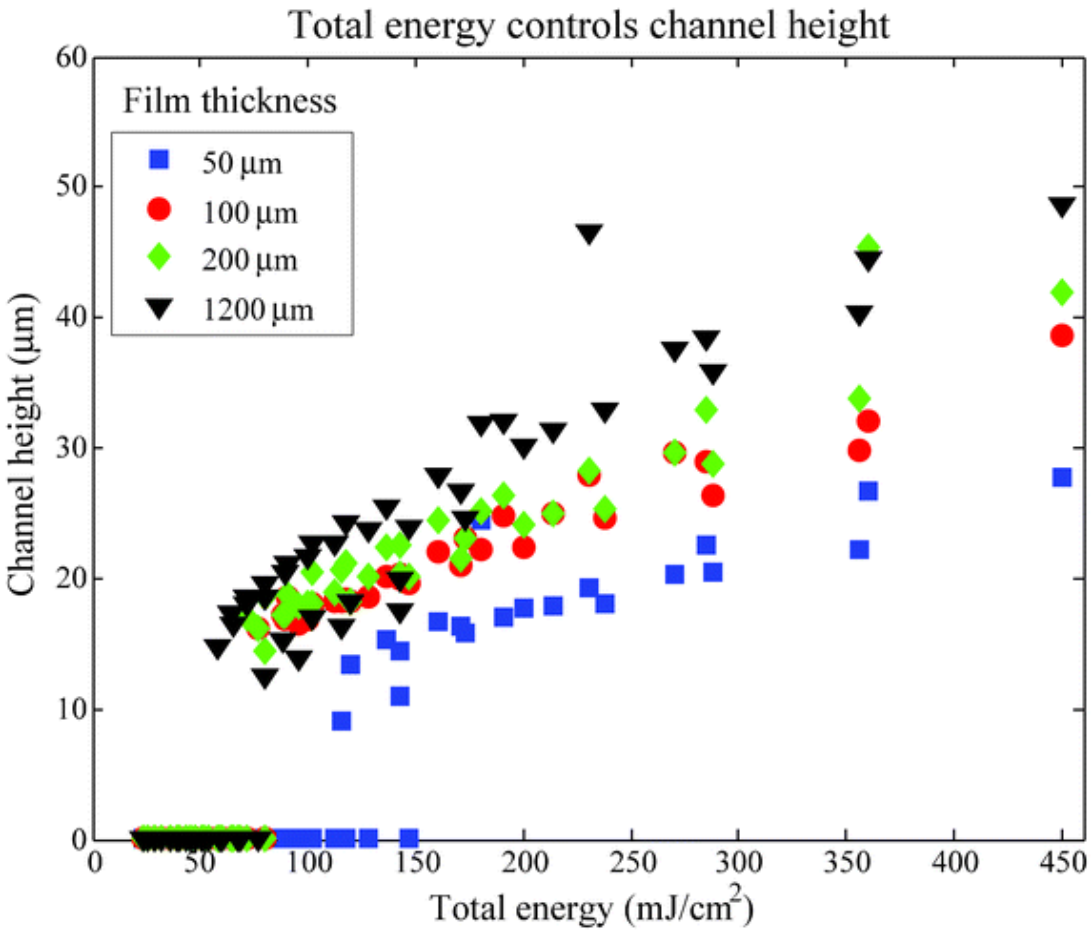

Fig. 6.4 Using pGS photomasks, the total amount of energy used to expose the photoresist can be controlled using gray scale level and/or exposure time allowing for the fabrication devices with multiple channel heights in a single UV exposure. Total energy is calculated using the percent gray value, exposure time, and the intensity of the UV transilluminator as described by eqn (1).

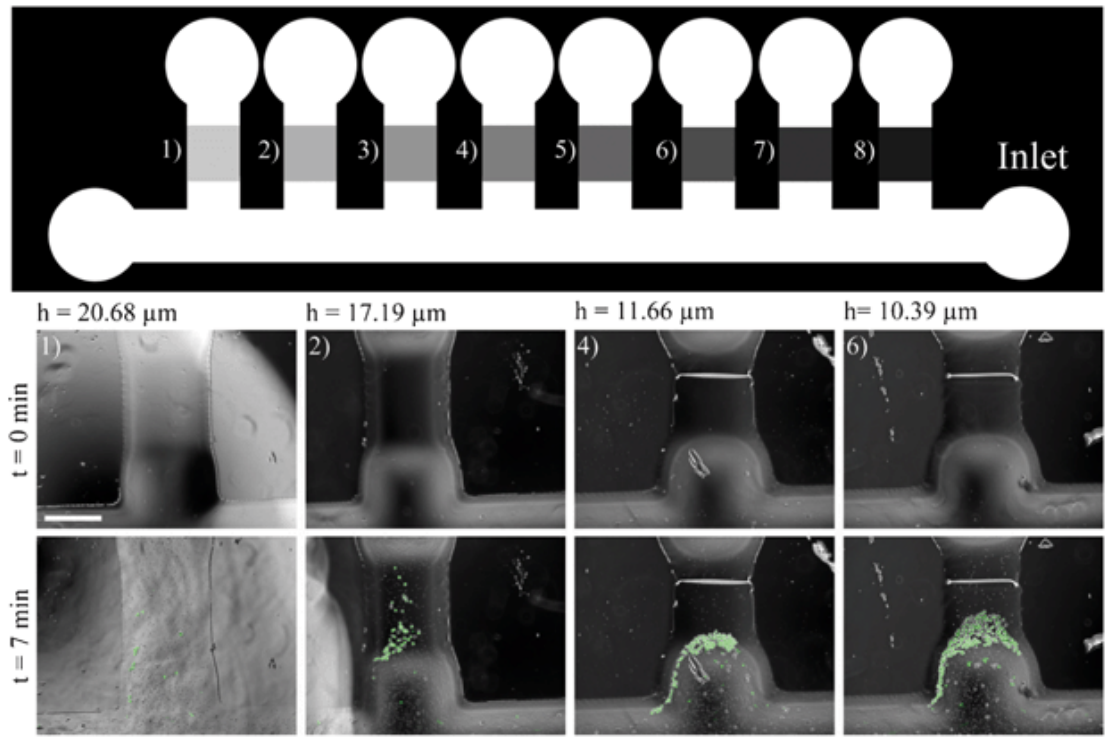

Fig. 6.5 pGS BDLL was used to produce PDMS microfluidic devices with 8 weir-type traps. PBS containing red blood cells and GFP-MDA-MB-231 cancer cells were passively driven through the weir-type traps by a 3 cm height differential to simulate the trapping and florescence microscopy was used for identification of CTCs trapped within the weir-type traps. The efficiency of weir-type traps depends on the height of the trap produced by pGS BDLL and is evidenced by the slippage and trapping of cancer cells while RBCs are allowed to freely pass through. Each channel is numbered to correspond with its position within the device. Scale bar: 500 µm.

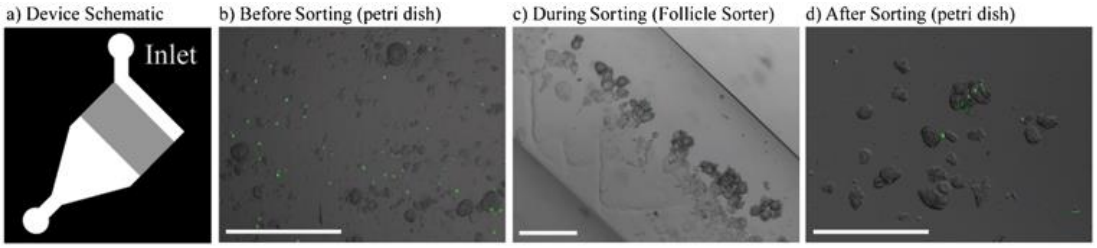

Fig. 6.6 Follicle sorting from GFP-MDA-MB-231 cancer cells. To further demonstrate the range of possible channel heights and their applications, a separate larger PDMS weir-type trap was produced with unspun SU-8 molds using pGS BDLL. Scale bar: 500 μm. a) Device schematic. b) Cancer cells were added into a solution containing primordial follicles within a petri dish. c) Follicles are trapped by weir-type traps while undigested collagen matrix squeezes through and cancer cells freely pass through. Flow was passive driven by a 7 cm height differential *via* suction of the outlet. d) The trapped follicles can be extracted from the device onto another petri dish by reversing the height differential of the inlet/outlet after a short flushing period with culture medium. The efficiency of cancer cell elimination is 88% and follicle recovery is 84%.

6.5 References

1. A. D. Stroock, *Science*, 2002, **295**, 647–651.
2. P. Wilding, L. J. Kricka, J. Cheng, G. Hvichia, M. A. Shoffner and P. Fortina, *Anal. Biochem.*, 1998, **257**, 95–100.
3. A. M. Skelley, O. Kirak, H. Suh, R. Jaenisch and J. Voldman, *Nat. Methods*, 2009, **6**, 147–152.
4. A. W. Browne, M. J. Rust, W. Jung, S. H. Lee and C. H. Ahn, *Lab Chip*, 2009, **9**, 2941.
5. A. Sayah, P.-A. Thivolle, V. K. Parashar and M. A. M. Gijs, *J. Micromech. Microeng.*, 2009, **19**, 085024.
6. M. L. Kovarik and S. C. Jacobson, *Anal. Chem.*, 2006, **78**, 5214–5217.
7. D. Lim, Y. Kamotani, B. Cho, J. Mazumder and S. Takayama, *Lab Chip*, 2003, **3**, 318.
8. Z. Huang, X. Li, M. Martins-Green and Y. Liu, *Biomed. Microdevices*, 2012, **14**, 873–883.
9. M. E. Wilson, N. Kota, Y. Kim, Y. Wang, D. B. Stolz, P. R. LeDuc and O. B. Ozdoganlar, *Lab Chip*, 2011, **11**, 1550.
10. C. J. Hansen, R. Saksena, D. B. Kolesky, J. J. Vericella, S. J. Kranz, G. P. Muldowney, K. T. Christensen and J. A. Lewis, *Adv. Mater.*, 2013, **25**, 96–102.
11. J. T. Borenstein, M. M. Tupper, P. J. Mack, E. J. Weinberg, A. S. Khalil, J. Hsiao and G. García-Cardeña, *Biomed. Microdevices*, 2009, **12**, 71–79.
12. H. Yu and G. Zhou, *Sensors Actuators B Chem.*, 2013.
13. X. Liu, Q. Wang, J. Qin and B. Lin, *Lab Chip*, 2009, **9**, 1200.
14. V. P. Korolkov, R. Shimansky, A. G. Poleshchuk, V. V. Cherkashin, A. A. Kharissov and D. Denk, ed. E.-B. Kley and H. P. Herzig, 2001, pp. 256–267.
15. B. Wagner, H. J. Quenzer, W. Henke, W. Hoppe and W. Pilz, *Sens. Actuators, A*, 1995, **46**, 89–94.
16. W. Däschner, P. Long, M. Larsson and S. H. Lee, *J. Vac. Sci. Technol., B*, 1995, **13**, 2729.
17. W. Däschner, P. Long, R. Stein, C. Wu and S. H. Lee, *Appl. Opt.*, 1997, **36**, 4675.
18. C. Chen, D. Hirdes and A. Folch, *Proc. Natl. Acad. Sci. U. S. A.*, 2003, **100**, 1499–1504.

19. J. Atencia, S. Barnes, J. Douglas, M. Meacham and L. E. Locascio, *Lab Chip*, 2007, **7**, 1567.

20. J.-H. Lee, W.-S. Choi, K.-H. Lee and J.-B. Yoon, *J. Micromech. Microeng.*, 2008, **18**, 125015.

21. A. Rammohan, P. K. Dwivedi, R. Martinez-Duarte, H. Katepalli, M. J. Madou and A. Sharma, *Sens. Actuators, B*, 2011, **153**, 125–134.

22. N. Futai, W. Gu and S. Takayama, *Adv. Mater.*, 2004, **16**, 1320–1323.

23. D. Lai, J. P. Frampton, H. Sriram and S. Takayama, *Lab Chip*, 2011, **11**, 3551.

24. S. Nagrath, L. V. Sequist, S. Maheswaran, D. W. Bell, D. Irimia, L. Ulkus, M. R. Smith, E. L. Kwak, S. Digumarthy, A. Muzikansky, P. Ryan, U. J. Balis, R. G. Tompkins, D. A. Haber and M. Toner,*Nature*, 2007, **450**, 1235–1239.

25. E. R. West, M. B. Zelinski, L. A. Kondapalli, C. Gracia, J. Chang, C. Coutifaris, J. Critser, R. L. Stouffer, L. D. Shea and T. K. Woodruff, *Pediatr. Blood Cancer*, 2009, **53**, 289–295.

26. J. S. Jeruss and T. K. Woodruff, *N. Engl. J. Med.*, 2009, **360**, 902–911.

27. D. B. Weibel, P. Garstecki and G. M. Whitesides, *Curr. Opin. Neurobiol.*, 2005, **15**, 560–567.

28. J. B. Smerage and D. F. Hayes, *Br. J. Cancer*, 2005, **94**, 8–12.

29. S. Braun and C. Marth, *N. Engl. J. Med.*, 2004, **351**, 824–826.

30. A. Rolle, R. Günzel, U. Pachmann, B. Willen, K. Höffken and K. Pachmann, *World J. Surg. Oncol.*, 2005, **3**, 18.

31. J. W. Song, S. P. Cavnar, A. C. Walker, K. E. Luker, M. Gupta, Y.-C. Tung, G. D. Luker and S. Takayama, *PLoS One*, 2009, **4**, e5756.

32. J. J. Eppig and A. C. Schroeder, *Biol. Reprod.*, 1989, **41**, 268–276.

Chapter 7

Label-Free Direct Visual Analysis of Hydrolytic Enzyme Activity Using Aqueous Two-Phase System Droplet Phase Transitions

Dextran hydrolysis-mediated conversion of polyethylene glycol (PEG)-dextran (DEX) aqueous two-phase system droplets to a single phase was used to directly visualize dextranase activity. Dextran droplets were formed either by manual micropipetting or within a continuous PEG phase by computer controlled actuation of an orifice connecting rounded channels formed by backside diffused light lithography. The time required for the two-phase to one-phase transition was dependent on the dextranase concentration, pH of the medium and temperature. The apparent Michaelis constants for dextranase were estimated based on previously reported catalytic constants, the binodial polymer concentration curves for PEG-DEX phase transition for each temperature and pH condition. The combination of a microfluidic droplet system and phase transition observation provides a new method for label-free direct measurement of enzyme activity.

7.1 Introduction

Assays for measuring the degradation of dextran either require the use of specially-prepared labeled polymers as surrogate substrates [1] or indirect measurement of degradation products, such as the amount of reducing sugar activity hydrolytically

released from dextran [2]. Here, we describe a label-free direct visualization assay for the measurement of dextranase activity that utilizes the observation of phase transitions of aqueous two-phase system (ATPS) droplets into one phase.

ATPSs are formed when two immiscible water-based solutions, usually composed of long-chain polymers, are mixed at concentrations above which it is thermodynamically favorable for the solutions to phase-separate into discrete regions [3]. This thermodynamic phenomenon is influenced by a variety of factors including pH, temperature, ionic content, solute/polymer concentration and the molecular weight of the phase-separating constituents [4]. For aqueous polymer solutions of a given weight/weight concentration, solutions composed of larger molecular weight polymers phase-separate more readily because of the smaller entropic cost to de-mix the smaller number of distinct polymer chains. Thus, when an enzyme hydrolyzes polymers within an ATPS, phase separation becomes less favorable because either the weight/weight concentrations of the long-chain polymer decrease or the long-chain polymers become fragmented into shorter chains. While observations of hydrolysis-triggered phase transitions of macroscopic ATPSs requires large amounts of enzyme, reducing the volume of the polymer substrate phases using microfluidic principles makes such phase transition processes practical for the measurement of enzyme activity, thereby increasing throughput and reducing the amounts of reagents used.

The polyethylene glycol (PEG)-dextran (DEX) ATPS is one of the most widely used ATPSs in laboratory science [5] and industry. The concentrations (typically expressed in terms of weight/weight) of PEG and DEX of certain molecular weights required for phase separation are described by binodial polymer concentration curves, as shown in Fig. 7.1. A two-phase system will transition to a single phase if the

concentrations of one or both polymers are decreased below the critical concentrations displayed by the binodial curve (Fig. 7.1A). If one considers a phase diagram based on molar concentrations (a less common way to present ATPS phase diagrams), as the polymer molecular weight decreases the binodal curve shifts up. This means that even if the molar concentration of DEX and PEG remains constant, as the DEX molecular weight decreases due to degradation, the binodal curve shifts such that the same molar concentrations of polymers no longer produce phase separation. Dextranase degrades DEX to cause the DEX microdroplets formed in the PEG phase solutions to disappear due to phase transition (Fig. 7.1A, right to left pointing horizontal arrow; Fig. 7.1B, shifting of the binodal curve).

Dextran hydrolysis by dextranase is of significance to both the sugar/carbohydrate polymer industry and dental medicine. Here, we apply the thermodynamic principle of phase transition to measuring the enzymatic activity of dextranase, an enzyme that hydrolyzes the alpha-(1,6) glycosidic bonds of dextran (DEX) to produce smaller oligosaccharides. We use well-plate and microfluidic droplet-based ATPS assays to demonstrate that the time it takes to transition a droplet-based PEG-DEX ATPS to a single phase depends on enzyme activity, as modulated by enzyme concentration, temperature and pH of the ATPS solution. Based on our data, this process is not diffusion limited for the droplet sizes and enzyme concentrations we tested. The Michaelis constants for dextranase activity are estimated for the various assay formats and enzyme conditions.

7.2 Materials and Methods

Chemicals and Reagents. DEX, average molecular weight 500,000, was purchased from Pharmacosmos (Denmark). Dextranase and PEG (average molecular weight 35,000) were both purchased from Sigma (MO, USA). Microfluidic devices were fabricated from Sylgard 184 polydimethylsiloxane (PDMS) and curing agent, both purchased from Dow Chemical (MI, USA). The master molds from which the microfluidic devices were replica-molded consisted of SU-8 from MicroChem (MA, USA) patterned on glass coverslips from Fisher Scientific (MA, USA).

Aqueous Two-Phase Systems. For the well-plate assays, a biphasic system composed of 2.5% PEG 35,000, 3.2% DEX T500 and PBS was formed. The equilibrated PEG and DEX phases were collected for dextranase testing. For the microfluidic tests, ATPSs were formed from near-critical point DEX (~3.2% w/w) + 0.01% w/w FITC-DEX and PEG (2.5% w/w) in PBS. The ATPSs were equilibrated at room temperature and centrifuged at 600 rcf before use. For all dextranase experiments, the pH was adjusted by addition of 1 N HCl to the PBS before incorporation of the polymers. Dextranase was added from a highly concentrated stock of 500 U/mL to achieve the appropriate concentration, where U is defined as 1 μmole of dextran degraded per minute in a pH 6.0 solution at 37 ˚C. Solutions were then stored on ice to prevent unwanted dextranase activity.

Dextranase Well-Plate Assays. Images were acquired at specific time points (up to 210 min) to test the effects of dextranase concentration (5, 2, 0.5, 0.2, 0.05 and 0.02 U/mL), pH (6.0 and 7.4) and temperature (25 °C and 37 °C) on DEX droplet degradation. After collection of the purified DEX and PEG phases, an appropriate amount of dextranase was first added only to the DEX phase. After a defined pre-incubation period, 0.5 μL droplets of DEX/enzyme mixture were micropipetted into

48-well assay plates containing 200 μL of PEG in each well. The micropipetting step took no longer than 5 sec. After 20 sec, images of the DEX droplets were captured to definitively confirm the loss of the phase boundary and rule out the possibility of misidentifying a phase boundary due to differences in the refractive index of the solutions. The appearance of a stable interface between the DEX droplets and the bulk PEG phase indicated phase separation. Droplet dynamics, including spreading or contraction after droplet addition, were also noted. For the relatively few time points where phase transition could not be definitively confirmed, additional time points were collected and the average time between the first indication of interface disappearance (dramatic droplet expansion due to loss of interfacial tension and barely visible phase boundary) and definitive interface disappearance (clearly no phase boundary) was considered as the DEX degradation time. This type of experiment with pre-incubation of a DEX phase only solution followed by periodic addition of small aliquots of the degraded DEX phase solution into a PEG phase is important for obtaining insights into the role of diffusion (or lack thereof) versus reaction, since all of the DEX reactions take place without diffusion into PEG until the DEX droplets are added to PEG. The procedure, however, is tedious. Thus, to demonstrate improved time resolution with less hands-on activity from the experimenter, we also performed experiments where we dispensed DEX droplets containing dextranase into the PEG solution and used time-lapse imaging every 2 sec from 0 to 120 min to observe DEX droplet degradation continuously using single small droplets.

Droplet Generating Device Fabrication. Microfluidic devices were fabricated using backside diffused light lithography, as described previously [6]. Briefly, an SU-8-

coated glass coverslip was exposed from the back (glass side) to UV illumination passing through a photomask. Rounded multilevel structures were developed in the photoresist using a discontinuous pattern on the photomask, such that light passing through the photoresist and the glass slide was scattered, exposing the SU-8 in the region corresponding to the discontinuity to less illumination. This diffuse light from both discontinuous ends joined to form a channel constriction (orifice) at the hydrodynamic focusing junction. The positive features from the photoresist were replica-molded using conventional soft lithography in PDMS to form elastomeric channels that were subsequently plasma-bonded to a PDMS membrane (100 μm thickness) fabricated by spin coating at 200 RPM for 240 seconds followed by 2000 RPM for 5 seconds. The channel geometries were designed to align with a Braille pin-array that was programmed to actuate the channel constriction to induce droplet formation, as described previously [7].

Microfluidic Droplet Formation. The appropriate amount of dextranase was added to the dextran solution, which was stored on ice to limit the dextranase activity. This solution was loaded into a cold syringe and placed on a syringe pump. Ice packs were used to keep the syringe and tubing connected to the device cool. Using the flow focusing channel, a threading regime was produced by syringe pump-driven flow at 0.01 mL/hour and 0.07 mL/hour for the DEX and PEG phases, respectively. An actuating Braille pin was placed underneath the orifice in the center channel to valve the flow of dextran at 0.8333 Hz. The Braille pin was controlled using a customized circuit-board connected to a computer through a universal serial bus (USB) with its own custom user interface. The entire process of loading the chilled DEX/dextranase solution and aligning the device prior to droplet generation lasted no longer than 15

min. Droplet flow was arrested by collapsing the upstream and downstream channel regions using clamps. This produced a closed system that allowed time-lapse imaging of droplet dynamics in the presence of dextranase. Droplets were imaged by fluorescence and brightfield microscopy (Nikon TS100, Tokyo, Japan), with images acquired every 30 seconds for the control and 0.02 U/mL dextranase conditions and every 10 seconds for the 5 U/mL dextranase condition. For microfluidic enzyme tests at temperatures above normal room temperature (~25 °C), the entire microscope room temperature was raised using climate control and further raised to 45 °C using a heat gun (Black & Decker, CT, USA). The temperature was continually monitored using a thermometer and the room thermostat. Heating the entire room guaranteed a constant temperature for the microfluidic device and limited the effects of thermal gradients on the PEG-DEX ATPS.

Calculation of Michaelis Constants. The phase transition weight percentages of DEX for different DEX chain lengths at 2.5 % PEG 35,000 for pH 7.4 at 25 °C were plotted and fitted with a power curve (Fig. 7.2). The points in the graph were based on experimental phase diagrams and previously published phase diagrams for PEG 35,000 and DEX 500,000 (Fig. 7.3), DEX 100,000 [8], DEX 40,000 [9] and DEX 10,000. The initial point of our ATPS corresponded to 2.5% PEG 35,000 and 3.2 % DEX 500,000. As dextranase digests the 500,000 g/mol dextran chain, the weight decreases proportionately to the fraction of the chain length digested. The expected molecular weight of dextran in the dextranase assay at which phase transition occurs following dextranase digestion is estimated to be 1.84% DEX 287,000 g/mol. The main products from digestion are glucose, isomaltose, isomaltotriose and larger

oligosaccharides [10]. We assumed that these products had insignificant contributions to phase formation.

The Michaelis-Menten kinetics allowed a comparison of the micro-well assays and the microfluidic assay. For a given pH, the K_{cat} of the assay is constant, while the Km changes. Varying the temperature from 37 °C to 25 °C changes the K_{cat} according to the Arrhenius Equation and also affects the K_m. The K_m is described as

$$K\mathrm{m} = \frac{[S]K\mathrm{cat}[E]t}{[P]} - [S],$$

where [E] is the enzyme concentration, [S] is the concentration of long chain DEX and [P] is the concentration of isomaltotriose. The rate constant at 37 °C is given by the manufacturer as 1.0 µmol/min/U. The activation energy, E_a, of Arrhenius equation was determined from a previous study [11]. Thus, the K_{cat} at 25 °C is 0.86 µmol/min/U. A dextranase concentration of 2.0 U/mL was used for the well-plate assay calculations and a concentration of 5.0 U/mL was used for the microfluidic assay calculations. Our experimental phase diagrams indicated that the phase transition weight percentage for DEX 500,000 varied only slightly with temperature and pH (from 1.466% to 1.543%). As such, identical values for [S] and [P] ($6.4*10^{-8}$ and $2.7*10^{-5}$ mol/mL, respectively) were used for each condition. [S] is based on the initial starting DEX concentration and [P] is calculated from the number of DEX chains ($6.4*10^{-8}$) multiplied by the number of isomaltotriose units (504.44 g/mol) released per chain as it is digested from 500,000 g/mol to 287,000 g/mol (422). In this model, [S] (mol/mL) is approximated to be constant over time. This is not unreasonable, as the molar concentration of long-chain DEX is assumed not to change

significantly within the time-frame of our experiments. Instead, the molecular weight of the DEX decreases with enzymatic digestion. As isomaltotriose is released from each DEX chain, the DEX chain length will decrease, as will the weight percentage of DEX. Thus, the K_m values for the various long-chain DEX polymers are expected to be similar. Based on these parameters, we calculated the Michaelis constants (K_m values) as shown in Table 7.1.

7.3 Results and Discussion

In this work, we maintained a constant PEG concentration, while degrading DEX by digesting it with dextranase. This resulted in a decrease in the weight/weight concentration of the largest molecular weight DEX species (Fig. 7.1A, right to left pointing horizontal arrow), while the molar concentration and total DEX-associated material mass of the system remained relatively constant. A two-phase to one-phase transition occurs when there is a decrease in weight/weight concentration of the original high molecular weight DEX (Fig 7.1A) or, if focusing on molar concentration of DEX of any molecular weight, when the molecular weights of the DEX decreases causing an upward shift of the binodal curve (Fig. 7.1B). In contrast, diluting the solution would decrease the concentrations of both PEG and DEX, and increase the overall volume of the solutions (Fig. 7.1A, arrow towards the origin and Fig. 7.1B).

We first tested enzymatic hydrolysis-mediated aqueous two-phase system transition using DEX solution droplets of 0.5 μL formed by pipetting into a well-plate filled with PEG solution. Dextranase activity was modulated using three parameters: pH, temperature and dextranase concentration (Fig. 7.4). Determination of two-phase

to one-phase conversion was based on time-lapse experiments where aliquots of DEX phase solutions pre-incubated with dextranase were added to a PEG phase at designated time intervals and the phase boundary at the DEX-PEG interface was observed immediately (~20 seconds) after addition to the PEG phase. At a few time points, only a portion of the boundary was visible. In those cases, the droplet system was determined to be in an intermediate state. In all cases, the intermediate state underwent two-phase to one-phase conversion by the time the next time point was observed. Increasing the pH from 6.0 to 7.4 increased the dextranase-mediated time to DEX droplet degradation (i.e., the conversion from having the ability to maintain two-phases when added to the PEG phase to immediately becoming a one-phase upon addition) by ~3 fold (Fig. 7.4a-b). Reducing the temperature from 37 °C to 25 °C also increased the time to DEX droplet degradation. Dextranase concentration was inversely proportional to time to DEX droplet degradation, displaying a nearly linear relationship; for example, when the dextranase concentration was increased by 10-fold, the DEX droplet degradation time decreased by ~10-fold. These experiments where the DEX phase solutions were degraded first then added to the PEG phase solutions are important for confirming that the inability of the degraded DEX phase solution to form a two-phase system is not dependent on diffusion of the degraded molecules away from the DEX phase droplet. Rather, when a DEX droplet fails to form a two-phase system, it is mainly because the DEX polymers have been degraded sufficiently that phase separation cannot occur even though all of the original DEX polymer materials are still present (Fig. 7.1). After dispensing the dextranase-degraded DEX droplets into the PEG phase, the droplets generally spread out due to their low interfacial tension with the PEG phase, which makes the droplets flatter (Fig. 7.4c). We also carried out a similar well-plate assay, in which DEX/FITC-

DEX/dextranase droplets were immediately place in a PEG-filled well and observed by time-lapse imaging at 2 sec intervals. The DEX droplet expanded over the course of imaging, before apparent voids began to appear in the droplet interior at ~35 min (Fig. 7.4d). By 50 min, the droplet was completely consumed. We considered the 35 minute time point to be the point at which two-phase to one-phase transition occurred in this assay.

This ATPS well-plate assay can be adapted for analysis of dextranase activity in other aqueous solutions such as industrial/manufacturing batch solutions, cell culture media and bacterial broth by simply observing DEX-PEG phase transition. For more sensitive detection that may be necessary to assess small-scale bacterial dextranase production, the assay detection limit can be lowered by decreasing the amount of dextran degradation required for two-phase to one-phase conversion. This can be achieved by using an ATPS composition that is closer to the binodial curve.

We next used a microfluidic device [12] to produce single- to sub-nanoliter dextran droplets to increase the throughput of the assay and demonstrate the potential for automated, chip-based analysis (Fig. 7.5a-c). Without actuation from a computer-controlled pin, a laminar stream of DEX was formed in the microfluidic channel, enclosed by two streams of PEG. Upon actuation, flow was interrupted, resulting in formation of DEX droplets carrying FITC-DEX as a tracer material (Fig. 7.5b). The FITC-DEX is not needed for purposes of measuring dextranase activity, but was included to help understand some of the dynamics of the degradation and droplet content release process, as will be explained below. We also monitored the droplets by brightfield microscopy.

In the absence of dextranase, the droplets maintained their size, fluorescence intensity and phase boundaries (Fig. 7.5c, first column). The addition of dextranase caused the degradation of the droplet emulsion into a single phase. At room temperature and a pH of 7.4, a high concentration of dextranase (5 U/mL) was required to degrade the DEX droplets in a timely manner as these conditions are enzymatically not optimal (Fig. 7.5c, second column). By adjusting the pH to 6.0 and increasing the temperature to 45°C (the optimal enzymatic conditions for dextranse), the DEX droplets could be degraded using much lower concentrations of dextranase (0.02 U/mL) (Fig. 7.5c third column). We confirmed the timescale of droplet disappearance under this condition using the pre-incubated well-plate assays (Fig. 7.5c, fourth column). These observations suggest various possibilities for designing rapid or gradual DEX-hydrolysis-triggered release of reagents from the DEX droplets.

To compare the different assay formats and enzyme degradation conditions, we calculated the Michaelis constants based on Michaelis-Menten kinetics and the binodial polymer concentration curves for the PEG-DEX ATPS (Table 7.1; binodial curves shown in Fig. 7.2). The similarities in time to transitioning to one-phase between the DEX droplets pre-incubated with dextranase before PEG addition and those that were incubated after addition to PEG, and the mechanistic explanation of Fig. 7.1B suggest that the process of DEX/PEG two-phase to one-phase transition due to dextranase degradation of DEX is not limited by diffusing away of degraded DEX. That is, DEX degradation products do not have to diffuse away for the phase transition to occur. Thus, our assay should be minimally influenced thermodynamically by changes in droplet scale. We do note, however, that there is slightly more ambiguity as to exactly when one considers a droplet to have

transitioned to one phase (e.g. Fig. 4D 35 min) for larger droplets compared to smaller drops. As expected, the Michaelis constant decreased under conditions that were more favorable to enzymatic degradation of DEX (i.e., higher temperature and lower pH).

7.4 Conclusions

Our droplet dispersion technology has applications in the field of microfluidics [13], where in the future it may be applied for microfluidic chemical reactions [14] or creating dynamic chemical gradients for studying cell signaling applications by compartmentalizing and releasing reagents or cell signaling factors. Since eukaryotic cells typically do not produce dextran and have few important glycosidic bonds hydrolyzed by dextranase on their surface, the process may serve as a mild, cell culture-friendly, and localized controlled reagent-release mechanism. Dextranase is also of interest in clinical dentistry as it is secreted by oral bacteria that modify the formation of dental plaques and use the plaque constituents (including dextran) as a source of nutrients [1]. With the ability to detect dextranase activities as low as 0.020 U/mL in less than 90 minutes (robust oral dextranase-producing bacteria such as P. Oralis secrete extracellular dextranase up to 0.490 U/mL [1]), it may be possible to analyze oral microbial flora using our system. Finally, highly sensitive dextranase activity testing can be helpful in the sugarcane industry for early detection of costly and potentially destructive contamination, as well as for standardization of dextranase enzymes used industrially to prevent dextran accumulation during sugar production [15]. While we focus on just the analysis of dextranase activity, the concept of using aqueous two-phase system droplet transitions to directly visualize polymer hydrolyzing enzyme activity may be applicable to other biopolymer ATPSs as well.

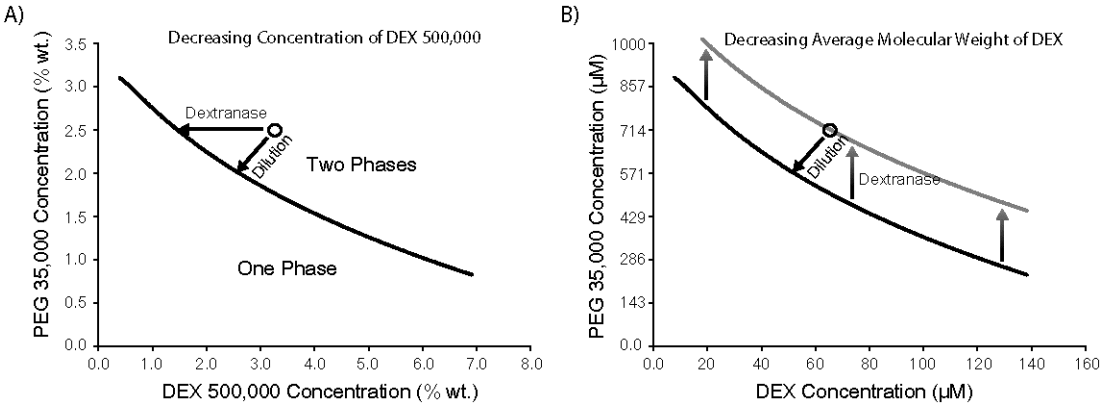

Fig. 7.1 The binodial phase diagram for the PEG 35,000/DEX 500,000 system. A) A two-phase system can be converted to a single phase either by dilution or by degradation of DEX by dextranase. This graph focuses on the weight % concentration of DEX 500,000. B) Another representation of how a two-phase system can be converted to a single phase either by dilution or by degration of DEX by dextranase. This graph focuses on the the molar concentration of long chain DEX of various molecular weights. As dextranase digests DEX, the molar concentration remains the same for a significant time, but the average long chain DEX molecular weight decreases. As the molecular weight of DEX decreases, the molar concentration of DEX does not decrease, but the binodal curve shifts up because a higher concentration of PEG is required to form an ATPS with the same molar concentration of lower molecular weight DEX. The molar concentration point designated by the circle corresponds to 2.5% PEG 35,000/3.2% DEX 500,000.

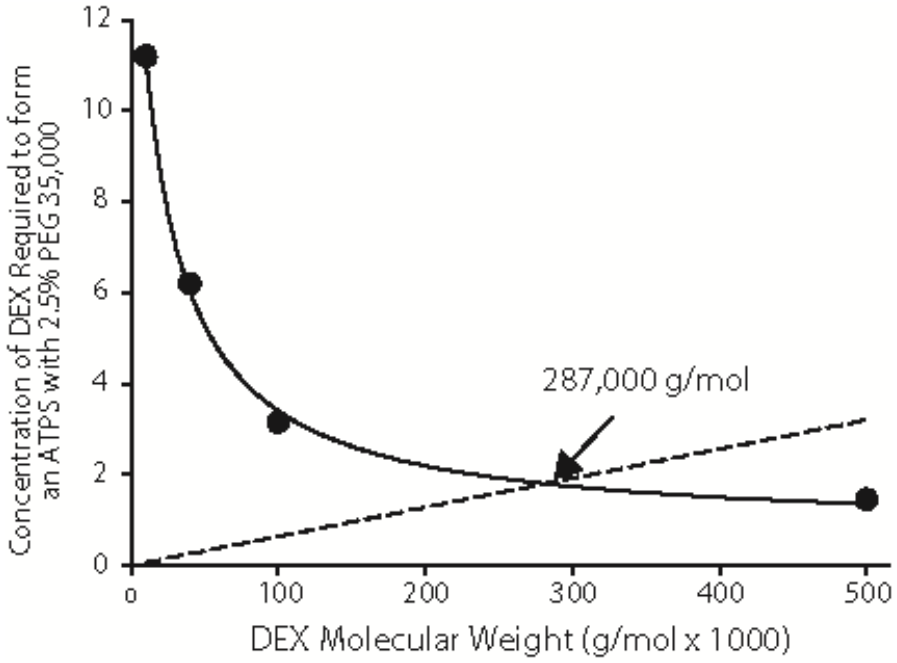

Fig. 7.2 DEX chain length vs. concentration of DEX required to form an ATPS with 2.5% PEG 35,000. This plot was used to determine the amount of DEX chain shortening required for the degraded 3.2% DEX 500,000 to no longer form an ATPS with 2.5% PEG. As dextranase digests the 500,000 g/mol dextran chain, the dotted line represents the weight decreasing proportionately to the fraction of the chain length digested.

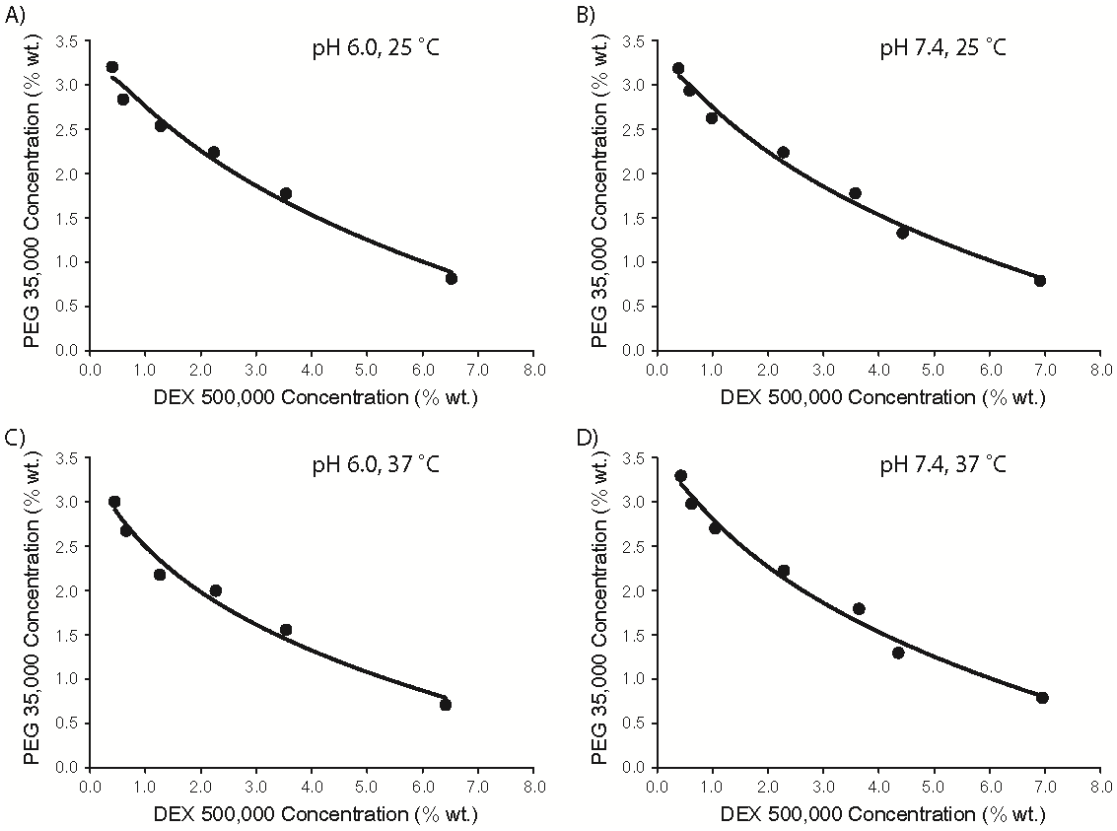

Fig. 7.3 Binodial Curves for the PEG 35,000/DEX 500,000 ATPS at the pH values and temperatures used for the dextranase assay.The binodal concentration of DEX at 2.5% PEG are A) 1.51%, B) 1.50%, C) 1.58% and D) 1.49%.

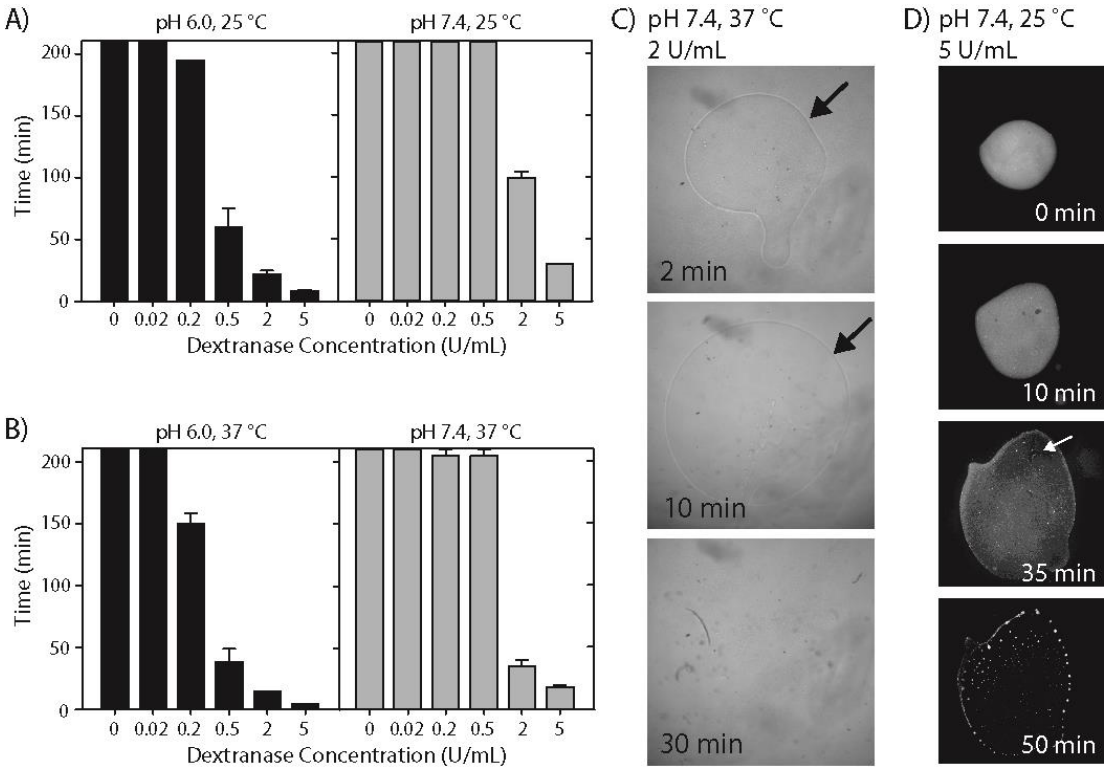

Fig. 7.4 Two-phase to one-phase conversion occurs following dextranase-mediated DEX degradation. (A-B) Dextranase activity can be assessed in a well-plate by recording the time at which DEX droplets pre-incubated with dextranase no longer form phase boundaries with PEG. DEX droplet degradation times vary by pH, temperature and dextranase concentration. A maxium incubation time of 210 min was used for these assays. (C) Phase separation (or lack thereof) of DEX droplets pre-incubated with 2 U/mL dextranase for 2 min, 10 min and 30 min at pH 7.4, 37 °C as they are added into PEG. The black arrows indicate the phase boundary. (D) Phase separation of DEX droplets containing FITC-DEX and 5 U/mL dextranase (without pre-incubation) in PEG, as recorded by fluorescence time-lapse imaging. The white arrow indicates the initial location of the void that indicated droplet degradation and the conversion of the ATPS to a single phase. The 35 minute time point was considered the trasition point from two phases to one phase.

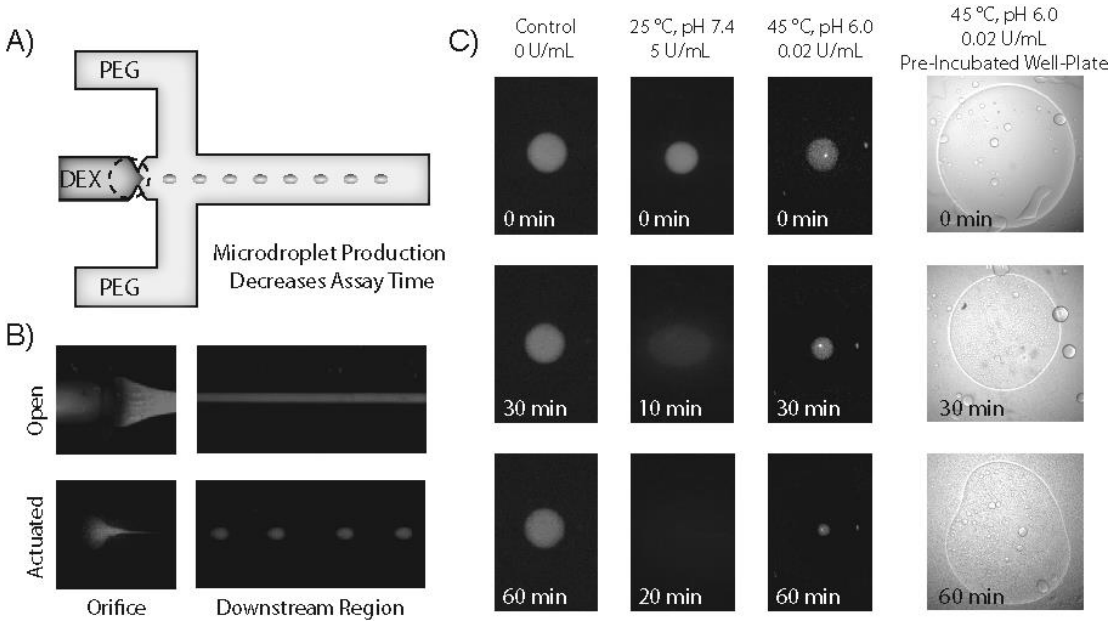

Fig. 7.5 Operating principle of the droplet-generating device. (A) A central DEX inlet is flanked by two PEG inlets. The channel constriction is actuated by a computer controlled pin positioned at the black dashed circle. (B) Without actuation this constriction is open, resulting in the formation of a laminar stream of DEX in the center of the channel. Pin actuation at an appropriate frequency closes the constriction to produce droplets of DEX. The DEX phase was visualized using a FITC-DEX tracer. (C) Droplets generated microfluidically allow sensitive detection of enzyme activity. Droplet degredation was not observed when dextranase was absent from the ATPS. (D) The pre-incubated well- plate assay produces comparable results for 0.02 U/mL dextranse at pH 6.0, 45 °C.

Enzyme Condition	Time (min)	K_m (M)
Well-Plate Assay (Pre-Incubation)		
pH 7.4, 25 °C	100	3.4×10^{-4}
pH 7.4, 37 °C	35	1.0×10^{-4}
pH 6.0, 25 °C	22	2.4×10^{-5}
pH 6.0, 37 °C	15	7.1×10^{-6}
Well-Plate Assay (Time-Lapse)		
pH 7.4, 25 °C	35	7.9×10^{-5}
Microfluidic (Time-Lapse)		
pH 7.4, 25 °C	30*	5.8×10^{-5}

Table 7.1 Catalytic data for the various dextranase conditions and assay formats. *10 minutes was added to the time point shown in Fig. 7.3b (20 min) to account for the additional time (including the time where temperature was kept low) that the DEX solution was exposed to dextranase during microfluidic droplet generation preparation.

7.5 References

1. Igarashi, T.; Yamamoto, A.; Goto, N., Detection of dextranase-producing gram-negative oral bacteria. *Oral microbiology and immunology* **1998,** *13* (6), 382-6.

2. Kaster, A. G.; Brown, L. R., Extracellular dextranase activity produced by human oral strains of the genus Bifidobacterium. *Infection and immunity* **1983,** *42* (2), 716-20.

3. (a) Dobry, A.; Boyer-Kawenoki, F., Phase separation in polymer solution. *Journal of Polymer Science* **1947,** *2* (1), 90-100; (b) Albertsson, P. A. k., *Partition of cell particles and macromolecules : separation and purification of biomolecules, cell organelles, membranes, and cells in aqueous polymer two-phase systems and their use in biochemical analysis and biotechnology*. 3rd ed.; Wiley: New York, 1986; p 346 p.

4. Albertsson, P. A., Partition of cell particles and macromolecules in polymer two-phase systems. *Advances in protein chemistry* **1970,** *24*, 309-41.

5. (a) Tsukamoto, M.; Taira, S.; Yamamura, S.; Morita, Y.; Nagatani, N.; Takamura, Y.; Tamiya, E., Cell separation by an aqueous two-phase system in a microfluidic device. *The Analyst* **2009,** *134* (10), 1994-8; (b) Yamada, M.; Kasim, V.; Nakashima, M.; Edahiro, J.; Seki, M., Continuous cell partitioning using an aqueous two-phase flow system in microfluidic devices. *Biotechnology and bioengineering* **2004,** *88* (4), 489-94; (c) Soohoo, J. R.; Walker, G. M., Microfluidic aqueous two phase system for leukocyte concentration from whole blood. *Biomedical microdevices* **2009,** *11* (2), 323-9; (d) Tavana, H.; Jovic, A.; Mosadegh, B.; Lee, Q. Y.; Liu, X.; Luker, K. E.; Luker, G. D.; Weiss, S. J.; Takayama, S., Nanolitre liquid patterning in aqueous environments for spatially defined reagent delivery to mammalian cells. *Nature materials* **2009,** *8* (9), 736-41; (e) Tavana, H.; Mosadegh, B.; Takayama, S., Polymeric aqueous biphasic systems for non-contact cell printing on cells: engineering heterocellular embryonic stem cell niches. *Adv Mater* **2010,** *22* (24), 2628-31.

6. (a) Futai, N.; Gu, W.; Takayama, S., Rapid Prototyping of Microstructures with Bell-Shaped Cross-Sections and Its Application to Deformation-Based Microfluidic Valves. *Advanced Materials* **2004,** *16* (15), 1320-1323; (b) Lai, D.; Frampton, J. P.; Sriram, H.; Takayama, S., Rounded multi-level microchannels with orifices made in one exposure enable aqueous two-phase system droplet microfluidics. *Lab on a chip* **2011,** *11* (20), 3551-3554.

7. Gu, W.; Zhu, X.; Futai, N.; Cho, B. S.; Takayama, S., Computerized microfluidic cell culture using elastomeric channels and Braille displays. *Proceedings of the National Academy of Sciences of the United States of America* **2004,** *101* (45), 15861-6.

8. Boreyko, J. B.; Mruetusatorn, P.; Retterer, S. T.; Collier, C. P., Aqueous two-phase microdroplets with reversible phase transitions. *Lab on a Chip* **2013**, *13* (7), 1295-1301.

9. Long, M. S., Dynamic and asymmetric protein microcompartmentation in aqueous two-phase vehicles. *Penn State University Doctoral Dissertation* **2005**, Accessed on 2/15/2014 at https://etda.libraries.psu.edu/paper/6801/.

10. Fukumoto, J.; Tsuji, H.; Tsuru, D. Studies on mold dextranases. *Journal of Biochemistry* **1971**, *69*, 1113-1121.

11. El-Tanash, A. B.; El-Baz, E.; Sherief, A. A., Properties of Aspergillus subolivaceus free and immobilized dextranase. *European Food Research and Technology* **2011**, *233*, 735-742.

12. Lai, D.; Frampton, J. P.; Hari, S. A.; Takayama, S., Rounded multi-level microchannels with orifices made in one exposure enable aqueous two-phase system droplet microfluidics. *Lab on a chip* **2011,** *11* (20), 3551-3554.

13. (a) Sugiura, S.; Nakajima, M.; Iwamoto, S.; Seki, M., Interfacial Tension Driven Monodispersed Droplet Formation from Microfabricated Channel Array. *Langmuir : the ACS journal of surfaces and colloids* **2001,** *17* (18), 5562-5566; (b) Sugiura, S.; Nakajima, M.; Seki, M., Effect of Channel Structure on Microchannel Emulsification. *Langmuir : the ACS journal of surfaces and colloids* **2002,** *18* (15), 5708-5712; (c) Basu, A. S., Droplet morphometry and velocimetry (DMV): a video processing software for time-resolved, label-free tracking of droplet parameters. *Lab on a chip* **2013,** *13* (10), 1892-901; (d) Zeng, S.; Pan, X.; Zhang, Q.; Lin, B.; Qin, J., Electrical control of individual droplet breaking and droplet contents extraction. *Analytical chemistry* **2011,** *83* (6), 2083-9.

14. (a) Trivedi, V.; Doshi, A.; Kurup, G. K.; Ereifej, E.; Vandevord, P. J.; Basu, A. S., A modular approach for the generation, storage, mixing, and detection of droplet libraries for high throughput screening. *Lab on a chip* **2010,** *10* (18), 2433-2442; (b) Schudel, B. R.; Choi, C. J.; Cunningham, B. T.; Kenis, P. J. A., Microfluidic chip for combinatorial mixing and screening of assays. *Lab on a chip* **2009,** *9* (12), 1676-1680.

15. Eggleston, G.; Monge, A., Optimization of sugarcane factory application of commercial dextranases. *Process Biochemistry* **2005,** *40* (5), 1881-1894.

APPENDICES

Appendix A

Lab-on-a-chip biophotonics: its application to assisted reproductive technologies

With the benefits of automation, sensitivity and precision, microfluidics has enabled complex and otherwise tedious experiments. Lately, lab-on-a-chip (LOC) has proven to be a useful tool for enhancing non-invasive assisted reproductive technology (ART). Non-invasive gamete and embryo assessment has largely been through periodic morpohological assessment using optical microscopy and early LOC ART was the same. As we realize that morphological assessment is a poor indication of gamete or embryo health, more advanced biophotonics has emerged in LOC ART to assay for metabolites or gamete separation via optoelectrical tweezers. Off-chip, even more advanced biophotonics with broad spectrum analysis of metabolites and secretomes has been developed that show even higher accuracy to predicting reproductive potential. The integration of broad spectrum metabolite analysis into LOC ART is an exciting future that merges automation and sensitivity with the already highly accurate and strong predictive power of biophotonics.

A.1 Introduction

Microfluidics is a relatively new field studying the physical principles of fluid behaviour that have already been extensively applied in chemistry[1] and molecular biology[2]. More recently, microfluidics has also become increasingly applied to

cellular behaviour and interaction studies[3-5]. The scalability of microfluidics allows for unprecedented cost efficiency due to the minute amount of reagents necessary allowing for the execution of otherwise expensive experiments and automation provided by embedded microfluidic features can allow for high sensitivity without user variability. For cell culture applications, the small volumes can enhance autocrine effects although nutrient depletion and waste accumulation also becomes faster. At the microscale, the flow of even familiar fluids like water and aqueous solutions also becomes dramatically different due to a low Reynolds number, the ratio between inertial forces and viscous forces. When viscous forces dominate, a phenomenon called laminar flow results that where the fluid quickly and reliably moves in response to external forces. When two or more streams converge in laminar flow conditions, they do not mix save for the effects of diffusion due to a lack of turbulence.

These small volume and low Reynolds number flow conditions can be utilized to more closely resemble *in vivo* conditions of insemination and embryo culture than classical *in vitro* methods using culture dish, test tube or drops of media. In 1979, it was first reported that the microenvironment holds a dramatic importance in embryo handling and culture[6]. More recently, it has been shown that dynamic stimulation of oocytes increase fertilization rates[7] as well as increase in oocyte health[8].

Microfluidic devices are typically composed of a transparent elastomer and plastics such as PDMS and polystyrene. This allows many lab-on-a-chip (LOC) applications to use biophotonics for data acquisition. For assisted reproductive technologies (ART), microfluidics provides a tool for non-invasive cell quality assessment especially for precious cell samples such as oocytes and embryos. The speed at which

samples can be sorted using microfluidic operations also allow for high-throughput screening in ART particularly for sperm samples.

A.2 Basic Use of Biophotonics in LOC ART

Less than half of *in vitro* fertilization (IVF) cycles result in a live birth even for women below the age of 35 that causes severe physical, emotional and financial stress[9]. The success decreases even more with frozen embryos and age. Thus embryo, oocyte and sperm quality assessment is an important procedure to identify the healthiest oocytes and sperm for IVF and the embryos with the highest reproductive potential for implantation. However even now, embryo morphology and cleavage rates are the most common form of embryo quality assessment. Early LOC ART technology also involved direct quality assessment with periodic morphology assessment mostly based on optical and at times fluorescence imaging.

LOC morphology assessment of oocytes and embryos

It was first shown in 2000 that microfluidic channels supported normal embryo development[10] and later in 2001 to show that many microfabrication materials showed good biocompatibility with murine embryos[11]. Both studies used periodic optical microscopy to assess embryo morphology. Degree of biocompatibility was reported as the percentage of two-cell embryos developing into blastocysts by 96 hours compared to petri dish control.

Microfluidic devices later showed functionality of high-throughput single oocyte trapping, fertilization and embryo culture. Allowing multiple embryos to be individually monitored and tracked during their development showing comparable

fertility rates and embryo development to petri dish control[12]. The device improved upon classic embryo culture methods with ease of use through automation that simplified an otherwise labour intensive media changing process in IVF. Due to the scale at which the microfluidic device operates, it only required a small amount of sperm sample for successful fertilization as opposed to its macro-scale counterparts[13].

Meanwhile with specialized channel architecture to produce dynamic fluid mechanical stimulation while maintaining autocrine factor distribution that mimic *in vivo* microenvironments (Fig. A.1), embryos cultured in microenvironments more resembling *in vivo* conditions had more reproductive potential than petri dish controls[14]. This too used periodic optical microscopy and morphology assessment for measure showing an increase in blastocyst development as well as blastocyst cell number as determined by terminal invasive evaluation on fixed and stained embryos. Rare among LOC ART, this study used viability assessment such as implantation percentage and ongoing pregnancy as a primary outcome and showed over 20% improvement by using dynamic microfluidic culture. The device was driven using peristaltic actuation of Braille pins allowing for portability and convenience without the need for extensive syringe pumps and lines connected to the device common to many microfluidic devices. The microfunnel architecture also provided accessibility of the oocytes in both insertion into and extraction from the device via simple pipetting. As opposed to culture in small droplets in a petri dish, LOC ART devices are capable of extracting media during culture through the outlet channel to prevent accumulation of toxic metabolic waste such as ammonia[15] which may harm embryos[16].

LOC sperm morphology assessment

Currently, the most successful treatment for male infertility is using intracytoplasmic sperm injection (ICSI) where oocytes are fertilized via direct injection of sperm. Requiring only a small amount of viable sperm, ICSI drastically increases chances of contraception even for severe cases of sperm-based infertility. While theoretically only one viable sperm is required per harvested oocyte, identifying and isolating the most viable sperm is challenging[17]. Typically samples are purified using centrifugation methods but for difficult samples, laboratories may even hand-sort semen samples consisting of mostly dead sperm and debris to isolate the most motile sperm with healthy morphology. In some cases of extremely low sperm counts, the procedure could take hours making automated sperm sorting a welcome technology in ARTs.

Using microfluidic channel that produce mild, biomimetic sorting mechanism based on sperm motility which avoids centrifugation reported to cause sublethal damage to sperm[17, 18]. Fluid flow using laminar flow regime consists of multiple streamlines. These streamlines are parallel to one another according to channel geometry with the absence of turbulent mixing. Dead sperm, nonmotile sperm and debris are unable to move on their own and thus are simply carried by the streamline they reside in towards the waste reservoir. However, motile sperm are able to swim under their own power and are capable of moving across streamlines into a secondary reservoir designated to contain only motile sperm for extraction[19]. With surface tension and gravity as the driving force, the channel geometry or loading conditions can be controlled to adjust initial surface tension to vary the motility threshold of sperm collected and purity.

A device using fluorescence was design using a built-in micro-cuvette for male subfertility screening. A long microfluidic channel connected the sample chamber to the micro-cuvette produced a barrier that allowed only highly motile sperm to reach the micro-cuvette. Calcein-AM dyed sperm can be quantified using a microfluorometer to assess the level of sperm motility[20] where higher fluorescent signal indicates higher motile sperm count. With signal recorded every 30s for 50 minutes, a profile of sperm motility can be deduced.

Pitfalls of morphology assessments

It cannot be ignored that morphology is a poor indicator of viability such as viable fetus and live birth. A major pitfall for basic use of biophotonics in LOC ART applications that limits their capability for translational human ART research, it opens a large demand for much more sophisticated biophotonics to provide more accurate primary outcome assessments. An issue spanning all fields of ART, not just LOC, it has allowed for an opportunity in ART for advanced predictive algorithms for long term viability assessment using data from simple photonics equipment that can eventually be integrated into LOC to improve primary outcome assessments.

A.3 Advanced Use of Biophotonics in LOC ART

With the increasing popularity of biophotonics, the integration of this technology into LOC ART has been exciting. In recent years, the use of continuous imaging, optical tweezers, traps and broad spectrum spectroscopy has widened the amount of non-invasive analysis for ART purposes that provide quantitative information other than qualitative morphology assessments.

Sperm quality assessment and sorting

In cases of extreme male infertility with the absence of motile sperm, ICSI is still capable of producing live births with non-motile but live sperm. This leaves a great need for the identification of live sperm, even if they are non-motile; a task that is labour intensive and currently requires single sperm isolation and exposure to hypo-osmotic solutions and visualization of membrane swelling[21]. Devices were coated with a polyethylene glycol (PEG) antifouling layer and layered with a photosensitive layer to be used for optoelectronic tweezer (OET) applications. Projected light reduces the impedance on the photosensitive layer to create regions of high electric field. The field generated produces dielectrophoretic force to manipulate micro- and nanoparticles. It was shown that OET is capable of non-invasive sorting of viable non-motile sperm from non-viable sperm without introducing DNA damage[22]. Due to a live cell's ability and a dead cell's inability to keep intact a charge gradient between its cytoplasm and extracellular microenvironment, they respond differently to an electric field. Since live cells have a higher dipole moment by maintaining an ionic gradient across its cell membrane, live cells experience attractive forces toward regions of high electric field while dead or dying cells have no or repulsive forces to the electric field (Fig. A.4)[23]. This OET selection process improves upon existing technologies to retrieve viable sperm independent of its motility overcoming significant challenges in the ICSI sperm selection process particularly for those with extreme infertility complications.

In situations with an abundance of motile sperm, the selection process for the ideal sperm for ICSI is often arbitrary. A group in 2008 developed an automatic microscope system for high-throughput sperm analysis and sorting using an annular laser trap[24]

that previously required laborious joystick control. In addition to recording sperm swim speed using automated cell tracking technology, the system is capable of relocating sperm and releasing them at normal or tangential enter angles against an annular laser trap to which the swim behaviour in response to annular trap is assessed and categorized into three major groups: speeding up in response to and penetrating the annular trap, sperm changing its swimming trajectory and slides briefly along the annular trap, and sperm changing its swimming trajectory and slides along the annular trap for an extended period of time (20s) showing signs of fatigue.

Although not used routinely for human ART, biophotonics combined with microfluidic flow cytometry is now routinely applied for sex preselection of sperm in the agricultural industry. Sperm is extracted from the bull and its DNA stained with Hoescht 33342. Using an argon laser for excitation, the resulting fluorescence signal allow accurate and high-throughput identification resulting fetal sex according to difference in DNA content, and therefore difference in fluorescence intensity between X- and Y- chromosome carrying sperm (approximately a 3.8% increase in signal due to larger X chromosome). After identification of sex, the droplet containing the sperm is charged according to the sex and deflected using a charged plate into collection tubes (Fig. A.5). Flow cytometry combined with fluorescence detection and downstream cell sorting were capable of preselecting the sex of calves with 90% accuracy and produced live calves without anatomical or neurological abnormalities. This system is capable of high-throughput sperm sorting up to 25,000 spermatozoa per second[25]. Although both cytometer and detector are capable of much higher speeds, 25,000 spermatozoa per second was empirically determined as optimal due to

limitations stemming from the need to individually encase each spermatozoa in its own droplet for accurate DNA assessment.

Direct oocyte or embryo quality assessment

Like morphology assessment of spermatozoa, selection of mature oocytes is also often subjective. A quantifiable measure is needed to eliminate subjectivity for optimal selection of the healthiest oocytes for IVF. However the need for non-invasive tests limits the number of biophotonic spectroscopies appropriate for direct analysis of precious cell samples.

Oocytes are positioned in the middle of two optical fibres within a microfluidic device by holding micropipettes commonly used in IVF micromanipulators for ICSI. With a white light illumination fibre and a collection fibre, the absorption spectra can be measured. The absorption spectra provided a quantifiable measure of oocyte maturity by comparing different spectra maxima and width. A fully immature oocyte was found to have maxima of ~630nm wavelength and a width of ~270nm while a fully mature oocyte was found to have maxima of ~580nm and a width of ~210nm (Fig. A.6)[26]. Using the absorption spectra, the subjectivity of determining maturity has been eliminated with quantifiable measures.

Optoelectric tweezers were also used to separate normal oocytes from abnormal oocytes. Via the same mechanism as for sperm, normal oocytes are able to move against gravity under OET induced electric field while abnormal oocytes stay stationary at their initial starting point[27, 28]. With selective discrimination of healthy oocytes, OET induced electric fields provide another non-subjective mechanism for selecting oocytes with the best developmental potential.

The advancement of LOC ART optical microscopy from periodic to continuous imaging has enabled the control of osmotic shock associated with oocyte cryopreservation. Vitrification is the transformation of a substance into glass and the vitrification of oocytes has recently been shown to be more successful than classical slow-freezing cryopreservation in establishing pregnancy[29]. However to prepare oocytes into vitrification solution, a highly hyperosmotic solution, oocytes are transferred stepwise into ever increasing concentrated CPA solutions while suffering from an osmotic shock on each step. Studies have been conducted to show that using extra transfer steps with less change in concentration on each step decreases osmotic shock and increases cryopreservation quality[30] but at the cost of practicality as the transfer of oocytes is delicate, prone to accidents and requires extensive training[31]. With the precision and sensitivity afforded by microfluidics, LOC is capable of exposing oocytes to a continuous profile of gradually increasing CPA concentrations. With a continuous profile, essentially an infinite amount of steps, and microfluidic automation and continuous optical microscopy, the oocytes were shown to be successfully exposed to vitrification solutions with dramatically less osmotic shock and labour than manual controls[32].

Indirect oocyte or embryo quality assessment

As understanding of reproduction and associated technologies become more advanced, simple measures of oocyte quality such as morphology and maturity become insufficient[33]. Indirect oocyte or embryo quality assessment opens the full field of biophotonic spectroscopies to quantify cell quality. Indirect assessments typically perform spent media analysis to calculate oocyte or embryo metabolism. Embryo metabolism provides a much clearer indication of embryo health. For example, mouse

blastocysts with low glycolytic activity (closer to *in-vivo* levels) have been shown to indicate high viability[34] and human blastocysts with the highest glucose uptake were correlated with the highest reproductive potential[35].

An automated, computer-controlled microfluidic device was designed for continuous embryo culture with integrated spent media analysis on-chip. Using a versatile Braille display for pumping and valving, the chip is capable of automated glucose measurement assays with fluidic sampling, pumping, mixing and washing steps (Fig. A.7)[36]. The glucose assay uses coupled glucose oxidase-peroxidase reaction to produce fluorescent resorufin from colourless amplex red reagent at a 1:1 stoichiometry. The long emission wavelengths of resorufin (587nm) allow for sensitive fluorescent quantification of glucose. The chip is capable of real time and continuous culture with measurements every 5 seconds for over 6 hours. Use of a glucose assay that utilizes long excitation wavelengths (488 nm) that are safer for embryos than typical ultraviolet light used in NADPH-linked glucose assays previously used for off-chip embryo metabolism measures was important to prevent exposure of embryos to damaging UV light.

The need of shielding embryos from harmful UV light was the basis of other groups using two devices to perform LOC embryo metabolism measurements to separate embryo cultures from the metabolite assay device later to be subject to UV light. This method was capable of measuring more metabolites using shorter excitation wavelengths but required periodic manual transfer of spent media from embryo culture to microfluidic device. Spent media was extracted via pipetting from microdrops containing embryos on a petri dish and transferred into a microfluidic device. Upon manual loading of spent media sample and reagents necessary for

performing glucose, pyruvate, and lactate enzymatic assays in full automation involving enzyme cocktail aliquotting, mixing of reagents, data acquisition, and data analysis[37]. The device is also capable of serial measurements of metabolites within 5 minutes and full automated analysis of 10 samples with intermittent calibration in a 3 hour period.

A.4 Future of Biophotonics in LOC ART

Due to low pregnancy rates per embryo transferred in IVF, IVF treatments typically transfer multiple embryos simultaneously to increase pregnancy potential. However with each addition of an embryo, the chance of multiple births dramatically increases. Single embryo transfer (SET) is an effective technique to minimize risks of multiple pregnancies but its acceptance is limited due to the inaccuracy of embryo reproductive potential assessments[38]. For SET to gain popularity, a more selective process for the embryo with highest reproductive potential is needed. Biophotonics has made significant advances particularly in metabolic profiling for ART. However current LOC metabolic profiling requires assaying for a specific metabolite of interest. When multiple metabolites of interest are involved, the LOC quickly becomes convoluted in design. The integration of LOCs with external optics also becomes more difficult due to the need to place supporting optics syringe pumps within close proximity to the device. However groups within the biophotonics community, although not on LOC devices, have shown the use of spectroscopy capable of capturing a broad spectrum of metabolites without the need to assay for a specific metabolite.

Although not photonics, nuclear magnetic resonance (NMR) spectroscopy is a powerful technique for non-invasive examination of biological fluids. Based an atomic nuclei's magnetic properties, NMR provides data rich in simultaneous structural and quantitative information capable of screening urine samples for hundreds of pathophysiological conditions in a single spectral measurement[39]. However the technique is expensive in both time and financial costs, although some measurements can take less than a minute, some may take a few hours. NMR also requires highly specialized personnel not always available in a clinical setting to operate equipment and analyse results.

Mass spectroscopy (MS) has also emerged as a popular tool for metabolic profiling providing advantages over other spectroscopies such as the ability to detect many metabolites at physiological conditions from μM concentrations with a high mass accuracy in parts per million[40]. MS was shown to not only be able to detect metabolites consumed by embryos, but also the secretomes of mouse and human embryo. Noting a dramatic difference in secretomes of degenerating embryos and a developing blastocyst[41], MS is providing a new field of opportunities to understand embryonic physiology.

Although not as specific and detailed in information provided compared to NMR, a group used spent embryo media with near-infrared (NIR) spectroscopy to distinguish viable embryos from non-viable embryos independent of morphology. Spectral regions (ROH, -SH, C=C, -OH and –NH groups) of metabolic profiles were quantified using inverse least-squares regression and leave-one-out cross validation to produce a relative embryo viability score to assess embryo reproductive potential[42]. NIR broad spectrum metabolic profiling was shown to be superior to morphology

assessment for selective embryos for SET to produce an on-going pregnancy[43]. At day 2 after SET, metabolic profiling was shown to be 40% more accurate in assessing viable embryos than morphology (69% and 27.6%). At day 3 after SET, it was 15% more accurate with 53.6% accuracy with NIR metabolic profiling as opposed to 38.5% for morphology. The study showed a large inter-patient or inter-embryo variability with regards to the calculated viability score and more studies are needed to identify the causes of this variability. Nevertheless, a low viability score was highly predictive of poor pregnancy. In another study, NIR was shown to have 75% sensitivity at predicting embryo implantation and resultant delivery between binary groups of patients (0 or 100% implantation rates)[42]. With each study, NIR metabolic profiling proves to be a powerful analysis to be used in embryo selection for SET.

Raman spectroscopy uses a laser of monochromatic light that provides similar but complimentary results to NIR spectroscopy. Raman spectroscopy is superior to NIR for aqueous samples due to water producing very weak Raman signals. Raman spectroscopy based metabolic profiling by itself was capable of 80.5% accuracy for predicting (100%) implantation and associated delivery or (0%) failed implantation[44]. In agreement with previously described studies of metabolic profiling, there is a clear correlation between metabolism and reproductive potential for human embryos leaving no question that metabolic profiling is a powerful tool for clinical screening for the best embryos for procedures such as SET in the future.

Currently, embryo cultures were done in microdrops consisting of 50 µL media. Raman and NIR spectroscopy can be performed with 15 µL of spent media in approximately one minute[42]. Its integration into LOC technology will provide quantitative information on how recreating physiological conditions during culture

increase embryo reproductive potential. Using only a fraction of media necessary with conventional microdrop embryo culture, spent media from LOC devices will have a higher ratio between embryos and surrounding media allowing for higher concentrations of secretomes for heightened detector sensitivity to embryo secretion rates. Automation provided by LOC ART promises a less laborious process as well as elimination of operator variability.

The advancement from periodic to continuous imaging alone delivered incredible insight on human embryo development. Continuous monitoring with dark field microscopy is capable of predicting human embryo development into the blastocyst stage with 93% sensitivity by measuring only three parameters by day 2 after fertilization (Fig. A.8)[45]. This study used an automatic computer algorithm for real-time embryo development monitoring and prediction showing that with continuous imaging, promise of advanced diagnosis of embryo potential. The integration of this highly accurate predictive technology to LOC ART applications will greatly increase its viability assessment power and address one major pitfall to LOC ART applications translational human research.

Integration of spectroscopy with microfluidics that allows for broad spectrum analysis of metabolites or secretomes poses significant challenges. LOC automation typically necessitates microfluidic operations embedded into the device. With each operation (mixing, diluting, valving), the device often becomes much more complicated requiring supporting equipment off-chip such as additional syringe pumps (Fig. A.9). For this reason, LOC is often a lab-on-a-chip-in-a-lab of specialized equipment, a major challenge to many biology and chemistry labs adopting the technology. Flexibility of operations such as valve timings is limited due to the built-

in automation nature of LOC. So often when rather small features need adjustment, entirely new masters need to be prepared using photolithography, a specialized technique involving equipment also not available to most chemistry and biology labs. To address these issues to increase the usability of LOC technologies to a broader scientific community, many groups make progress in developing ease fabrication techniques without the use of photolithography[46] and using intelligent design built-in micro geometries to implement microfluidic operations without the use of additional supporting equipment[47].

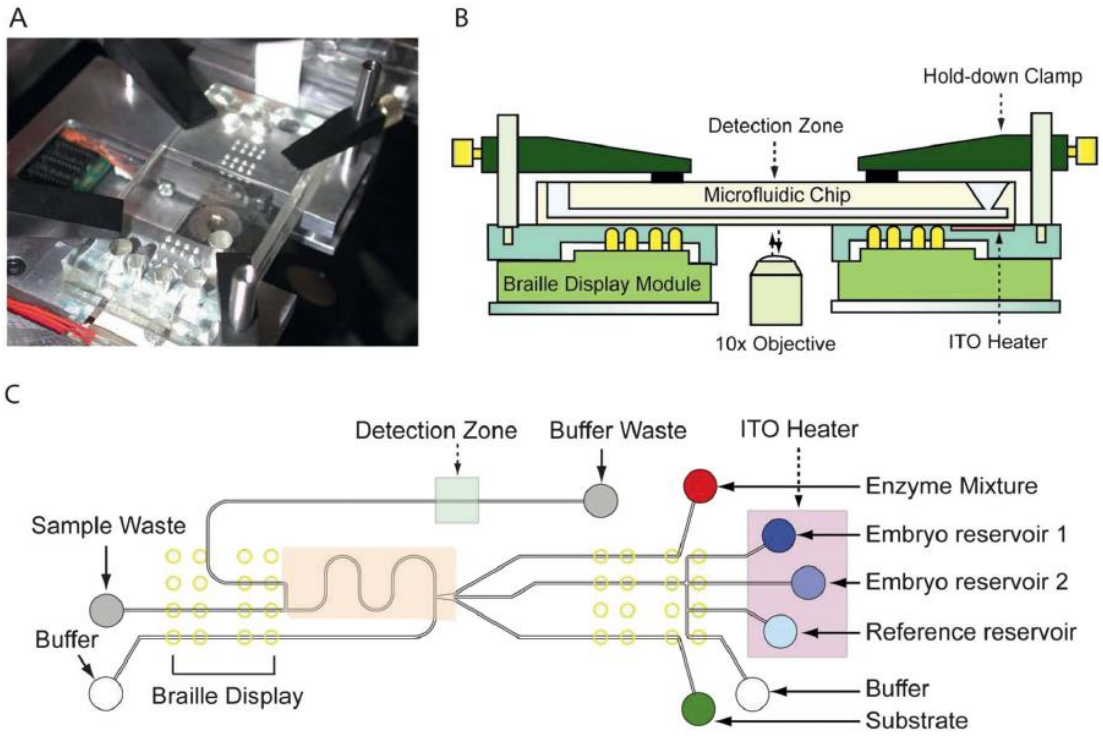

Fig. A.1 Integration of LOC with simple biophotonics [35]. Currently most advanced LOC requires a large amount of supporting equipment, limiting its integration into complex photonics. Progress in implementation of microfluidic operations without the addition of supporting equipment will make LOC integration with highly complex photonics practical.

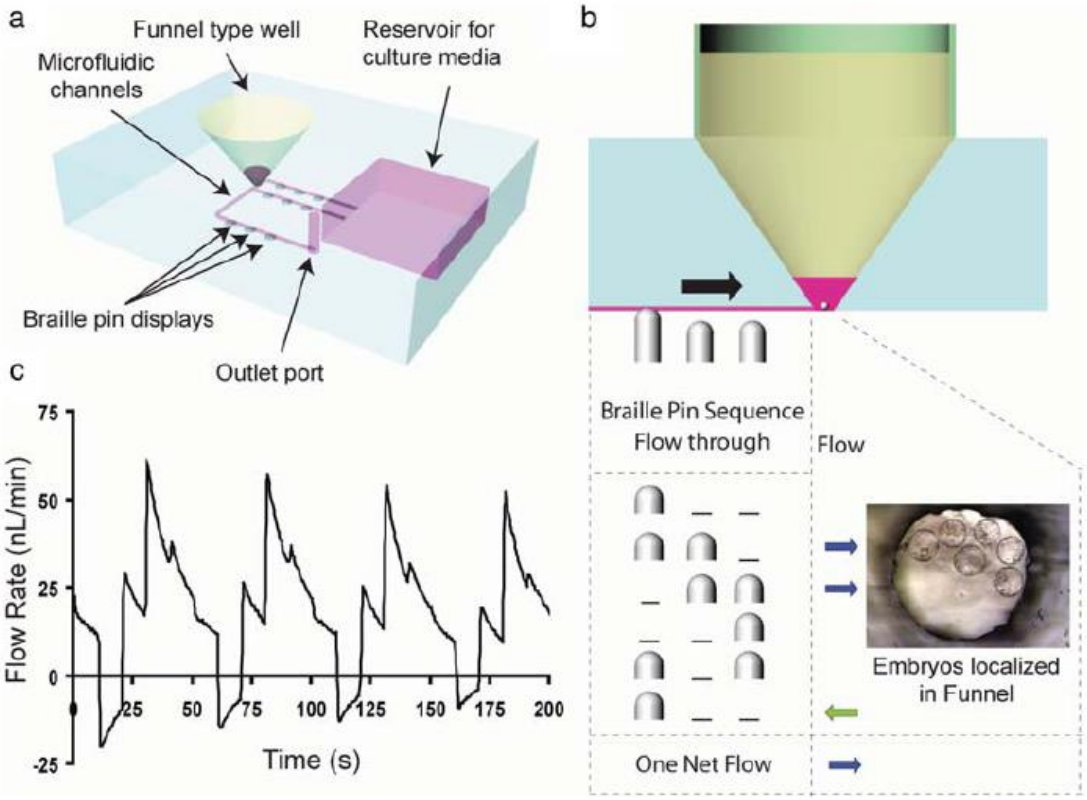

Fig. A.2 (A,C) Dynamic microfunnel architecture provides both autocrine factor retention and mechanical stimulation . (B) The accessibility of the funnel allows for easy embryo introduction into and extraction from the device via simple pipetting. Outlet channel also provided an effective method to prevent the accumulation of toxins from metabolic waste [14].

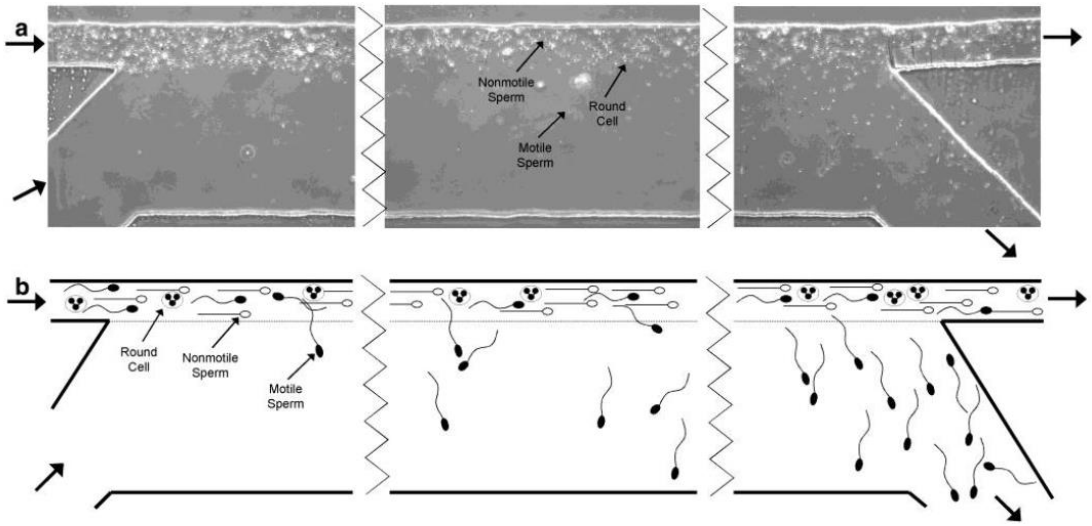

Fig. A.3 A passively driven sperm sorter was built using surface tension and gravity as a driving force and laminar flow regime. Flow is from left to right. Sperm sample is loaded in the reservoir at the top left. Dead sperm, non-motile sperm and debris are carried straight across the top stream while motile sperm are able to swim under their own power and cross streamlines into the collection reservoir in the bottom right [19].

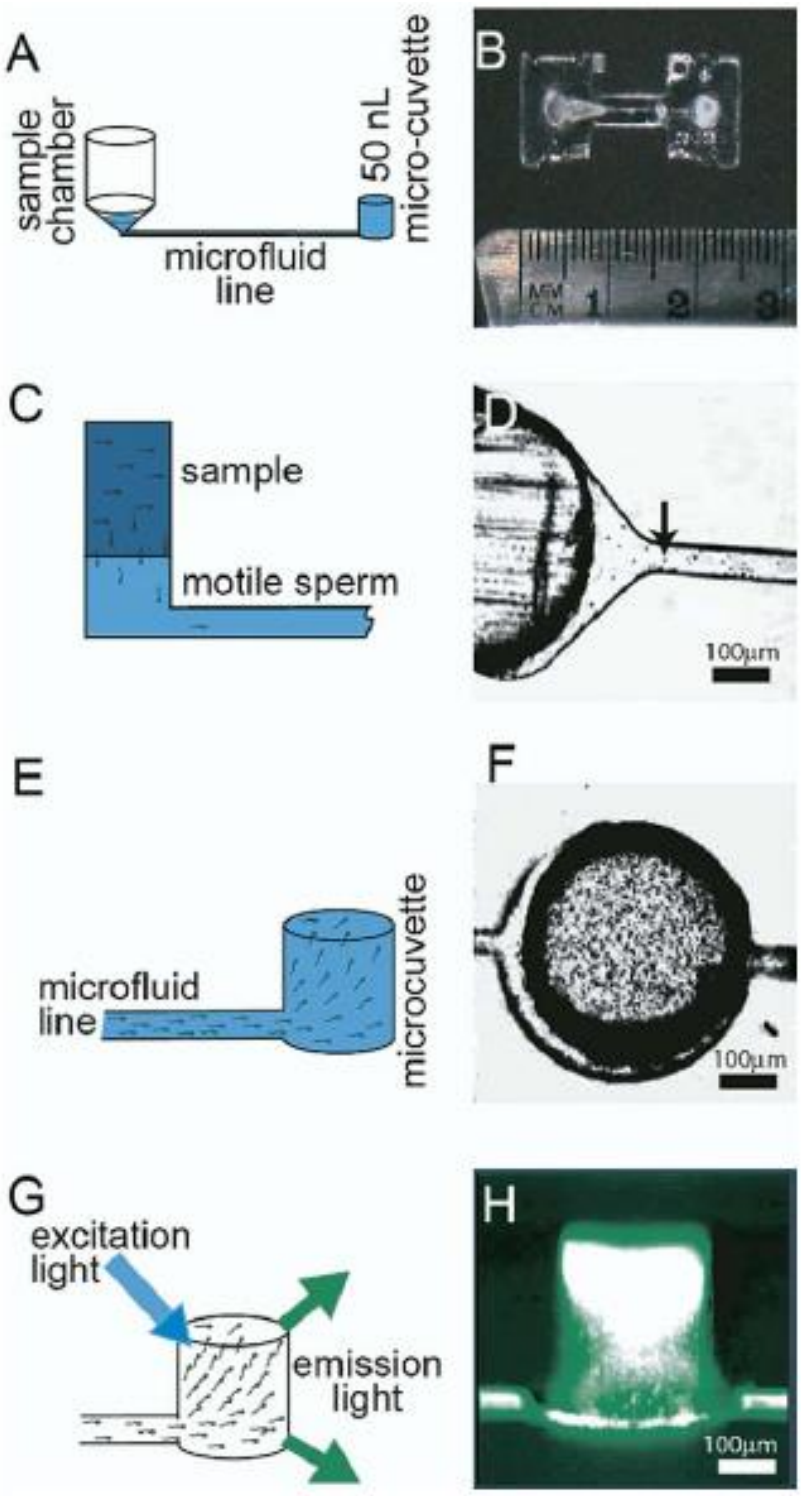

Fig. A.4 (A-B) A microfluidic line connects the sample reservoir to a 50nL micro-cuvette. (C-D) The microfluidic line which serves as a selective filter to separate motile sperm from dead sperm, non-motile sperm and debris is 52 μm^2 in cross section and 6 mm in length. (E-H) Sperm is labelled with Calcein-AM and upon reaching the micro-cuvette are excited by excitation light and the fluorescent light emission is detected to assess the number of motile sperm reaching the micro-cuvette over a 50 minute period [20].

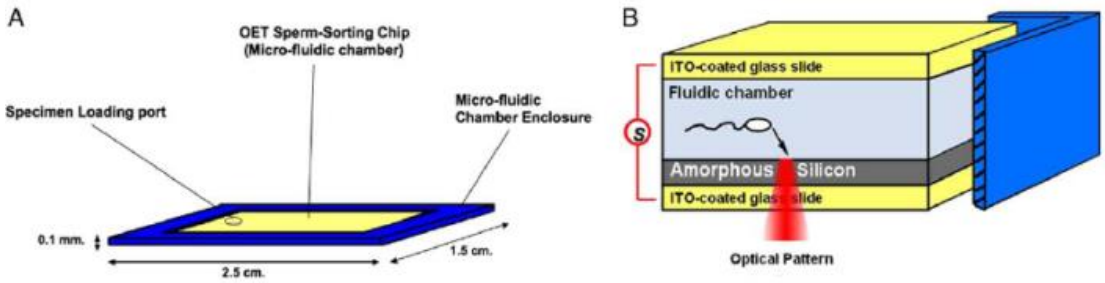

Fig. A.5 Live cells due to the ability to maintain an ionic gradient to the extracellular space are highly polarized in an electric field. While dead cells have no gradient are not polarized. (A) sample is loaded into a microfluidic chamber for OET sorting. (B) Live cells experience attractive forces towards regions of high electric field while dead or dying cells will have weak or no repulsive forces [23].

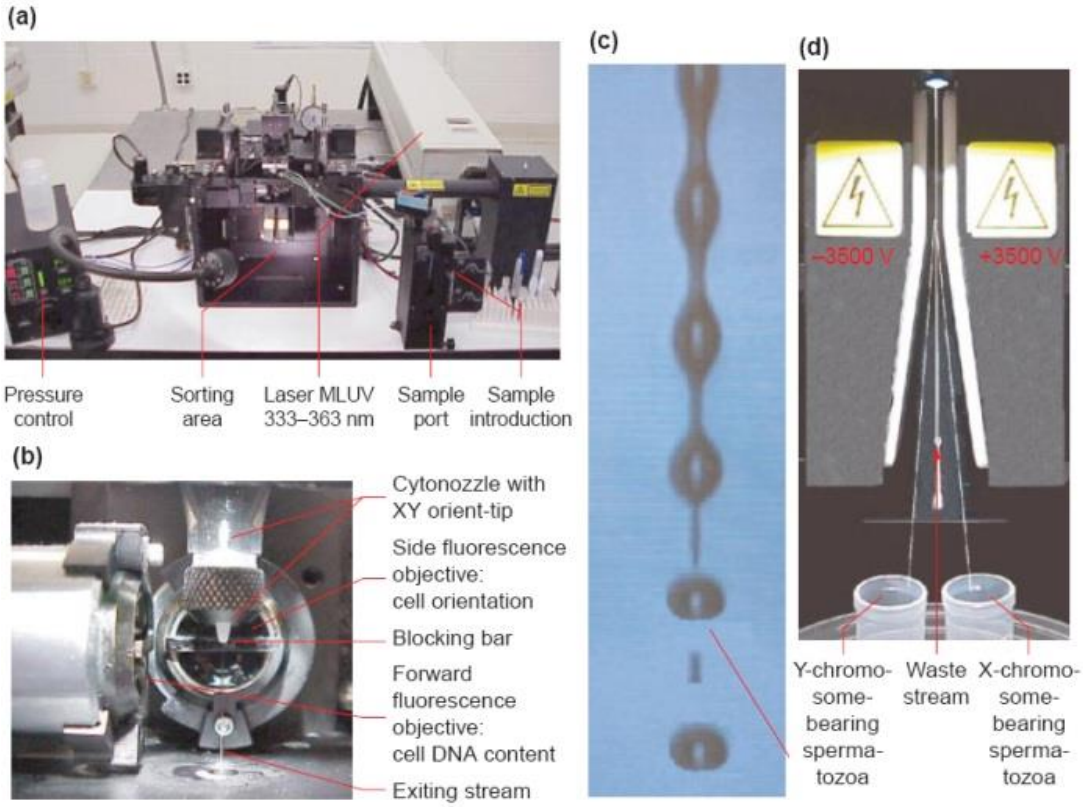

Fig. A.6 (A) Overview of sperm sorter set up. Computer not included. (B) Integration of optics and hydrodynamics. (C) Instabilities in the stream are applied via mechanical vibrations. (D) Droplets are given either a negative or positive charge depending on their sex. Under an electric field, the droplets experience a horizontal force that directs them into the collection tubes [25].

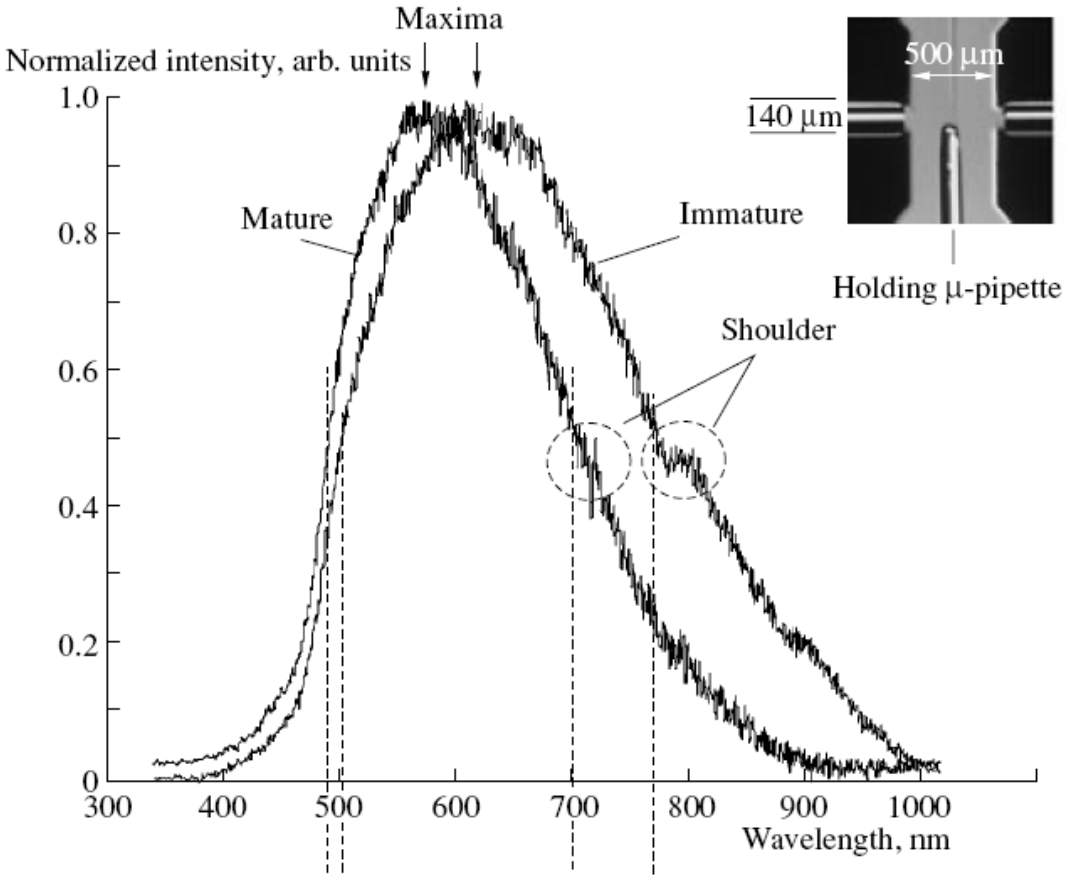

Fig. A.7 The degree of oocyte maturity can be analysed using the absorption spectra by assessing the location of maxima and spectral width [26].

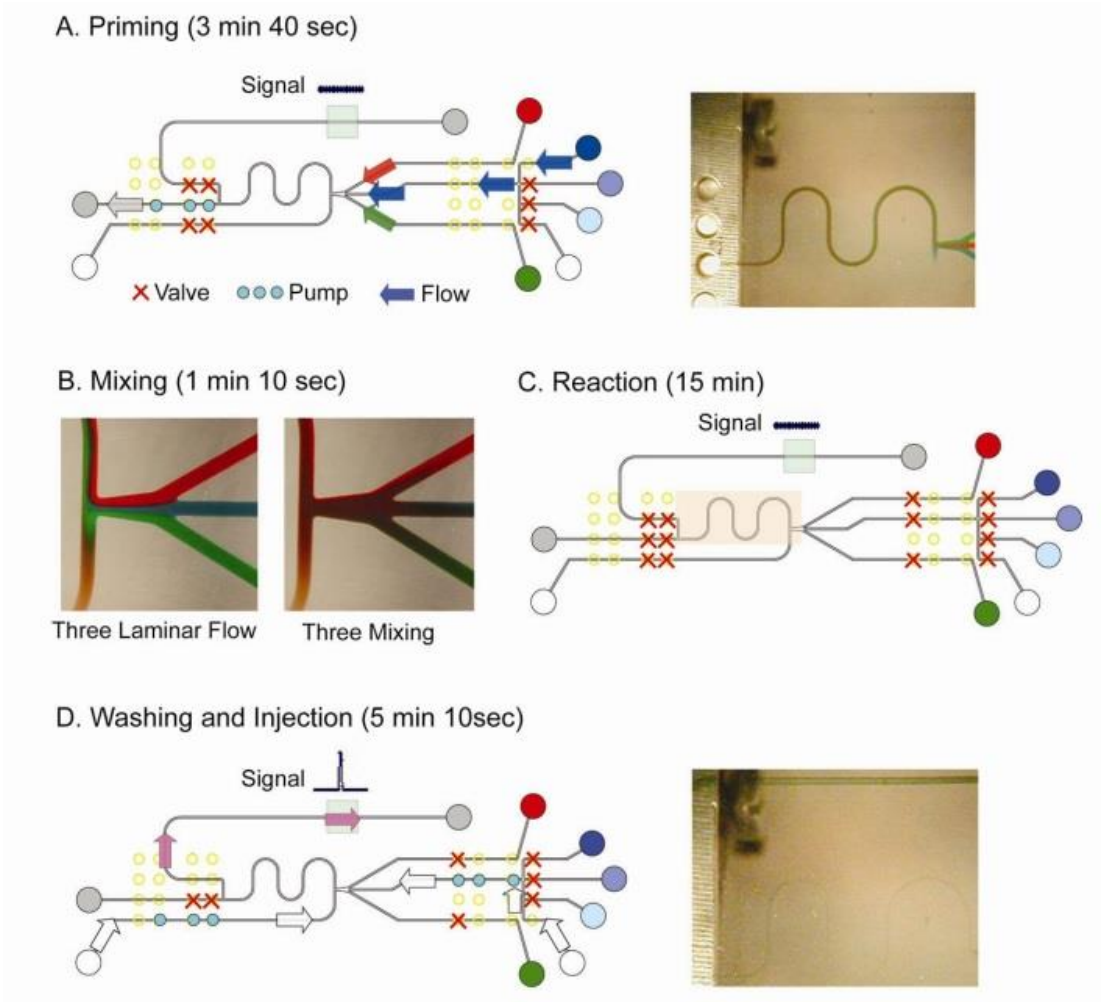

Fig. A.8 Braille-driven device is highly programmable capable of complex operations such as (A) priming, (B-C) mixing and reactions, and (D) washing and injection with minimal support from external sources unlike typical syringe-driven devices that typically require additional syringe pumps for complex operations [36].

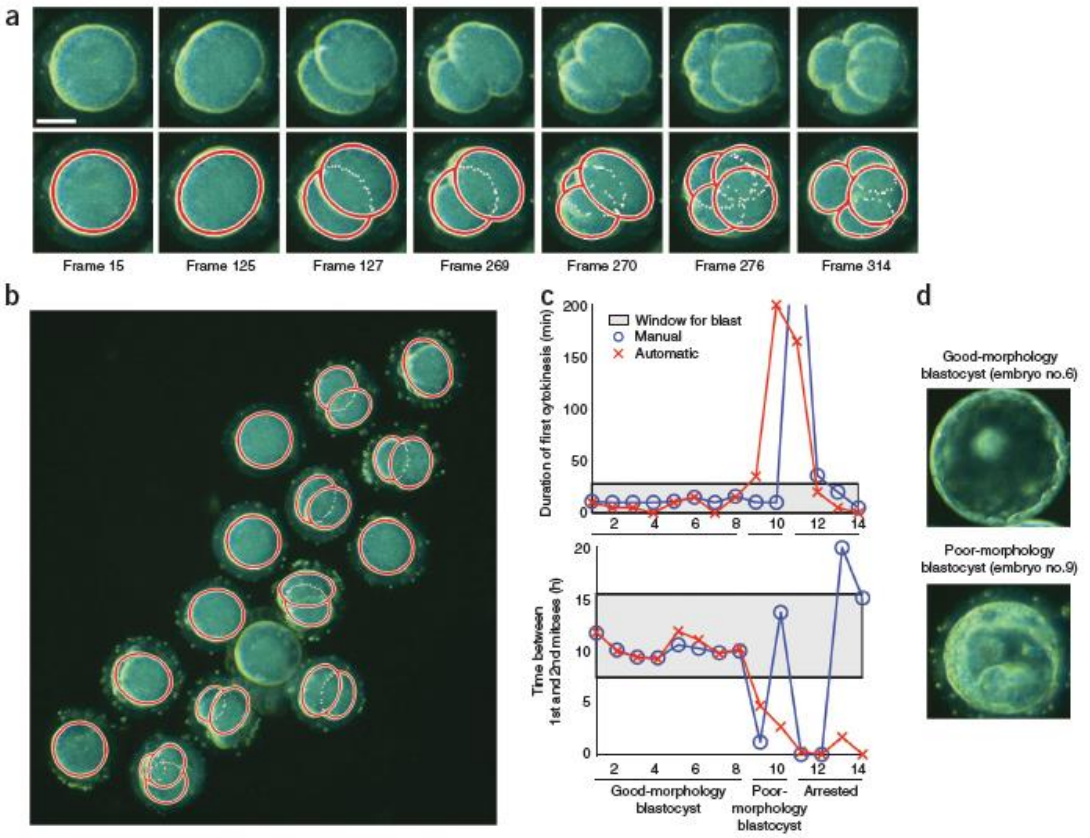

Fig. A.9 (A-B) Continuous imaging combined with automatic monitoring algorithm. (C-D) By analysing parameters such as duration of first cytokinesis and time between 1st and 2nd mitoses, the algorithm is capable of predicting whether embryos will develop with good and bad morphology [45].

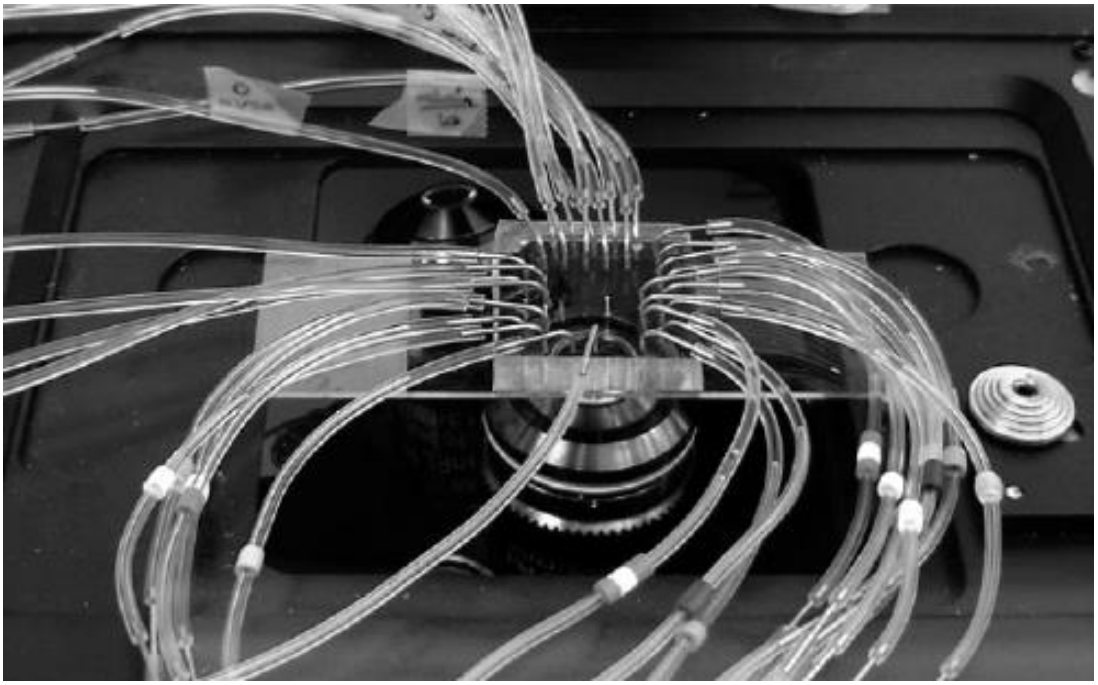

Fig. A.10 With each additional operation in syringe-driven LOC devices, more supportive equipment is necessary (each tube is typically connected to a syringe pump not pictured). With complicated LOCs, it becomes increasingly difficult to integrate with also complicated optics due to spatial limitations [37].

A.5 References

1. A. J. Tomlinson, N. A. Guzman, and S. Naylor, J Capillary Electrop **6**, 247-66 (1995).
2. D. Beebe, M. Wheeler, H. Zerinque, E. Walters, and S. Raty, Theriogenology **57**, 125-35 (2002).
3. J. Shim, T. F. Bersano-Begey, X. Zhu, A. H. Tkacyk, J. J. Linderman, and S. Takayama, Curr Top Med Chem **3**, 687-703 (2003).
4. S. Chung, R. Sudo, V. Vickerman, I. K. Zervantonakis, and R. D. Kamm, Ann Biomed Eng **38**, 1164-77 (2010).
5. A Folch, and M. Toner, Ann Biomed Eng **2**, 227-56 (2000).
6. S. M. Willadsen, Nature **277**, 298-300 (1979).
7. A. Nir, J Theor Biol **214**, 171-9 (2002).
8. H. B. Croxatto, Reprod Biomed Online **4**, 160-9 (2002).
9. Society for Assisted Reproductive Technologies. ART Success Rates report. (2009).
10. J. A. Davis, S. Raty, D. T. Eddington, I. K. Glasgow, H. C. Zeringue, M. B. Wheeler, and D. J. Beebe, in: Microtechnologies in Medicine and Biology, 1st Annual International Conference, Lyon, France, 2000, (IEEE, Lyon, 2000), pp. 307–10.
11. I. K. Glasgow, H. C. Zeringue, D. J. Beebe, S. J. Choi, J. T. Lyman, N. G. Chan, and M. B. Wheeler, IEEE T Bio-Med Eng **48**, 570-8 (2001).
12. C. Han, Q. Zhang, R. Ma, L. Xie, T. Qiu, L. Wang, K. Mitchelson, J. Wang, G. Huang, J. Qian, and J. Cheng, Lab Chip **10**, 2848-54 (2010).
13. R. S. Suh, N. Phadke, D. A. Ohl, S. Takayama, and G. D. Smith, Hum Reprod **21**, 477-83 (2006).
14. Y. S. Heo, L. M. Cabrera, C. L. Bormann, C. T. Shah, S. Takayama, and G. D. Smith, Hum Reprod **25**, 613-22 (2010).
15. D. K. Gardner, and M. Lane, Biol Reprod **48**, 377-85 (1993).
16. M. Lane, and D. K. Gardner, Biol Reprod **69**, 1109-17 (2003).
17. S. Smith, S. Hosid, and L. Scott, Fertil Steril **63**, 591-7 (1995).
18. J. G. Alvarez, J. L. Lasso, L. Blasco, R. C, Nunez, S. Heyner, P. P. Caballero, and B. T. Storey, Hum Reprod **8**, 1087-92 (1993).
19. B. S. Cho, T. G. Schuster, X. Zhu, D. Chang, G. D. Smith, and S. Takayama, Anal Chem **75**, 1671-5 (2003).

20. M. C. McCormack, S. McCallum, and B. Behr, J Urology **175**, 2223-7 (2006).

21. R. S. Jeyendran, H. H. van der Ven, M. Perez-Palaez, B. G. Crabo, and L. J. D. Zaneveld, J Reprod Fertil **70**, 219-28 (1984).

22. A. T. Ohta, M. Garcia, J. K. Valley, L. Banie, H. Y. Hsu, A. Jamshidi, S. L. Neale, T. Lue, and M. C. Wu Lab Chip **10**, 3213-7 (2010).

23. M. M. Garcia, a. T. Ohta, T. J. Walsh, E. Vittinghof, G. Lin, M. C. Wu, and T. F. Lue, J Urology **184**, 2466-72 (2010).

24. L. Shi, B. Shao, T. Chen, and M. Berns, J Biophotonics **2**, 167-77 (2009).

25. G. E. Seidel, and D. L. Garner, Reproduction **124**, 733-43 (2002).

26. R. Zeggari, B. Wacogne, C. Pieralli, C. Roux, and T. Gharbi, Laser Phys **16**, 294-302 (2006).

27. H. Hwang, D. H. Lee, W. Choi, and J. K. Park, Biomicrofluidics **3**, 014103 (2009).

28. J. K. Valley, P. Swinton, W. J. Boscardin, T. F. Lue, P. F. Rinaudo, M. C. Wu, M. M. Garcia, Plos One **5**, e10160 (2010).

29. G. D. Smith, P. C. Serafini, J. Fioravanti, I. Yadid, M. Coslovsky, P. Hassun, J. R. Alegretti, and E. L. Motta, Fertil Steril **94**, 2088-95 (2010).

30. M. Kuwayama, S. Fujikawa, and T. Nagai, Cryobiology **31**, 415-22 (1994).

31. M Antinori, E. Licata, G. Dani, F. Cerusico, C. Versaci, and S. Antinori, Reprod Biomed Online **14**, 72-9 (2007).

32. Y. S. Heo, H. J. Lee, B. A. Hassell, D. Irimia, T. L. Toth, H. Elmoazzen, and M. Toner, Lab Chip **11**, 3530-7 (2011).

33. A. Borini, C. Lagalla, M. Cattoli, E. Sereni, R. Sciajno, Carlo Flamigni, and G. Cotcchio, Reprod Biomed Online **10**, 653-68 (2005).

34. M. Lane, and D. K. Gardner, Hum Reprod **11**, 1975-8 (1996).

35. D. K. Gardner, D. M. Lane, J. Stevens, and W. B. Schoolcraft, Fertil Steril **76**, 1175-80 (2001).

36. Y. S. Heo, L. M. Cabrera, C. L. Bormann, G. D. Smith, and S. Takayama, Lab Chip (2012) DOI: 10.1039/c21c21050a.

37. J. P. Urbanski, M. T. Johnson, D. D. Craig, D. L. Potter, D. K. Gardner, and T. Thorsen, Anal Chem **80**, 6500-7 (2008).

38. D. R. Brison, F. D. Houghton, D. Falconer, S. A. Roberts, J. Hawkhead, P. G. Humpherson, B. A. Lieberman, and H. J. Leese, Hum Reprod **19**, 2319-24 (2004).

39. J. K. Nicholson, J. Connelly, J. C. Lindon, and E. Holmes, Nat Rev Drug Discov **1**, 153-61 (2002).

40. W. B. Dunn, Phys Biol **5**, 011001 (2008).

41. M. G. Katz-Jaffe, W. B. Schoolcraft, and D. K. Gardner, Fertil Steril **86**, 678-85 (2006).

42. E. Seli, D. Sakkas, R. Scott, S. C. Kwok, S. M. Rosendahl, and D. H. Burns, Fertil Steril **88**, 1350-7 (2007).

43. C. G. Vergouw, L. L. Botros, P. Roos, J. W. Lens, R. Schats, P. G. A. Hompes, D. H. Burns, and C. B. Lambalk, Hum Reprod **23**, 1499-504 (2008).

44. R. Scott, E. Seli, K. Miller, D. Sakkas, K. Scott, and D. H. Burns, Fertil Steril **90**, 77-83 (2008).

45. C. C. Wong, K. e. Loewke, N. L. Bossert, B. Behr, C. J. De Jonge, T. M. Baer, and R. A. Reijo Pera, Nat Biotechnol **28**, 1115-21 (2010).

46. C. S. Chen, D. N. Breslauer, J. I. Luna, A. Grimes, W. C. Chin, L. P. Lee, and M. Khine, Lab Chip **8**, 622-4 (2008).

47. B. Mosadegh, C. H. Kuo, Y. C. Tung, Y. Torisawa, T. Bersano-Begey, H. Tavana, and S. Takayama, Nat Phys **6**, 433-7 (2010).

Appendix B

Thinking big by thinking small: application of microfluidic technology to improve ART

In Vitro Fertilization (IVF) laboratories often carry a penchant to resist change while in the pursuit of maintaining consistency in laboratory conditions. However, implementation of new technology is often critical to expand scientific discoveries and to improve upon prior successes to advance the field. Microfluidic platforms represent a technology that has the potential to revolutionize the fundamental processes of IVF. While the focus of microfluidic application in IVF has centered on embryo culture, the innovative platforms carry tremendous potential to improve other procedural steps and represents a possible paradigm shift in how we handle gametes and embryos. The following review will highlight application of various microfluidic platforms in IVF for use in maturation, manipulation, culture, cryopreservation and non-invasive quality assessment; pointing out new insights gained into functions of sperm, oocytes and embryos. Platform design and function will also be discussed, focusing on limitations, advancements and future refinements that can further aid in their clinical implementation.

B.1 Introduction

Within the field of assisted reproductive technologies (ART), like many other fields, there is an ongoing endeavor to improve outcomes and optimize efficiency. Achieving this goal is facilitated by various scientific discoveries regarding the development and function of gametes and preimplantation embryos, of which more are revealed each day. Importantly, technological innovations, several of which are developed with entirely different disciplines in mind, permit many of these new discoveries. Furthermore, in addition to novel information gained from their application, these new technologies may be adapted to change the fundamental approaches used for everyday laboratory procedures, like cell culture. Microfluidics represents such a technological advancement.

While the focus of microfluidic application in ART has recently been centered on embryo culture,[1,2] the innovative platforms carry tremendous potential to revolutionize all aspects of ART and represents a possible paradigm shift in how we handle gametes and embryos (Fig. B.1). The following review will highlight applications of various microfluidic platforms in ART, pointing out new insights gained into functions of sperm, oocytes and embryos, while also highlighting the platforms themselves; specifically focusing on limitations, advancements and future refinements that can further aid in their widespread clinical implementation .

B.2 Andrology

One of the earliest applications of microfluidic platforms in ART entailed assessment of spermatozoa. The constrictive nature of microfluidic platforms and ability to create

complex networks of channels and reservoirs proved a useful combination in assessing characteristics of motile sperm.

As early as 1993, simple microchannel devices made of silicone were used to evaluate rudimentary aspects of sperm function *via* interactions with cervical mucus, hyaluronan, spermicide and anti-sperm antibody beads as motile sperm traversed various network layouts.[3] Follow-up studies demonstrated the ability to perform quantitative sperm counts and motility assessments on etched glass microchannel devices.[4] While these early devices did not integrate active fluid flow or utilize the unique physical aspect of fluids during flow through microfluidic channels, they did provide insight into the potential applications of the platforms. As design and fabrication processes have advanced, application of microfluidics in andrology has grown.

Sperm counts

A microfluidic chip was recently developed consisting of channels etched on a glass wafer fabricated to perform sperm counts. Directing sperm movement at varying velocity by adjusting height of fluid columns from two media reservoirs, cells were able to pass along a microfluidic channel flanked on either side with planar electrodes. The resulting electrical impedance measurements recorded as sperm passed the electrodes permitted estimation of sperm concentration.[5] While the simple media flow generated by gravity and hydrostatic pressure is easy-to-use, careful regulation is required to ensure proper speed of sperm for accurate assessment. Importantly, the approach was able to distinguish sperm from polystyrene beads and HL-60 cells, which is important for clinical application due to other debris in seminal plasma. With refinements and considerations to production costs, a similar system could be

envisioned for use for routine semen analysis to streamline and standardize sperm counts.

Sperm separation

Perhaps the most widespread application of microfluidic technology in andrology entails use for sperm separation. Many of these approaches rely on devices that generate fluid flow from media reservoirs through some sort of microchannel. Devices designed using microfluidic channels for sperm separation are highly dependent upon variables affecting the laminar flow and velocity of the fluid streams in motion. Factors like channel width, height, depth, as well as fluid velocity and viscosity are all critical parameters that must be considered when trying to optimize separation of a specific sperm population. This task is further complicated by the varying viscosity of semen and presence of cellular debris in addition to sperm. Despite these sometimes difficult variables, several modern devices have addressed some of these issues.

One of the earlier reports using microfluidic technology for separation of motile sperm from semen samples utilized a polydimethylsiloxane (PDMS) passive gravity-driven device where the hydrostatic pressure of two separate inlet reservoirs drove media flow down a converging microfluidic channel[6] (Fig. B.2) The principle of the device took advantage of the fact that only motile sperm can traverse the border that separates the parallel streams of diluted semen and fresh medium. Thus, the laminar flow properties exhibited by media in microchannels allowed motile sperm to swim away from non-motile sperm, debris, and seminal plasma and collect in a separate outlet reservoir. Follow-up experiments demonstrated this microfluidic device design was not only biocompatible with human sperm, but that it could isolate motile,

morphologically normal cells.[7]The novel approach appeared to offer a feasible alternative to isolate sperm from oligozoospermic patients for use in intra-cytoplasmic sperm injection (ICSI).

Another approach employing microfluidics for sperm sorting utilized mouse sperm placed into a PDMS/glass device, to isolate sperm based on motility, but also *via* chemotaxis towards cumulus cells.[8] Sperm were placed into an inlet reservoir and allowed to swim down a straight channel, whose dimensions were optimized for motile sperm recovery. Sperm were then collected in a small central reservoir, where video imaging could occur, before swimming onward into 1 of 2 branching channels, each leading to separate collection reservoir. Other microfluidic devices to explore sperm chemotaxis also exist and offer further unique tools to explore sperm function.[9]

In another use of microfluidic technology for andrology, a PDMS/glass device was constructed that directed sperm flow within microchannels to separate, align and orient sperm of mouse, bull and human,[10]providing potential applications for ICSI. Utilizing the fact that motile sperm orient themselves against media flow within these devices, and that motile sperm can swim against media flow of certain velocity, a series of three reservoirs and four microfluidic channels allow processing of sperm *via* hydrostatic media flow. Of note, this device requires very precise regulation of media volumes within the reservoirs to regulate hydrostatic pressure.

Utilizing these advantages of a microfluidic device for sperm isolation, implementation of a microfluidic sperm sorter manufactured out of quartz has begun in clinical IVF. A preliminary report indicates human semen can be processed rapidly and isolated motile sperm can be used to successfully fertilize human oocytes following ICSI[11] (Fig. B.2). Follow up studies by the same group have since produced

PDMS versions of the sperm separation device that have widened microfluidic channels to help isolate sperm with higher velocity and are more cost-effective to permit clinical application.[12]

Due to the limitations inherent in a microfluidic sperm sorting device, utilization of the technology must provide some added benefit over conventional processing methods. Conventional sperm preparation methods, such as serial centrifugation, density gradient separation or swim-up, are reported to induce sperm DNA damage, perhaps to exposure to reaction oxygen species (ROS).[13–15] Preliminary data indicate that sperm isolated using a microfluidic sperm sorting device had significantly lower levels of DNA damage and higher motility compared to these more conventional approaches.[16] Thus, microfluidic sperm sorting may allow for selection of higher quality sperm, potentially leading to improved embryo quality. With the above mentioned applications, one can envision a microfluidic device that assesses sperm concentration, motility, progression and then separates sperm based on various qualities or characteristics. This isolated sperm could then be manipulated in a fashion to make it suitable for ICSI within the same microfluidic platform to streamline the current practice of moving sperm from dish-to-dish. This approach could prove a powerful tool in reducing variability in andrology laboratory testing and processing and help improving ART outcomes. However, it should be noted that, despite the ability of microfluidic devices to perform high-speed and high-throughput sperm sorting, selection is based solely on motility. Thus, the approach is unable to identify non-motile but viable sperm for ICSI, which is relevant for patients suffering from severe or complete asthenozoospermia.

B.3 Embryology

Employing microfluidic technology for embryology requires considerations unique from microfluidic devices utilized with adherent cells, or even those used for sperm assessment. The main obstacle to consider is reliability of cell recovery. While it may be acceptable to recover only a portion of an initial cell population when dealing with hundreds of thousands or millions of cells, 100% recovery is essential for applications involving oocytes and embryos. Thus, platform design must make accessibility and recovery of paramount importance, and it must do so without limiting the inherent properties of microfluidics that make it advantageous to cell biology, namely the constrictive nature. In addition, the added effort and cost of applying microfluidics must be offset by a measurable benefit on gametes or embryos to justify implementation of the technology. Fortunately, many of these issues are actively being addressed, and, as a result, platforms have begun to receive initial testing in all aspects of embryology, including *in vitro* oocyte maturation (IVM),*in vitro* fertilization (IVF) and embryo culture.

Oocyte maturation

In vitro oocyte maturation is an especially appealing approach for human ART considering the tremendous advantages offered, including reduced cost and reduced health risk to disorders such as ovarian hyperstimulation syndrome (OHSS).[17] However, IVM is still an inefficient practice. Fortunately, microfluidic approaches offer the potential to improve current IVM success rates. In the first report of oocyte maturation using microfluidics, a microfluidic channel flanked by two media reservoirs with no regulated media flow, did not result in porcine oocytes maturing efficiently in silicone devices (2% Metaphase II; MII). However, when these

oocytes were matured in PDMS devices, they matured at a significantly higher rate compared to control microdrops (2% *vs.* 71% to MII, respectively).[18] Interestingly, cumulus cell expansion was noticeably diminished in oocytes matured in microchannels compared to larger microdrops. This observation may be indicative of quality oocyte cytoplasmic maturation, as oocytes regulate cumulus cell development and function.[19] Thus, while the size and/or volume limitations of microchannels may improve nuclear maturation, they may also have some limiting effect on porcine oocyte cytoplasmic properties, or physically restrict cumulus expansion. In contrast, subsequent follow-up experiments by Walters and coworkers from the same research group suggest oocyte cytoplasmic maturation may actually be enhanced in static microchannels. Pig oocytes matured in 250 μm wide PDMS/borosilicate glass microchannels produced significantly higher numbers of 2-cell embryos following IVF and embryo culture in microdrops compared to oocytes matured in 500 μl drops (67 *vs.* 49%).[20] Unfortunately, pronuclear formation, embryo development past the maternal-zygotic transition, or blastocyst cell numbers as measures of improved oocyte developmental competence were not reported. The differential results from these studies in similar designed devices of differing materials suggest that material selection is of paramount importance for the sensitive oocyte.

Interestingly, preliminary studies indicate bovine oocytes matured in PDMS microfunnels with Braille pin regulated media flow actually yields improved blastocyst development following IVM compared to static matured oocytes (unpublished results). Despite these preliminary findings, the field awaits peer reviewed publications examining effects of fluid flow in microfluidic devices on more informative markers of oocyte developmental competence. Toward this end, a

microfluidic device does exist that utilizes magnetically actuated manipulators in conjunction with ultrasonic vibration for single cell manipulation.[21] This device can move and orient porcine oocytes and may be modified for potential micromanipulation purposes. Interestingly, a vibrating culture platform was previously shown to enhance porcine oocyte developmental competence when applied to standard culture dishes with larger volumes.[22] Thus, the vibrational aspect of the previously mentioned microfluidic device used to move oocytes may also offer some benefit to oocyte cytoplasmic maturation and could be potentially modified to improve IVM.

In vitro fertilization

Another demonstration of microfluidic application in ART can be seen in insemination performed "on chip". Insemination is a particularly difficult procedural step in ART, as sperm motility characteristics and interactions with oocytes in microfluidic channels are highly dependent upon fluid flow rate. The speed of fluid movement influences sperm motion and a threshold exists where sperm are no longer capable of independent movement.[23] Furthermore, sperm motion paths can be influenced by the contours of the device. These qualities have immense implications for success of fertilization within microfluidic platforms.

The first attempt at the procedural step of insemination was performed using porcine oocytes placed into PDMS/borosilicate microchannels (Fig. B.3). Sperm were added in a manner where hydrostatic pressure differences created from differing volume of media added to reservoirs at either end of the microchannel resulted in gravity-driven fluid flow of sperm past oocytes, which were immobilized at a constriction point within the microchannel. Fertilization in this device resulted in

significantly lower rates of polyspermic penetration compared to fertilization in control microdrops.[24] Reduced polyspermic penetration rates were attributed to the physical characteristics of the microfluidic device, mimicking the environment *in vivo*. It was hypothesized that microfluidic devices served to limit time of oocyte exposure to sperm, as sperm were not confined to the vicinity of the oocytes, but allowed to flow past the eggs.

Subsequently, Suh and colleagues demonstrated successful fertilization of mouse oocytes on a more complex microfluidic device that consisted of a series of open slots within a microchannel[25] (Fig. B.3). Although initial experiments utilizing high concentrations of sperm revealed that overall fertilization rates were decreased on the microfluidic device compared to control microdrops, subsequent experiments demonstrated that, by lowering sperm concentration, fertilization rates in microfluidic devices were actually higher than controls. These results appear to be the result of chip design, as authors observed increased concentration of sperm in the vicinity of the oocyte in microfluidic devices.

More recently, fertilization has been performed on a microfluidic microwell device[26,27] (Fig. B.3). Similar to previous devices, platforms were made of PDMS and constructed with an inlet and outlet reservoir, which generated media flow using gravity. Microchannels leading from each reservoir connect to a larger microchamber that housed individual square microwells containing individual oocytes. Microwell depth was optimized to permit retention of oocytes while allowing adequate debris removal and sperm interaction with oocytes. Media and sperm could then be flowed over the microwells housing the oocytes. Using this approach, similar rates of mouse oocyte fertilization were obtained compared to controls (69.0 *vs.* 71.4%).[26] An

alternate device from the same research group with differing design to incorporate multiple procedural steps also yielded promising fertilization results.[27] Additional microfluidic devices incorporating insemination with other procedural steps have also been developed and are discussed later.[26]

Other oocyte manipulations

In addition to maturation and insemination, other oocyte manipulations are common during routine IVF procedures. Microfluidic devices have been developed that can perform some of these tasks. Cumulus cell removal can be performed in a series of microchannels.[28,29] Utilizing fluid flow driven manually *via* attached syringes, exposing oocytes to chemical and physical manipulation, cumulus cells could be removed, leaving the oocyte intact. A similar approach has also been successful in removing the zona pellucida.[30] More recently, a system combining microfluidic channels and an optical ablation laser was used to manipulate clam oocytes through a series of channels, which permitted media exchange and positioning of cells for laser ablation.[31] Application of a similar device that could rotate cells[32] could be envisioned as useful for clinical procedures like assisted hatching.

Embryo culture

Exhaustive studies have been conducted aimed at optimizing preimplantation embryo culture system *in vitro*, and, similar to IVM and IVF, a microfluidic platform may aid in this endeavor. The initial report on embryo culture using microfluidics by Raty and colleagues indicated that 2-cell mouse embryos could be cultured to the blastocyst stage within static microchannels[33,34] (Fig. B.4A). Compared to 30 μl control microdrops, culture within these microchannels containing about 500 μl of media

resulted in significantly greater 16-cell/morula formation at 24 h, greater blastocyst formation at 48 h and 72 h, and a greater portion of hatched blastocysts at 72 and 96 h. However, impact on implantation or live birth was not evaluated. Subsequent experiments utilizing a similar device by Walters and coworkers from the same research group showed that *in vivo* derived 4-cell porcine embryos could be cultured to blastocyst and transferred, resulting in live birth.[35] However, in these follow-up experiments, no observable beneficial effects on embryo development were seen when compared to culture in control organ-well dishes. Furthermore, cell recovery issues were apparent when culturing cells in microchannels.

Building upon their initial microchannel static embryo culture studies, Hickman *et al.* examined mouse embryo development in microchannels with media flow, controlled *via* an external large syringe infusion pump.[36] Flow rates examined (0.1 and 0.5 μl h^{-1}) did not enhance development compared to static culture. In fact, a flow-rate of 0.5 μl h^{-1} resulted in significantly lower development of 2-cell mouse embryos to morula and blastocyst stages, while producing higher numbers of abnormal embryos compared to controls. Thus, flow rate and manner of flow delivery appeared to be important variables for embryo culture in microfluidic devices. Indeed, embryos can sense sheer stress, which can induce apoptosis and be detrimental to embryo development.[37] However, it is questionable if flow rates necessary for dynamic fluid flow in microfluidic channels would approach velocities high enough to cause concern. Additionally, it should be noted that these data on the impact of media flow and flow-rate on embryo development should be re-assessed, as culture conditions may have been suboptimal. In this particular study, control mouse embryos cultured in control static microchannels did not improve embryo development as

previously reported by Raty and colleagues from the same research group.[33] One possible source of variation requiring future study was the increased number of embryos cultured in each device, a factor which undoubtedly would have an impact due to influence of group embryo culture,[38,39] especially within the confines of a microfluidic platform.

Yet another approach to culturing embryos within microfluidic device employed not only dynamic media flow, but also co-culture. Mizuno and coworkers developed a "womb-on-a-chip", where endometrial cells can be grown in a lower chamber, while embryos are cultured in an upper chamber, separated from the lower by a thin membrane[40,41] (Fig. B.5A). The design permits embryo exposure to secreted factors from the endometrial cells, while avoiding direct cell contact. In their preliminary report, authors demonstrated that mouse ova fertilized on and resulting embryos cultured in these devices showed similar cleavage to 2-cell and similar blastocyst formation rates compared to 50 ul control microdrops.[40] Furthermore, cell number was significantly higher in blastocysts fertilized/cultured in microfluidic devices. Subsequently, blastocysts obtained from microfluidic devices were transferred to recipient female mice and resulted in live offspring at rates similar to embryo cultured in static microdrops. A similar co-culture approach was taken by the same group, culturing 2-cell mouse embryos to blastocyst stage on the refined OptiCell microfluidic device. OptiCell microfluidic co-culture culture yielded chromosomally normal embryos, capable of yielding live offspring.[42]Mizuno and colleagues later published an abstract reporting the first instance of human embryo culture within their co-culture microfluidic devices. Donated 2–4 stage frozen human embryos were cultured to the blastocyst stage, resulting in significantly higher rates of blastocyst

development from microfluidic devices compared to control microdrops.[41] Additionally, visual scoring of microfluidic-derived blastocyst development revealed higher quality blastocysts with significantly higher cell numbers compared to static controls. A similar device was later constructed using a microporous membrane to separate mouse embryos from endometrial cells[43] (Fig. B.5B). Unfortunately, co-culture confounds interpretation of results obtained, as it is impossible to discern if beneficial effects are attributed to co-culture or the physical properties of the microfluidic device/design.

Notably, a braille pumping system using tiny electric piezo actuators has been used successfully to grow embryos by peristaltic media motion along microchannels formed in PDMS through a microfunnel housing the cells[44–47] (Fig. B.4B) This approach is unique from other microfluidic devices used in ART, in that it permits precise computerized regulation of speed and flow patterns, rather than passive media flow due to gravity, or the more course media flow provided by external syringes. It was demonstrated that regardless of media flow pattern (back and forth *vs.* flow-through) or speed (fast *vs.* slow), 1-cell mouse embryos cultured in these microfluidic devices showed greater hatching of blastocysts and significantly higher cell number than static controls, yielding numbers similar to those obtained from *in vivo* derived blastocysts.[45,47] It was also shown that this approach produced greater number of mouse embryos reaching morula stage at 48 h, blastocyst at 72 h and hatched blastocyst at 96 h compared to control static chips, while significantly more bovine embryos reached the blastocyst stage at 144 h in microfluidic devices compared to control static devices.[44] Follow up experiments indicated that beneficial effects of embryo culture in the dynamic culture device are additive and require a minimum 48

h of culture at the beginning or end of 96 h culture periods.[46,47] Importantly, this device was the first report that a microfluidic dynamic culture platform could not only improve preimplantation embryo development, but that quality of embryos cultured in a microfluidic device with media flow are superior to those grown in static systems, as evidenced by increased implantation rates, lower rates of absorption and higher ongoing pregnancy rates in mouse.[47] Also important to note, the studies were eloquently controlled using static controls within the microfunnel platform, which permitted the conclusion that the media flow as responsible for beneficial effects, rather than simply an effect of the material or microfunnel design. Subsequently, a modified microfunnel constructed for clinical trials was able to support human blastocyst formation, while producing higher quality embryos on day 3 with lower levels of fragmentation[48] (Fig. B.4C)

More recently, at least one study has used a tilting culture system in conjunction with microfluidic channels to gently agitate embryos during culture. Bovine embryos were tilted 10° over 1 min and cultured inside straight microchannels or microchannels with a 150–160 μm constriction. Though no difference in blastocyst formation was observed, and the influence of the tilting system alone was not examined, authors suggest that combining an embryo tilting system with a 169 um constricted microchannel may offer a means of improving bovine embryo cleavage, yielding higher rates of 8-cell development after 44 h or culture compared to straight channels (56.7 *vs.* 23.9%).[49] It should be pointed out, however, that the tilting approach is simply agitation and doesn't necessary remove or replenish the existing media like perfusion systems. A similar microchannel system from the same group also examined use of a micromodulated syringe pump for culturing bovine embryos to

supply mechanical stimulation.[50] Similar methods of combining a simplified microchannel or microfluidic devices with other dynamic methods of inducing fluid movement, generally used at the macro-level, such as vibration or agitation, may be helpful, as gentle agitation appears to beneficial for human embryos.[51,52] Though the more recent dynamic culture platforms that agitate media and embryos by simply placing traditional culture dishes with microdrops or larger volumes of media on a moving or vibrating platform have been examined and appear promising,[51–54,22,49] in the context of this review, these aren't considered microfluidic culture platforms and may not utilize the full potential of the constrictive microenvironments offered by microfluidic approaches.

Regardless, microfluidic systems with perfusion, or some other means of agitation, may benefit embryo development for a variety of reasons. One intriguing possibility is the idea that gentle mechanical stimulation, either through fluid flow or gentle movement of the embryos, could be beneficial. This "Active Embryo Hypothesis", theorizes that gentle physical stimulation of embryos can activate embryotrophic signaling pathways and promote embryo development.[55] However, excessive forces can be detrimental. Indeed, it is well known that various sensory mechanotranduction systems are evident in a variety of cells types, usually manifested by regulation of ion channels.[56] The same may hold true in embryos, or even oocytes, as it is known that embryos can sense sheer forces for rotating embryo culture or other pipetting, which activates various signaling cascades.[37,57] Whether beneficial signaling pathways are activated in mammalian oocytes or embryos within these dynamic culture platforms, what these pathways may be, or whether they are responsible for observed benefits, remains unknown.

Finally, another aspect of novel microfluidic culture devices that may convey an unexpected benefit to developing embryos is the use of novel materials. While these materials may be initially selected due to ease of manufacturing intricate designs using techniques such as photolithography, the platforms surfaces themselves may improve embryo development. Indeed, it has been postulated that coating of platform surfaces with specific molecules may benefit embryo development, either through direct physical effects, or through modifications of the chemical environment.[2,55] Thus, the actual material used in device construction may also impact the culture microenvironment. This was found to be the case when using PDMS for culture device construction, as the material is absorptive and caused detrimental osmolality shifts unless a specialized parylene coating was applied.[58] It was later reported that PDMS embryo culture devices that were "softer" supported better embryo development.[59] In comparing polystyrene of high stiffness, with a softer PDMS or collagen, it was found that softer surfaces improved embryo and placental development. However, due to the zona pellucida as a barrier preventing direct contact to the embryo, the stiffness of the polymer or substrate likely played no role. Rather, the absorptive nature of the varying surfaces likely differed and differently impacted media characteristics. Interestingly, it was recently reported that standard polystyrene petri dishes, as most commonly used to culture embryos, may weaken cells, as evidenced by reduced proliferative capacity along a vertical wall of adherent cell lines[60] Specifically, it found a subtle softening and swelling of the polystyrene surface due to interactions with water that created nanoscopic layers of hydroxide ions that altered localized pH and induced a layer of ROS. This may have ramifications for optimizing embryo culture and use of more appropriate surfaces or materials may be warranted.

B.4 Cryopreservation

Expanding upon the application of microfluidic devices for specific procedural steps within ART, the precise fluid control offered by these dynamic platforms may be especially well-suited to exposure to cryoprotectants. Conditions of cryoprotectant exposure can impact cell function and survival, with factors like concentration and time of exposure as crucial variables.[61] This is especially true for vitrification approaches, which utilize very high concentrations of cryoprotectant agent (CPA) and require very low exposure times to prevent toxicity. Detrimental effects of CPA exposure on genotoxicity, even without cryopreservation, have been shown.[62] Even sub-lethal genotoxicity such as DNA fragmentation[63] can still cause catastrophic outcomes.[64] Thus, given the fact that oocyte vitrification procedure successes to date have been achieved despite the lack of a quantitative understanding of the mechanical and chemical effects different CPAs and CPA exchange procedures can have on gametes and embryos, microfluidics may permit optimizing CPA exchange procedures and reduce sub-lethal damages.

Importantly, practical issues exist with current manual cryoprotectant exposure regimes that limit preciseness and repeatability. There is inherent variability in timing of manual procedures between individuals. Also, discrete manual dilution steps are required to make cryoprotectant exposure feasible. While logistically important for the embryologist, these approaches may not be ideal for the cell. Thus, it is clear that currently, laboratories lack the tools needed to perform CPA exchange precisely at the cellular level.

Although the two or three step CPA exchange concept is now relatively broadly accepted for embryo or oocyte vitrification, the exact procedure differs from lab to lab contributing to the variability in cryopreservation success rates. More fundamentally, there is a problem that there are more potential combinations of CPAs and CPA exchange procedures that could be utilized than can be efficiently and reliably tested for by trial and error experiments alone. The approach of using specialized bioengineered devices to design vitrification CPA exchange protocols, where manual dilutions do not limit efficacy, might help alleviate both the osmotic shock (mechanical effects) and CPA toxicity (chemical effects). A more gradual, rather than sudden stepwise increases in CPA concentration, is known to increase viability.[65] There is a practical and capability limit, however, in terms of how many exposure steps and in what time the CPA exchange can be performed using the current gold standard; manual pipetting. Furthermore, the transfer of cells from solution to solution for each step involves rapid pipetting that can introduce mechanical stress.[57]

To address these current limitations with manual approaches, microfluidic devices have been designed where, rather than moving the oocyte from one CPA solution to another by pipetting, the oocyte will be stationary and the CPA solutions will be pumped over it by computer control. This permits continuous and gradual, rather than discrete step increases, in CPA concentrations that the oocyte is exposed to. Preliminary reports indicate potential of this approach. Controlled CPA exposure with a microfluidic platform reduced the size change of oocytes compared to traditional approaches, which may be important for cell viability[66](Fig. B.6A). However, the platform design yields limited access to cells for loading and removal, which is

problematic in terms of clinical practicality. A similar approach for using computerized control of media exposure to permit gradual cryoprotectant exchange to limit large osmolality changes have been used with embryos[67] (Fig. B.6B). Perhaps more importantly, use of a microfluidic platform for gradual CPA removal during oocyte/embryo warming may be beneficial in further optimizing cryosurvival. This application remains to be explored.

Another obstacle that has hindered rapid and wide-spread acceptance of vitrification approaches has centered on ease-of-use issues of vitrification devices. There are numerous commercially available and in-house devices to contain oocytes or embryos for low temperature storage following vitrification.[68] These utilize very small volumes of vitrification solution to permit the vitrification process and avoid damaging ice crystal formation. While both open and close containers can be used successfully, the combination of the low volume and rapid time needed to load devices to prevent toxicity from cryoprotectant exposure can be problematic, especially compared to 0.25 cc straws used with slow-rate approaches. A novel microfluidic platform regulating CPA solution exposure to oocytes, that integrates a novel vitrification device, could simply bypass the current step-wise procedure and eliminate errors with manual dilutions and movement of cells through various media and loading of complicated devices.

B.5 Future Directions

Though incremental advances in application of microfluidic technology to enhance current ART protocols should now be readily apparent, the full potential of the

approach has yet to be recognized. Much of this is due to the limitations in design and function, both perceived and actual. However, emerging studies are pushing the envelope to harness the capability of these novel devices. Three main areas in microfluidic refinement that hold tremendous promise for revolutionizing efficiency of IVF include ability to implement multiple IVF procedural steps on a single device, automation of procedural steps and implementation of diagnostic inline assays. If implemented in a clinically feasible platform, these advancements may lead to improved culture conditions, reduction of *in vitro* stressors, as well as improved embryo selection; ultimately culmination in improvement in ART outcomes.

Multiple ART procedural steps on a single device

Many of the above mentioned studies implement a single procedural step on a microfluidic device. However, implementation of multiple steps on the same device would be advantageous, as it would reduce cell handling and the associated environmental stressors. Keeping the delicate cells in place, while gradually changing media, or gently rolling the cell to a new location may produce a less stressful environment and help optimize the *in vitro* culture system.

One of the first examples of integration of multiple procedural steps on a single microfluidic platform was presented by Clark and coworkers. Their preliminary data demonstrated that both IVM and IVF of porcine oocytes could be performed on the same microfluidic device without removal of the cells between procedures.[69] Media within devices were changed by withdrawing from the 2 reservoirs and sperm added *via* manual pipetting without disturbing oocytes, which were housing in a connecting microchannel. Although there were no observable benefits achieving cleavage to 2-cell compared to control treatments (49% *vs.* 51%), this demonstrated

that multiple tasks of *in vitro* embryo production could be performed upon the same microfluidic platform.

Another example of integrating multiple IVF steps on a single platforms entails separation of porcine sperm using laminar flow in a microfluidic device, and then fertilizing oocytes that were then placed in a chamber near the exit point of the separated, motile sperm.[70] Rates of monospermic penetration varied depending on oocyte location in the exit chamber. Subsequent analysis revealed that the microfluidic device yielded higher rates of normal fertilization and subsequent blastocyst development compared to standard insemination protocols in petri dishes.

More recently, mouse embryos have been cultured successfully in microwells housed on the same microfluidic device where fertilization occurred. Han *et al.*[26] demonstrated that oocytes could be fertilized in microwells using media and sperm movement *via* gravity driven hydrostatic pressure . Fertilization media was then replaced with embryo culture media by flowing media though the channels on the same device and embryos cultured. Though there was no active media flow during the 96 h of embryo development, similar high rates of blastocyst formation were obtained following culture in microwells compared to controls (87.5*vs.* 87.8%). Similarly, using a revised device design employing the "octacolumn" to house oocytes/embryos rather than microwells, the same group again demonstrated mouse oocyte fertilization and subsequent embryo development on the same microfluidic platform, yielding high rates of blastocyst formation, similar to controls (86.9% *vs.* 85.3%).[27] Another device also exists that performs IVF and embryo culture without removing the cells.[40]

More ambitious and complex devices are emerging. One report details a device that incorporates a variety of procedural steps from oocyte manipulation, insemination and embryo culture.[27] Similarly, another "chip" has been developed that attempts to integrate each step of the IVF process including oocyte positioning, sperm screening, fertilization and embryo culture with media replacement.[26]

Most recently, a miniaturized embryo array has been developed that can trap multiple zebrafish embryos, holding them in individual locations while utilizing microfluidic perfusion to supply fresh media or pharmacologic compounds to examine effects over time.[71] Integrated with a perfusion pump, stage heater and valves to help regulate flow and remove waste, this platform is also combined with real-time video analysis. A similar approach could be envisioned for use with mammalian embryo culture, where real-time embryo imaging devices placed in incubators has received widespread attention.[72,73] Using a miniaturized approach, each microfluidic "chip" could in theory have its own thermal heat source below the embryos, contain a miniaturized camera and self-contained LED light source for observation, and even maintain their individual atmosphere in isolated chambers. This would be a large departure from multiple dishes/patients sharing a large common incubator, where dishes are removed on a regulator basis for microscopic observation and subject to changes in temperature and pH.

Automation

Automation of intricate step-wise procedures performed on microfluidic platforms within the ART laboratory is a potential method to reduce variability and perhaps improve ease-of-use. Others have already conjectured that some level of automation may be the future of the IVF laboratory.[74] As an example of the promise of this

approach, automation of blastomere visualization/tracking during mitosis and use of a predictive algorithum for automatic embryo selection has been utilized.[72,73] Additionally, more complex procedures that could utilize a microfluidic platform, such as automated microinjection have been explored.[75,76]Toward this end, an automated microfluidic device aimed at sorting, collecting, orienting *xenopus* oocytes for subsequent microinjection has been developed.[77] Authors claimed a dramatically improved efficiency, reducing the time needed to process 400 oocytes from 1 day to ~4 h. While this may have application for large scale animal production purposes, the relevance to human oocytes, which are limited in number for each case, may not be as significant. It does, however, introduce the ability to reduce variability and stress in the culture system. Automation of vitrification procedures has also been examined as a way to reduce variability in this highly sensitive approach,[67] and may prove to be an instrumental tool in further improving success.

Inline diagnostic assays

Implementation of inline diagnostic assays to aid in selection of viable gametes for use or embryos for transfer would further help realize the immense potential of microfluidics in ART.[78] Microfluidic devices have been developed to assess embryo metabolism[79] (Fig. B.7A) and oxygen consumption,[80] though these devices were not developed with extended culture or cell recovery for subsequent use in mind. More recently, a promising approach of measuring glucose consumption in the same microfluidic device where embryos are cultured has been developed[78,81] (Fig. B.7B). This approach may permit real-time metabolic assessment of embryos, ultimately providing a profile of metabolism over time. Such a profile could be used in

conjunction with similar profiles collected over time, such as those collected using emerging morphokinetic time-lapse analyses. Combining multiple real-time analytic profiles would undoubtedly provide greater insight into embryo development and permit better selection for transfer.

B.6 Conclusions

It is clear that microfluidics offer many opportunities to revolutionize the ART laboratory as we currently know it. Importantly, these technologies would not negate the need for an embryologist. Rather, they would serve to streamline processes, act as an adjunct to reduce stress imposed upon gametes and embryos, reduce variability between personnel/lab, and serve to help optimize the culture environment. Though personnel would be required to change their current procedures and likely undergo extensive training to learn to operate and troubleshoot new microfluidic or automated systems, this should be viewed as enhanced job training; a necessity in any position that attempts to constantly improve upon past successes. That being said, it is acknowledged that microfluidic devices are generally designed with functionality first and foremost, with little or no regard to ease of clinical applications. In this respect, future designs should consider simplicity and usability to facilitate the adoption of microfluidics in the clinical ART laboratory.

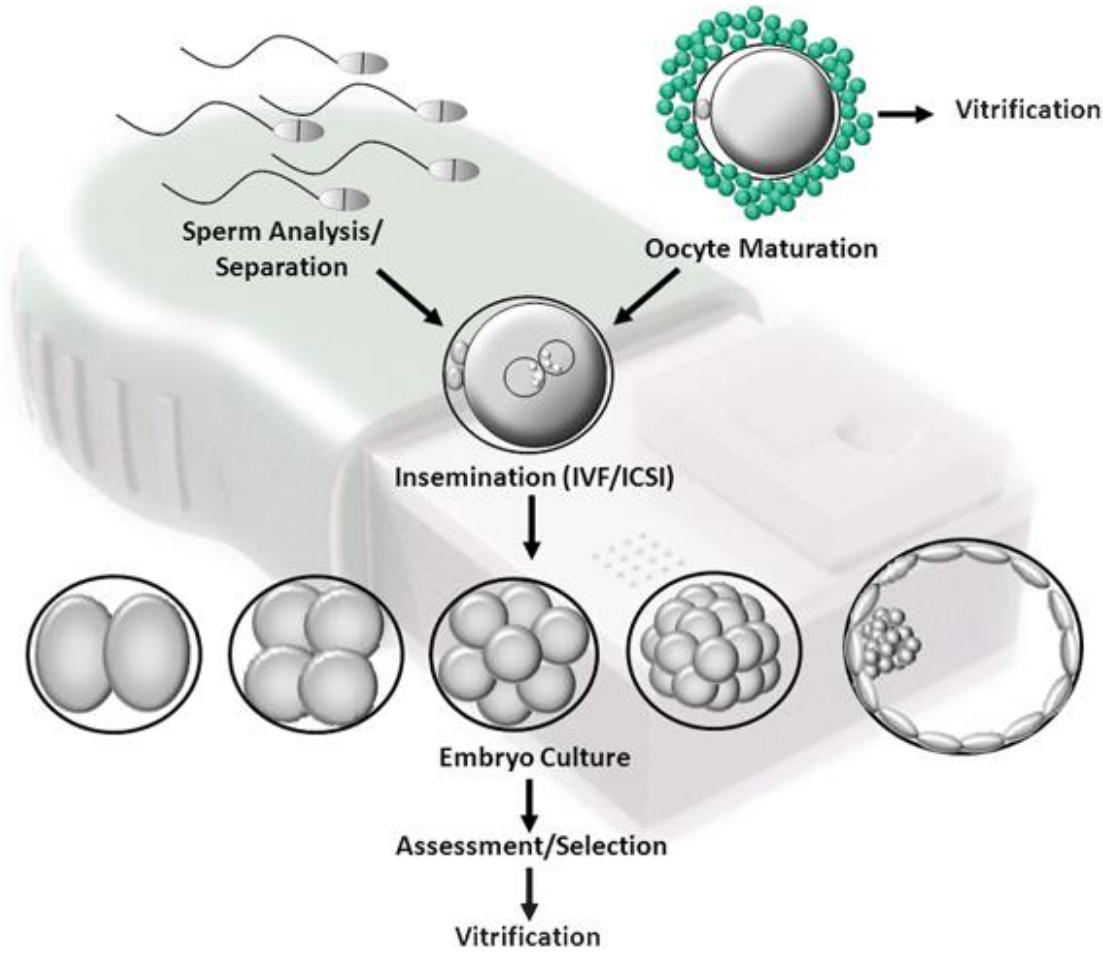

Fig. B.1 Schematic of basic steps involved in the *in vitro* fertilization process that have utilized microfluidic devices.

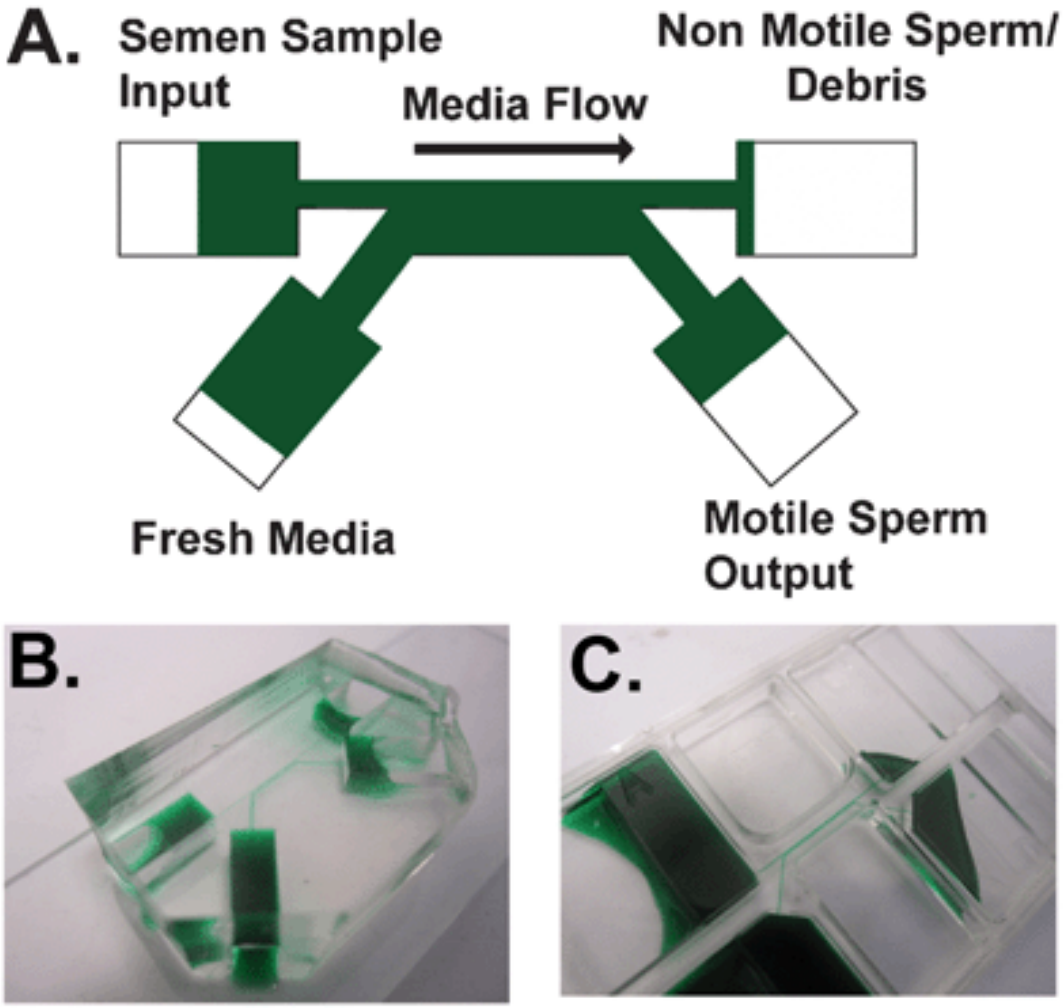

Fig. B.2 A) Schematic of a microfluidic device created for sperm sorting. Passively driven by a difference in surface tension, the separation of motile sperm relies on laminar flow of the merging fluid streams, and motile sperm can swim across the interface to collect in a reservoir.[7] B) Sperm sorter device made of PDMS used in initial design and testing. C) Modification of the microfluidic sperm sorting device made of polystyrene suitable for clinical use.

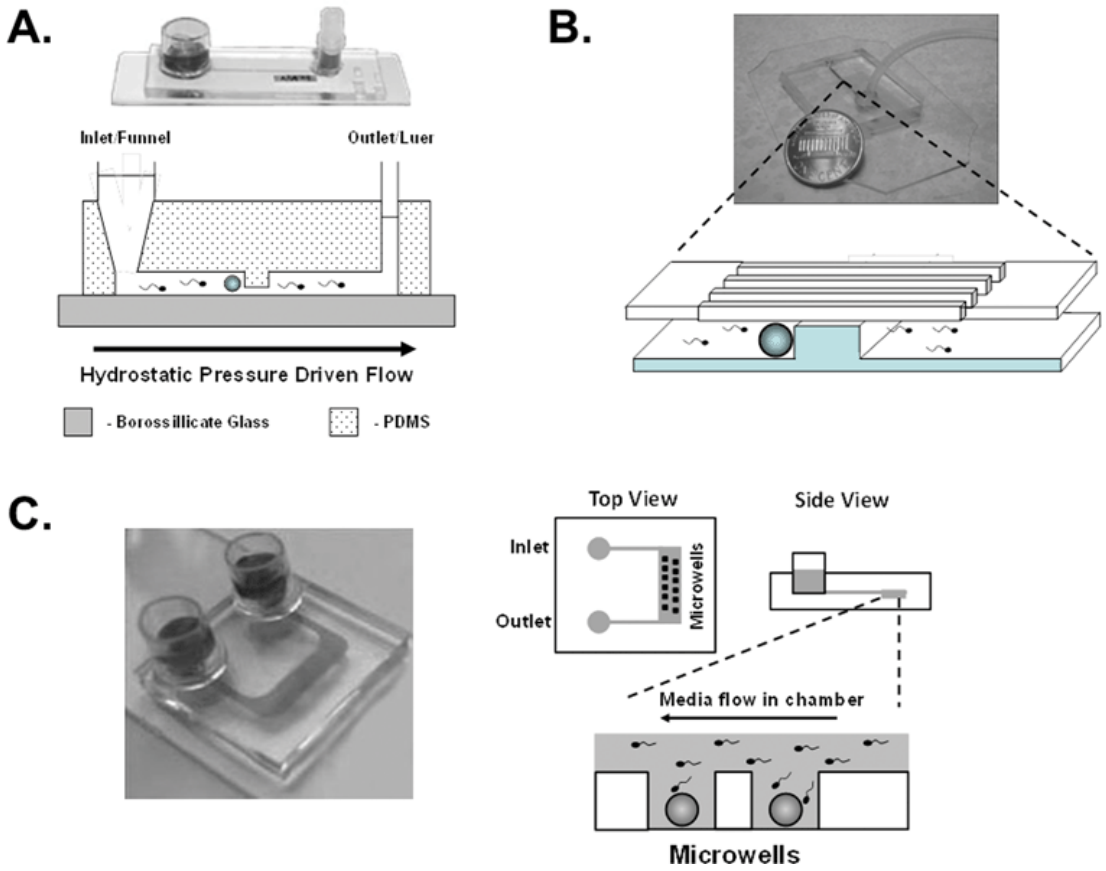

Fig. B.3 A) First device design used to successfully perform fertilization of pig oocytes using microfluidics.[24,69] This device utilized a straight microchannel with a small constriction point to prevent oocytes from rolling the length of the channel, while permitting sperm to flow past the oocyte. This particular device utilized gravity driven media flow and was not engineered to sustain controlled fluid flow over time. A similar device was used for oocyte maturation.[69] B) A modified microfluidic platform used to successfully perform fertilization of mouse oocytes.[25] C) Alternate fertilization device using microwells.[26,27]This device may create a more suitable microenvironment, while also permitting individual identification of zygotes following fertilization. All of the aforementioned fertilization microdevices are designed with controlled width/depth/height of microwells or channels tailored accordingly to account for oocyte size of each respective species.

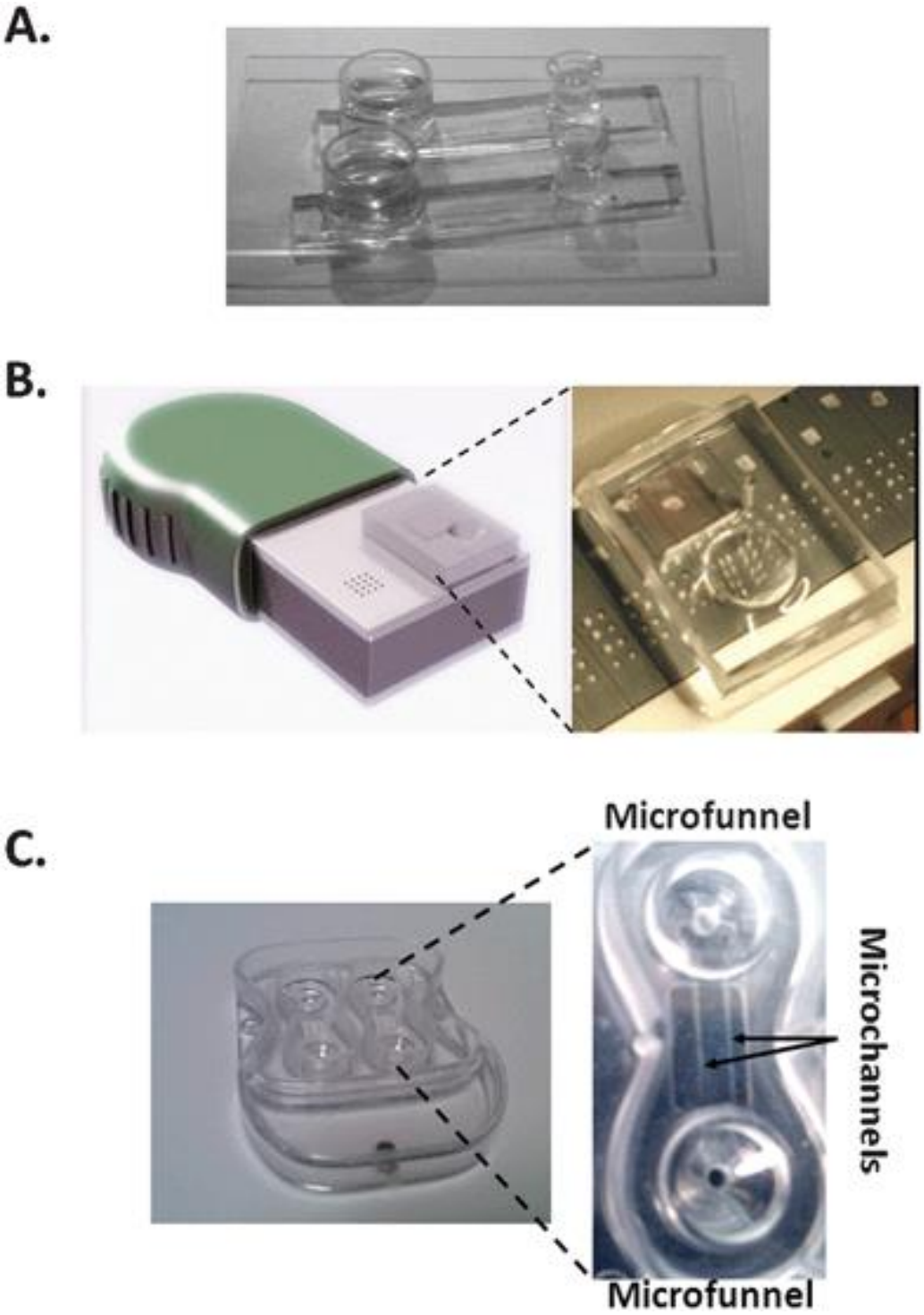

Fig. B.4 A) First microfluidic channel used to culture mammalian embryos.[33,34] Microchannels are problematic with regard to cell access and consistent recovery. B) First microfluidic platform using microfunnels formed in PDMS with actively controlled media flow *via* use of Braille pin actuators for culture of mouse embryos that was shown to improve implantation and live birth outcomes.[45,47] C) Modified microfunnel platform made of polystyrene to permit automated media flow suitable for clinical use.[48] The microfunnel design for embryo culture provided ease of access to the embryo for clinical purposes, while maintaining effective fluidic stimulation for enhanced outcomes.

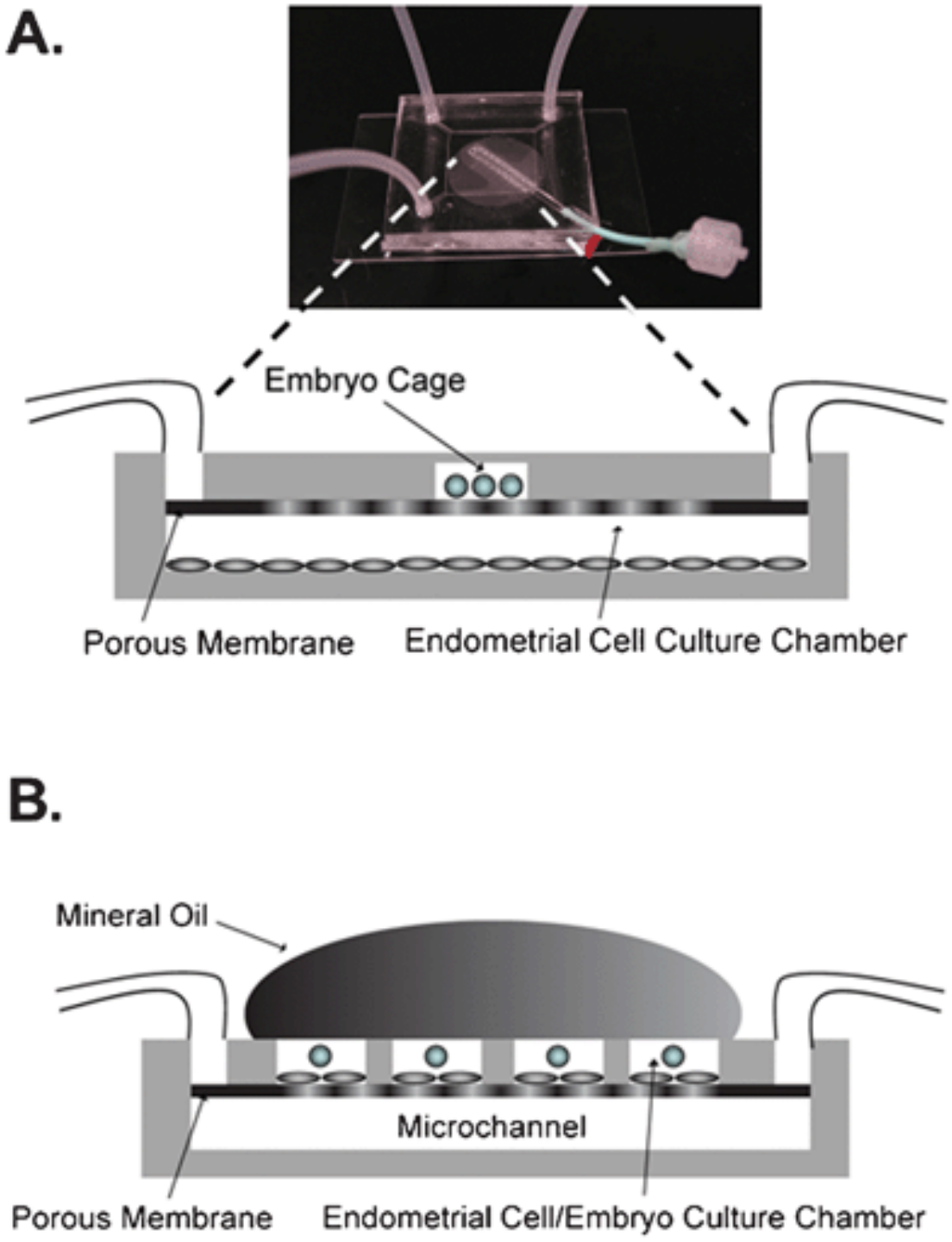

Fig. B.5 A) Microfluidic platform used for endometrial co-culture of mouse and human embryos.[40,41] B) Alternate microfluidic device using a microporous membrane to separate mouse embryos during co-culture with endometrial cells.[43] Both devices have porous membranes as an essential part of design. However, within the field of IVF, there has been a movement away from co-culture towards use of more define culture systems.

A.

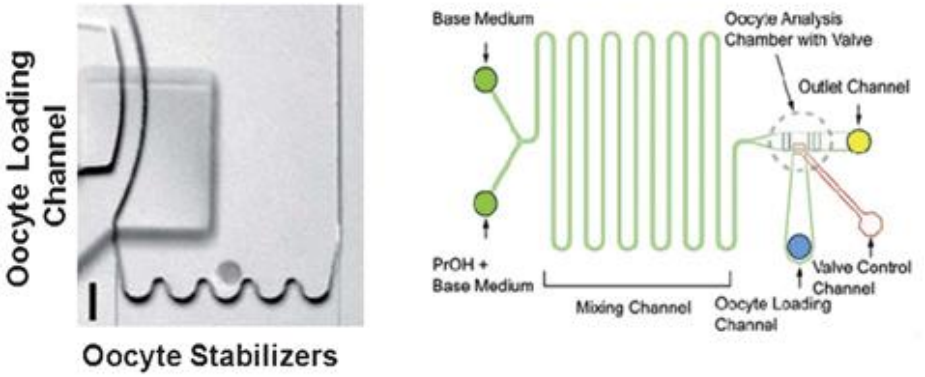

B.

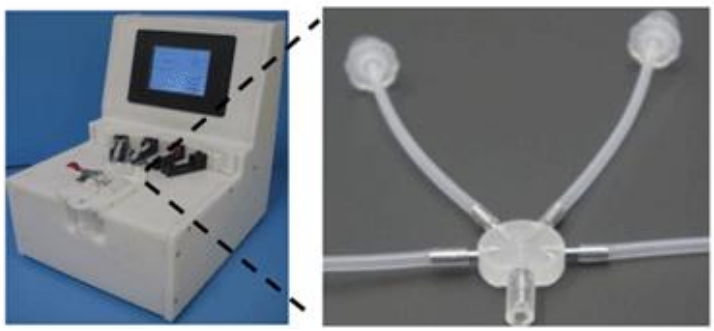

Fig. B.6 A) Microfluidic device used to optimize cryoprotectant exposure schemes for oocytes by measuring volume changes.[66] Serpentine channels were used to effectively mix two solutions of temporally changing flow rates to produce a gradual cryoprotectant exposure scheme. A valving mechanism was also introduced to lock the oocyte inside the analysis chamber during flow. B) Alternate device used to automate gradual cryoprotectant exposure for embryos.

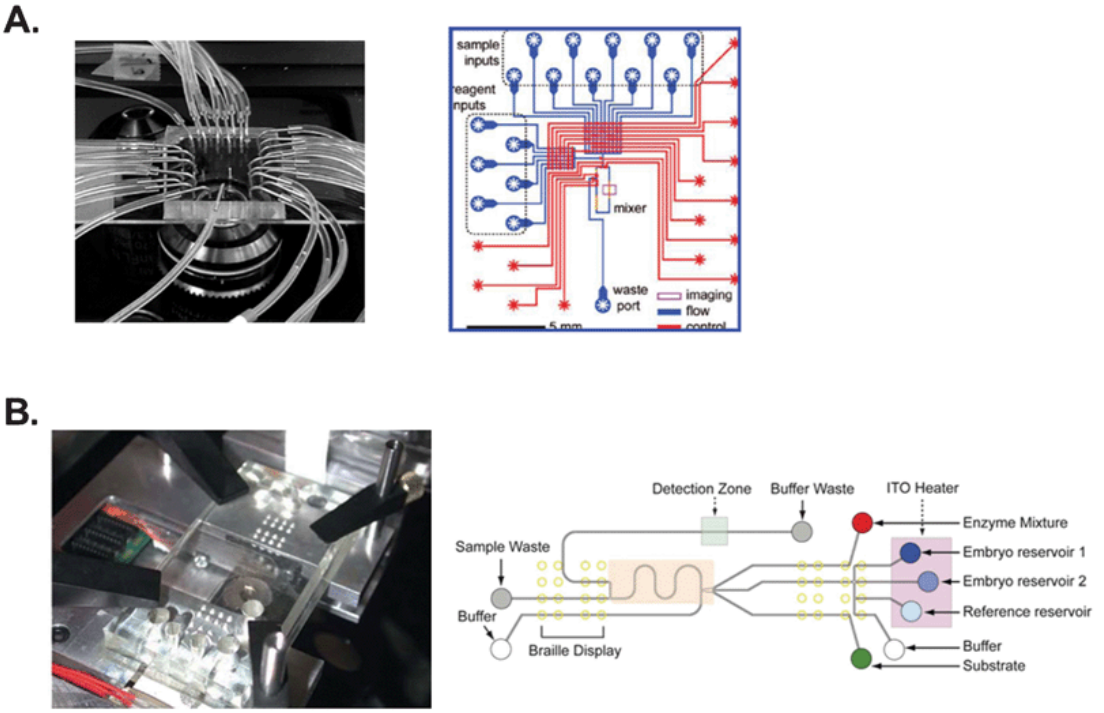

Fig. B.7 A) Microfluidic device used to analyze embryo metabolism.[82] External tubing used for pneumatics or syringe driven inlets can be cumbersome and problematic for clinical application B) Microfluidic device used to culture embryos, while simultaneously permitting assessment of glucose utilization as a means of non-invasive embryo assessment on the same device.[81] Clinical usability is preserved by using a preprogrammed Braille display to drive flow.

B.7 References

1. G. D. Smith, S. Takayama and J. E. Swain, *Biol. Reprod.*, 2012, **86**, 62.
2. J. E. Swain and G. D. Smith, *Hum. Reprod. Update*, 2011, **17**, 541–557.
3. L. J. Kricka, I. Faro, S. Heyner, W. T. Garside, G. Fitzpatrick, G. McKinnon, J. Ho and P. Wilding, *J. Pharm. Biomed. Anal.*, 1997, **15**, 1443–1447.
4. L. J. Kricka, O. Nozaki, S. Heyner, W. T. Garside and P. Wilding, *Clin. Chem.*, 1993, **39**, 1944–1947.
5. L. I. Segerink, A. J. Sprenkels, P. M. ter Braak, I. Vermes and A. van den Berg, *Lab Chip*, 2010, **10**, 1018–1024.
6. B. S. Cho, T. G. Schuster, X. Zhu, D. Chang, G. D. Smith and S. Takayama, *Anal. Chem.*, 2003, **75**, 1671–1675.
7. T. G. Schuster, B. Cho, L. M. Keller, S. Takayama and G. D. Smith, *Reprod. BioMed. Online*, 2003, **7**, 75–81.
8. L. Xie, R. Ma, C. Han, K. Su, Q. Zhang, T. Qiu, L. Wang, G. Huang, J. Qiao, J. Wang and J. Cheng, *Clin. Chem.*, 2010, **56**, 1270–1278.
9. S. Koyama, D. Amarie, H. A. Soini, M. V. Novotny and S. C. Jacobson, *Anal. Chem.*, 2006, **78**, 3354–3359.
10. D. Seo, Y. Agca, Z. Feng and J. Critser, *Microfluid. Nanofluid.*, 2007, **3**, 561–570.
11. D. Shibata, H. Ando, A. Iwase, T. Harata, F. Kikkawa and K. Naruse, *Fertil. Steril.*, 2007, **88**, S110.
12. K. Matsuura, M. Takenami, Y. Kuroda, T. Hyakutake, S. Yanase and K. Naruse, *Reprod. BioMed. Online*, 2012, **24**, 109–115.
13. A. Agarwal, I. Ikemoto and K. R. Loughlin, *Arch Androl*, 1994, **33**, 157–162.
14. M. Shekarriz, D. M. DeWire, A. J. Thomas Jr. and A. Agarwal, *Eur. Urol.*, 1995, **28**, 31–35.
15. M. Fraczek, D. Sanocka and M. Kurpisz, *Int. J. Androl.*, 2004, **27**, 69–75.
16. R. Schulte, Y. Chung, D. Ohl, S. Takayama and G. Smith, *Fertil. Steril.*, 2007, **88**, S76.
17. R. C. Chian, J. H. Lim and S. L. Tan, *Curr. Opin. Obstet. Gynecol.*, 2004, **16**, 211–219.
18. E. Walters, D. Beebe and M. Wheeler, *Theriogenology*, 2001, **55**, 497.
19. R. B. Gilchrist, L. J. Ritter, S. Myllymaa, N. Kaivo-Oja, R. A. Dragovic, T. E. Hickey, O. Ritvos and D. G. Mottershead, *J. Cell Sci.*, 2006, **119**, 3811–3821.

20. P. Hester, H. Roseman, S. Clark, E. Walters, D. Beebe and W. MB, *Theriogenology*, 2002, **57**, 723.

21. M. Hagiwara, T. Kawahara, Y. Yamanishi, T. Masuda, L. Feng and F. Arai, *Lab Chip*, 2011, **11**, 2049–2054.

22. Y. Mizobe, M. Yoshida and K. Miyoshi, *J. Reprod. Dev.*, 2010, **56**, 285–290.

23. M. D. Lopez-Garcia, R. L. Monson, K. Haubert, M. B. Wheeler and D. J. Beebe, *Biomed. Microdevices*, 2008, **10**, 709–718.

24. S. G. Clark, K. Haubert, D. J. Beebe, C. E. Ferguson and M. B. Wheeler, *Lab Chip*, 2005, **5**, 1229–1232.

25. R. S. Suh, X. Zhu, N. Phadke, D. A. Ohl, S. Takayama and G. D. Smith, *Hum. Reprod.*, 2006, **21**, 477–483.

26. C. Han, Q. Zhang, R. Ma, L. Xie, T. Qiu, L. Wang, K. Mitchelson, J. Wang, G. Huang, J. Qiao and J. Cheng, *Lab Chip*, 2010, **10**, 2848–2854.

27. R. Ma, L. Xie, C. Han, K. Su, T. Qiu, L. Wang, G. Huang, W. Xing, J. Qiao, J. Wang and J. Cheng, *Anal. Chem.*, 2011, **83**, 2964–2970.

28. H. C. Zeringue and D. J. Beebe, *Methods Mol. Biol.*, 2004, **254**, 365–374.

29. H. C. Zeringue, J. J. Rutledge and D. J. Beebe, *Lab Chip*, 2005, **5**, 86–90.

30. H. C. Zeringue, M. B. Wheeler and D. J. Beebe, *Lab Chip*, 2005, **5**, 108–110.

31. C. Chandsawangbhuwana, L. Z. Shi, Q. Zhu, M. C. Alliegro and M. W. Berns, *J. Biomed. Opt.*, 2012, **17**, 015001.

32. C. Leung, Z. Lu, X. P. Zhang and Y. Sun, *IEEE Trans. Biomed. Eng.*, 2012, **59**, 1049–1056.

33. S. Raty, E. M. Walters, J. Davis, H. Zeringue, D. J. Beebe, S. L. Rodriguez-Zas and M. B. Wheeler, *Lab Chip*, 2004, **4**, 186–190.

34. S. Raty, J. Davis, D. Beebe, S. Rodriguez-Zas and M. Wheeler, *Theriogenology*, 2001, **55**, 241.

35. E. Walters, S. Clark, H. Roseman, D. Beebe and M. Wheeler, *Theriogenology*, 2003, **59**, 441.

36. D. Hickman, D. Beebe, S. Rodriguez-Zas and M. Wheeler, *Comp. Med.*, 2002, **52**, 122–126.

37. Y. Xie, F. Wang, W. Zhong, E. Puscheck, H. Shen and D. A. Rappolee, *Biol. Reprod.*, 2006, **75**, 45–55.

38. M. Reed, *The Clinical Embryologist (online)*, 2006, **9**, 5–19.

39. M. Reed, B. Woodward and J. Swain, *J. Reprod. Stem. Cel. Biol.*, 2011, **2**, 77–87.

40. J. Mizuno, S. Ostrovidov, H. Nakamura, K. Akaishi, H. Inui, Y. Sakai, T. Fujii, K. Anzai and A. Watanabe, *Proceeding from ESHRE*, 2007.

41. J. Mizuno, S. Ostrovidov, Y. Sakai, T. Fujii, H. Nakamura and H. Inui, *Fertil. Steril.*, 2007, **88**, S101.

42. H. Nakamura, J. Mizuno, K. Akaishi, H. Inui, H. Busujima, N. Watanabe, E. Kuriki, K. Anzai and A. Watanabe, *Hum. Reprod.*, 2007, **22**, i170.

43. H. Kimura, H. Nakamura, T. Akai, T. Yamamoto, H. Hattori, Y. Sakai and T. Fujii, *IEEE Trans. NanoBiosci.*, 2009, **8**, 318–324.

44. C. Bormann, L. Cabrera, Y. Heo, S. Takayama and G. Smith, *Biol. Reprod.*, 2007, 89.

45. L. Cabrera, Y. Heo, J. Ding, S. Takayama and G. Smith, *Fertil. Steril.*, 2006, **87**, S43.

46. C. Bormann, L. Cabrera, Y. Heo, S. Takayama and G. Smith, *Proceedings from the 14th World Congress on In Vitro Fertilization*, 2007, 84.

47. Y. S. Heo, L. M. Cabrera, C. L. Bormann, C. T. Shah, S. Takayama and G. D. Smith, *Hum. Reprod.*, 2010, **25**, 613–622.

48. J. R. Alegretti, B. Barros, P. Serafini, E. Motta and G. Smith, *Fertil. Steril.*, 2011, **96**, s58.

49. M. S. Kim, C. Y. Bae, G. Wee, Y. M. Han and J. K. Park, *Electrophoresis*, 2009, **30**, 3276–3282.

50. C. Bai, M. Kim and J. Park, *BioChip J.*, 2011, **5**, 106–113.

51. V. Isachenko, R. Maettner, K. Sterzik, E. Strehler, R. Kreinberg, K. Hancke, S. Roth and E. Isachenko, *Reprod. BioMed. Online*, 2011, **22**, 536–544.

52. E. Isachenko, R. Maettner, V. Isachenko, S. Roth, R. Kreienberg and K. Sterzik, *Clin. Lab.*, 2010, **56**, 569–576.

53. T. Koike, K. Matsuura, K. Naruse and H. Funahashi, *J. Reprod. Dev.*, 2010, **56**, 552–557.

54. K. Matsuura, N. Hayashi, Y. Kuroda, C. Takiue, R. Hirata, M. Takenami, Y. Aoi, N. Yoshioka, T. Habara, T. Mukaida and K. Naruse, *Reprod. BioMed. Online*, 2010, **20**, 358–364.

55. J. Swain, T. Pool, S. Takayama and G. Smith, in *Textbook of Assisted Reproductive Technologies*, ed. D. Gardner, A. Weissman, C. Howles and S. Zeev, Informa Healthcare, Boca Raton, 3rd edn, 2009, ch. 63, pp. 843–858.

56. P. Syntichaki and N. Tavernarakis, *Physiol. Rev.*, 2004, **84**, 1097–1153.

57. Y. Xie, F. Wang, E. E. Puscheck and D. A. Rappolee, *Mol. Reprod. Dev.*, 2007, **74**, 1287–1294.

58. Y. S. Heo, L. M. Cabrera, J. W. Song, N. Futai, Y. C. Tung, G. D. Smith and S. Takayama, *Anal. Chem.*, 2007, **79**, 1126–1134.

59. K. S. Kolahi, A. Donjacour, X. Liu, W. Lin, R. K. Simbulan, E. Bloise, E. Maltepe and P. Rinaudo, *PLoS One*, 2012, **7**, e41717.

60. A. P. Sommer, M. K. Haddad and H. J. Fecht, *J. Bionic Eng.*, 2012, **9**, 353–357.

61. J. Swain and S. GD, in *Fertility Cryopreservation*, ed. R. Chian and P. Quinn, Cambridge, 2010, ch. 4, pp. 24–38.

62. A. Berthelot-Ricou, J. Perrin, C. Di Giorgio, M. De Meo, A. Botta and B. Courbiere, *Fertil. Steril.*, 2011, **95**, 1452–1457.

63. H. Men, R. L. Monson, J. J. Parrish and J. J. Rutledge, *Mol. Reprod. Dev.*, 2003, **64**, 245–250.

64. C. Vincent and M. H. Johnson, *Oxf. Rev. Reprod. Biol.*, 1992, **14**, 73–100.

65. M. Kuwayama, S. Fujikawa and T. Nagai, *Cryobiology*, 1994, **31**, 415–422.

66. Y. S. Heo, H. J. Lee, B. A. Hassell, D. Irimia, T. L. Toth, H. Elmoazzen and M. Toner, *Lab Chip*, 2011, **11**, 3530–3537.

67. L. Meng, X. Huezo, B. Stone, K. Back, G. Ringler and R. Marrs, *Fertil. Steril.*, 2011, **96**, s207.

68. P. Quinn, in *Fertility Cryopreservation*, ed. R. Chian and P. Quinn, Cambridge, 2010, ch. 16, pp. 131–143.

69. S. Clark, E. Walters, D. Beebe and M. Wheeler, *Theriogenology*, 2003, **59**, 441.

70. H. Sano, K. Matsuura, K. Naruse and H. Funahashi, *Theriogenology*, 2010, **74**, 863–870.

71. J. Akagi, K. Khoshmanesh, B. Evans, C. J. Hall, K. E. Crosier, J. M. Cooper, P. S. Crosier and D. Wlodkowic, *PLoS One*, 2012, **7**, e36630.

72. C. C. Wong, K. E. Loewke, N. L. Bossert, B. Behr, C. J. De Jonge, T. M. Baer and R. A. Reijo Pera, *Nat. Biotechnol.*, 2010, **28**, 1115–1121.

73. S. L. Chavez, K. E. Loewke, J. Han, F. Moussavi, P. Colls, S. Munne, B. Behr and R. A. Reijo Pera, *Nat. Commun.*, 2012, **3**, 1251.

74. M. Meseguer, U. Kruhne and S. Laursen, *Fertil. Steril.*, 2012, **97**, 1277–1286.

75. Z. Lu, X. Zhang, C. Leung, N. Esfandiari, R. F. Casper and Y. Sun, *IEEE Trans. Biomed. Eng.*, 2011, **58**, 2102–2108.

76. L. S. Mattos, E. Grant, R. Thresher and K. Kluckman, *IEEE Trans. Inf. Technol. Biomed.*, 2009, **13**, 822–831.

77. S. F. Graf, T. Madigou, R. Li, C. Chesne, A. Stemmer and H. F. Knapp, *J. Lab. Autom.*, 2011, **16**, 186–196.

78. D. Lai, G. D. Smith and S. Takayama, *J. Biophotonics*, 2012, **5**, 650–660.

79. J. P. Urbanski, M. T. Johnson, D. D. Craig, D. L. Potter, D. K. Gardner and T. Thorsen, *Anal. Chem.*, 2008, **80**, 6500–6507.

80. C. O'Donovan, E. Twomey, J. Alderman, T. Moore and D. Papkovsky, *Lab Chip*, 2006, **6**, 1438–1444.

81. Y. S. Heo, L. M. Cabrera, C. L. Bormann, G. D. Smith and S. Takayama, *Lab Chip*, 2012, **12**, 2240–2246.

82. J. Urbanski, M. Johnson, D. Craig, D. Potter, D. Gardner and T. Thorsen, *Fertil. Steril.*, 2007, **88**, S36.

Appendix C

Microfluidic Automation Using Elastomeric Valves and Droplets: Reducing Reliance on External Controllers

This paper gives an overview of elastomeric valve- and droplet-based microfluidic systems designed to minimize the need of external pressure to control fluid flow. This Concept article introduces the working principle of representative components in these devices along with relevant biochemical applications. This is followed by providing a perspective on the roles of different microfluidic valves and systems through comparison of their similarities and differences with transistors (valves) and systems in microelectronics. Despite some physical limitation of drawing analogies from electronic circuits, automated microfluidic circuit design can gain insights from electronic circuits to minimize external control units, while implementing high-complexity and high-throughput analysis.

C.1 Introduction

Two key features of microfluidics are small volumes and fluid flows. These two traits give rise to many compelling advantages for microfluidic bioassays such as: reduced reagent use, rapid mixing for reactions and assays, rapid serial analysis such as in droplet microfluidics, spatio-temporal micropatterning of biochemical for cellular analysis, and recreating physiological fluid mechanical microenvironments.[1–4] These benefits and well-established microfabrication technology make microfluidic devices promising for high-throughput and complex analysis. Accordingly, microfluidic

devices are becoming increasingly sophisticated, integrating increasingly larger numbers of passive components such as channels and chambers as well as components that need active control such as valves and regulators. While the cost associated with increasing the number of microfluidic component features in these complex devices is small, the cost associated with increasing the number of the external control units to operate the microfluidic components is still large because even single external pressure control units such as a pump is relatively expensive. With increased recognition of this control-challenge that hampers broader use of microfluidic devices for high-throughput and high-complexity analysis, microfluidic engineers are searching for new ways to enable sophisticated on-chip control without increasing the number of large external controllers.

In this Concept paper, we focus on schemes to minimize the use of off-chip *mechanical pressure* controllers in elastomeric valve and droplet microfluidic devices for high-throughput analysis. Other microfluidic control schemes also have the potential to minimize mechanical pressure controllers: Interested readers can find good reviews or studies on centrifugal,[5] capillary microfluidics,[6] and microfluidic control using viscoelastic polymer solutions.[7] On the other hand, digital microfluidics by electrowetting[8] and electrokinetic flows[9] are excluded because their flows are directly controlled by electricity. Also, we exclude fluidic automation schemes using pipetting robots[10] because they extensively rely on external controllers. In Section 2, we explain the history of fluidic automation. Section 3 introduces the working principles of elastomeric valve circuits along with their biochemical applications. Section 4 presents droplet circuits focusing on key functions for autonomous rapid

serial processing. To conclude, in Section 5, we discuss the outlook for design of more sophisticated automated microfluidic circuits in the near future.

C.2 History of Macroscale Fluidic Control

The history of automatic fluidic control can be traced to the legendary water clock, which was made by Ctesibius (around 250 BC), a Greek physicist and inventor.[11] His clock was operated by a self-regulating water supply similar to the mechanism for flushing toilets nowadays. More recently, in the 1800s to early 1900s, pneumatic systems, or vacuum- and compressed-air-based fluidic systems, became a major mechanism for the operation and control of machinery (Fig C.1). We see remnants of these control systems even today in the pneumatic tube system used to transport light and small items that must be delivered rapidly across a building such as money and medical samples.[12]

Interestingly in the 1950s and 60s, during the transient time from pneumatic to solid-state electronic control circuitry, there was very active development of fluidic logic circuits and they can be classified into three categories: (i) high Reynolds number flow-driven fluid logic (HRFL), (ii) pneumatic logic, and (iii) hydraulic control. HRFL refers to technology that takes advantage of a jet of fluid (air or water) having high Reynolds number to create logic elements that have no moving parts.[13] A jet of fluid is to be deflected by a side-striking control jet, resulting in non-linear amplification and other logic operations. On the other hand, pneumatic logic particularly refers to high pressure, low mass flow, on/off control systems that utilize millimeter to centimeter scale pneumatically actuated valves. Pneumatic logic is

different from HRFL in that it has pressure-actuated moving solid parts. The pneumatic logic systems are highly reliable and are still used today in specialized control settings where compressed air is the only energy source available, the danger of spark generation exists, or high concentration of dust/moisture is present.[13] Hydraulic control circuits also exist. Despite their long time delays and requirement for high operating pressures, they offer higher accuracy in delivering force and are still used today in systems such as the braking system of cars.[14]

As electronic components became more readily available, many of the fluidic controls were replaced by electronics. This transition accelerated with the development of solid-state "electronic valves"—more commonly known today as transistors—and the commercial rollout of integrated microelectronic circuits in the 1960s. Fluid logic devices normally cannot compete with their electronic counterpart because the size and the speed of electronic logic circuits are far more advantageous. With the increased use of microfluidics for biomolecular studies, however, the need for fluidic controls with minimal external units has also increased, leading to a renewed interest in fluidic components analogous to electronic circuits. Recently, use of a viscoelastic polymer solution, flux stabilizer, a bistable flip-flop memory, and flow rectifier have been implemented.[7] It is important to realize that these and other microfluidic circuits developed recently are very different in size and operating mechanism from the millimeter to macroscale fluidic logic systems investigated decades ago. Much of the difference arises due to use of smaller channel sizes and in some cases also to introduction of mechanically compliant materials for device construction. Key considerations for operation of these newer generations of microfluidic devices include: (i) elasticity of the material, (ii) viscosity, and (iii) interfacial phenomena of

fluids. In the next sections, we present elastomeric-valve-utilizing and droplet-based microfluidic devices that take advantage of these features. Elastomeric microfluidic devices extensively use the first two properties and droplet devices exploit the last two.

C.3 Advent of Elastomeric Microfluidic Devices

Because of the great success of microelectronics, size similarity in terms of being miniaturized, and electrohydraulic analogies, electronic circuits have inspired much of what is developed in microfluidics. With only a power source, an electronic circuit implements sophisticated autonomous functions (i.e., no aid by other external units).[15, 16] Such functions are enabled by the smart arrangement of electronic transistors, resistors, and capacitors, which are the key components of electronic circuits. Notably, an interesting analogy exits between electric and microfluidic parameters: voltage corresponds to pressure and current to flow rate. Owing to the similarity in equations between electric/electronic and microfluidic components, electric resistors correspond to microfluidic channels having fluids, capacitors to chambers having elastomeric membranes, and electronic transistors to elastomeric valves.

Such elastic property of microfluidic components comes from polydimethylsiloxane (PDMS, Young's modulus of ~1 MPa),[17] a widely used material for soft lithography that is to make microstructures by molding. Owing to its moderately stiff elastic property, microfluidic valves and capacitors containing PDMS membranes have appropriate operational pressure-ranges for microfluidic devices. Elastomeric valves

are suitable for parallel processing of biochemicals, thereby implementing high-throughput analysis. Some of the applications like digital polymerase chain reaction (PCR)[18] need only one control source because all valves are on/off simultaneously. In many cases, however, valves should be controlled individually for sequential processes; thus typically requiring many control lines and sources. In this section, for the minimal external control, we introduce microfluidic analogues of electronic components, present their working principle, and show related biochemical applications.

Key Components

Multiplexer and Demultiplexer

A multiplexer is a component that selects one out of many possible inputs and connects that input to a single output. Control lines regulate the selection process and the number of external controllers can be significantly reduced through a smart arrangement of control lines. Fig. C.2A depicts the process of how one out of 4 input channels is selected by the manipulation of 4 control channels in a binary multiplexer.[19] The vertical lines are flow input channels (I*i*) transferring input liquids and the horizontal lines are control channels (C*i*) containing hydraulic rectangular membrane valves. As shown in the cross-section of the multiplexer valve (Fig. C.2A), I*i* is formed under membrane valves of C*i*.[20] Note that a particular valve (shown in squares of the right panel) is considered "on" when it is open with regards to flow through I*i*. Two C*i* constitute one bit. Note that, in each bit, on-off states of valves in the two C*i* are opposite; for example, in bit 0, when valves in $C_1$are on, valves in C_2 are off. Thus, each bit has only two states (state 0 and 1); for instance, in bit 0, state 0 is valves-off in C_1 and valves-on in C_2 and state 1 is C_2 off and C_1 on. Fig.

C.2A shows bit 0 and 1 are both in state 1 so I_3 is selected to be output (i.e., $1 \times 2^0 + 1 \times 2^1 = 3$). Because of this binary characteristic and a smart arrangement of valves, *n* control lines (or *n*/2 bits) can regulate up to $2^{n/2}$ flow channels. A greater saving of the control lines can be achieved by using a ternary, a quaternary, and a combinatory multiplexer that can regulate up to $3^{n/2}$, $4^{n/2}$, and $n!/((n/2)!)^2$ flow channels, respectively, with *n* control lines (or *n*/2 bits).[21, 22] The efficiency of the multiplexers is summarized in Fig. C.2B.

Compared to the multiplexer, a demultiplexer functions conversely. That is, it connects a single input channel to a selected output channel out of multiple possible outlets; thus working as an output selector. As a result, input and output channels in a demultiplexer are simply reversed from that of a multiplexer.[23] Even with the use of multiplexers and demultiplexers, multiple control sources are still necessary to address many flow channels individually. Additionally, only 1 input or output can be selected at a time making this type of control unsuitable for some applications. In the next section, we show that logic gates in combination with multiplexers and demultiplexers have potential to save more control line resources.

Logic Gates for Boolean Operations

Logic gates are components that implements Boolean functions such as AND, OR, NOT, and XNOR operations.[24] They are the elementary building blocks of digital circuits. The power of digital circuits is that more complex components like shift registers can be implemented by cascading logic gates, theoretically enabling the control of unlimited number of outputs with a set small number of control signal inputs. Both pneumatic and hydraulic logic systems have been implemented microfluidically. Both logic systems have the capability to control a biochemical

analysis unit when the logic systems and the analysis unit are monolithically integrated in a device.

A key element of the microfluidic pneumatic logic (i.e., channels are filled with air or vacuum) is a normally closed (NC) valve. The NC valve is analogous to a p-channel enhanced mode MOSFET in that the valve has three terminals (gate, source, and drain) and the closed valve is on only when the source minus gate pressure is greater than some value (threshold pressure).[25] As shown in Fig. C.3A, source and drain terminals are in the same plane (see left panel or black areas of right panel), but there is a valve seat between them (left panel); the gate terminal is the only access port to the bottom chamber (gray area of right panel) that is under the membrane, the gray line is connected to the gate, and the black lines are linked to source and drain. NC valves can directly be pneumatic NOT gates[26, 27] depending on their pressure connections. As shown in the right panel of Fig. C.3A, gate is used as an input (I_1), and drain is connected to control (C_1) at a constant vacuum and to output (O_1) channel. We define positive and vacuum pressures as state 0 and 1, respectively. When the pressure of I_1 is positive (state 0, i.e., pushing membrane upward), NC valves is off (closed), making O_1 at vacuum (state 1). On the other hand, when I_1 channel is at high vacuum (state 1), NC valve is on (open) because source pressure is higher than gate pressure (i.e., pushing membrane downward). At that moment, because fluidic resistance in C_1 is designed to be greater than that in O_1 channel, air dominantly flows to O_1 channel thus making the pressure of O_1 positive (state 0). As a result, pressure states of I_1 and O_1 (= 1_1) are always opposite; thus making the unit an analogue of the electronic NOT gate.

The more logic units are cascaded, the more sophisticated a system can be implemented. For example, two NOT gates can make a gated D latch (Fig. C.3B) and its behavior is illustrated in Fig. C.3C. In contrast to a single NOT gate, I_1 is connected to the source terminal of a valve. As long as clock pulse (E) is in state 1 (i.e., the valve is on for I_1), O_1 follows I_1 because O_1 is directly connected to I_1through the valve controlled by E. Note that even after E is in state 0, O_1 maintains (i.e., latches) the original I_1 state when E is in state 1. This is because, as shown in Fig. C.3B, O_1 and O_1 bar can retain their original states when the valve controlled by E is off. As such, cascading structures with 23 NOT gates can be made to constitute a 4-bit shift register, which can decode the sequential inputs from a single port into 4 parallel output ports.[26] When a shift register's outputs are connected to the control lines of a multiplexer, the outputs can regulate the control lines. Theoretically, by increasing the number of bits a shift register can handle, an arbitrarily large number of control lines can thus be regulated using the same number of external control units.

The basic building block of the hydraulic logic gates (i.e., channels are filled with liquids) is a normally open (NO) valve; it is analogous to an electronic p-channel junction gate field-effect transistor and makes a pressure gain.[28] Note that definition of state in hydraulic logic is the opposite of that in the pneumatic logic just described. That is, high pressure (~100 kPa) and atmospheric pressure are state 1 and 0, respectively. Fig. C.3D shows an AND gate; dark gray, light gray, and black lines in the right bottom panel are bottom, middle, and top channels, respectively; and when gate pressure is high (state 1), the membrane containing a stiff disk (marked in white of left bottom panel) deflects upward and flow from the top to middle channel is prevented (valve-off). Control line C_1 is always at high pressure and $C_2$is at

atmospheric pressure. Only when the two inputs (I_1 and I_2) are both at high pressures (state 1), thus closing the two NO valves (off), does the output also take on state 1. The OR gate can be defined in a similar way (Fig. C.3E). A static latch consists of two OR and one AND gate (Fig. C.3F). Here the state of each input or output (I_1, E, or O_1) is similar to that of the pneumatic latch (Fig. C.3C). The difference is that the hydraulic static latch needs two clock inputs (E and E bar) but have one output (O_1). The advantage of the hydraulic logic over the pneumatic logic is that it prevents potential bubble formation due to the lack of a vacuum line and latching times can be permanent. However, as the hydraulic logic system serially cascades more logic gates, it suffers significant pressure drops compared to pneumatic logic because viscosity of water is two orders of magnitude greater than that of air.

Constant-Input-Driven Oscillators

A constant-input-driven oscillator is a device that converts constant input (flow or pressure) to an oscillatory output flow. Because the device does not need dynamic external control units such as solenoid valves, it can simplify the need of off-chip control units. The generated output can be used as an on-chip timing source for microfluidic logic gates. Also, when a biochemical solution is used as an input, the output itself can be used to directly manipulate biomolecules. To date, constant flow- and pressure-driven oscillators have been presented.

A constant-flow-driven oscillator uses NC valves, which are analogous to p-type metal-oxide-semiconductor field-effect transistors (pMOSFETs), as a key element.[29, 30] Fig. C.4A shows how the drain and gate terminals of two NC valves (the NC valve structure is shown in Fig. C.3A) are connected to each other to make the two valves alternate on-off states with an opposite phase to each other. This happens

because when the difference between the source and gate pressure surpasses a threshold pressure causing a valve to open and release its pressure, the flow output increases the gate pressure in the other valve causing it to close. Then, owing to the constant inflow, the pressure in the newly closed valve accumulates until the pressure surpasses a threshold value at which point the valve opens increasing the gate pressure in the other valve and closing it. In this way, the two valves open and close alternately. To control the duty cycle of the outflow, the opening width (w_o) of the two valves can be made asymmetric. This geometrical difference in the valve design changes the threshold pressure of opening for each valve. This in turn causes the pressure accumulation time of the two valves to become different, thereby changing the duty cycle or the relative duration that each valve is on.[30]

A constant-pressure-driven oscillator uses a free-standing flexible disk (Fig. C.4B).[31] Because the disk edge is not bonded to the device, flow passes through the disc edge when the disc deflects. Significant inertial force of flow initiates at a high-pressure input (70 kPa) and, by the interaction of the elastic force of the disk, vibration of the disk occurs, thereby oscillating the outflow (~100 Hz at the order of 1 mL/min flow rates). Another constant-pressure-driven oscillator is a pneumatic ring resonator, which uses cascaded odd numbers of NOT gates using NC valves.[32] The drains of the valves are connected to a common atmospheric pressure and the other gate terminal. Because of the pressure condition and the internal capacitance of each valve, the membranes (or drain pressures) of the valves oscillate alternately and the frequency range is reported at 1–100 Hz. The ring oscillator is used as an on-chip timing source for a finite-state machine capable of sequential metering, mixing, and flushing.[33] The operating oscillation frequency of two constant-pressure-driven oscillators are fast

(~100 Hz) compared to that of the constant-flow-driven oscillators (< ~ 1 Hz). It is because these pressure-driven oscillators either have very high operational pressure ranges owing to utilization of inertial effects[31] or use air[32] that gives rise to much lower fluidic resistance than that of water.

Other Useful Components

A device that controls the flow-rate ratio of two outflows using a single periodic pressure source has been described.[34] In this device, two flow channels merge at the outlet and each flow channel has two membrane fluidic capacitors serially connected through fluidic resistors and a NC valve. In each flow channel, a combination of two capacitors work as a bi-directional pump at a specific range of pressure excitation frequency because the second capacitor functions like a bandpass filter. The frequency range can be tuned by the product of capacitance and resistance in the channel. The NC valve changes the bi-directional flow into a uni-directional flow because the gate is at atmospheric reference pressure and source pressure of the valve alternates between positive and negative values. As a result, when two channels have different ranges of working excitation pressure frequency, the flow-rate ratio of the two outflows is controlled by the excitation frequency.

Another interesting component is a peristaltic micropump, which uses a single periodic pressure source.[35] The device has different size, quasi NC valves connected in series through source and drain terminals, and the gate terminals are linked to each other. The smaller valves have faster response times owing to the small, internal membrane capacitance. Because the size of the connected valve increases (or decreases) along the flow direction, the valves close sequentially by the arrival of a single pressure pulse, thus enabling pumping.

Biochemical Applications

To date, compelling biochemical applications using microfluidic logic gates, oscillators, frequency-specific flow controllers are not reported. This may be because such components are at a primitive stage and they have limited operational ranges and flexibility compared to those extensively depending on external controllers. On the other hand, with the combination of external controllers, microfluidic multiplexers using elastomeric valves have been widely used for the parallel processing of biochemicals. An initial compelling application of the multiplexers was protein crystallization.[36, 37] For crystallization, metering and mixing of reagents while keeping a constant nL-scale reaction-volume are essential.[36] Owing to the microscale of the devices' chamber, the assay can highly concentrate precise amounts of target molecules and can mix reagents rapidly; more recently, these advantages have also been utilized in the study of protein binding kinetics.[38, 39] Compared to the crystal growth of conventional microbatch and hanging-drop formats, the device implemented faster growth and higher hit rate of crystals. The device also measured phase behavior of xylanase crystallization systematically (Fig. C.5A-D).[37] Two 4-bit binary multiplexer arrays (Fig. C.5A) select one of 16 reagents and 16 buffers separately, thereby enabling 144 parallel chemical reactions. The selected solutions are metered and injected as consecutive slugs (~80 pL each) through a positive displacement cross-injection junction (Fig. C.5B) into the ring structure (Fig. C.5C) and then mixed in less than 3 s (Fig. C.5D). Because such a process is done systematically, protein phase-space for crystallization (Fig. C.5E) was completely mapped efficiently.

Multiplexers can also be used for cell culture systems: Gomez-Sjoberg et al. developed an automated cell culture and screening system that provide arbitrary culture media in 96 chambers having 60 nL individual volume.[40] Composition of the media provided through 16 inputs could be changed with high temporal resolution. Human primary mesenchymal stem cells (hMSCs) were cultured for weeks to examine effects of osteogenic stimulation on differentiation, proliferation, and cell motility. Multiplexers can also be applied to other cell applications such as a single-cell analysis[41–43] and arrayed cell analysis.[44, 45] In single-cell analysis, each cell is seeded in parallel multiple chambers individually and its response is individually analyzed; thus enabling cyclopedic data collections. For detection of target intracellular materials such as DNA or mRNA, they are extracted and their concentrations are increased through PCR to a detectable level.[41, 42]

C.4 Droplet Circuits

Droplet circuits are appropriate for rapid serial processing of biochemicals because the droplet generation frequency can be over a kHz and subsequent droplet processing and analysis can also be rapidly performed. Many factors affect generation of droplets.[46] Important factors are size and shape of channel junctions, viscosity of immiscible phases, interfacial tension between phases and channel walls. For example, between two phases, a less viscous phase tends to be droplets such as air droplets in water and water droplets in oil. Typically, high interfacial tension between two phases is necessary for spontaneous droplet formation; to make droplets in two phases that have low interfacial tension like aqueous two-phase system, additional mechanical perturbations are necessary.[47, 48] Also, like water (or oil) droplets in a hydrophobic (or

hydrophilic) channel, a relatively less wettable channel with respect to the phase that forms the droplets is necessary. After the generation of droplets, other serially connected components perform key functions. In this section, we introduce key functions of droplet circuits. Although some of the functions are not directly analogous to that of electronic circuits, the overall system is inspired by electronic circuits in that the modularity of each component is essential for the serial processing. We briefly discuss their working principle and show how they are used in the overall system for rapid biochemical processing.

Key Components

Droplet Sorter, Mixer, and Splitter

Passive sorting mechanisms are based on droplet size and weight. Sorting of different size droplets can use channel geometry that vary the ratio of shear forces.[49] When a droplet meets bifurcating channels, it flows into a branch with a relatively high shear force because the force drives the droplet into the branch instantaneously. Small droplets select low-resistance channel because higher flow rate of the channel results in high shear force (left panels of Fig. C.6A). On the other hand, with increasing droplet size, the droplet gets higher shear force toward the high-resistance channel because droplet's effective area to that direction increases. Accordingly, large droplet flows into the high-resistance channel (right panels of Fig. C.6A). A device using gravity also works for sorting of the droplets having different size and weight.[50] Despite its simplicity and high efficiency, the device requires relatively small sample velocities to allow gravity to take effect over designed flow distances (sedimentation of ~200 μm over 2.5 cm in channel length at 1 mL/h sample velocity). Droplet sorting is also achieved via electric fields that generate a force to steer

droplets into branching downstream channels depending on its fluorescence output,[51] and complex traffic operations were achieved with droplet sorting into five individual channels.[52] In addition, passive droplet rearrangement can be achieved with a channel loop design.[53] For example, a droplet traveling in series ABCDE can be rearranged to be ACDBE through the change of flow resistance in channels.

At high interfacial tension, droplet fusion will occur spontaneously with channel geometry[54, 55] between the two droplets containing different reactants (Fig. C.6B). Further rapid mixing (~2 ms) is achieved through chaotic advection through a long serpentine channel (Fig. C.6C).[56] Using bifurcating channels or T channels, a passive splitter makes a monodisperse mother droplet into evenly split two sister droplets.[57] The ratio of droplet volume splitting is roughly equal to daughter channel length ratio or inversely proportional to the daughter channel flow rate. This process can be repeated numerously in series achieve the desired droplet number or droplet size for both single and double emulsions (Fig. C.6D).[58] Droplets can also be actively split or mixed repeatedly via electrofusion,[59] one that is advantageous for mixing droplets at low interfacial tensions. Although active forms of droplet operations are capable of complex droplet manipulations,[60] external control technologies have yet to produce droplet operations at the rate of flow-focusing droplet generation.

Another recent passive operation is the passive droplet dilutor. This technique is capable of high-throughput dilution and screening of nanoliter droplets via a passively activated side valve geometric design[61] (pillar structures of Fig. C.6E). A large droplet is trapped in a dilution chamber and forms the mother droplet containing contents to be diluted. Subsequent input droplets contain the diluent that fuses with the mother droplet, thus diluting the mother droplet. The increased volume of the mother droplet

closes the side valve, and shear force to the downward channel increases thereby generating output droplet from the mother droplet until the side valve is re-opened. As this process repeats, concentrations of mother and output droplets are significantly diluted with high precision.

Traffic Control via Boolean Operations, Flip-Flop Switching, and Synchronization

Other droplet microfluidic analogues of electronic circuits such as logic gates, switches, and synchronizers make elegant use of channel geometry (Fig. C.6F).[62] The existence of a droplet affect the flow of the other droplet, thereby enabling Boolean functions. The working principle is similar to the passive sorter in that designed flow resistance and shear force govern the traffic of the droplets, thus implementing embedded functions. Further characterization of the synchronizer geometry was studied by Ahn et al.[63] and is useful for synchronizing droplets for downstream droplet fusion. In the synchronizer, the leading droplet experiences higher resistance than the lagging droplet, allowing for the lagging droplet to have higher velocity and catch up. When the droplets are synchronized, the pressures differences stabilize and the droplets exit the ladder network synchronized and traveling at the same velocity.

Biochemical Applications

Droplet microfluidics is well suited for the applications that require rapid analysis such as high-throughput single-cell analysis, protein analysis, and PCR requiring ultrafast reaction times. Rapid single-cell analysis can be performed through the sequence of single-cell encapsulation, exposure to stimulant of choice via droplet fusion, short or long-term incubation times and finally assay and signal acquisition

(Fig. C.7).[64] The advantages of such applications are the ability to keep precise amounts of reactants separate until the desired conditions are met for them to be mixed and after mixing as started, the small diffusion lengths allow for rapid reaction times for high-throughput functionality. Through the use of a few simple electrodes, complex operations can be performed on protein for a multi-step assay with fluorescent readout.[64, 65] This device greatly simplifies an otherwise laborious laboratory protocol at a greatly reduced cost on both operator cost and material costs through automation and miniaturization. Similarly through automation and miniaturization, droplet microfluidics is capable of performing a commonly used technique: PCR with 1.5 million amplifications in parallel at over 99% accuracy.[66] Purified genomic DNA and reactants necessary for PCR are encapsulated into droplets at the specified concentrations. Using mostly passive operations and a simple electrode for electrofusion, the device enables complex droplet operations and droplet fusion to achieve appropriate delivery and mixture of droplet components at the correct sequence and conditions for PCR to occur.

Owing to its relatively simple device geometry, droplet microfluidic devices are relatively easy to design, serially cascade, and fabricate. However, the device may be inappropriate for applications that need to keep target biomolecules in the droplet while removing and changing solutions, and for assays requiring immobilization of biomolecules on channel surfaces. Although elastomeric microfluidic devices are conceptually more complex and need more expertise to design, they would be more suitable for these latter types of applications.

C.5 Outlook and Perspectives

Although microfluidic control circuits that are analogues of electronic circuits are in their infancy, they have the potential to minimize external control units and to perform autonomous, embedded functions. Nevertheless, to make development of such electronics-inspired microfluidic circuits more useful, we should understand the (i) operational, and (ii) physical limitations behind the analogy. There are many types of electronic circuits but some electronic circuit designs may be more appropriate for conversion into fluidic circuits than others. Given the nice analogy between electronic and microfluidic circuits in terms of designing and analyzing microfluidic circuits, what might the analogy provide in terms of fruitful directions for future development?

In terms of operation, both elastomeric and droplet microfluidic circuits have an inherent limitation because, once such devices are fabricated, their functions and operational ranges are more restricted than those that extensively use external controllers. For example, in the microfluidic oscillator circuit, the input flow rate or pressure determines the oscillation period for a given device. In other words, flow rate and oscillation period cannot be independently regulated; thus limiting flexibility. Also, the range of oscillation periods is narrower compared to those relying on external controllers. This also applies to droplet circuits where flow rate in conjunction with the bifurcating channel's shape and size determine droplet size and its generation frequency. Nevertheless, when specific operational ranges are determined and the devices are designed accordingly, they will be useful like application-specific integrated circuit (ASIC) chips in electronics.

Physical limitation exists in elastomeric microfluidic circuits. To perform even relatively simple digital functions using Boolean operations, elastomeric valve circuits need relatively large number of valves. In the 4-bit shift resistor, ~60 valves were

necessary to convert sequential signals of a single source to 4-bit parallel signals. As the number of Boolean operations increase, as required for more sophisticated functions, the number of serially connected valves drastically increases due to the nature of the modular approach (functional partition by elementary components). In electronic circuits, however, this serial/modular approach is plausible. For example, the Intel Itanium 2 processor, which is a microprocessor introduced in 2004, has $\sim 6 \times 10^8$ transistors with each having sizes on the order of $\sim$100 nm.[67]Because electrical resistance of integrated wires and transistors can be easily regulated, the processor performs sophisticated digital computing (Boolean operation) with an acceptable internal voltage drop. In contrast, if microfluidic valves were to be fabricated with such high density and small size, control of pressure would become a significant issue. Threshold pressures of microfluidic valves would be high due to their small, stiff membranes. More importantly, the pressure drop would be enormous due to the reduced channel size and the serial connection of channels. For instance, a 10-fold reduction of channel radius (e.g., 100 to 10 μm) results in a 10^4-fold increase of flow resistance. Also, total resistance linearly increases with the increasing number of serially connected channels and valves. Such analysis suggests limits in effectively transferring digital circuit design concepts that use Boolean operations to microfluidics.

In this regard, microfluidic circuits may gain more fruitful insights from analog electronics, where electric components and transistors give continuous output voltages and currents. Microfluidic analogues of analog electronic-circuits are oscillators,[29–32] peristaltic pumps,[35] and frequency-specific flow controller.[34] Notably, they have simpler structures; thus implying easier fabrication and less pressure drop. Also, their

own feedback control and continuous output enable their input flows directly to be output flows. In contrast, digital microfluidic circuits using Boolean operations are designed to indirectly control biochemical solutions.[26–28] Parallel biochemical processing with such analog microfluidic circuits, however, has not been demonstrated yet except for a very simple immunoassay.[29] A clever arrangement of microfluidic valves, capacitors, and resistors in conjunction with selection of control input would be needed to enable more sophisticated parallel biochemical processing. Such devices can be inspired by analog electronics because they perform parallel processing with electric resistors, capacitors, and transistors.

In droplet circuits, on the other hand, a serial/modular approach is plausible and, through the approach, droplet circuits have already demonstrated several rapid/serial biochemical processing. Because each component of droplet circuits is simple and does not suffer high pressure drop, components like droplet generators, splitters, and sorters are serially connected without high pressure drops. Nevertheless, despite seemingly facile serial modularity, integrating each component can result in unexpected issues due to the relatively small actuation forces generated and susceptibility to fluctuations and disturbances. By overcoming such obstacles and finding good biochemical applications, droplet circuits have become excellent tools for rapid serial processing of biochemicals.

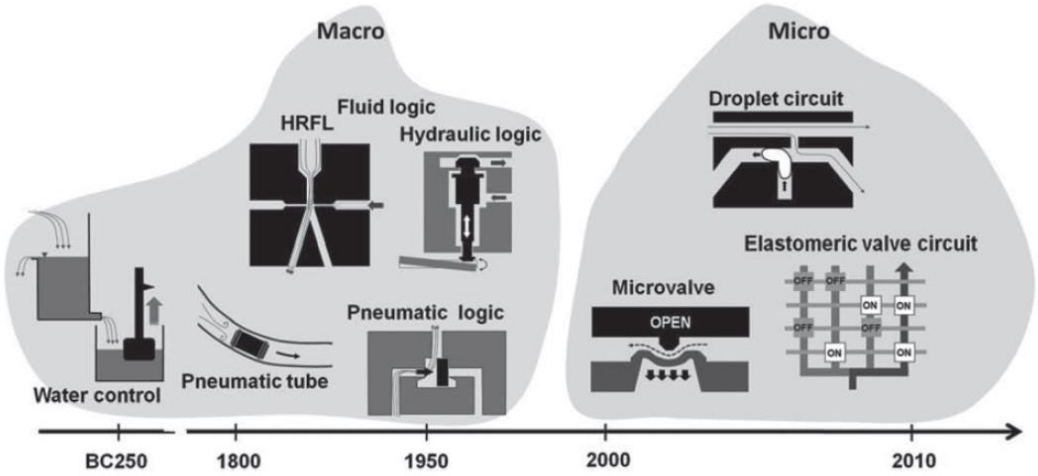

Fig. C.1 Timeline showing development of macroscopic and microscopic fluidic actuation and control systems.

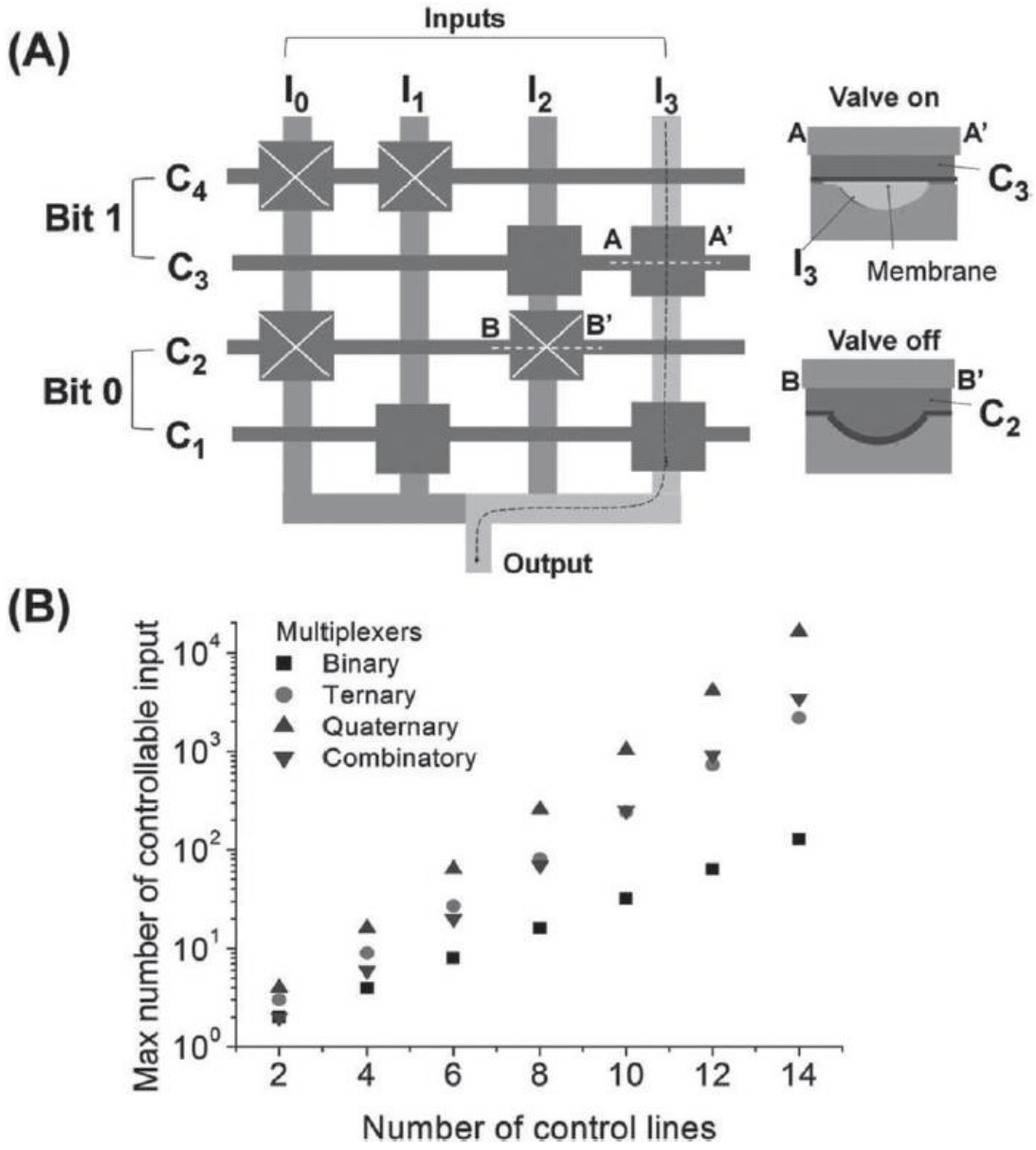

Fig. C.2 Microfluidic multiplexers. A) Binary multiplexer. Horizontal and vertical lines are control (C*i*) and input (I*i*) flow channels, respectively. Cross-sections (AA' and BB') of the valves show that control and input liquids are in top and bottom channels, respectively, and depict on- and off-states. In each bit, on-off states of valves in the upper and lower C*i* are opposite; state 1 (or 2) is upper valves off (or on) and lower valves on (or off). The diagram shows that bit 0 and 1 are both in state 1 and thus I_3 is selected to be an output. B) Maximum number of controllable flow channels in different multiplexers.

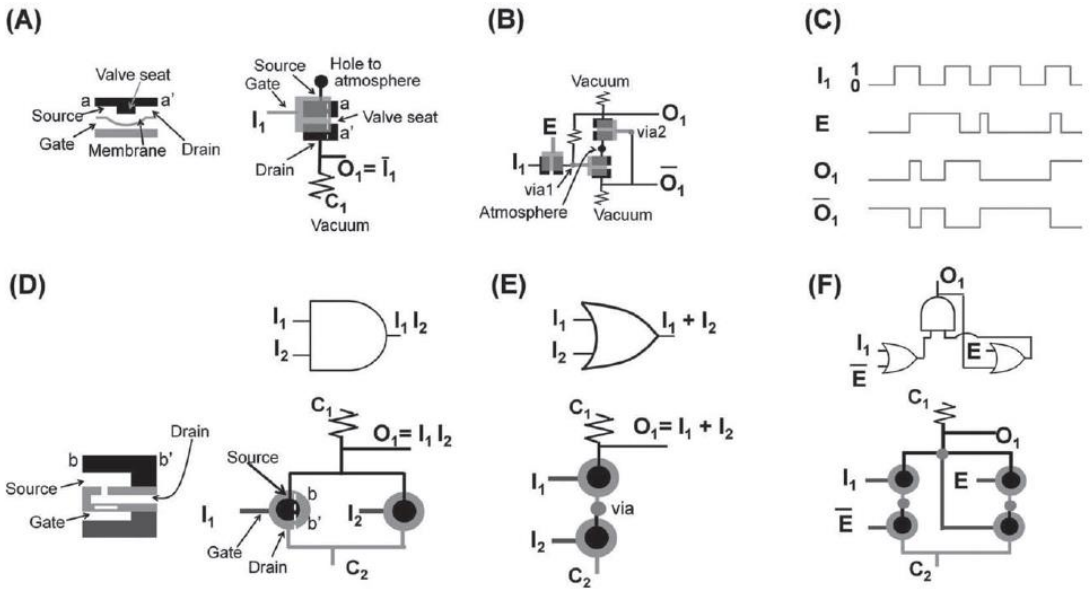

Fig. C.3 Microfluidic logic gates. A) Pneumatic NOT gate. Cross-section of a valve shows the valve-on state; source and drain terminals are in the top channel; and a gate terminal locates at the bottom channel under the membrane. In the top view of the valve, black area is in top channel and gray area is in bottom channel. B) Pneumatic gated D latch consisting of NOT gates. C) State of each line in gated D latch. Vacuum and atmospheric pressure are defined as state 1 and 0, respectively. D) Hydraulic AND gate. Cross-section shows a normally open valve, which has a pressure gain with a rigid disk (white bar above gate in left panel); valve is off when gate pressure is sufficiently high to deflect the membrane containing the disk upward and to close a hole. In the top view of the valves, black, light gray, and dark gray areas are in the top, middle, and bottom channels, respectively. E) Hydraulic OR gate. F) Hydraulic static latch consisting of AND and OR gates. State of each line coincides that in (C). Note that high and low pressures are defined as state 1 and 0, respectively, and it is the opposite of pneumatic logic.

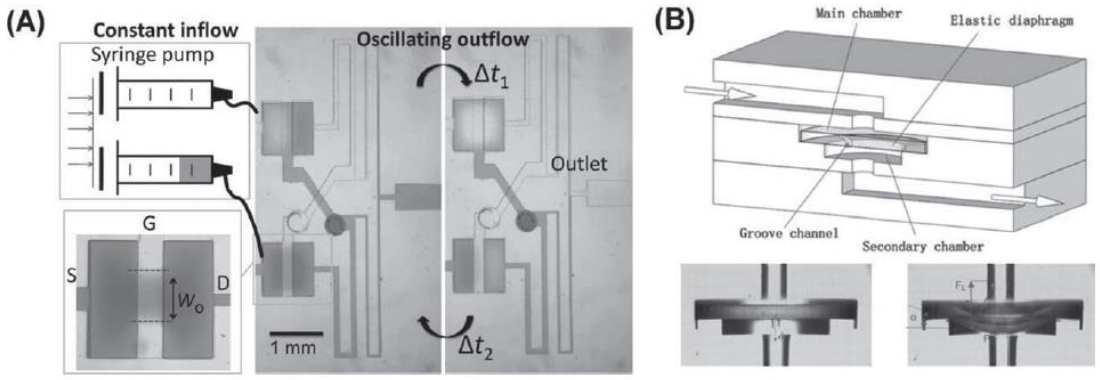

Fig. C.4 Constant-input-driven microfluidic oscillator. A) Constant-flow-driven oscillator. In the two normally closed valves, one valve's drain is connected to the other valve's gate, thereby making alternating pressure accumulation and release of each valve. Reproduced with permission.[30] Copyright 2012, American Chemical Society. B) Constant-pressure-driven oscillators. Vibration of free-standing, flexible disk results in outflow oscillation. Reproduced with permission.[31] Copyright 2012, Royal Society of Chemistry.

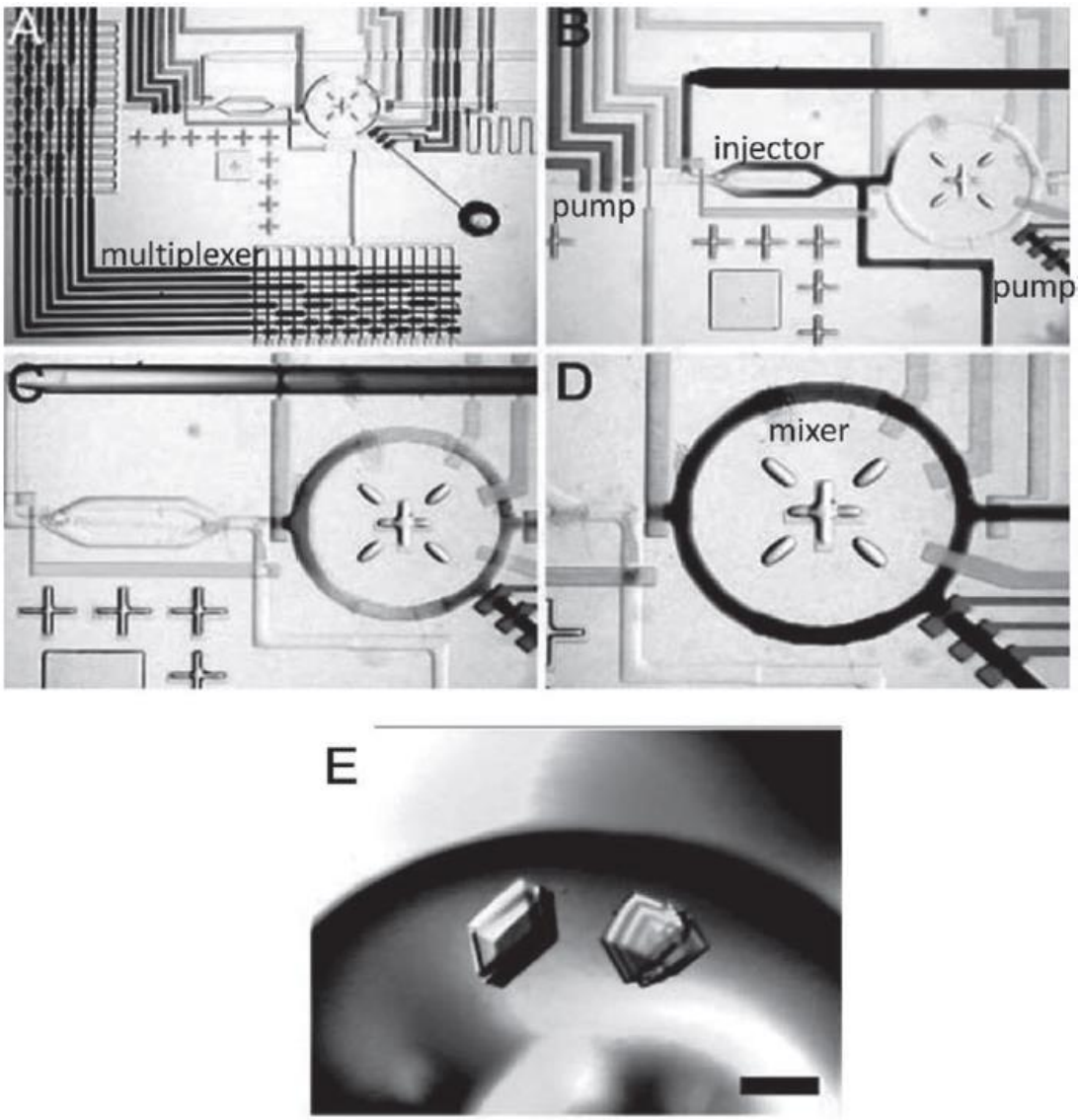

Fig. C.5 Applications of microfluidic multiplexers. A–D) Optical micrographs of "Formulation chip". E) Large, single, 3D crystals grown directly from optimal screen. A–E, reproduced with permission.[37] Copyright 2004, National Academy of Sciences, USA.

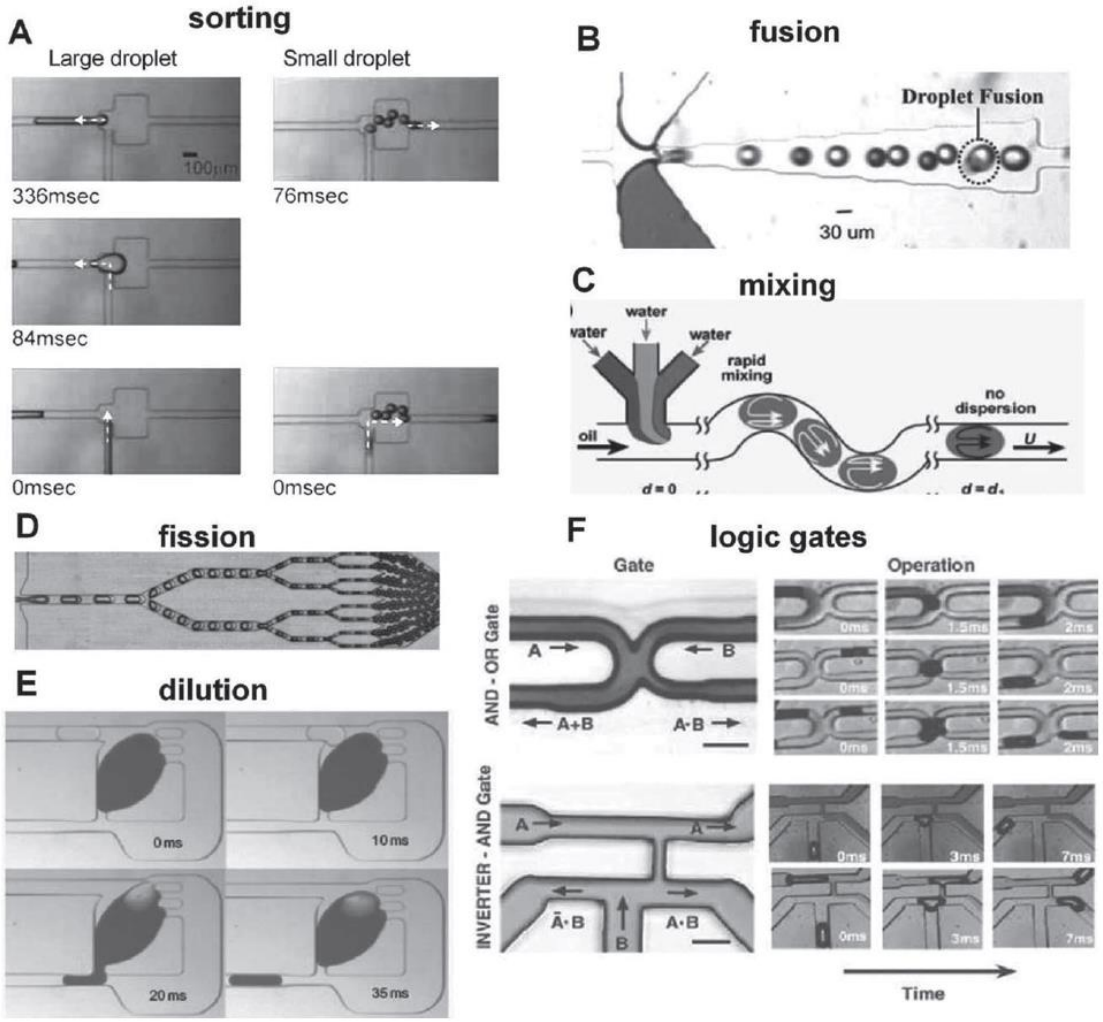

Fig. C.6 Droplet microfluidic operations. A) Sorting by size. Reproduced with permission.[49] Copyright 2008, Springer. B) Spontaneous fusion. Reproduced with permission.[55] Copyright 2006, Royal Society of Chemistry. C) Mixing by chaotic advection. Reproduced.[56] D) Droplet fission. Reproduced with permission.[58] Copyright 2011, Royal Society of Chemistry. E) Dilution. Reproduced with permission.[61] Copyright 2011, Nature Publishing Group. F) Microfluidic analogues of electric logic gates. Reproduced with permission.[62] Copyright 2007, American Association for the Advancement of Science.

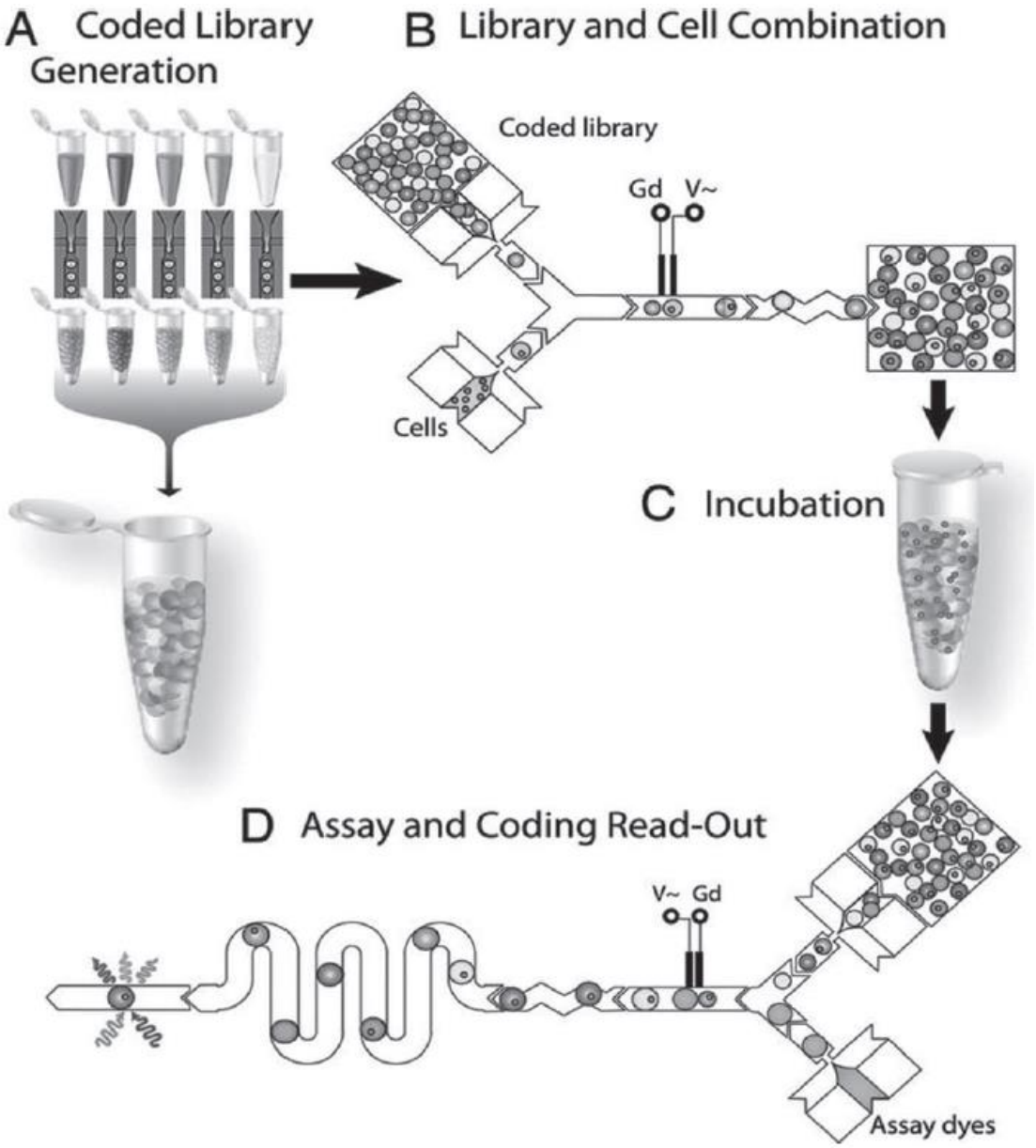

Fig. C.7 Droplet microfluidic application flowchart. A) Cell stimulants are encapsulated into droplets and stored off chip. B) Stimulants are mixed together or with single-cell encapsulated droplets via fusion operations. C) After fusion, the droplets can then be recollected and incubated off chip if necessary. D) Droplets are once again loaded into a droplet device with fusion operations with separate reagents for protein assay. Fluorescence signals can then be acquired downstream after chaotic advection mixing to determine effects of stimulants on single cells. Reproduced.[64]

C.6 References

1 P. S. Dittrich, A. Manz, *Nat. Rev. Drug Discovery* 2006, **5**, 210–218.

2 S. Vyawahare, A. D. Griffiths, C. Merten, *Chem. Biol.* 2010, **17**, 1052–1065.

3 G. M. Whitesides, *Nature* 2006, **442**, 368–373.

4 P. Liu, R. A. Mathies, *Trends Biotechnol.* 2009, **27**, 572–581.

5 a) D. Mark, S. Haeberle, G. Roth, F. von Stetten, R. Zengerle, *Chem. Soc. Rev.* 2010, **39**, 1153–1182; b) R. Gorkin, J. Park, J. Siegrist, M. Amasia, B. S. Lee, J.-M. Park, J. Kim, H. Kim, M. Madou, Y.-K. Cho, *Lab Chip* 2010, **10**,1758–1773.

6 a) A. W. Martinez, S. T. Phillips, G. M. Whitesides, E. Carrilho, *Anal. Chem.* 2010, **82**, 3–10; b) M. R. McNeely, M. K. Spute, N. A. Tusneem, A. R. Oliphant, *Proc. SPIE* 1999, **3877**, 210–220; c) S.-J. Kim, Y. T. Lim, H. Yang, Y. B. Shin, K. Kim, D.-S. Lee, S. H. Park, Y. T. Kim, *Anal. Chem.* 2005, **77**, 6494–6499; d) M. Zimmermann, H. Schmid, P. Hunziker, E. Delamarche, *Lab Chip* 2007, **7**, 119–125.

7 a) A. Groisman, M. Enzelberger, S. R. Quake, *Science* 2003, **300**, 955–958; b) A. Groisman, S. R. Quake, *Phys. Rev. Lett.* 2004, 094501.

8 a) R. Schoch, J. Han, P. Renaud, *Rev. Mod. Phys.* 2008, **80**, 839–883; b) R. B. Fair, *Microfluid. Nanofluid.* 2007, **3**, 245–281.

9 K. Horiuchi, P. Dutta, *Lab Chip* 2006, **6**, 714–723.

10 H. Erfle, B. Neumann, U. Liebel, P. Rogers, M. Held, T. Walter, J. Ellenberg, R. Pepperkok, *Nat. Protoc.* 2007, **2**, 392–399.

11 J. G. Landels, in *Engineering in the ancient world*, University of California Press, Berkeley, California 2000.

12 G. A. Audsley, in *The art of organ-building: a comprehensive historical, theoretical, and practical treatise on the tonal appointment and mechanical construction of concert-room, church, and chamber organs*, Dover Publications, 1965.

13 H. L. Stewart, in *Hydraulic and Pneumatic Power for Production*, Industrial Press, New York 1977.

14 T. Gilles, in *Automotive service: inspection, maintenance repair*, Delmar Cengage Learning, 2011.

15 C. Alexander, M. Sadiku, *Fundamentals of electric circuits*, McGraw-Hill, New York, 2008.

16 R. C. Jaeger, T. N. Blalock, *Microelectronic Circuit Design*, McGraw-Hill, New York, 2003.

17 G. M. Whitesides, E. Ostuni, S. Takayama, X. Jiang, D. E. Ingber, *Annu. Rev. Biomed. Eng.* 2001, **3**, 335–373.

18 E. A. Ottesen, J. W. Hong, S. R. Quake, J. R. Leadbetter, *Science* 2006, **314**, 1464–1467.

19 T. Thorsen, S. J. Maerkl, S. R. Quake, *Science* 2002, **298**, 580–584.

20 D. Maier-schneider, J. Maibach, E. Obermeier, O. F. Pan, E. T. Al, *J. Microelectromech. Syst.* 1995, **4**, 238–241.

21 D. W. Lee, Y.-H. Cho, *Lab Chip* 2009, **9**, 1681–1686.

22 Z. Hua, Y. Xia, O. Srivannavit, J.-M. Rouillard, X. Zhou, X. Gao, E. Gulari, *J. Micromech. Microeng.* 2006, **16**, 1433–1443.

23 W. H. Grover, R. H. C. Ivester, E. C. Jensen, R. A. Mathies, *Lab Chip* 2006, **6**, 623–631.

24 S. G. Shiva, in *Introduction to logic design*, 2nd ed, M. Dekker, New York 1998, Ch. 2 and Ch 4.

25 H. Takao, M. Ishida, K. Sawada, *J. Microelectromech. Syst.* 2002, **11**, 421–426.

26 M. Rhee, M. A. Burns, *Lab Chip* 2009, **9**, 3131–3143.

27 E. C. Jensen, W. H. Grover, R. a Mathies, *J. Microelectromech. Syst.* 2007, **16**, 1378–1385.

28 J. A. Weaver, J. Melin, D. Stark, S. R. Quake, M. A. Horowitz, *Nature Phys.* 2010, **6**, 218–223.

29 B. Mosadegh, C.-H. Kuo, Y.-C. Tung, Y.-suke Torisawa, T. Bersano-Begey, H. Tavana, S. Takayama, *Nature Phys.* 2010, **6**,433–437.

30 S.-J. Kim, R. Yokokawa, S. C. Lesher-Perez, S. Takayama, *Anal. Chem.* 2012, **84**, 1152–1156.

31 H. M. Xia, Z. P. Wang, W. Fan, A. Wijaya, W. Wang, Z. F. Wang, *Lab Chip* 2012, **12**, 60–64.

32 P. N. Duncan, T. V. Nguyen, E. E. Hui, in *Proceedings of the μTAS 2010 Conference*, Groningen, Netherlands, Oct 3–7, 2010, pp.1838–1840.

33 T. V. Nguyen, S. Ahrar, P. N. Duncan, E. E. Hui, in *Proceedings of the μTAS 2011 Conference*, Seattle, USA, Oct 2–6, 2011,741–743.

34 D. C. Leslie, C. J. Easley, E. Seker, J. M. Karlinsey, M. Utz, M. R. Begley, J. P. Landers, *Nature Phys.* 2009, **5**, 231–235.

35 H. Lai, A. Folch, *Lab Chip* 2011, **11**, 336–42.

36 C. L. Hansen, E. Skordalakes, J. M. Berger, S. R. Quake, *Proc. Natl. Acad. Sci. USA* 2002, **99**, 16531–16536.

37 C. L. Hansen, M. O. A. Sommer, S. R. Quake, *Proc. Natl. Acad. Sci. USA* 2004, **101**, 14431–14436.

38 S. R. Bates, S. R. Quake, *Appl. Phys. Lett.* 2009, **95**, 073705–3.

39 S. J. Maerkl, S. R. Quake, *Science* 2007, **315**, 233–237.

40 R. Gómez-Sjöberg, A. A. Leyrat, D. M. Pirone, C. S. Chen, S. R. Quake, *Analytical Chemistry* 2007, **79**, 8557–8563.

41 R. J. Taylor, D. Falconnet, A. Niemistö, S. A. Ramsey, S. Prinz, I. Shmulevich, T. Galitski, C. L. Hansen, *Proc. Natl. Acad. Sci. USA*2009, **106**, 3758–3763.

42 J. F. Zhong, Y. Chen, J. S. Marcus, A. Scherer, S. R. Quake, C. R. Taylor, L. P. Weiner, *Lab Chip* 2008, **8**, 68–74.

43 S. Tay, J. J. Hughey, T. K. Lee, T. Lipniacki, S. R. Quake, M. W. Covert, *Nature* 2010, **466**, 267–271.

44 L. M. Fidalgo, S. J. Maerkl, *Lab on a Chip* 2011, **11**, 1612–1619.

45 G. A. Cooksey, C. G. Sip, A. Folch, *Lab on a Chip* 2009, **9**, 417–426.

46 S.-Y. Teh, R. Lin, L.-H. Hung, A. P. Lee, *Lab Chip* 2008, **8**, 198–220.

47 I. Ziemecka, V. van Steijn, G. J. M. Koper, M. Rosso, A. M. Brizard, J. H. van Esch, M. T. Kreutzer, *Lab Chip* 2011, **11**, 620–624.

48 D. Lai, J. P. Frampton, H. Sriram, S. Takayama, *Lab Chip* 2011, 3551–3554.

49. Y. C. Tan, Y. L. Ho, A. P. Lee, *Microfluid. Nanofluid.* 2008, **4**, 343–348.

50 D. Huh, J. H. Bahng, Y. Ling, H. H. Wei, O. D. Kripfgans, J. B. Fowlkes, J. B. Grotberg, S. Takayama, *Anal. Chem.* 2007, **79**,1369–1376.

51 J. C. Baret, O. J. Miller, V. Taly, M. Ryckelynck, A. El-Harrak, L. Frenz, C. Rick, M. L. Samuels, J. B. Hutchison, J. J. Agresti, D. R. Link, D. A. Weitz, A. D. Griffiths, *Lab Chip.* 2009, **9**, 1850–1858.

52 L. Wang, L. A. Flanagan, N. L. Jeon, E. Monuki, A. P. Lee, *Lab Chip.* 2007, **7**, 1114–1120.

53 Y. C. Tan, J. S. Fisher, A. I. Lee, V. Cristini, A. P. Lee, *Lab Chip.* 2004, **4**, 292–298.

54 L. Mazutis, J. C. Baret, A. D. Griffiths, *Lab Chip.* 2009, **9**, 2665–2672.

55 L. H. Hung, K. M. Choi, W. Y. Tseng, Y. C. Tan, K. J. Shea, A. P. Lee, *Lab Chip.* 2006, **6**, 174–178.

56 H. Song, J. D. Tice, R. F. Ismagilov, *Angew. Chem. Int. Ed.* 2003, **42**, 768–772

57 D. R. Link, S. L. Anna, D. A. Weitz, H. A. Stone, *Phys. Rev. Lett.* 2004, **92**, 054503.

58 A. R. Abate, D. A. Weitz, *Lab Chip* 2011, **11**, 1911–1915.

59 S. K. Cho, H. Moon, C. J. Kim, *J. Microelectromech. S.* 2003, **12**, 70–80.

60 P. Paik, V. K. Pamula, R. B. Fair, *Lab Chip.* 2003, **3**, 253–259.

61 X. Niu, F. Gielen, J. B. Edel, A. J. deMello, *Nature Chem.* 2011, **3**, 437–442.

62 M. Prakash, N. Gershenfeld, *Science* 2007, **315**, 832–835.

63 B. Ahn, K. Lee, H. Lee, R. Panchapakesan, K. W. Oh, *Lab Chip.* 2011, **11**, 3956–3962.

64 E. Brouzes, M. Medkova, N. Savenelli, D. Marran, M. Twardowski, J. B. Hutchison, J. M. Rothberg, D. R. Link, N. Perrimon, M. L. Samuels, *P. Natl. Acad. Sci. USA.* 2009, **106**, 14195–14200.

65 L. Mazutis, J. C. Baret, P. Treacy, Y. Skhiri, A. F. Araghi, M. Ryckelynck, V. Taly, A. D. Griffiths, *Lab Chip.* 2009, **9**, 2902–2908.

66 R. Tewhey, J. B. Warner, M. Nakano, B. Libby, M. Medkova, P. H. David, S. K. Kosopoulos, M. L. Samuels, J. B. Hutchison, J. W. Larson, E. J. Topol, M. P. Weiner, O. Harismendy, J. Olson, D. R. Link, K. A. Frazer, *Nat. Biotechnol.* 2009, **27**, 1025–1031.

67 www.ni.com/white-paper/8564/en, accessed on May 2012